UNIVERSIDADE DA BEIRA INTERIOR

Engenharia

Control of Modular Multilevel Converters in High Voltage Direct Current Power Systems

Majid Mehrasa

Tese para obtenção do Grau de Doutor em
Engenharia Electrotécnica e de Computadores
(3º ciclo de estudos)

Orientador:	Doutor João Paulo da Silva Catalão
Co-orientador:	Doutora Maria do Rosário Alves Calado
Co-orientador:	Doutor Edris Pouresmaeil

Covilhã, Junho de 2019

UNIVERSITY OF BEIRA INTERIOR

Engineering

Control of Modular Multilevel Converters in High Voltage Direct Current Power Systems

Majid Mehrasa

Thesis submitted in fulfillment of the requirements for the Ph.D. degree in

Electrical and Computer Engineering

(3rd cycle of studies)

Supervisor: Dr. João Paulo da Silva Catalão
Co-supervisor: Dr. Maria do Rosário Alves Calado
Co-supervisor: Dr. Edris Pouresmaeil

Covilhã, June 2019

This work was supported by FEDER funds through COMPETE 2020 and by Portuguese funds through FCT, under Projects SAICT-PAC/0004/2015 - POCI-01-0145-FEDER-016434 (ESGRIDS) and 02/SAICT/2017 - POCI-01-0145-FEDER-029803 (UNiTED).

UNIÃO EUROPEIA

Fundos Europeus
Estruturais e de Investimento

Acknowledgments

Firstly, I would like to express my sincere gratitude to my Ph.D. advisors, Dr. João Catalão, Dr. Maria Calado and Dr. Edris Pouresmaeil, for the continuous support of my Ph.D. studies and related research, for their patience, motivation and immense knowledge. Their constructive guidance, advice, and comments helped me at all times during the research and writing of this thesis.

I would like to thank to my fellow colleagues in the "Sustainable Energy Systems Lab" especially Dr. Sérgio Santos, Dr. Gerardo Osório, Dr. Radu Godina and Dr. Eduardo Rodrigues for providing a great environment and dealing with all needs in the Lab during the past years.

Last but not least, I would like to thank my family, especially my mother, my wife and all my friends who have been beside me in the last years.

Resumo

Esta tese visa proceder a uma análise abrangente de conversores multinível modulares (MMC) para transmissão a alta tensão em corrente contínua (HVDC), almejando apresentar novos modelos matemáticos em sistemas dinâmicos e projetar novas estratégias de controlo. Na primeira etapa são introduzidos dois novos modelos matemáticos dinâmicos que usam *differential flatness theory* e as componentes de correntes circulantes. Ainda, é estabelecida uma modelação matemática para o controlo preciso dos MMCs, operando em modo inversor ou modo retificador. Depois de apresentar as novas equações matemáticas, as técnicas de controlo mais adequadas são delineadas. Devido às características não lineares dos MMCs, são projetadas duas estratégias de controlo não-lineares baseadas no método direto de *Lyapunov* e no controlo do tipo *passivity theory-based* combinado com controlo por modo de deslizamento através do uso de modelos dinâmicos baseados em correntes circulantes para fornecer uma operação estável aos MMCs em aplicações de HVDC sob várias condições de operação. Os efeitos negativos das perturbações de entrada, erros de modelação e incertezas do sistema são suprimidos através da definição da função de controlo de *Lyapunov* para alcançar os termos de integração-proporcionalidade dos erros de saída para que possam finalmente ser adicionados às entradas iniciais. Os resultados da simulação computacional realizados em ambiente MATLAB/SIMULINK verificam os efeitos positivos dos modelos dinâmicos propostos e das novas estratégias de controlo em todas as condições de operação dos MMCs no modo inversor, retificador e em aplicações HVDC.

Palavras Chave

Conversor Multinível Modular, Potência Ativa e Reativa, Método de Lyapunov, Controlo por Modo de Deslizamento, Transmissão a Alta Tensão em Corrente Contínua.

Abstract

This thesis focuses on a comprehensive analysis of Modular Multilevel Converters (MMC) in High Voltage Direct Current (HVDC) applications from the viewpoint of presenting new mathematical dynamic models and designing novel control strategies. In the first step, two new mathematical dynamic models using differential flatness theory (DFT) and circulating currents components are introduced. Moreover, detailed step-by-step analysis-based relationships are achieved for accurate control of MMCs in both inverter and rectifier operating modes. After presenting these new mathematical equations-based descriptions of MMCs, suitable control techniques are designed in the next step. Because of the nonlinearity features of MMCs, two nonlinear control strategies based on direct Lyapunov method (DLM) and passivity theory-based controller combined with sliding mode surface are designed by the use of circulating currents components-based dynamic model to provide a stable operation of MMCs in HVDC applications under various operating conditions. The negative effects of the input disturbance, model errors and system uncertainties are suppressed by defining a Lyapunov control function to reach the integral-proportional terms of the flat output errors that should be finally added to the initial inputs. Simulation results in MATLAB/SIMULINK environment verify the positive effects of the proposed dynamic models and control strategies in all operating conditions of the MMCs in inverter mode, rectifier mode and HVDC applications.

Keywords

Modular Multilevel Converter, Active and Reactive Power, Lyapunov Method, Sliding Controller, High Voltage Direct Current Transmission.

Contents

Acknowledgments iv

Resumo v

Abstract vi

Contents vii

List of Figures xii

List of Tables xviii

List of Symbols xix

Relevant Acronyms xxviii

Chapter 1 1

Introduction 1

1.1 Background 1

1.2 Research Motivation and Problem Definition 2

1.3 Research Questions, Objectives and Contributions of the Thesis 4

1.4 Methodology 8

1.5 Notation 8

1.6 Organization of the Thesis 8

Chapter 2 11

Novel Control Strategy for Modular Multilevel Converters Based on Differential Flatness Theory 11

2.1 Introduction 11

2.2 Proposed Control Technique 13

2.2.1 Dynamic Analysis of the Proposed MMC-based Model 13

2.2.2 The Proposed DFT-Based Control Technique 16

2.3 Effects of the Control Inputs Perturbations 20

2.4 Simulation Results 24

2.4.1 Control Technique Effect Assessment 24

2.4.2 Load Variation Evaluation 26

2.4.3 Parameters Variation Evaluation 28

2.5 Chapter Conclusions 31

Chapter 3 32

A Multi-Loop Control Technique for the Stable Operation of Modular Multilevel Converters in HVDC Transmission Systems 32

3.1 Introduction 32

3.2 The Proposed Differential Equation of MMC 34

3.2.1 Proposed Six Order Dynamic Model of MMCs 35

3.2.2 Capability Curve Analysis of MMCs Active and Reactive Power 38

3.3 Control Discussion 40

3.3.1 The Design of Outer Loop Controller (OLC) 41

3.3.2 Design of the Central Loop Controller (CLC) 43

3.3.3 The Design of Inner Loop Controller (ILC) 46

3.4 Convergence Evaluation and Stability Analysis 47

3.4.1 The Load Compensation Capability Analysis of MMC2 47

3.4.2 Dynamic Model Analysis of the DC-Link Voltage 48

3.5 Convergence Evaluation and Stability Analysis 50

3.5.1 The Load Variations Based Assessment of the Proposed Control Technique 51

3.5.2 The Parameter Variations Based Assessment of the Proposed Control Technique 55

3.6 Chapter Conclusions 60

Chapter 4 61

Function-Based Modulation Control for Modular Multilevel Converters under Varying Loading and Parameters Conditions 61

4.1 Introduction 61

4.2 The Proposed Modulation Functions 63

4.2.1 Calculation of The MMC' Arms Currents 63

4.2.2 The Proposed Modulation Function 65

4.3 Evaluation of the Instantaneous Power of the MMC Arms 67

4.3.1 Calculation of The MMC' Arms Currents 67

4.3.2 Instantaneous Power of the Arm's Resistance and Inductance 68

4.4 Determination of $\boldsymbol{Im}$and $\boldsymbol{\alpha}$ 70

4.5 Accurate Sizing of the Equivalent Sub-Module Capacitors 71

4.6 Simulation Results 73

4.6.1 Load Changes Evaluation 75

4.6.2 Parameters Changes Evaluation 79

4.7 Chapter Conclusions 83

Chapter 5 84

A Novel Modulation Function-Based Control of Modular Multilevel Converters for High Voltage Direct Current Transmission Systems 84

5.1 Introduction 84

5.2 Modular Multilevel Converter's Alternating Current-Side Voltages 86

5.3 Analysis of Proposed Modulation Function 88

5.3.1 Parameters Variation Effects on the Proposed Modulation Function 90

5.3.2 Input Current Variation Effects on the Proposed Modulation Function 92

5.4 Simulation Results 94

5.4.1 Parameter Variation Evaluation 95

5.4.2 Evaluation of Modular Multilevel Converter Input Current Variation 97

5.5 Chapter Conclusions 99

Chapter 6 100

Dynamic Model, Control and Stability Analysis of MMC in HVDC Transmission Systems 100

6.1 Introduction 100

6.2 The Proposed MMC-Based HVDC Model 102

6.3 Steady State Analysis 105

6.4 Dynamic Stability Analysis 107

6.5 Capability Curve Analysis of the MMCs 111

6.6 DC-Link Voltage Stability Analysis 113

6.7 Simulation Results 116

6.7.1 DC-Link and AC Voltages Evaluation 117

6.7.2 Analysis of MMC Currents 119

6.7.3 Active and Reactive Power Sharing Assessment 123

6.8 Chapter Conclusions 126

Chapter 7 127

Conclusions, Directions for Future Work and Contributions 127

7.1 Main Conclusions 127

7.2 Directions for Future Works 130

7.3 Relevant Contributions of this Work 130

7.3.1 Publications in Peer-Reviewed Journals 130

7.3.2 Publications in International Conference Proceedings 131

Bibliography 132

Appendices 148

Appendix A 149

Appendix B 150

Appendix C 151

List of Figures

Figure 2.1	The circuit diagram of the proposed MMC-based model.....	14
Figure 2.2	The proposed control technique of DFT (a) the component of u_1 (b) the component of u_2.....	20
Figure 2.3	The perturbation effect of first control input on (a) the first flat output (b) the second flat output.....	22
Figure 2.4	The effects of second control inputs on (a) the first flat output (b) the second flat output.....	23
Figure 2.5	The single diagram of simulated model.....	24
Figure 2.6	SM's voltages of MMC.....	25
Figure 2.7	Voltage at PCC in phase "a".....	25
Figure 2.8	Active power of MMC, load and AC filter.....	25
Figure 2.9	Reactive power of MMC, load and AC filter.....	26
Figure 2.10	SM's voltages of MMC with load variations at t=0.4 s.....	27
Figure 2.11	PCC voltage of phase "a" with load variations at t=0.4 s.....	27
Figure 2.12	Active power of MMC, load and AC filter with load variations at t=0.4.....	28
Figure 2.13	Reactive power of MMC, load and AC filter with load variations at t=0.4s.....	28
Figure 2.14	SM's voltages of MMC with parameters variations at t=0.4 s.....	29
Figure 2.15	PCC voltage of phase "a" with parameters variations at t=0.4 s.....	29
Figure 2.16	Active power of MMC, load and AC filter with parameters variations at t=0.4 s.....	30

Figure 2.17 Reactive power of MMC, load and AC filter with parameters variations at t=0.4 s..... 30

Figure 3.1 Schematic diagram of the MMC-HVDC system. (a) Single-line diagram model and (b) circuit diagram of the back-to-back MMC..... 35

Figure 3.2 (a) Power curve of MMCs (b) R and L changes effects on MMCs power curve..... 40

Figure 3.3 The proposed outer loop controller for (a) MMCs currents (b) MMCs circulating currents..... 44

Figure 3.4 The Proposed Central Loop Controller for (a) MMCs currents (b) MMCs circulating currents..... 46

Figure 3.5 The Proposed Inner Loop Controller for (a) the MMC2 reference currents (b) the MMC1 reference currents..... 47

Figure 3.6 The phase diagrams of the DC-link voltage (a) a>0 and (b) a<0..... 49

Figure 3.7 Block diagram of the proposed control technique for the MMC-HVDC system in Figure 3.1..... 51

Figure 3.8 The upper and lower switching functions of phase “a’ of (a) MMC1 (b) MMC2, under load changes..... 53

Figure 3.9 MMCs DC-link and Sub-Module’s voltages with load changes..... 53

Figure 3.10 MMCs AC voltages with load changes..... 54

Figure 3.11 MMCs Circulating currents with load changes..... 54

Figure 3.12 Active and reactive power of MMCs, load, and AC filter with load changes..... 55

Figure 3.13 Parameters changes for (a) the resistance of MMCs (b) the inductance of MMCs..... 56

Figure 3.14 The upper and lower switching functions of phase “a’’ of (a) MMC1 (b) MMC2, under MMC parameters changes..... 57

Figure 3.15 MMCs DC-link and SM's voltages with parameters changes..... 58

Figure 3.16 MMCs AC voltages with the parameters changes..... 58

Figure 3.17 MMCs circulating currents with parameters changes..... 59

Figure 3.18 Active and reactive power of MMCs, load, and AC filter with parameters changes..... 59

Figure 4.1 (a) The proposed MMC, (b) sub-module..... 64

Figure 4.2 The equivalent capacitor of (a) upper sub-modules (b) lower sub-modules..... 72

Figure 4.3 The overall structure of the proposed controller..... 73

Figure 4.4 In load changes process, a) The proposed three-phase upper and lower modulation functions with its carrier waves, b)the generated switching signals for upper sub-modules in phase "a" c) the generated switching signals for lower sub-modules in phase "a"..... 75

Figure 4.5 (a) The sub-module voltages of phase "a" (b) The output voltages of MMC before and after connecting AC filter capacitor under load change condition..... 76

Figure 4.6 (a) The output and circulating currents of the MMC. (b) Active and reactive power of the MMC under load changes condition..... 77

Figure 4.7 Angle Difference between output MMC voltages and Currents under load changes condition..... 78

Figure 4.8 In parameters changes condition, a) The proposed three-phase upper and lower modulation functions with its carrier waves, b)the generated switching signals for upper sub-modules in phase "a" c) the generated switching signals for lower sub-modules in phase "a"..... 79

Figure 4.9 (a) The sub-modules voltages of phase "a" (b) Output voltages of MMC before and after connecting AC filter under parameters change condition..... 80

Figure 4.10 (a) Output and circulating currents of the MMC (b) Active and reactive power of the MMC under parameters changes condition..... 81

Figure 4.11 Angle Difference between output MMC voltages and Currents under parameters changes condition..... 82

Figure 5.1 (a) The proposed three-phase modular multilevel converter (MMC) based model; and (b) sub-module (SM)..... 85

Figure 5.2 The proposed modulation functions for phase "a"..... 89

Figure 5.3 The proposed modulation index and function as to parameters given in Table 5.1..... 89

Figure 5.4 The proposed modulation index and function based on parameters variations given in Table 2..... 90

Figure 5.5 A typical shifted-level pulse width modulation (PWM) for proposed upper modulation function with parameter changes..... 91

Figure 5.6 A typical shifted-level PWM for proposed lower modulation function with parameter changes..... 91

Figure 5.7 The proposed modulation index and function based on input variable variations..... 92

Figure 5.8 A typical shifted-level PWM for proposed upper modulation function with input current changes..... 92

Figure 5.9 A typical shifted-level PWM for proposed lower modulation function with input current changes..... 93

Figure 5.10 The overall structure of the proposed modulation functions for MMC..... 93

Figure 5.11 SM voltages of MMC with parameter variations..... 94

Figure 5.12 DC-link voltage of MMC with parameter variations..... 95

Figure 5.13 MMC current of phase "a" with parameter variations..... 95

Figure 5.14 The active and reactive power of MMC with parameter variations..... 95

Figure 5.15 Circulating current of MMC in phase "a" with parameter variations..... 96

Figure 5.16 SM voltages of MMC with input MMC current variation..... 97

Figure 5.17 DC-link voltage of MMC with input MMC current variations..... 97

Figure 5.18 MMC current of phase "a" with MMC input current variations..... 97

Figure 5.19 The active and reactive power of MMC with MMC input current variations..... 98

Figure 5.20 Circulating current of MMC in phase "a" with input MMC current variations..... 98

Figure 6.1 General model of the proposed MMC-based HVDC system..... 102

Figure 6.2 Equivalent circuits of: (a) Dynamic model based on MMC output currents, (b) dynamic model based on circulating currents..... 103

Figure 6.3 Calculation of MMC output currents..... 105

Figure 6.4 Switching functions based on MMC output currents (a) d-component, (b) q-component..... 105

Figure 6.5 Switching functions based on circulating currents (a) d-component, (b) q-component, (c) 0-component..... 106

Figure 6.6 Different states of v_{dc} and dv_{dc}/dt..... 109

Figure 6.7 Capability curve of MMCs (a) increasing $i_{dc} > 0$, (b) decreasing $i_{dc} < 0$..... 111

Figure 6.8 Nyquist diagram of DC-link voltage variations for $i_{dci} > 0$ due to (a) d-component variations of MMC current (f_{i1}) (b) q-component variations of MMC current (f_{i2}) (c) DC-link current variations (f_{i3})..... 113

Figure 6.9 Nyquist diagram of DC-link voltage variations for $i_{dci} < 0$ due to: (a) d-component variations of MMCs currents (f_{i1}), (b) q-component variations of MMCs currents (f_{i2}), and (c) DC-link current variations (f_{i3})..... 114

Figure 6.10 Overall structure of the proposed controller..... 115

Figure 6.11 SM voltages and DC and AC side voltages of MMCs without DLM..... 116

Figure 6.12 SM voltages and DC and AC side voltages of MMCs with DLM..... 117

Figure 6.13 Circulating, DC-link and AC-side currents of the interfaced MMCs without DLM..... 118

Figure 6.14 Circulating, DC-link and AC-side currents of the interfaced MMCs with DLM..... 119

Figure 6.15 d and q components of MMCs currents without DLM..... 120

Figure 6.16 d and q components of MMCs currents with DLM..... 121

Figure 6.17 MMC1 and MMC2 active and reactive power waveforms without DLM..... 122

Figure 6.18 MMC1 and MMC2 active and reactive power waveforms with DLM..... 123

List of Tables

Table 2.1	The proposed MMC model specifications with related loads.....	26
Table 2.2	The second parameters for the proposed MMC model.....	29
Table 3.1	Simulation Parameters.....	50
Table 4.1	The parameters of the proposed MMC in load changes conditions.....	73
Table 4.2	The parameters of the proposed MMC in parameters changes conditions.....	74
Table 5.1	Simulated system parameters. AC: alternating current; DC: direct current.....	90
Table 5.2	Changes in MMC parameters in Condition 2.....	90
Table 6.1	Units for magnetic properties.....	115

List of Symbols

The main notations used in Chapters 2, 3, 4, 5 and 6 are listed below. Other symbols are defined where they first appear.

Chapter 2

Sets and Indices

i	1,2
j	1,2
k	a,b,c

Parameters

L	Output inductance of MMC
R	Output resistance of MMC
L_t	Arm's inductance of MMC
R_t	Arm's resistance of MMC
C_f	AC Filter Capacitor
C_{dc}	DC-link Capacitor
N	Sub modules numbers in per arm

Variables

i_k	Output Currents of MMC
i_{uk}	Upper's arm Currents of MMC
i_{lk}	Lower's arm Currents of MMC
i_{cirk}	Circulating Currents of MMC
i_{dq}	Output Currents of MMC in d-q reference frame
i_{cir0}	Circulating Currents of MMC in 0dq reference frame
v_{dc}	DC link voltage of MMC
v_{uk}	Upper's SM voltages of MMC
v_{lk}	Lower's SM voltages of MMC
u_k	The control factors of MMC

u_{dq}	The control factors of MMC in d-q reference frame
v_k	PCC voltages
v_m	The maximum magnitude of PCC voltages
v_{dq}	PCC voltages in d-q reference frame
P	Instantaneous active power of MMC
Q	Instantaneous reactive power of MMC
y_{12}	Flat Outputs
x_{123}	The state variables
u_{12}	The control inputs
e_{i1}	The proportional errors of the flat outputs
e_{i2}	The integral errors of the flat outputs
Δy_i	The perturbations of flat outputs
Δu_i	The perturbations of control inputs

Chapter 3

Indices

K	*a, b, c*
J	*1,2*

Parameters

$1/\xi_{(dq)}$	Proportional gain
L	Inductance of the MMCs
R	Resistance of the MMCs
L_p	Arm's inductance
C_{eq}	Equivalent *DC*-link capacitor
R_{dc}	Equivalent *DC*-link resistance
R_{dq0j}	Injection resistances
f_{ac}	*AC*-side frequency

f_s	Switching frequency
n	Numbers of SMs in each arm
C	Capacitor of SM
C_{fi}	Capacitor of *AC* filter
$\omega_{(dq)2}, \omega_{(dq)\max 2}$	Cut-off frequency
$\omega_{p(dq)2} / \xi_{(dq)}$	Integral gain
$k_{(dq)j}$	Positive constant of CLC
$\psi_{cir(dq)j}$	Positive constant of CLC
$\psi_{(dq)j}$	Positive constant of CLC

Variables

Q_j^*	Reference values of Reactive power of MMCs
$H_{(dq)j}(s)$	Transfer function
Z_{dqj}	Error vector
E_{dqj}	Total saved energy
S_{dqj}	Time-variable sliding surface
v_c	Rated capacitor voltage
$S_{(ul)jk}$	Switches of the MMCs
$v_{(ul)kj}$	Lower and upper arms voltages
v_{kj}	Output voltages of the MMCs
v_{dc}	*DC*-link voltage
u_{kj1}	First equivalent modulation function of the respective SM stacks
u_{kj2}	Second equivalent modulation function of the respective SM stacks

$v_{sm(ul)kj}$	SMs voltages
$v_{t(dq)j}$	*AC*-side voltages of the MMCs
$v^*_{(dq)j}$	Reference value of output voltages of the MMCs
v^*_{dc}	Reference value of *DC*-link voltage
i_{kj}	Currents of MMCs
i_{cirkj}	Circulating currents of the MMCs
$i_{(ul)kj}$	Lower and upper arms currents
i_{dcj}	MMCs *DC*-link currents
$i_{sm(ul)kj}$	Currents of SMs
$i^*_{(dq)j}$	Reference values of MMCs currents
$i^*_{cir(dq)j}$	Reference values of circulating currents
$i_{l(dq)j}$	Load currents
$I_{av(dq)j}$	Average currents of the MMCs
$i_{(dq)\max j}$	Maximum value of MMCs currents
$\sum_{h=1}^{\infty} i_{l(dq)h}$	Total harmonic current components of loads
P_j	Injected active power of MMCs
Q_j	Injected reactive power of MMCs
P^*_j	Reference values of active power of MMCs

Chapter 4

Indices

k	a,b,c
j	0,-1,1
i	u,l

Parameters

L	Output inductance of MMC
R	Output resistance of MMC
L_t	Arm's inductance of MMC
R_t	Arm's resistance of MMC
L_{eq}	Equivalent inductance of MMC
R_{eq}	Equivalent resistance of MMC
ω	Angular frequency of MMC
$\beta_{i(012)}$	Harmonically coefficients of sub-module powers
$\beta_{xi(012)}$	Harmonically coefficients of arm's inductance and resistance powers
a	Angle Difference between output MMC voltages and Currents
Θ_i	Phase angle of modulation functions

Variables

i_k	Input MMC Currents
i_{lk}	Arm Currents of MMC
i_{cirk}	Circulating Currents of MMC
i_{dc}	MMC DC-link Current
v_{dc}	MMC DC-link Voltage
v_{ik}	Sub-modules Voltages of MMC
v_k	Output voltages of MMC
v_{ix}	The voltage of arm's resistance and inductance
p_{ik}	Sub-modules power of MMC

p_{ix}	The power of arm's resistance and inductance
$p_{3\varphi}$	Output Active power of MMC
$q_{3\varphi}$	Output Reactive power of MMC
I_{dc}	DC component of DC-link current
i_{dcrip}	Ripple parts of DC-link current
$\tilde{i}_{dcrip}$	Derivative of DC-link current ripple parts
I_m	Magnitude of output MMC Currents
V_m	Maximum Magnitude of output MMC Voltages
V_{mi}	Magnitude of the proposed modulation functions

Chapter 5

Parameters

L_k	Input inductance of MMC
R_k	Input resistance of MMC
L_{kul}	Arm's inductance of MMC
R_{kul}	Arm's resistance of MMC
L_{kt}	Equivalent arm's inductance of MMC
R_{kt}	Equivalent arm's resistance of MMC
ω	Angular frequency of MMC

Variables

i_k	Input MMC currents
I_{mk}	Magnitude of input MMC currents
i_{ku}	Upper arm currents
i_{kl}	Lower arm currents
I^*_{mk}	Reference values of input MMC currents
v_{ks}	Input MMC voltages

v_{kl}	AC-side voltages
v_m	Magnitude of input MMC voltages
v_m^*	Reference value of input MMC voltage
v_{ku}	Upper arm voltages
v_{kl}	Lower arm voltages
v_{DC}	MMC DC-link voltage
u_{ku}	Switching function for Upper's arms
u_{kl}	Switching function for Lower's arms
m_k	Proposed modulation index
a_k	Angle between input MMC voltages and currents
α_k^*	Reference value of α_k
V_{kt}	Magnitude of upper and lower voltage difference
θ_{kt}	Angle of upper and lower voltage difference

Chapter 6

Indices

k	a,b,c
i	1,2

Parameters

L	MMC inductance
R	MMC resistance
L_{ul}	Upper and lower arm inductance
R_{ul}	Upper and lower arm resistance
L_t	Equivalent inductance of MMC arm
R_t	Equivalent resistance of MMC arm
C_{dc}	The equivalent capacitance of MMCs
R_{dc}	The total switching loss of MMCs
ω	Angular frequency of MMC voltage

$a_{(1\text{-}5)i}$	Coefficients of DLM controller

Variables

i_{ki}	MMC currents
i_{ulki}	Upper and Lower arm currents
i_{cirki}	Circulating currents of MMCs
i_{dci}	DC link currents of MMCs
i_{dqi}	MMC currents in dq frame
$i_{cirdq0i}$	Circulating currents in dq0
i^*_{dqi}	Reference currents of MMC
$i^*_{cirdq0i}$	Reference circulating current
i^*_{dci}	Reference DC link current
$\Delta\, i_{dqi}$	MMC currents variations
$\Delta\, i_{dci}$	DC link currents variations
I_{avdqi}	Average values of MMC currents
v_{ki}	Output voltages of MMC
v_{ulki}	Upper and Lower arm voltages of MMC
$v_{dc,}$	DC link voltage
v_{dqi}	MMC output voltages in dq frame
v^*_{dqi}	Reference MMC output voltages
v^*_{dc}	Reference DC link voltage
v_{tdqi}	Terminal voltages of MMC
Δv_{dc}	DC link voltage variation
Δv_{dci}	MMC effects on DC link voltage
P_i	MMC active power
ΔP_i	MMC active power variation
Q_j	MMC reactive power
ΔQ_j	MMC reactive power variation
$u_{k(1,2)i}$	MMC switching functions
$u^*_{dq0(12)i}$	Reference MMC switching functions
$u_{dq0(1,2)i}$	MMC switching function in dq frame

$\Delta u_{dq0(1,2)i}$	Dynamic of MMC switching function
$(-\psi, -x)$	The center of i_{di}-i_{qi} curve
r	The radius of i_{di}-i_{qi} curve
$(-\psi', -x')$	The center of P_i-Q_j curve
r'	The radius of P_i-Q_j curve

Relevant Acronyms

AC	Alternating Current
ASD	Adjustable-Speed Drive
AVM	Average-Value Model
CB-PWM	Carrier-Based Pulse With Modulation
CC	Capability Curve
CCSC	Circulating Current Suppression Control
CHB	Cascaded H-bridge Converters
CLC	Central Loop Controller
CM	Common-Mode
CPS-PWM	Carrier-Phase-Shift Pulse-Width-Modulation
DERs	Distributed Energy Resources
DFT	Differential Flatness Theory
DLM	Direct Lyapunov Method
FACTS	Flexible Alternating Current Transmission Systems
HVDC	High-Voltage, Direct Current
ILC	Inner Loop Controller
KCL	Kirchhoff's Current Law
KVL	Kirchhoff's Voltage Law
LPF	Low Pass Filter
MIMO	Multi-Input Multi-Output
MMC	Modular Multilevel Converter
MMCC	Modular Multilevel Cascade Converter
MPC	Model Predictive Control
MSHE	Multilevel Selective Harmonic Elimination
MSHE-PWM	Multilevel Selective Harmonic Elimination Pulse-Width Modulation
NLC	Nearest Level Control
NLM	Nearest Level Modulation
OLC	Outer Loop Controller
PCC	Point of Common Coupling
PD	Phase-Disposition
PI	Proportional-Integral
PSC	Phase-Shifted Carrier
PWM	Pulse-Width-Modulation
RESs	Renewable Energy Resources
SLPWM	Shifted Level Pulse Width Modulation

SM	Sub-Modules
SMC	Sliding Mode Control
SMO	Sliding Mode Observer
SS	Switching Signals
STATCOM	Static Synchronous Compensator
SUPWM	SM unified PWM
SV	Singular Value
THD	Total Harmonic Distortion
VSC	Voltage-Source Converter
ZSS	Zero Sequence Signals

Chapter 1

Introduction

1.1 Background

HVDC (high-voltage direct current) is a highly efficient alternative for transmitting the electricity generated through the large scale of renewable energy resources (RESs) included off/on-shore wind farms over long distances and for special purpose applications. For this reason, HVDC transmission systems have been becoming more and more important in an energy landscape that is featured by enhancing the controllers for the used distributed generations. In fact, HVDC systems are able to help three-phase grids get more stabilized and also connected to green power. The future grid can hopefully rely on such systems because of their aforementioned key roles.

Due to the stated issues, HVDC systems have been widely investigated in recent years. To pursue more recent literatures, both control and protection of multi-terminal HVDC systems have been an important research topic that is accomplished in [1]. Optimized algorithms-based methods have also been considered for reaching more stability for HVDC systems [2], [3]. Another important theme related to HVDC systems is the harmonic elimination that has been discussed in [4], [5]. Moreover, unbalanced grid conditions have been realized at solving this challenge for HVDC system [6]. As a good selection for HVDC systems, among the power converters used for HVDC applications, modular multilevel converters (MMCs) have been recently chosen as the main core of HVDC structures because of their characteristics, such as high reliability capability, modular structure, high efficiency, seamlessly DC link, effective redundancy, and excellent output with eliminated harmonic components and minimum passive filter.

Reference [7] has presented several reduced-order small-signal models for MMC in HVDC applications to investigate the criteria including singular values (SVs) of the frequency response, dynamic response in the time domain, and the largest absolute error of SVs. Some MMC energy-based control strategies have been analyzed in [8], VSC-HVDC Links. The expansion of renewable energy resources and their various structures have been involved with MMCs. The subjects pertaining to RERs such as high penetration problems [9], [10], integration of small-scale renewable energy sources into power grid [11], the harmonic current and reactive power compensation [12], microgrid systems [13], etc., will show the importance of an accurate analysis of MMCs for RERs-based applications.

For instance, a Static Synchronous Compensator (STATCOM) has been designed for offshore wind farm applications based on a modular multilevel cascade converter (MMCC) in which its asymmetrical reactive power capability has been accurately analyzed as well [14]. Various modulation strategies applied to MMCs have been investigated in [15] for renewable energy integration. The carrier-based pulse with modulation (CB-PWM) techniques, the CB-PWM methods adapted with an additional cell ranking and selection algorithm, the state-of-the-art of zero sequence signals (ZSS) applied on three-phase inverters, the alliance between the ZSS with the CB-PWM, as well as the nearest level modulation (NLM) have been discussed in [15]. As another use of MMCs for RERs [16], the conception of MMCs for high-scale photovoltaic generation based on efficiency criteria has been studied in [17].

1.2 Research Motivation and Problem Definition

The necessity of choosing a suitable converter for high power generation and transmission, especially HVDC systems, has led to proposing a modular converter in [18]. For the full investigation and stable operation of the converter that has been named MMC, many dynamic models have been considered to be proposed [19]. Thus, in the first step, the best mathematical-based description for MMC should be defined from the viewpoint of differential equations.

A phasor format-based model in the rotating d-q coordinate frame has been proposed in [20] for MMC that the modelled for power-flow and parameter studies. The coordinate frame has been shaped at double the fundamental frequency, in steady state. Also, a substantial analytical basis is presented to facilitate direct mathematical manipulations of nonlinear terms in the rotating frame [20].

The reference [21] has designed a continuous model to accurately simulate the blocked state that is very important for accurate simulation of faults. This model is very useful in high-voltage DC applications [21].

Three dynamic linear state-space models of the modular multilevel converter (MMC), which are suitable for small-signal dynamic studies and controller design, have been proposed in [22]. The three models consist of two, six and ten states, respectively. The 2nd- and 6th-order models ignore the dynamics of the second harmonics and circulating current suppression control (CCSC). As the main challenges of dynamic analytical modelling of MMC, the multiplication nonlinear terms are directly converted to the rotating d-q frame.

An average-value model (AVM) of the MMCs considering the sub-module capacitor voltage ripple is proposed in [23] to investigate the control dynamic performance of MMCs. In addition, the sub-module capacitors voltage ripple on the MMC dynamic behavior is explored. Also, the equivalent impedances of the DC and AC sides of the MMC are accurately evaluated [23]. Moreover, using the achieved equivalent impedances, a particular AVM of MMCs, consisting of the equivalent capacitors reflecting the capacitor voltage ripple, has been proposed in [23].

Accurate investigation of the aforementioned dynamic models shows that some of them lack circulating current parts with the aim of suppressing this current. also, other dynamic models have not considered step-by-step analysis of all state variables of MMC. Considering both mentioned features is crucial for presenting an appropriate controller for MMC.

Another important issue related to MMC is the nonlinearity features that should be considered for designing any controller for MMC. Many nonlinear control techniques included input-output feedback linearization [24], [25], direct Lyapunov method [26]–[28], sliding mode controller [29], passivity theory-based control technique [30], [31], etc.

A nonlinear robust multi-loop controller has been designed in [32] for two shunt MMC-based voltage source converters and one series capacitor, via control Lyapunov function to reach fast tracking performance, and robustness against system uncertainties and disturbances. By the use of Lyapunov theorem, stability of the closed-loop nonlinear system is proved as well. In addition, the proposed controller has been decentralized using adaptive observer to estimate the nonlocal system parameters [32].

Since MMCs are multi-input multi-output (MIMO) nonlinear systems, a feedback linearization-based current control strategy can be a suitable option for applying to an MMC system, which has been proposed in [33]. In the first step, the nonlinear state function model of the MMC has been driven and then transformed to a linearized and decoupled form with the help of the input-output feedback linearization technique [33]. Based on the linearized system, simple linear controllers are employed to regulate the output and inner differential currents of the MMC.

Reference [34] has proposed a fault detection method based on a sliding mode observer (SMO) and a switching model of a half-bridge for modular multilevel converters which is capable of locating a faulty semiconductor switching device in the circuit. This method can appropriately address the whole stable operations of MMC.

A sliding mode control (SMC) based method has been proposed for the MMC in [35]. The analyses accomplished for the system dynamics under the proposed control method, relations among control parameters and their validity conditions can be driven providing a guidance for systematic controller design [35]. The proposed SMC-based method provides comparable steady state performance and fast dynamic responses, without compromising the computational effort or requirement for a precise system model.

As it can be understood from the mentioned literatures with the role of designing nonlinear controllers, considering both load and parameters variations in the duties frame of their proposed control technique were not carefully discussed. Thus, it is necessary to design a comprehensive nonlinear control technique for simultaneously reaching the aforementioned aims in which a complete dynamic model is also used.

1.3 Research Questions, Objectives and Contributions of the Thesis

This thesis presents two new mathematical models including the flat outputs-based dynamic model with active and reactive power state variables, as well as a comprehensive six-order dynamic model by considering all effects of d-q components of circulating currents. Also, to describe the best performance of MMC, two comprehensive analyses regarding all MMC currents and voltages, as well as the ultimate reference switching functions, are executed in this thesis.

In addition, using comprehensive analyses, two novel control strategies have been proposed for MMC so that the controllers have the robustness feature against parameters and load variations. Except for the analysis-based control techniques, several nonlinear control strategies have been designed for MMC in HVDC applications to stabilize the behaviors of all considered state variables. It should be stated that the stable response for MMC is aimed to reach in both steady state and dynamic operating conditions in all accomplished researches.

In particular, the following research questions are addressed:

- How can various parts of the dynamic model of the MMC impact on providing an accurate power sharing of renewable energy resources-based HVDC in the presence of model uncertainties and errors?
- What are the results of using the proposed multi-loop control technique on the stable operation of MMCs in HVDC Transmission Systems, and how will each loop with its duties be appropriately led to stable outputs in various operating conditions?

- Which state variables should be more important in a detailed analysis of the MMC structure at reaching flexible modulation functions when the parameter alterations exist in the overall performance of the power system?
- How much considering detailed calculations of MMC PWM modulation functions can ease reaching the desired values for the modulation index and phase, and also what is the effect of the system parameters considered by proposing the modulation index and phase?
- Whether by considering the circulating currents components can cause that the ultimate designed controller shows positive results at controlling MMC in the HVDC system or not?
- What results can be achieved by accurately analyzing the proposed detailed curve based on the active and reactive power generated through MMC and which factors can be used to show other aspects of the proposed curve?

The main objectives of this thesis are as follows:

- To investigate on existing mathematical dynamic models of renewable energy resources-based MMC in various applications and inquire the nonlinearity features of MMC along with their proportional nonlinear control techniques;
- To present a different statement for the dynamic model of MMC based on the defined flat outputs enhanced with robustness ability against both load and parameters variations;
- To develop an appropriate control method by considering sliding mode surface for approaching the state variables errors of MMC to zero for the steady state and dynamic operation of a renewable energy resources-based HVDC transmission while parameters changes are taken into account;
- To present a detailed step-by-step analysis of MMC for achieving the appropriate switching functions that are able to provide the control aims with very high accuracy;
- To extract the detailed specifications of various parts of MMC switching functions ignored by existing related works that can enhance the stability of both sides of the HVDC transmission system;
- To develop the existing dynamic models by considering the circulating currents effects in both steady and dynamic states operations;
- To provide a global asymptotical stability for renewable energy resources-based HVDC systems by considering total saved energy of the system in the presence of load changes in both AC sides;
- To present a new algorithm for both MMC currents and power that leads to a new capability curve employed for both steady state and dynamic analysis.

The contributions of this thesis (all already published in prestigious venues) are summarized as follows:

- A novel control strategy for MMC is designed based on differential flatness theory (DFT), in which instantaneous active and reactive power values are considered as the flat outputs. Using this model, the flat outputs-based dynamic model of MMC is obtained to reach the initial value of the proposed controller inputs. In order to mitigate the negative effects of input disturbance, model errors and system uncertainties on the operating performance of the MMC, the integral-proportional terms of the flat output errors are added to the initial inputs. This can be achieved through defining a control Lyapunov function which can ensure the stability of the MMC under various operating points. This contribution is published in **"IEEE Journal of Emerging and Selected Topics in Power Electronics"** [36];
- A multi-loop control strategy based on a six-order dynamic model of the modular multilevel converter (MMC) is presented for the high-voltage direct current (HVDC) applications. For the initial analysis of the operation of MMC, a capability curve based on active and reactive power of the MMC is achieved through a part of the six order dynamic equations. According to the MMC's control aims, the first loop known as the outer loop is designed based on passivity control theory to force the MMC state variables to follow their reference values. As the second loop with the use of sliding mode control, the central loop should provide appropriate performance for the MMC under variations of the MMC's parameters. Another main part of the proposed controller is defined for the third inner loop to accomplish the accurate generation of reference values. By implementing an accurate coordination between the designed control loops, stable responses for all involved state variables are achieved. This contribution has been published in **"International Journal of Electrical Power & Energy Systems" (ELSEVIER)** [37].
- A new function-based modulation control technique for modular multilevel converters (MMC) is proposed. The main contributions of the proposed controller are: 1) two separate modulation functions to attain the switching signals of upper and lower sub-modules; 2) the simplicity of the designed controller, especially in comparison with the existing methods; and 3) maintaining stable operation during parameters varying condition due to its structure. Moreover, the effects of the MMC parameters and currents changes are considered as the assessment factors of the proposed modulation functions performance in both steady-state and dynamic conditions. In addition, using the proposed functions, the instantaneous powers of the MMC arms and the equivalent capacitors of the upper and lower sub-modules are evaluated. This contribution is published in **"IET Generation, Transmission and Distribution"** [38].

- A novel modulation function-based method including analyses of the modulation index and phase is proposed for operation of modular multilevel converters (MMCs) in high voltage direct current (HVDC) transmission systems. The proposed modulation function-based control technique is developed based on thorough and precise analyses of all MMC voltages and currents in the a-b-c reference frame in which the alternating current (AC)-side voltage is the first target to be obtained. Using the AC-side voltage, the combination of the MMC upper and lower arm voltages is achieved as the main structure of the proposed modulation function. The main contribution of the proposed work is to obtain two very simple new modulation functions to control MMC performance in different operating conditions. The features of the modulation function-based control technique are as follows: (1) this control technique is very simple and can be easily achieved in a-b-c reference frame without the need of using Park transformation; and (2) in addition, the inherent properties of the MMC model are considered in the proposed control technique. Considering these properties leads to constructing a control technique that is robust against MMC parameters changes and also is a very good tracking method for the components of MMC input currents. These features lead to improving the operation of MMC significantly, which can act as a rectifier in the HVDC structure. This contribution published in **"Energies"** [39].
- A dynamic model, control and stability analysis of MMC-HVDC transmission systems is presented. The main contributions are fourfold: (1) obtaining a comprehensive dynamic model in d-q frame for MMC-based HVDC system with six independent dynamical state variables, including two AC currents, three circulating currents, and the DC-link voltage, (2) developing the dynamic parts of switching functions by the use of DLM to reach globally asymptotical stability, (3) deriving a detailed capability curve (CC) based on active and reactive power of the MMC for the proposed system, investigating the impacts of various values of the DC-link currents on CC; it can be used to verify the maximum capacity of interfaced MMC for the injection of active and reactive power into the power grid, (4) performing a comprehensive investigation of MMC output and DC-link current variations effects on DC-link voltage stability by using small-signal analysis. This contribution published in **"IEEE Transactions on Power Delivery"** [40].

1.4 Methodology

The mathematical models developed in this thesis are based on the MMC state variables included output voltages, output currents, circulating currents, input voltages, input currents, DC link voltage, active power and reactive power. In order to achieve the main research objectives, beyond the simulation models, this thesis develops the existence of dynamic models by considering circulating currents components and detailed step-by-step analysis of MMC state variables to reach stable responses for the HVDC power system under uncertainty, and a dramatically changing power generation scheme over time.

On the other hand, because of the nonlinearity characteristics of MMC dynamics, the proposed nonlinear control techniques include Flatness theory, direct Lyapunov method, passivity theory-based method, and sliding mode controller, all implemented in MATLAB© SIMULINK environment to considered MMCs in various structures.

1.5 Notation

The present thesis uses the notation commonly used in the scientific literature, harmonizing the common aspects in all sections, wherever possible. However, whenever necessary, in each section, a suitable notation may be used. The mathematical formulas will be identified with reference to the subsection in which they appear and not in a sequential manner throughout the thesis, restarting them whenever a new section or subsection is created. Moreover, figures and tables will be identified with reference to the section in which they are inserted and not in a sequential manner throughout the thesis.

Mathematical formulas are identified by parentheses (x.x.x) and called “Equation (x.x.x)” and references are identified by square brackets [xx]. The acronyms used in this thesis are structured under synthesis of names and technical information coming from both the Portuguese or English languages, as accepted in the technical and scientific community.

1.6 Organization of the Thesis

This thesis encompasses seven chapters that are organized as follows:

Chapter 1 presents a background of the work in the first step. Then, the research motivations and the problem definition are discussed. Subsequently, the next part of this chapter focuses on the research questions and contributions of this thesis. Also, the used methodologies of the thesis are given. In addition, the adopted notations are discussed in the next part. Finally, the chapter concludes by outlining the structure of the thesis.

Chapter 2 concentrates on a novel control strategy based on differential flatness theory (DFT) for MMC. Introduction is the first section of this chapter. Then, the second section consists of two sub-sections of dynamic analysis of the proposed MMC-based model as well as the proposed DFT-based control technique. The stability analysis of this chapter is provided by investigating the effects of the control inputs perturbations as the next section. Simulation results and the highlighted points of the chapter are provided afterwards.

Chapter 3 presents a multi-loop control technique for the stable operation of MMCs in HVDC transmission systems. Except for the introduction which is the first section of this chapter, the next section discusses about the proposed differential equation of MMC. This section contains two subsections including the proposed six order dynamic model of MMCs and capability curve analysis of MMCs active and reactive power. Three loops of the proposed control technique are discussed in the control section that encompasses the issues of the design of the outer loop controller (OLC), the design of the central loop controller (CLC) and the design of the inner loop controller (ILC). Convergence evaluation and stability analysis are regarded as the evaluation section of this chapter. The load compensation capability analysis of MMC and dynamic model analysis of the DC-link voltage are discussed in the evaluation section in detail. Finally, simulation results in MATLAB/Simulink environment are presented.

Chapter 4 presents a function-based modulation control for MMCs under varying loading and parameters conditions. Introduction and the proposed modulation functions discussion are the first sections of the chapter. Second section investigates the calculation of the MMC' arms currents, and the proposed modulation function. Then, the evaluation of the instantaneous power of the MMC arms are executed by calculation of the MMC' arms currents and instantaneous power of the arm's resistance and inductance. Next section focuses on the determination of $\boldsymbol{I_m}$ and $\boldsymbol{\alpha}$. Accurate sizing of the equivalent sub-module capacitors is also provided in the next section. Simulation results and highlighted points of this chapter are the last sections, respectively.

Chapter 5 proposes a novel modulation function-based control of MMCs for HVDC transmission systems. Introduction is written in the first section. Then, the detailed calculation of the alternating current-side voltage is accomplished in the next section. The analysis section includes parameters and input current variations effects on the proposed modulation function are accurately discussed. Simulation results are discussed as well.

Chapter 6 discusses about dynamic Model, control and stability analysis of MMC in HVDC transmission systems. After introduction, the model of MMC-based HVDC system is proposed. Steady state and dynamic stability analysis are presented in two other sections, respectively. In the next section, capability curve analysis of the MMCs is presented. DC-link voltage stability analysis is placed in the next section. Simulation results and highlighted points of this chapter are given in the next sections.

Chapter 7 presents the main conclusions of this work. Guidelines for future works in this field of research are provided. Moreover, this chapter reports the scientific contributions that resulted from this research work and that have been published in journals, book chapters or in conference proceedings of high standard (IEEE).

Chapter 2

Novel Control Strategy for Modular Multilevel Converters Based on Differential Flatness Theory

This chapter aims to present a novel control strategy for Modular Multilevel Converters (MMC) based on differential flatness theory (DFT), in which instantaneous active and reactive power values are considered as the flat outputs. To this purpose, a mathematical model of the MMC taking into account dynamics of the AC-side current and the DC-side voltage of the converter is derived in a d-q reference frame. Using this model, the flat outputs-based dynamic model of MMC is obtained to reach the initial value of the proposed controller inputs. In order to mitigate the negative effects of the input disturbance, model errors and system uncertainties on the operating performance of the MMC, the integral-proportional terms of the flat output errors are added to the initial inputs. This can be achieved through defining a control Lyapunov function that can ensure the stability of the MMC under various operating points. Moreover, the small-signal linearization method is applied to the proposed flat output-based model to separately evaluate the variation effects of controller inputs on flat outputs. The proficiency of the proposed method is researched via MATLAB simulation. Simulation results highlight the capability of the proposed controller in both steady-state and transient conditions in maintaining MMC currents and voltages, through managing active and reactive power.

2.1 Introduction

Considering the issues concerning to the renewable energy resources [41], [42], investigating high-power and Medium-voltage converters has been attracted attention more and more. High-power and Medium-voltage power electronics-based converters have been continuously employed in high-technology industries, traction systems and regenerative energy sources, since they offer effective power structures, flexible designed controllers, various dynamic models, and effective pulse-width-modulation (PWM) techniques [43]–[46]. These features can lead to low harmonic components, fast responses against dynamic changes, improved power factors as well as power quality in grid-connected systems, not to mention a ride-through capability and/or a redundant converter design in various operating conditions [47]–[49]. Among existing power electronic-based converters, modular multilevel converters (MMCs) have been gaining popularity due to their full modularity and easy extend ability to meet different voltage and power level requirements in various applications i.e., photovoltaic systems, large wind turbines, AC motor drives, HVDC systems, DC-DC transformers, battery electric vehicles, distributed energy resources (DERs), and flexible alternating current transmission systems (FACTS) [50]–[55].

However, the MMCs commonly demand complex control configurations in compression with other converter topologies. Therefore, designing an appropriate control technique for the control and operation of the MMC in power systems is essential. To this end, several studies in the literature have addressed the control concept of the MMCs in power systems which will be briefly presented as follows [56]–[66]. A nearest level control (NLC) along with an optimized control strategy is proposed to govern the MMC operation in [56], which is based on the dynamic redundancy and the utilization ratio of the sub-modules.

A model predictive direct current control is provided for the MMC in [57]. The proposed control technique can maintain the load current within strict bounds around sinusoidal references and minimize capacitor voltage changes and circulating currents. In recent years, dynamic models for MMCs have been the topics of several work [58]–[60]. In [60], a new switching-cycle state-space model is designed for a MMC in which a respective switching-cycle control approach is also proposed by considering the unused switching states of the converter. Through using the average voltage of all the sub-modules (SMs) in each control cycle, a fast voltage-balancing control along with a numerical simulation model are proposed for the MMC in [61]. The sinusoidal common-mode (CM) voltage and circulating currents are employed for designing various control techniques in MMCs. In fact, in order to attenuate the low-frequency components of the SM capacitor voltage, the sinusoidal common-mode voltage and circulating current are used to design a control strategy for the MMC in [62]. In [63], optimized sinusoidal CM voltage and circulating current are used to limit the SM capacitor voltage ripple and the peak value of the arm current. Also, for adjustable-speed drive (ASD) application under constant torque low-speed operation, two control techniques based on injecting a square-wave CM voltage on the AC-side and a circulating current are proposed to reduce the magnitude of the SM capacitor voltage ripple [64]. Furthermore, a control strategy based on a sinusoidal CM voltage and circulating current is proposed for an MMC-based ASD over the complete operating speed region [65]. In addition, the peak value of the sinusoidal common mode voltage can be a key solution for analyzing the SM capacitor voltage ripple [66].

In this chapter, a novel control strategy based on differential flatness theory (DFT), inspired by that was used for the control of converters in [36], [67]–[70], is presented to control the operation of MMC in power systems. The flat outputs required for the DFT based control technique are the instantaneous active and reactive power of the MMC. The initial values of the proposed controller inputs can be driven by a new dynamic equation of the MMC, achieved as per the flat outputs. Then, a control Lyapunov function based on the respective integral-proportional errors of flat output is utilized to provide a stable operation against input disturbance, model errors, and system uncertainties.

Also, in order to evaluate the variation effects of controller inputs on flat outputs, the relevant transfer functions are obtained through the small signal model of the flat outputs-based dynamic equations. In comparison with other existing control techniques for MMC, the proposed controller exhibits several considerable advantages in terms of the stability issues for robustness enhancement, highly improvements of MMC power sharing ability, less overshoot and undershoot for SM voltages and transient through considering simultaneously all the input disturbance, model errors, and system uncertainties and applying directly the MMC active and reactive power as the state variables. The simulation analysis using Matlab/Simulink clearly demonstrates the effectiveness of the DFT-based control strategy in the proposed MMC-based model under different operating modes.

2.2 Proposed Control Technique

Figure 2.1 depicts a circuit diagram of the proposed MMC-based model. The MMC consists of six sub-modules in series in each upper and lower arm. Each sub-module can be modeled as a half-bridge IGBT-diode switch-based rectifier. Two resistance-inductance loads are connected to the PCC in which the second load enters in operating mode by means of the switch at a determined time. Also, a capacitor filter is considered at the PCC of the MMC to improve output AC voltages. Since the dynamic equations of the proposed model are considered in the design of the proposed control strategy; thus, these basic equations as well as a new dynamic model based on the outputs of DFT are extracted in this section.

2.2.1 Dynamic Analysis of the Proposed MMC-based Model

As can be seen in Figure 2.1, the series connection of sub-modules in both upper and lower arms of the MMC are represented by the controllable voltage sources of v_{uk} and v_{lk} respectively.

These voltages play a key role in controlling the MMC in different operating conditions. As per Figure 2.1, the relationships between arm's currents and AC voltages of the MMC, taking into account the DC-link voltage and controllable voltage sources, can be expressed as,

$$v_k + L\frac{di_k}{dt} + Ri_k + L_t\frac{di_{uk}}{dt} + R_t i_{uk} - \frac{v_{dc}}{2} + v_{uk} = 0 \tag{2.1}$$

$$v_k + L\frac{di_k}{dt} + Ri_k + L_t\frac{di_{lk}}{dt} + R_t i_{lk} + \frac{v_{dc}}{2} - v_{lk} = 0 \tag{2.2}$$

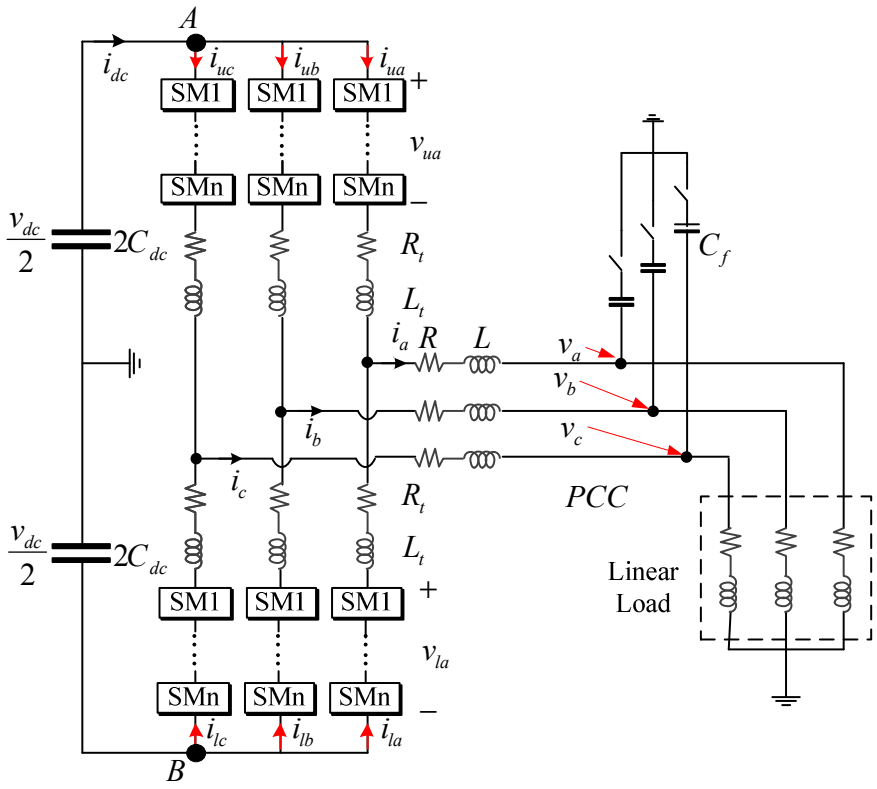

Figure.2.1. - The circuit diagram of the considered MMC-based model.

By summing (2.1) and (2.2), the basic dynamic model of the proposed MMC-based model can be obtained as,

$$\left(\frac{2L+L_t}{2}\right)\frac{di_k}{dt}+\left(\frac{2R+R_t}{2}\right)i_k+u_k+v_k=0 \tag{2.3}$$

where $i_{uk}+i_{lk}=i_k$. The control factor of u_k is equal to $u_k=(v_{uk}-v_{lk})/2$ which reflects the effect of both controllable voltage sources. In addition, the DC-link voltage term is eliminated in (2.3). By applying KCL's law in the determined points of A and B in Figure 2.1, the relationships between the MMC's arm currents and the DC-link voltage are stated respectively as,

$$C_{dc}\frac{dv_{dc}}{dt}=-\left(i_{ua}+i_{ub}+i_{uc}\right) \tag{2.4}$$

$$C_{dc}\frac{dv_{dc}}{dt}=\left(i_{la}+i_{lb}+i_{lc}\right) \tag{2.5}$$

Considering circulating currents as $i_{cirk}=(i_{uk}-i_{lk})/2-i_{dc}/3$ and summing up equations (2.4) and (2.5), the dynamic equation of DC-link voltage can be obtained as,

$$C_{dc}\frac{dv_{dc}}{dt}+i_{cira}+i_{cirb}+i_{circ}+i_{dc}=0 \tag{2.6}$$

Thus, the dynamics of the proposed MMC in the abc reference frame can be obtained as (2.7),

$$\begin{bmatrix}\left(\frac{2L+L_t}{2}\right)\frac{di_a}{dt}\\ \left(\frac{2L+L_t}{2}\right)\frac{di_b}{dt}\\ \left(\frac{2L+L_t}{2}\right)\frac{di_c}{dt}\\ C_{dc}\frac{dv_{dc}}{dt}\end{bmatrix}=\begin{bmatrix}-\left(\frac{2R+R_t}{2}\right) & 0 & 0 & 0 & 0 & 0\\ 0 & -\left(\frac{2R+R_t}{2}\right) & 0 & 0 & 0 & 0\\ 0 & 0 & -\left(\frac{2R+R_t}{2}\right) & 0 & 0 & 0\\ 0 & 0 & 0 & -1 & -1 & -1\end{bmatrix}\begin{bmatrix}i_a\\ i_b\\ i_c\\ i_{cira}\\ i_{cirb}\\ i_{circ}\end{bmatrix}-\begin{bmatrix}u_a\\ u_b\\ u_c\\ 0\end{bmatrix}-\begin{bmatrix}v_a\\ v_b\\ v_c\\ i_{dc}\end{bmatrix} \tag{2.7}$$

The park transformation matrix is considered as,

$$\begin{bmatrix}m_d\\ m_q\\ m_0\end{bmatrix}=\frac{2}{3}\begin{bmatrix}\cos(\omega t) & \cos(\omega t-2\pi/3) & \cos(\omega t+2\pi/3)\\ -\sin(\omega t) & -\sin(\omega t-2\pi/3) & -\sin(\omega t+2\pi/3)\\ 1/2 & 1/2 & 1/2\end{bmatrix}\begin{bmatrix}m_a\\ m_b\\ m_c\end{bmatrix} \tag{2.8}$$

In (2.8), the variables of 'm' represent all state variables of the proposed MMC. By applying the Park transformation matrix of (2.8) to (2.7), the basic dynamic model of the proposed MMC-based model in d-q frame is driven as,

$$\left(\frac{2L+L_t}{2}\right)\frac{di_d}{dt}+\left(\frac{2R+R_t}{2}\right)i_d-\omega\left(\frac{2L+L_t}{2}\right)i_q+u_d+v_d=0 \tag{2.9}$$

$$\left(\frac{2L+L_t}{2}\right)\frac{di_q}{dt}+\left(\frac{2R+R_t}{2}\right)i_q+\omega\left(\frac{2L+L_t}{2}\right)i_d+u_q+v_q=0 \tag{2.10}$$

$$C_{dc}\frac{dv_{dc}}{dt}+\sqrt{3}i_{cir0}+i_{dc}=0 \tag{2.11}$$

Equations (2.9)-(2.11) present a basic dynamic model of the MMC-based model. These equations are used to propose the new dynamic model utilized to project the DFT-based control technique and to evaluate the variation effects of controller inputs on flat outputs.

2.2.2 The Proposed DFT-Based Control Technique

The DFT as an effective nonlinear approach is used to design an appropriate controller to represent the nonlinear properties of the proposed MMC-based model [67]–[70]. Flatness properties were firstly introduced by Fliess et al. [70]. A nonlinear system can be called as a flat one if all state variables, control inputs and a finite number of the control inputs time derivatives of the nonlinear system can be stated based on the system outputs without any integration [67]. For this flat system, the outputs are considered as the flat outputs. In the next consequence, the output variables of the flat system should be achieved as functions of the state variables, the input variables, and a finite number of their time derivatives. The mathematical description of a flat system can be explained as follows. Considering the general form of the system as (2.12),

$$\begin{aligned} \dot{x} &= f\left(x,u\right) \\ y &= h\left(x,u\right) \end{aligned} \tag{2.12}$$

Based on the flat definition, (2.13) should be governed as,

$$y = g\left(x,u,\dot{u},\ddot{u},\ldots,u^{(\lambda)}\right) \tag{2.13}$$

Also, another property of a flat system can be written as,

$$x = \psi\left(y,\dot{y},\ddot{y},\ldots,y^{(\chi)}\right) \tag{2.14}$$

$$y = \phi\left(y, \dot{y}, \ddot{y}, ..., y^{(\kappa)}\right) \tag{2.15}$$

Based on these aforementioned descriptions, defining appropriate flat outputs, control inputs and state variables of the proposed model as the basic requirements of the DFT is firstly considered as follows. According to the basic dynamic model of the MMC, the DFT variables are given as,

$$\begin{aligned} y &= \begin{bmatrix} y_1 & y_2 \end{bmatrix} = \begin{bmatrix} P & Q \end{bmatrix} \\ u &= \begin{bmatrix} u_1 & u_2 \end{bmatrix} = \begin{bmatrix} u_d & u_q \end{bmatrix} \\ x &= \begin{bmatrix} x_1 & x_2 & x_3 \end{bmatrix} = \begin{bmatrix} i_d & i_q & v_{dc} \end{bmatrix} \end{aligned} \tag{2.16}$$

Based on (2.16), the instantaneous active and reactive power of MMC defined as $P=v_d i_d+v_q i_q$ and $Q=v_q i_d-v_d i_q$ (with $v_q=0$), is determined as flat outputs. The relations between flat outputs and MMC state variables can be expressed as,

$$x_1 = \psi\left(y_1\right) = \frac{y_1}{v_d}, x_2 = \psi\left(y_2\right) = \frac{y_2}{-v_d} \tag{2.17}$$

According to DFT properties, the proposed MMC-based model is flat, if a set of state variables, so-called flat outputs, from its dynamic model can be found. Therefore, the differential part of the flat output can be expressed by determined state variables and control inputs without any integration. Thus, through equations (2.9), (2.10), and (2.17), the dynamic representation of specified flat outputs in the proposed control technique can be achieved as,

$$\frac{dy_1}{dt} = \dot{v}_d x_1 - \left(\frac{2R+R_t}{2L+L_t}\right) v_d x_1 + \omega v_d x_2 - \left(\frac{2}{2L+L_t}\right) v_d u_1 - \left(\frac{2}{2L+L_t}\right) v_d^2 \tag{2.18}$$

$$\frac{dy_2}{dt} = \frac{\dot{v}_d y_2}{v_d} - \left(\frac{2R+R_t}{2L+L_t}\right) y_2 + \omega y_1 + \left(\frac{2}{2L+L_t}\right) v_d u_2 - \left(\frac{2}{2L+L_t}\right) v_d^2 \tag{2.19}$$

Equations (2.17), (2.18) and (2.19) are used to attain the initial values of the control technique inputs as,

$$u_1 = \left(\frac{2L+L_t}{2}\right)\frac{\dot{v}_d y_1}{v_d^2} - \left(\frac{2R+R_t}{2}\right)\frac{y_1}{v_d} - \left(\frac{2L+L_t}{2}\right)\frac{\omega y_2}{v_d} - v_d - \left(\frac{2L+L_t}{2v_d}\right)\dot{y}_1 \tag{2.20}$$

$$u_2 = \left(\frac{2L+L_t}{2v_d}\right)\dot{y}_2 - \left(\frac{2L+L_t}{2}\right)\frac{\dot{v}_d y_2}{v_d^2} + \left(\frac{2R+R_t}{2}\right)\frac{y_2}{v_d} - \left(\frac{2L+L_t}{2}\right)\frac{\omega y_1}{v_d} \tag{2.21}$$

In order to obtain a robust control system against the input disturbance, model errors, and system uncertainties, proportional-integral errors of the flat outputs are defined as,

$$e_{i1} = y_i^* - y_i, e_{i2} = \int_0^t \left(y_i^*(h) - y_i(h)\right)dh \tag{2.22}$$

The flat output errors are entirely considered through e_{i1} and e_{i2} that can lead to designing a proper controller for decreasing the various errors of MMC active and reactive power sharing. The effects of the flat output errors on the proposed control inputs can be specified by the stability evaluation of the following Lyapunov function as,

$$E\left(e_{11}, e_{12}, e_{21}, e_{22}\right) = \frac{1}{2}e_{11}^2 + \frac{1}{2}e_{12}^2 + \frac{1}{2}e_{21}^2 + \frac{1}{2}e_{22}^2 \tag{2.23}$$

The accurate operation of DFT with approaching the flat output errors to zero can be guaranteed by stability analysis of (2.23). The derivative of (2.23) is driven as,

$$\begin{aligned} \dot{E}\left(e_{11}, e_{12}, e_{21}, e_{22}\right) &= e_{11}\dot{e}_{11} + e_{12}\dot{e}_{12} + e_{21}\dot{e}_{21} + e_{22}\dot{e}_{22} \\ &= e_{11}\dot{e}_{11} + e_{12}e_{11} + e_{21}\dot{e}_{21} + e_{22}e_{21} \end{aligned} \tag{2.24}$$

Equations (2.22) and (2.24) can be rewritten based on (2.18) and (2.19), as follows,

$$\dot{E}\left(e_{11},e_{12},e_{21},e_{22}\right)=e_{11}\begin{pmatrix}\dot{y}_1^*-\dot{v}_d x_1+\left(\dfrac{2R+R_t}{2L+L_t}\right)y_1+\omega y_2\\+\left(\dfrac{2}{2L+L_t}\right)v_d u_1+\left(\dfrac{2}{2L+L_t}\right)v_d^2+e_{12}\end{pmatrix}$$
$$+e_{21}\begin{pmatrix}\dot{y}_2^*+\dot{v}_d x_2+\left(\dfrac{2R+R_t}{2L+L_t}\right)y_2-\\\omega y_1-\left(\dfrac{2}{2L+L_t}\right)v_d u_q+e_{22}\end{pmatrix} \tag{2.25}$$

By making flat outputs-based Lyapunov function globally asymptotically stable, (2.25) leads to the proposed control inputs as,

$$u_1=\frac{2L+L_t}{2v_d}\begin{pmatrix}-\dot{y}_1^*+\dot{v}_d x_1-\left(\dfrac{2R+R_t}{2L+L_t}\right)y_1-\omega y_2\\-\left(\dfrac{2}{2L+L_t}\right)v_d^2+e_{12}+\lambda_1 e_{11}\end{pmatrix} \tag{2.26}$$

$$u_2=\frac{2L+L_t}{2v_d}\begin{pmatrix}\dot{y}_2^*+\dot{v}_d x_2+\left(\dfrac{2R+R_t}{2L+L_t}\right)y_2-\omega y_1\\+e_{22}+\lambda_2 e_{21}\end{pmatrix} \tag{2.27}$$

The proposed control inputs of (2.26) and (2.27) lead to the global asymptotic stability of flat outputs errors-based Lyapunov function as,

$$\dot{E}\left(e_{11},e_{12},e_{21},e_{22}\right)=-\lambda_1 e_{11}^2-\lambda_2 e_{21}^2\le 0 \tag{2.28}$$

With λ_1 and λ_2>0, equation (2.28) verifies that the designed closed-loop control technique driven from (26) and (2.27) can provide a stable operation of the proposed MMC-based model. The block diagram of the proposed control technique is presented in Figure 2.2. The flat outputs errors and their integral are calculated from the measured instantaneous active and reactive power and the desired values of instantaneous power of the MMC as depicted in the block diagram. In order to reach global results for the proposed DFT based controller, $v_d=v_d^*$ for the term of $\dot{v}_d$ and consequently $\dot{v}_d=0$.

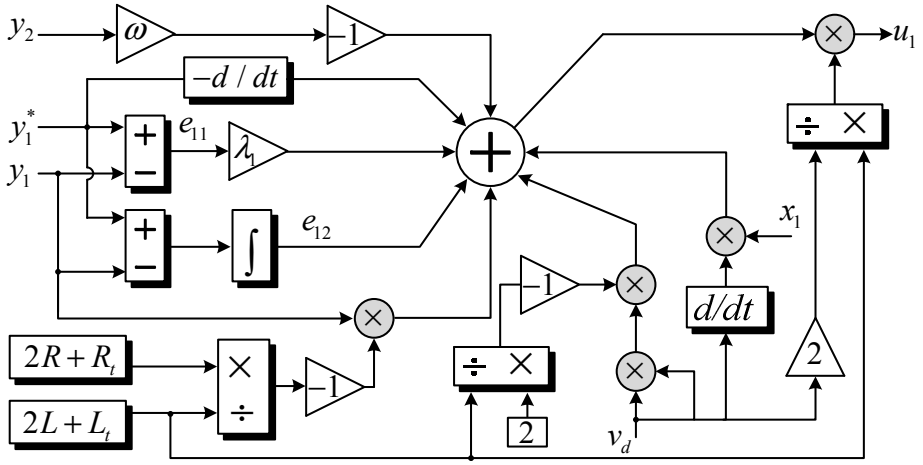

(a)

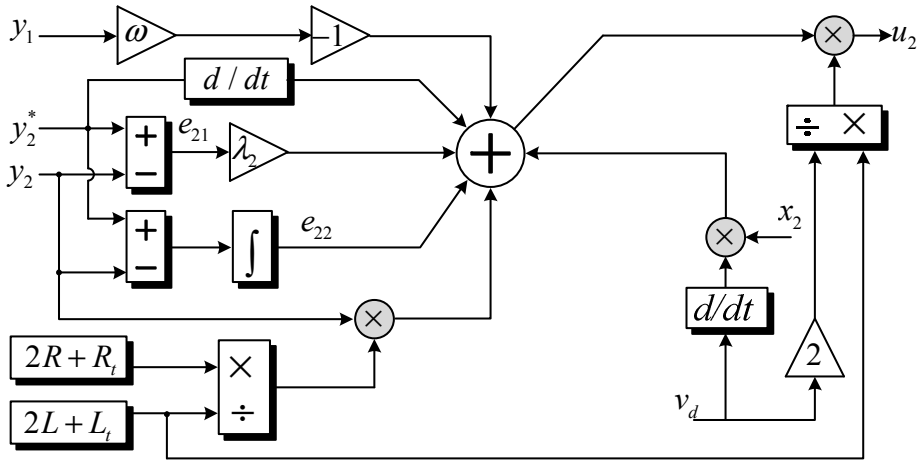

(b)

Figure 2.2 - The proposed control technique of DFT (a) the component of u_1 (b) the component of u_2.

2.3 Effects of the Control Inputs Perturbations

The MMC control inputs u_1 and u_2 aim to provide accurate tracking for the flat outputs. Thus, the MMC operation through presenting suitable active and reactive power sharing is highly dependent on the control inputs. The effects of control input variations on the flat outputs are investigated in this section. By applying (2.17) to (2.18) and (2.19) and using the small signal linearization technique, the relations between the perturbations of flat outputs and control inputs can be achieved as,

$$\Delta y_1 = F_{11}(s)\Delta u_1 + F_{12}(s)\Delta u_2 \tag{2.29}$$

$$\Delta y_2 = F_{21}(s)\Delta u_1 + F_{22}(s)\Delta u_2 \tag{2.30}$$

The transformation functions $\left(F_{ij}(S)\right)$ presented in (2.29) and (2.30) are defined as,

$$\begin{aligned}
F_{11}(s) &= \frac{-\left(s+\left(\frac{2R+R_t}{2L+L_t}\right)\right)\left(\frac{2}{2L+L_t}\right)v_d}{\Delta} \\
F_{12}(s) &= \frac{-\omega\left(\frac{2}{2L+L_t}\right)v_d}{\Delta}, \quad F_{21}(s) = \frac{\omega\left(\frac{2}{2L+L_t}\right)v_d}{\Delta} \\
F_{22}(s) &= \frac{-\left(s+\left(\frac{2R+R_t}{2L+L_t}\right)\right)\left(\frac{2}{2L+L_t}\right)v_d}{\Delta}
\end{aligned} \tag{2.31}$$

where the term of Δ in (2.31) is equal to,

$$\Delta = s^2 + 2\left(\left(\frac{2R+R_t}{2L+L_t}\right)\right)s + \left(\left(\frac{2R+R_t}{2L+L_t}\right)\right)^2 - \omega^2 \tag{2.32}$$

Each transformation function of $\left(F_{ij}(S)\right)$ is used to show the effect of the control inputs on their respective flat outputs. Furthermore, based on equations (29) and (30), each of flat outputs is affected by both control inputs. The Bode diagram is used to evaluate the impact of each control input on the flat outputs when the perturbation is being increased. The MMC parameters given in Table 2.1, are used in this section. The effects of the control inputs are separately considered as,

$$\begin{aligned}
\Delta y_{11} &= \Delta y_1\big|_{\Delta u_2=0} = F_{11}(s)\Delta u_1, \\
\Delta y_{12} &= \Delta y_1\big|_{\Delta u_1=0} = F_{12}(s)\Delta u_2 \\
\Delta y_{21} &= \Delta y_2\big|_{\Delta u_2=0} = F_{21}(s)\Delta u_1, \\
\Delta y_{22} &= \Delta y_2\big|_{\Delta u_1=0} = F_{22}(s)\Delta u_2
\end{aligned} \tag{2.33}$$

Figure 2.3 shows the Bode diagram of the proposed flat outputs with the perturbation variations of the first control input. As it can be seen from this figure, an increase in the perturbation of the first control input impacts on the second flat output is more considerable than that on the first flat output. It means that the perturbation of the first control input can lead to a significant deviation of the second flat output from its desired value during the MMC operation. The perturbation effect of the second control input is examined in Figure 2.4. As can be seen from the curves in Figure 2.4, in comparison with the second flat output, the first flat output is significantly affected by the perturbation variations of the second control input.

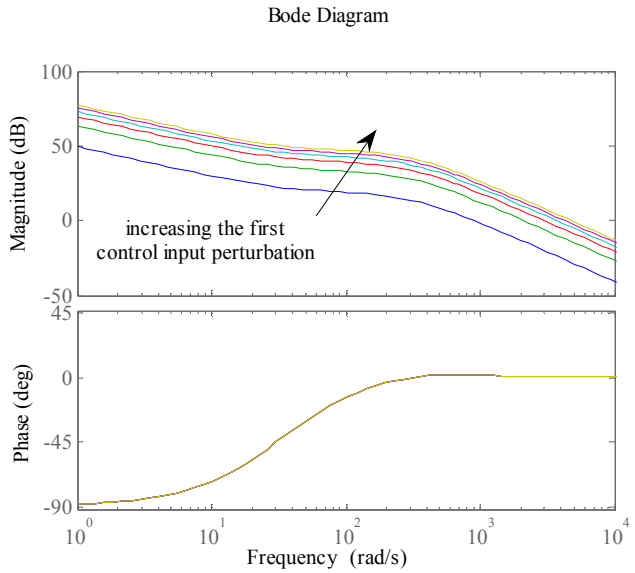

(a)

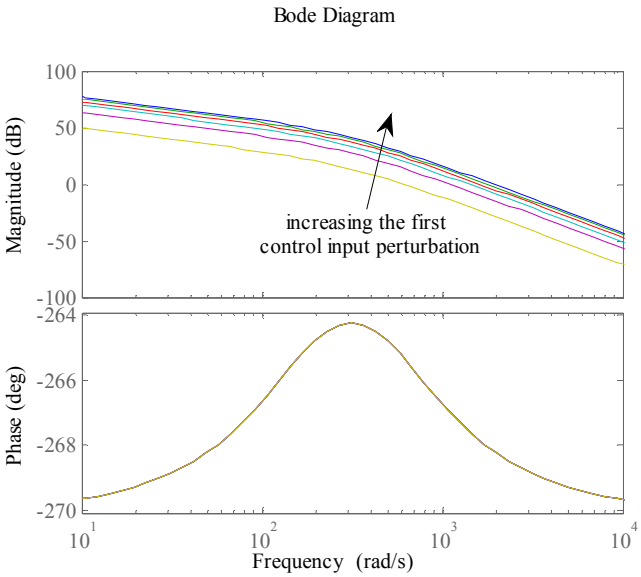

(b)

Figure 2.3 - The perturbation effect of first control input on (a) the first flat output (b) the second flat output.

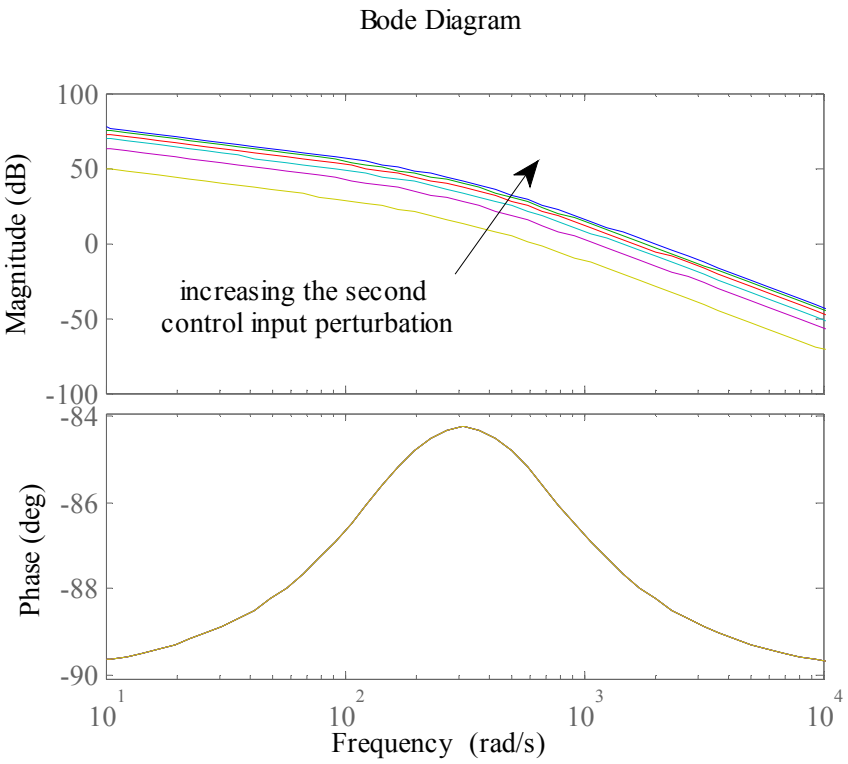

(a)

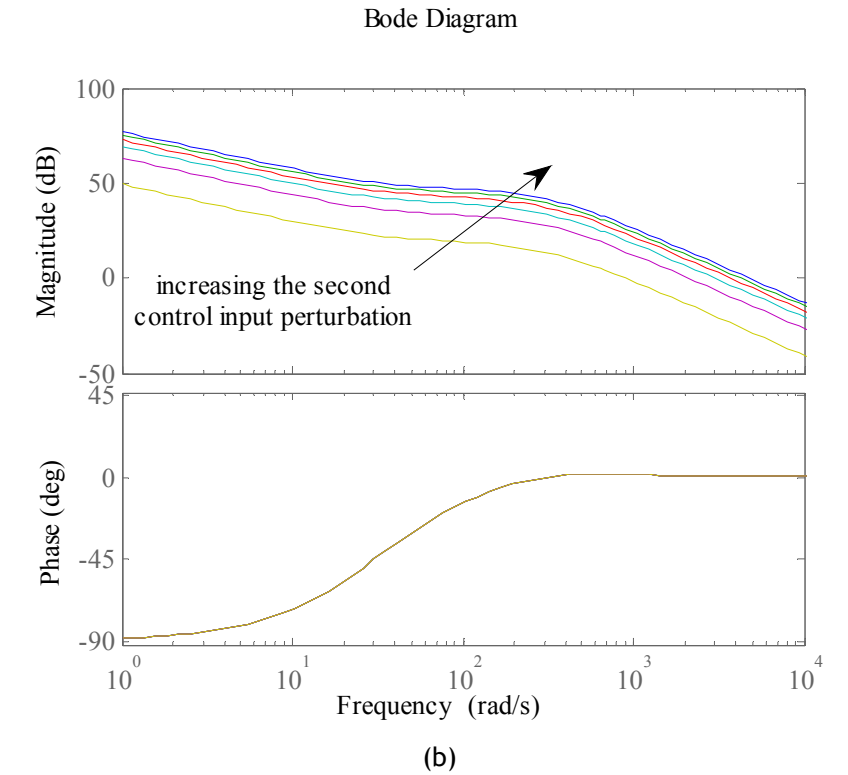

(b)

Figure 2.4 - The effects of second control inputs on (a) the first flat output (b) the second flat output.

2.4 Simulation Results

To verify the effectiveness of the proposed control technique, a detailed model of the aforementioned system as summarized in Figure 2.5 is implemented in the Matlab/Simulink. It is worth mentioning that the discrete mode with a sample time of 50 microsec is selected to execute the simulation of the MMC-based model in the Matlab environment. In order to assess the performance of the proposed technique, a load step change is applied to the system. Initially, in the steady state condition the MMC is regulated to provide the required power of 5.5MW+j2MVAR for a RL load. Then, in the load variation state, it is stepped up to 10 MW+j5MVAR.

2.4.1 Control Technique Effect Assessment

To assess the capability of the proposed DFT in a steady-state operation of the MMC, two time intervals are considered in this subsection. The first load, given in table I, is used in both operating conditions. In the first interval from 0 to 0.4, the control technique is applied to the MMC resulting in a stable voltage as shown in Figure 2.6. Then, at t=0.4 s, the designed control method is removed from the MMC. In consequence of the controller absence, the MMC SM voltages deviate from their desired values as depicted in Figure 2.7. In fact, the lack of the proposed control technique leads to an unbalanced and unstable voltage at PCC. Figure 2.8 and Figure 2.9 show the corresponding active and reactive power sharing among the MMC, load and capacitor filter. According to these figures, after removing the proposed control technique, all active and reactive power experience severe transient responses with high fluctuations, unable to track their reference values.

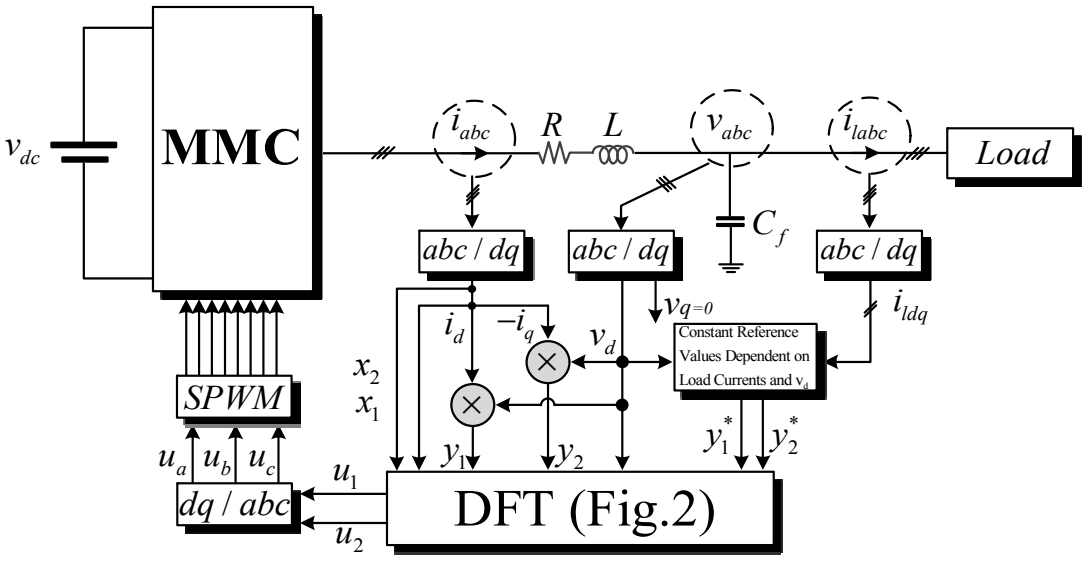

Figure 2.5 - The single diagram of simulated model.

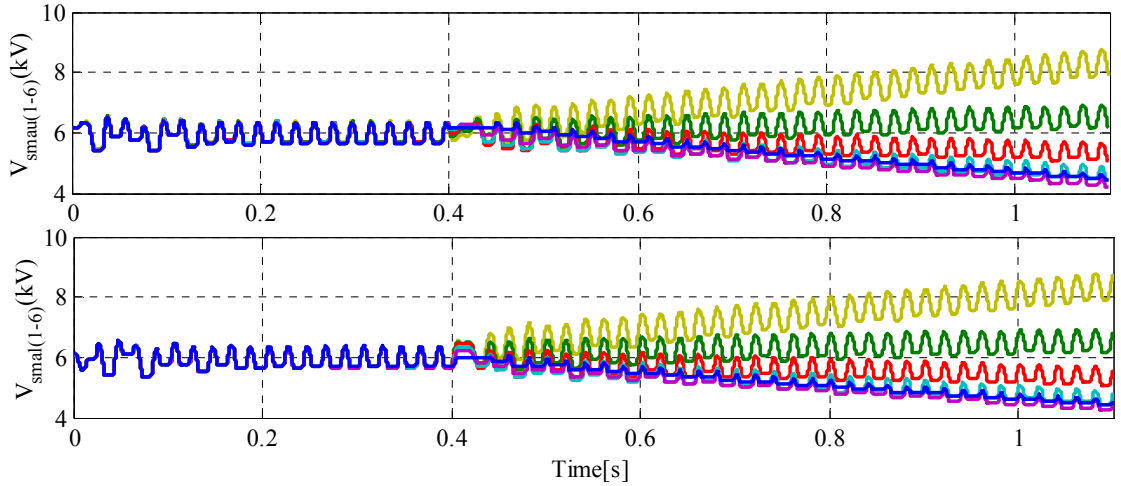

Figure 2.6 - SM's voltages of MMC.

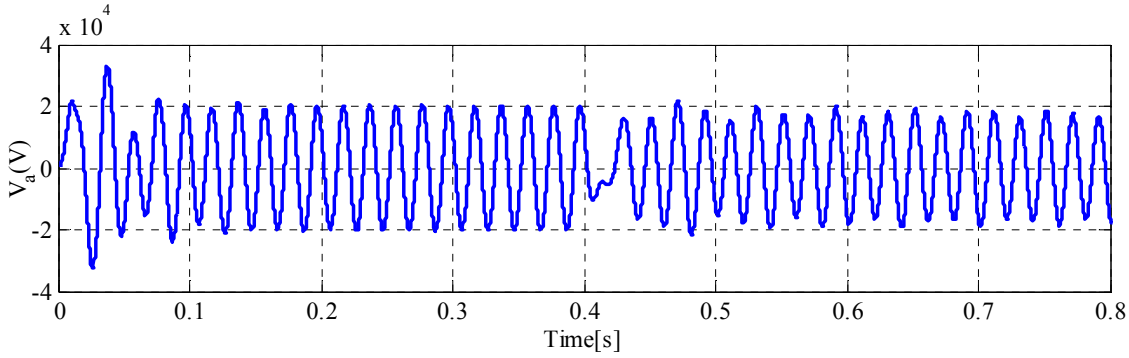

Figure 2.7 - Voltage at PCC in phase "a".

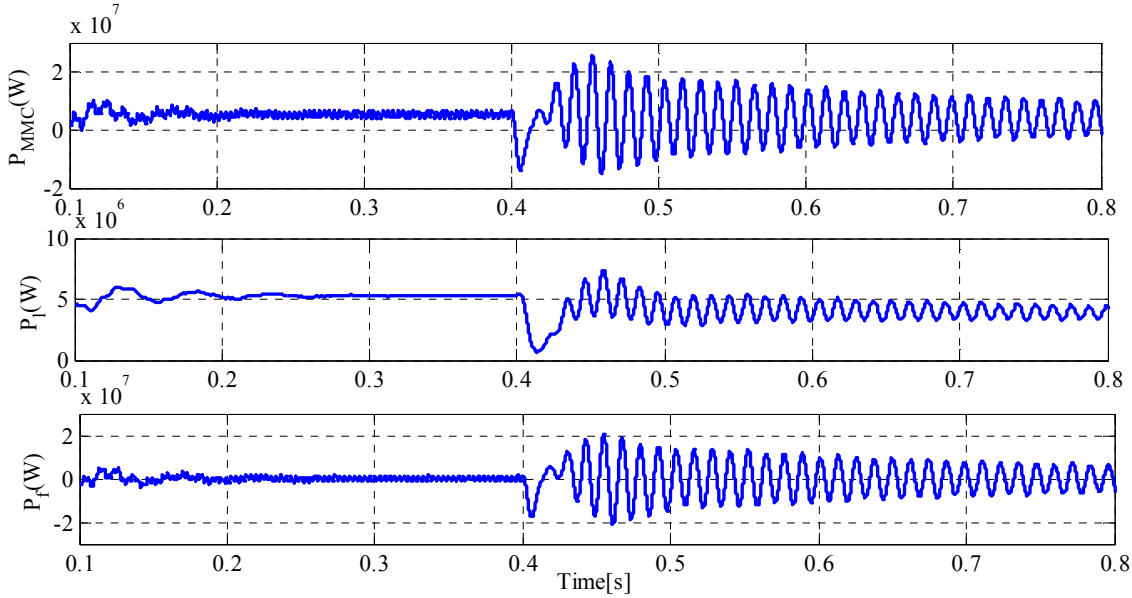

Figure 2.8 - Active power of MMC, load and AC filter.

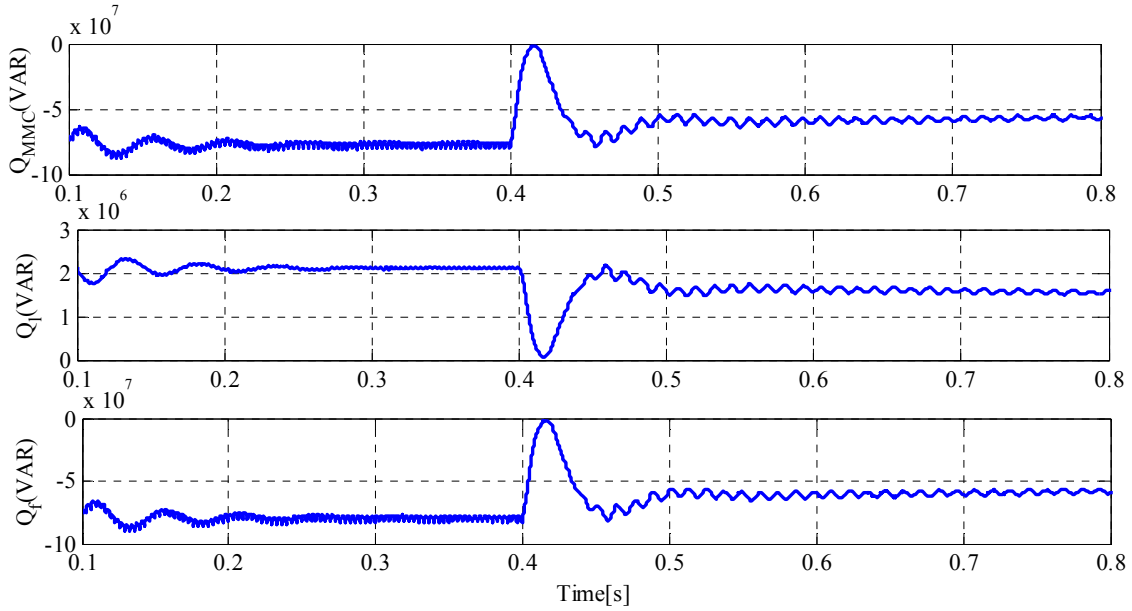

Figure 2.9 - Reactive power of MMC, load and AC filter.

2.4.2 Load Variation Evaluation

To evaluate the dynamic operation of the proposed control technique during transient state due to changes in loads connected to the PCC, MMC variables consisting of the flat outputs, output and SM voltages are taken into account. The proposed MMC model parameters for relevant loads are given in Table 2.1.

Figure 2.10 shows the SM's voltages of the phase "a" for a load change at t=0.4s. It can be seen that in spite of the load change the upper and lower SM's voltages maintain their reference values after a short transient period. In addition, the PCC voltage of phase "a" is illustrated in Figure 2.11. According to this simulation result, the proposed MMC model performs properly to maintain the output AC voltage regardless of the slight undershoot and overshoot due to a load variation at the starting point.

Table 2.1 - The proposed MMC model specifications with related loads

L_t (mH)	20	(N)	6
L (mH)	45	$f\,(Hz)$	50
C (mF)	20	C_f (mF)	0.6
R_t (□)	1	Load Active Power I	5.5 MW
R (□)	0.1	Load Reactive Power I	2 MVAR
v_{dc} (V)	36000	Load Active Power II	4.5 MW
v_m (V)	20000	Load Reactive Power II	3 MVAR

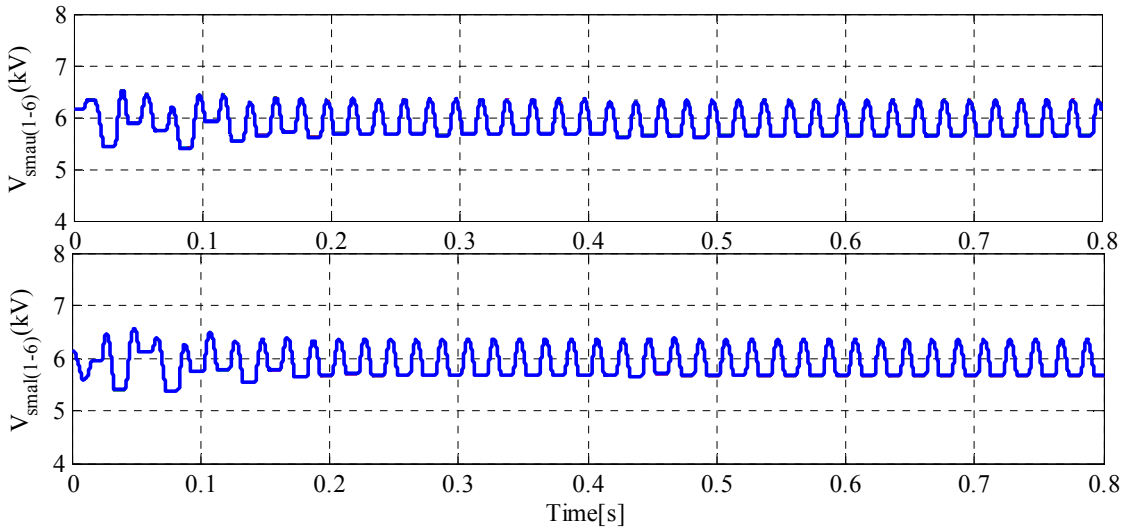

Figure 2.10 - SM's voltages of MMC with load variations at t=0.4 s.

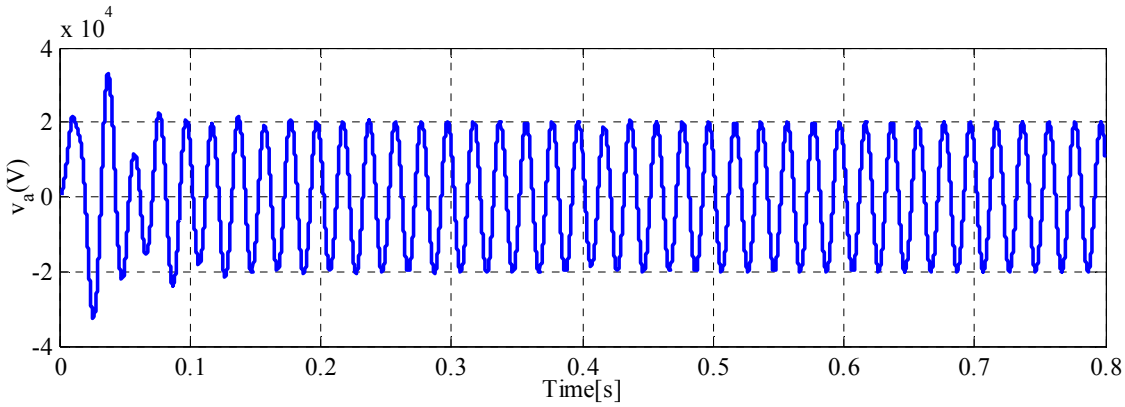

Figure 2.11 - PCC voltage of phase "a" with load variations at t=0.4 s.

The flat outputs including active and reactive power values are shown in Figure 2.12 and Figure 2.13. In steady state operation, the active power of the MMC follows properly the active power of load and the AC filter capacitor as depicted in Figure 2.12. Moreover, it can be seen from the responses during the time interval of [0.4, 0.8] that the proposed control technique is able to maintain the stability of the active power of the MMC after a short transient period. The MMC reactive power performance as the second flat output is evaluated in Figure 2.13. The reactive power demanded from the load to maintain PCC voltages can be appropriately provided by the proposed MMC model through the AC filter capacitor.

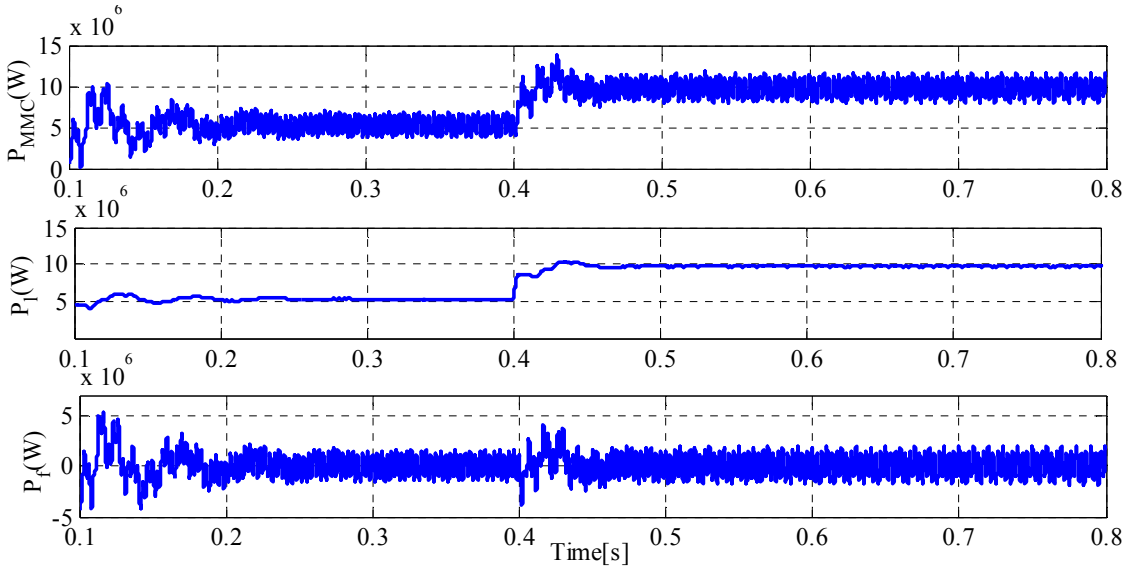

Figure 2.12 - Active power of MMC, load and AC filter with load variations at t=0.4 s.

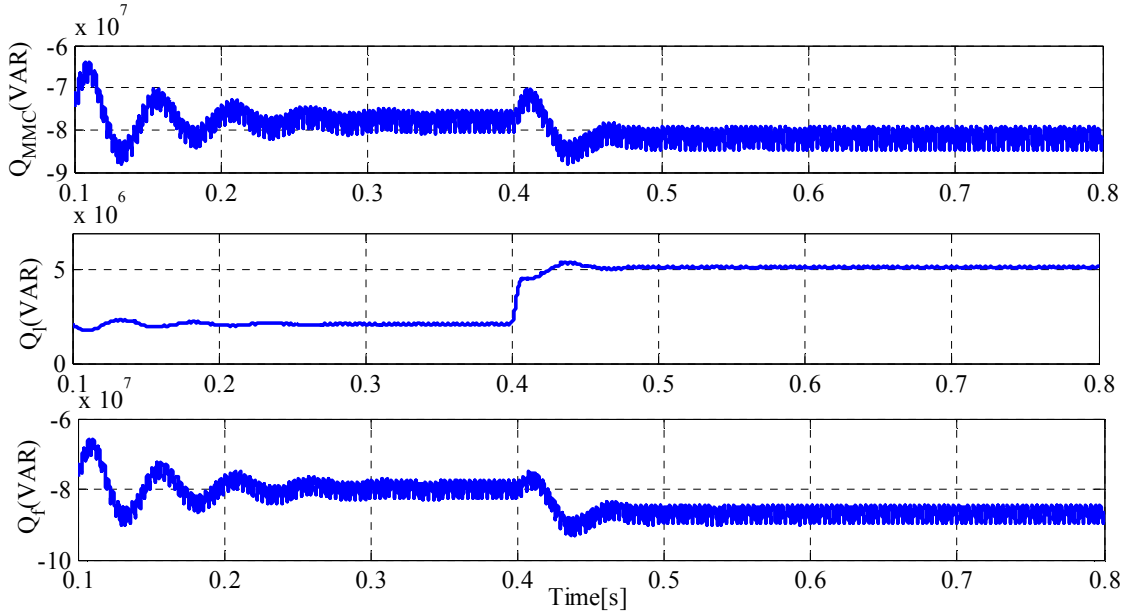

Figure 2.13 - Reactive power of MMC, load and AC filter with load variations at t=0.4 s.

2.4.3 Parameters Variation Evaluation

As discussed earlier, the proposed control technique can operate well under parameter variations. As per the MMC parameter patterns in both states presented in Table 2.1 and Table 2.2, SM's voltages of the MMC can be satisfied as shown in Figure 2.14. It should be noted that although the SM's voltages experience an undershoot immediately after parameters variation time, the reference values of this voltage can be followed by the MMC after a short transient period.

This confirms approaching the negative effects of the parameter variation to zero. While parameters variation takes place, the output voltage of MMC in phase “a” is involved with a short transient time as shown in Figure 2.15. Then, a sinusoidal pure waveform is achieved for MMC output voltage due to the stable operation of the proposed control technique.

As renewable energy systems are expected to make a significant contribution to supply worldwide electricity in a more secure and economic way, it is essential to carry on verifying the effeteness of control systems under the condition that there is an imbalance the generated and the consumed power. This research may be regarded as a basis for the development of modular multilevel converters and controllers in grid-connected systems to provide a long-term energy security.

Table 2.2 - The second parameters for the proposed MMC model

$L_{t2}(mH)$	35	$R_{t2}(\Omega)$	2.5
$L_2(mH)$	30	$R_2(\Omega)$	0.22

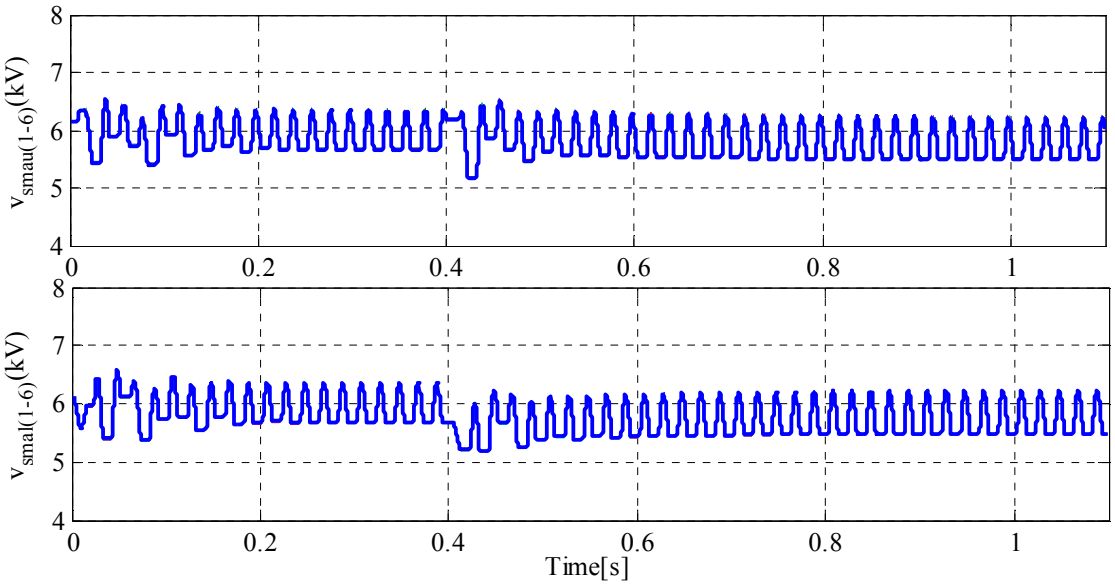

Figure 2.14 - SM’s voltages of MMC with parameters variations at t=0.4 s.

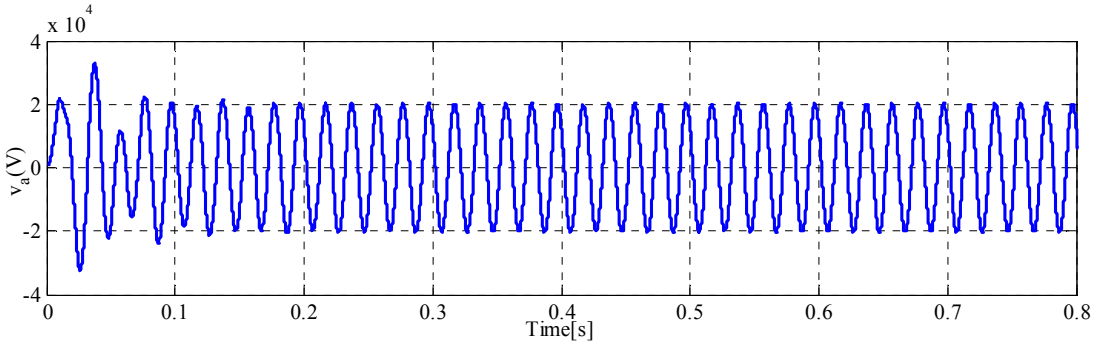

Figure 2.15 - PCC voltage of phase “a” with parameters variations at t=0.4 s.

To evaluate the ability of the proposed MMC-based model at reaching the desired value of its flat outputs under parameter variations, following scenario is given through Figure 2.16 and Figure 2.17. The MMC first operates in a steady state in which the MMC and the load active power approach to its target values. Then, after a parameter variation, the active power of the MMC, introduced as the first flat output experiences temporal fluctuations which will be attenuated after some short time cycles. In fact, the proposed control technique offers stable active power for the MMC, the load and the AC filter capacitor. In addition, the proposed technique contributes to provide the reactive power known as the second flat output of the MMC even parameter variation happens. As can be seen from Figure 2.17, the transient waveforms of the load and MMC reactive power during parameters variation can be damped and subsequently the desired reactive power can be achieved.

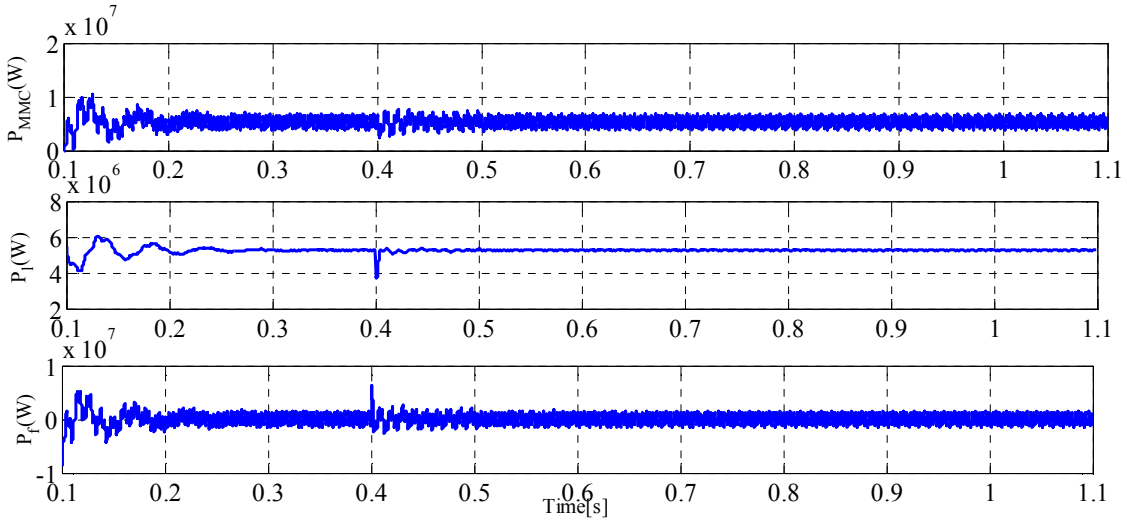

Figure 2.16 - Active power of MMC, load and AC filter with parameters variations at t=0.4 s.

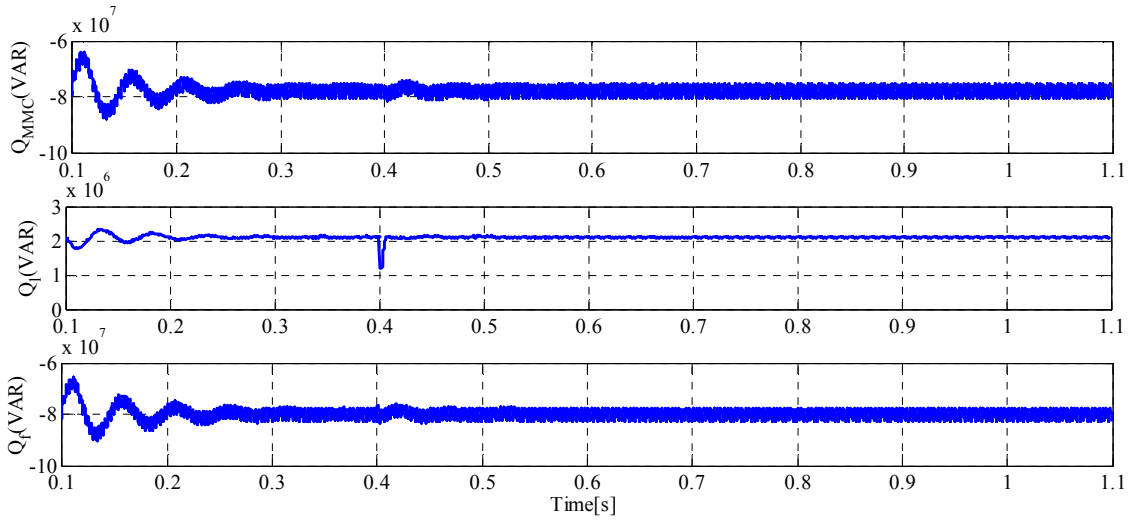

Figure 2.17 - Reactive power of MMC, load and AC filter with parameters variations at t=0.4 s.

2.5 Chapter Conclusions

This chapter addressed the differential flatness theory (DFT) used to control a modular multilevel converter (MMC), as a new contribution to earlier studies. Using the basic dynamic model of MMC in a d-q reference frame as well as defining appropriate flat outputs, new flat outputs-based dynamic equations were achieved. Then, these equations were used to obtain an initial value for controller inputs. In order to guarantee the stable operation of the MMC against the input disturbance, model errors and system uncertainties, a control Lyapunov function based on integral-proportional errors of the flat output was employed. In addition, the small-signal model of the flat outputs-based dynamic equation was developed and then the variation effects of controller inputs on flat outputs were accurately assessed. To evaluate the effectiveness of the proposed DFT-based control technique, Matlab simulations were carried out under challenging conditions, namely variations in parameters and load. The simulation results validated that the proposed control technique upholds the voltage levels accurately through providing active and reactive power. Overall, this novel DFT-based control scheme offered an efficient control design which can be upgraded to a varied range of complex converter topologies used for renewable energy applications.

Chapter 3

A Multi-Loop Control Technique for the Stable Operation of Modular Multilevel Converters in HVDC Transmission Systems

A multi-loop control strategy based on a six-order dynamic model of the modular multilevel converter (MMC) is presented in this chapter for the high-voltage direct current (HVDC) applications. For the initial analysis of the operation of MMC, a capability curve based on active and reactive power of the MMC is achieved through a part of the six order dynamic equations. According to the MMC's control aims, the first loop known as the outer loop is designed based on passivity control theory to force the MMC state variables to follow their reference values. As the second loop with the use of sliding mode control, the central loop should provide appropriate performance for the MMC under variations of the MMC's parameters. Another main part of the proposed controller is defined for the third inner loop to accomplish the accurate generation of reference values. Also, for a deeper analysis of the MMC's DC link voltage stability, two phase diagrams of the DC-link voltage are assessed. Matlab/Simulink environment is used to thoroughly validate the ability of the proposed control technique for the MMC in HVDC application under both load and MMC's parameters changes.

3.1 Introduction

The modular multilevel converter (MMC) topology has been a subject of increasing importance because of its special characteristics such as easy replacement of fault sub-modules (SMs), centralizing the distributed energies, modular structure, very low harmonic components and power losses, and also decreased rating values [18], [38], [71]–[73]. The MMCs have been widely utilized in various voltage/power levels of growing applications such as solar photovoltaic [74], large wind turbines [75], [76], AC motor drives [63], [77], high-voltage direct current (HVDC) transmission systems [39], [78], DC-DC transformers [79], battery electric vehicles [78], distributed energy resources (DERs) [43], [55], and flexible AC transmission systems (FACTS) [80]. Many researchers have focused on the control and modelling issues of the MMCs in various applications in recent years. Reference [81] deals with the fault condition of the MMC and tries to provide normal performance for the MMCs by the help of an energy-balancing control. A binary integer programming based model predictive control for the MMCs is proposed in [82] to optimize the multi-objective problem with minimum computing effort related to the control method.

A closed loop-needless PID controller along with increasing the arm inductance are considered to evaluate the effects of output voltage and current total harmonic distortion (THD) response in a modular multilevel converter [83]. Reference [84] presents a control strategy based on calculating the differential current references to provide desired operation for the MMCs in HVDC applications. Various dynamic models of the MMCs and their limitations in presenting robust control methods for these converters are investigated in [85]. In this work, a complete derivation of the proposed switching state functions without losing any circuital characteristics of the converter is accomplished and a switching-cycle control approach proposed based on unused switching states of the MMCs. A modulation technique is proposed in [60] based on a fixed pulse pattern fed into the SMs to maintain the stability of the stored energy in each SM, without measuring capacitor voltages or any other sort of feedback control. It also removes certain output voltage harmonics at any arbitrary modulation index and any output voltage phase angle. A current control design for independent adjustment of several current components and a systematic identification of current and voltage components for balancing the energy in the arms of an MMC is presented in [86]. In [87], a control strategy based on adding a common zero-sequence voltage to the reference voltages is proposed for balancing the arm currents of the MMCs under unbalanced load conditions. To reach it, a relationship between the DC-link active power and AC-link average active power is achieved and then, the DC component of the arm current is calculated through the AC-link average active power in the corresponding phase [87]. In the medium voltage systems, the energy storage can be embedded in MMC that causes several SMs to operate at significantly lower voltages [88]. In the structure presented in [89], the low-frequency components of the SM's output currents are removed by utilizing the interfaced batteries through the non-isolated dc/DC converters. Control algorithms proposed in this work are developed to balance the state of charge of batteries. A compact and clear representation of differential equations is obtained for the MMC by introducing two nonlinear coordinate transformations in [90]. In the proposed model, two candidate outputs leaded to the internal dynamics of second or third order and a quasi-static feedback generates a linear input-output behaviour. Other different aspects of MMC application in HVDC system such as DC fault and DC solid-state transformers operating conditions are assessed in the references of [91]–[94].

In many existing methods, simultaneously having robustness against MMC parameters changes and also having very good dynamic tracking responses against the MMC's load changes have not been considered in their designed control techniques. But, in this work, a multi-loop control strategy is aimed at providing a stable operation of the MMCs in HVDC application under both MMC's arm inductance and resistance parameters variations and also loads changes as well. This the first feature of the proposed controller that can increase the stability margins of the MMC performance with existence of more variations.

According to the achieved six order dynamic equations of the MMCs, firstly the outer loop formed by passivity based control technique is introduced to enable the convergence ability of the MMC's state variables for its reference values in dynamic changes. Then, sliding mode controller is used to prepare the MMCs for stable operation against the MMC's parameters variations as the central loop of the proposed controller. The inner loop is employed to help other loops have accurate reference values for its used state variables that as another feature of the proposed controller, can generate instantaneously the needed references values of both MMCs in various operating conditions. Also, a capability curve is obtained to specify the allowable area of the MMC's active and reactive power generation in HVDC application and also R and L variations effects on the curve are evaluated that can provide some control considerations to understand more about the simulation results of the MMC's performance. Stability analysis of DC-link voltage is done in final part of this chapter. Simulation results executed by Matlab/Simulink demonstrate the validity of the proposed control strategy in all operating conditions.

3.2 The Proposed Differential Equation of MMC

Figure 3.1 (a) shows the proposed HVDC system which is consisted of two back-to-back MMCs. The *AC*-side of the MMC1 comprises *AC*-system-1, a line with inductance of L and resistance of R, a three-phase step-down transformer and the input inductance and resistance of the MMC1. DC power is produced by MMC1 and then MMC2 uses this power to act as an inverter in HVDC structure. The resistance of R_{dc} represents total switching loss of MMCs which is paralleled with DC link. The *AC*-side of the MMC2 consists of the output inductance and resistance, an *AC* filter to trap dominant switching harmonics, a load and a three-phase step-up transformer. The employed MMCs are shown in Figure 3.1 (b). A half-bridge converter is the same SM in which three states are appeared for each SM as: (1) switch $S_{(ul)kj1}$is ON $\left(S_{(ul)kj2} \equiv off\right)$, in which the output voltage of the SM is equal to $v_{sm(ul)kj}$, (2) switch $S_{(ul)kj2}$ is ON $\left(S_{(ul)kj1} \equiv off\right)$ and consequently the SM's voltage becomes zero, and (3) as standby state, both upper and lower switches are not controlled $\left(S_{(ul)kj1} \equiv S_{(ul)kj2} \equiv off\right)$ and the capacitor of SM is pre-charged. Two first states will be considered in this chapter.

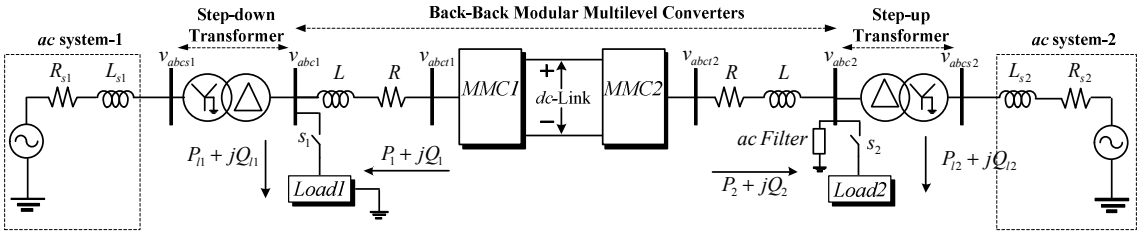

(a)

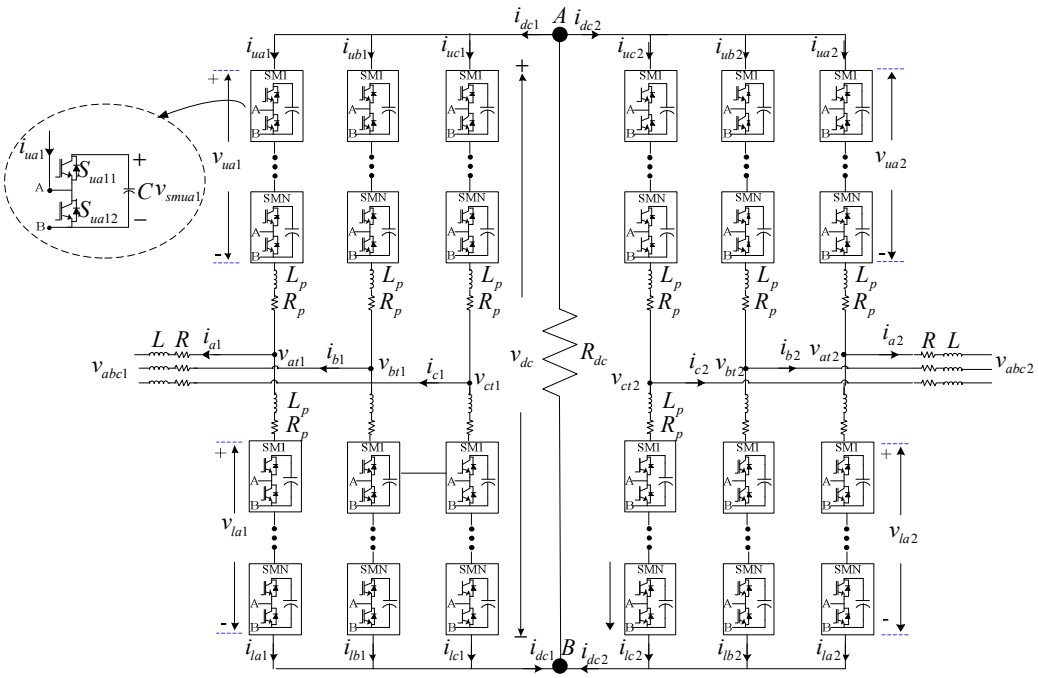

(b)

Figure 3.1 - Schematic diagram of the MMC-HVDC system. (a) Single-line diagram model and (b) circuit diagram of the back-to-back MMC.

3.2.1 Proposed Six Order Dynamic Model of MMCs

It can be realized from Figure 3.1(b) that the capacitor voltages of SM play a key role at generating DC-link voltage. Consequently, to regulate DC link voltage, $v_{(ul)kj}$ should be accurately controlled. The dynamic equation based on the MMC's currents can be achieved by the use of the Kirchhoff's voltage law (KVL) for Figure 3.1(b) as,

$$v_{kj} + L\frac{di_{kj}}{dt} + Ri_{kj} + L_p\frac{di_{ukj}}{dt} + R_p i_{ukj} - \frac{v_{dc}}{2} + v_{ukj} = 0 \tag{3.1}$$

$$v_{kj} + L\frac{di_{kj}}{dt} + Ri_{kj} - L_p\frac{di_{lkj}}{dt} - R_p i_{lkj} + \frac{v_{dc}}{2} - v_{lkj} = 0 \tag{3.2}$$

The MMC currents based dynamic model can be driven by summing up (3.1) and (3.2) as,

$$\left(L + \frac{L_p}{2}\right)\frac{di_{kj}}{dt} + \left(R + \frac{R_p}{2}\right)i_{kj} + v_{kj} + u_{kj1} = 0 \tag{3.3}$$

where,u_{kj1} can be calculated as,

$$u_{kj1} = \frac{\left(v_{ukj} - v_{lkj}\right)}{2} \tag{3.4}$$

To properly control the MMC currents for reaching desired values of active and reactive power sharing, DC-link voltage and SM voltages, the switching function of (3.4) is employed. Next important goal is decreasing the circulating currents of the MMCs which can be written as,

$$i_{cirkj} = \frac{i_{ukj} + i_{lkj}}{2} - \frac{i_{dcj}}{3} \tag{3.5}$$

The power losses of MMCs, the ripple magnitude of capacitor voltages and the total MMCs cost are increased because of existing circulating currents. By subtracting (3.1) from (3.2) and using (3.5), the circulating currents based differential equations can be achieved as (3.6),

$$L_p\frac{di_{cirkj}}{dt} + R_p i_{cirkj} + R_p\frac{i_{dcj}}{3} - \frac{v_{dc}}{2} + u_{kj2} = 0 \tag{3.6}$$

where, u_{kj2} is defined as,

$$u_{kj2} = \frac{\left(v_{ukj} + v_{lkj}\right)}{2} \tag{3.7}$$

According to points of A and B in Figure 3.1(b), the connection amid DC link voltage dynamic and MMC's arms currents is given as,

$$C_{eq}\frac{dv_{dc}}{dt}+\frac{v_{dc}}{R_{dc}}+\sum_{k=a}^{b,c}i_{uk1}+\sum_{k=a}^{b,c}i_{uk2}=0 \tag{3.8}$$

$$C_{eq}\frac{dv_{dc}}{dt}+\frac{v_{dc}}{R_{dc}}+\sum_{k=a}^{b,c}i_{lk1}+\sum_{k=a}^{b,c}i_{lk2}=0 \tag{3.9}$$

By summing up (3.8) and (3.9) and using (3.5), DC link voltage dynamic can be written in terms of DC link and circulating currents as (3.10),

$$C_{eq}\frac{dv_{dc}}{dt}+\frac{v_{dc}}{R_{dc}}+\sum_{k=a}^{b,c}i_{cirkj}+i_{dc1}+i_{dc2}=0 \tag{3.10}$$

Noting the switching states of SMs, the dynamics of voltage of SMs for the lower and upper arms can be summarized as,

$$C\frac{dv_{sm(ul)kj}}{dt}=\begin{cases} i_{(ul)kj} & S_{(ul)kj1}\equiv on \\ i_{sm(ul)kj}\to 0 & S_{(ul)kj1}\equiv off \end{cases} \tag{3.11}$$

According to (3.11), and considering an appropriate approximation for the operation of the symmetrical voltages of capacitors of SMs in two arms, dynamic of output voltage of SMs can be deduced through the MMCs or circulating currents. It leads that the proposed controller effectively be involved in an effective balanced condition for the SMs capacitors in different operating conditions. By transforming equations (3.3), (3.6) and (3.10) into dq reference frame, the proposed six order dynamic model of the MMCs in HVDC applications can be driven as,

$$\left(L+\frac{L_p}{2}\right)\frac{di_{dj}}{dt}+\left(R+\frac{R_p}{2}\right)i_{dj}-\omega\left(L+\frac{L_p}{2}\right)i_{qj}+u_{dj1}+v_{dj}=0 \tag{3.12}$$

$$\left(L+\frac{L_p}{2}\right)\frac{di_{qj}}{dt}+\left(R+\frac{R_p}{2}\right)i_{qj}+\omega\left(L+\frac{L_p}{2}\right)i_{dj}+u_{qj1}+v_{qj}=0 \tag{3.13}$$

$$L_p\frac{di_{cirdj}}{dt}+R_p i_{cirdj}-\omega L_p i_{cirqj}+u_{dj2}=0 \tag{3.14}$$

$$L_p\frac{di_{cirqj}}{dt}+R_p i_{cirqj}+\omega L_p i_{cirdj}+u_{qj2}=0 \tag{3.15}$$

$$L_p\frac{di_{cir0j}}{dt}+R_p i_{cir0j}+u_{0j2}-\frac{3\sqrt{2}v_{dc}}{2}+\sqrt{2}R_p i_{dcj}=0 \tag{3.16}$$

$$C_{eq}\frac{dv_{dc}}{dt}+\frac{v_{dc}}{R_{dc}}+\left(i_{cirdj}+i_{cirqj}+i_{cir0j}\right)+i_{dc1}+i_{dc2}=0 \tag{3.17}$$

3.2.2 Capability Curve Analysis of MMCs Active and Reactive Power

The MMC's potential in injection of maximum power is presented in this section. Based on Figure 3.1 (b), the MMCs DC-link and the AC side voltages are related to each other in d-q reference frame according to following equation,

$$v_{dc}i_{dcj}=v_{dtj}i_{dj}+v_{qtj}i_{qj} \tag{3.18}$$

By considering Figure 3.1(b) and applying KVL's law to the AC side of the proposed MMC based HVDC system, the relation between the output and AC-side voltages of the MMC in dq reference frame can be achieved as,

$$v_{dtj}=v_{dj}+L\frac{di_{dj}}{dt}+Ri_{dj}-\omega Li_{qj} \tag{3.19}$$

$$v_{qtj} = v_{qj} + L\frac{di_{qj}}{dt} + Ri_{qj} + \omega Li_{dj} \tag{3.20}$$

By substituting (3.19) and (3.20) in (3.18) and also assuming $di_{(dq)}/dt = I_{av(dq)}$, the following equation of a circle is driven as,

$$\left(i_{dj} + \frac{LI_{avdj} + v_{dj}}{2R}\right)^2 + \left(i_{qj} + \frac{LI_{avqj} + v_{qj}}{2R}\right)^2 = \frac{\left(LI_{avdj} + v_{dj}\right)^2 + \left(LI_{avqj} + v_{qj}\right)^2 + 4Rv_{dc}i_{dcj}}{4R^2} \tag{3.21}$$

The (3.21) determines the operation area of MMC's currents in d-q reference frame. By considering the MMC's active and reactive power as $P_j = v_{dj}i_{dj}$ and $Q_j = -v_{dj}i_{dj}$ and substituting in (3.21), the power curve of MMC in the proposed HVDC system can be obtained as [40],

$$\left(P_j + \frac{LI_{avdj}v_{dj} + v_{dj}^2}{2R}\right)^2 + \left(Q_j - \frac{LI_{avqj}v_{dj} + v_{dj}v_{qj}}{2R}\right)^2 = \frac{\left(LI_{avdj}v_{dj} + v_{dj}^2\right)^2 + \left(LI_{avqj}v_{dj} + v_{qj}v_{dj}\right)^2 + 4Rv_{dc}i_{dcj}v_{dj}^2}{4R^2} \tag{3.22}$$

The power curve of the proposed MMC based HVDC system in (3.22) is drawn in Figure 3.2 (a). It can be understood from this figure that the maximum and minimum amount of the MMC's active and reactive power are completely dependent on MMC's output parameters and also operation of the proposed MMC through the proposed controller. According to this figure, the center and radius of the power curve are definitely changed by MMC's output parameters, DC link specifications and also output currents and voltages of MMC in d-q reference frame. Figure 3.2 (b) and Figure 3.2 (c) show the various parameters effects of the MMC on the power curve. As can be seen, increasing the MMC's resistance (R) causes the power curve to become smaller with decreasing the radius and center. On the other hand, the scenario gets inverse when the MMC's inductance (L) increases as depicted in Figure 3.2 (c).

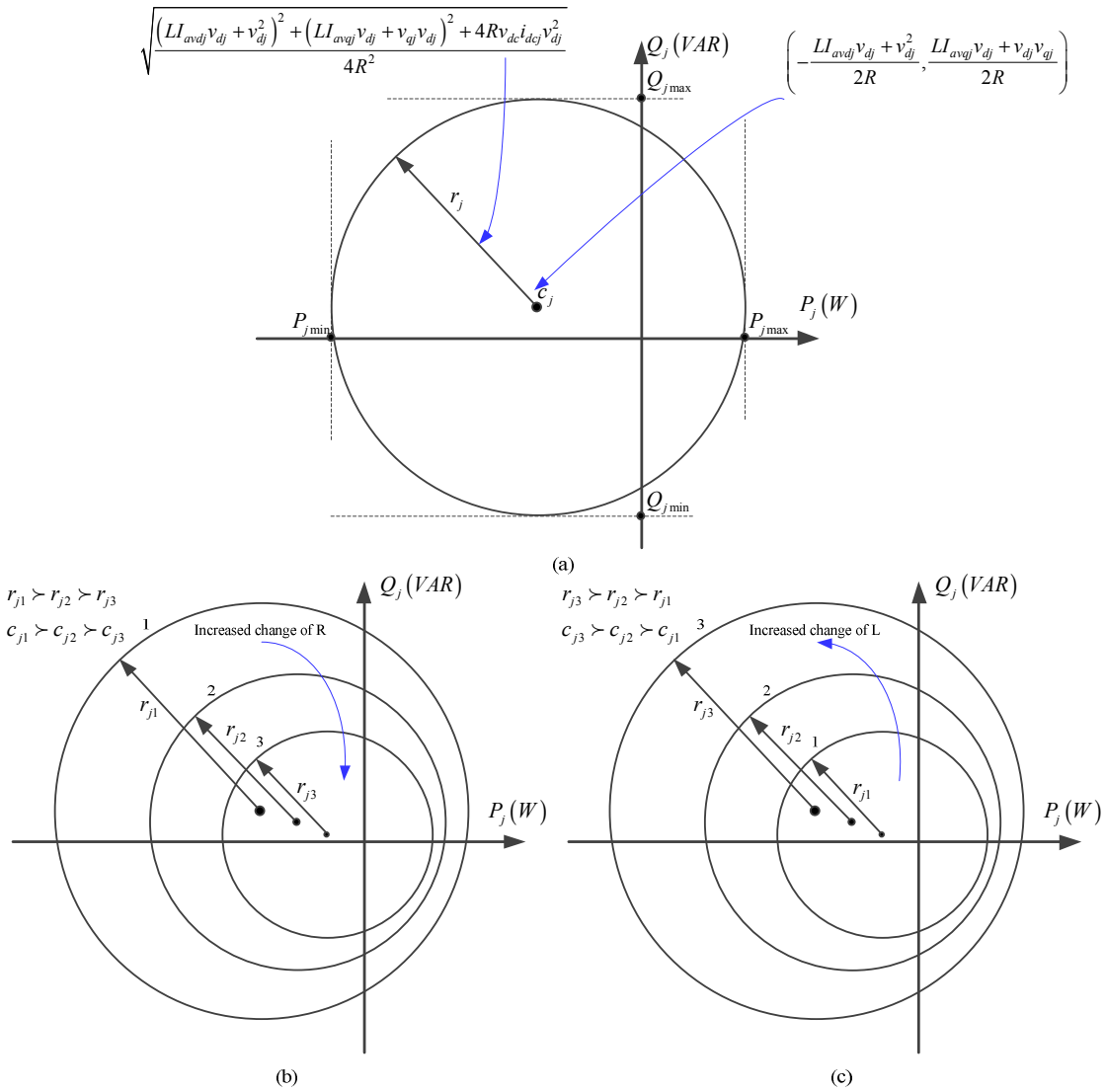

Figure 3.2 - (a) Power curve of MMCs (b) R and L changes effects on MMCs power curve [27].

3.3 Control Discussion

In this section, the sequent of designing process for the proposed multi-loop control technique is discussed in detail. The general aims of the proposed controller for the MMCs in HVDC applications are making stable operation under presence of both load and MMC's parameters changes that should be provided through the proposed three control loops i.e., outer, central and inner control loops (OLC, CLC, and ILC). OLC is aimed at leading the dynamic errors to attain zero value. The stable operation of the systems is assured with the CLC. Finally, the ILC provides reference currents for the both MMCs.

3.3.1 The Design of Outer Loop Controller (OLC)

The outer loop controller is designed in this sub-section to provide the ability of tracking the reference values of the MMCs state variables for final proposed controller with the existence of load changes. The Passivity based control technique is used in this section. Firstly the proposed six order dynamic equation of (3.12)-(3.17) is presented as (3.23),

$$T_{dq0j}\frac{dQ_{dq0j}}{dt}+X_{dq0j}Q_{dq0j}+P_{dq0j}+O_{dq0j}+Y_{dq0j}=0 \tag{3.23}$$

All the matrixes used in (3.23) are presented in Appendix A. The proposed error vector of the MMCs is written as,

$$\begin{aligned} Z_{dq0j} &= Q_{dq0j}-Q^{*}_{dq0j} \\ &= \left[i_{dj}-i^{*}_{dj} \quad i_{qj}-i^{*}_{qj} \quad i_{cirdj}-i^{*}_{cirdj} \quad i_{cirqj}-i^{*}_{cirqj} \quad i_{cir0j}-i^{*}_{cir0j} \quad v_{dc}-v^{*}_{dc} \right]^{T} \end{aligned} \tag{3.24}$$

To reach an effective error vector for OLC, the main control aims of regulating MMC power, DC link voltage and AC voltages should be considered in calculating its reference values. Using (3.23) and (3.24), the description of MMC closed-loop error differential equation can be achieved as,

$$T_{dq0j}\frac{dZ_{dq0j}}{dt}+X_{dq0j}Z_{dq0j}=-Q_{dq0j}-Y_{dq0j}-P_{dq0j}-\left(T_{dq0j}\frac{dQ^{*}_{dq0j}}{dt}+X_{dq0j}Q^{*}_{dq0j}\right) \tag{3.25}$$

Based on passivity control theory, injecting series resistances to the MMC closed-loop error differential equation can significantly enhance the convergence rate of outer loop controller. Equation (3.26) is used as series resistances,

$$R_{dq0j}=\begin{bmatrix} R_d & 0 & 0 & 0 & 0 & 0 \\ 0 & R_q & 0 & 0 & 0 & 0 \\ 0 & 0 & R_{cird} & 0 & 0 & 0 \\ 0 & 0 & 0 & R_{cirq} & 0 & 0 \\ 0 & 0 & 0 & 0 & R_{cir0} & 0 \\ 0 & 0 & 0 & 0 & 0 & \left(R_{dc}\right)^{-1} \end{bmatrix} \tag{3.26}$$

The completed closed-loop error differential equation of MMC can be obtained by adding the term of $R_{dq0j}Z_{dq0j}$ into the both sides of (3.25) as,

$$\begin{aligned} &T_{dq0j}\frac{dZ_{dq0j}}{dt}+X_{dq0j}Z_{dq0j}+R_{dq0j}Z_{dq0j}= \\ &-Q_{dq0j}-Y_{dq0j}-P_{dq0j}-\left(T_{dq0j}\frac{dQ^{*}_{dq0j}}{dt}+X_{dq0j}Q^{*}_{dq0j}-R_{dq0j}Z_{dq0j}\right) \end{aligned} \tag{3.27}$$

The desired operation of outer loop controller can be achieved by $Z_{dq0j}\rightarrow 0$. Thus,

$$T_{dq0j}\frac{dZ_{dq0j}}{dt}+X_{dq0j}Z_{dq0j}+R_{dq0j}Z_{dq0j}=0 \tag{3.28}$$

By applying (3.28) into (3.27), the proposed state variable error-based equation of outer loop controller can be obtained as,

$$-Q_{dq0j}-Y_{dq0j}-P_{dq0j}-\left(T_{dq0j}\frac{dQ^{*}_{dq0j}}{dt}+X_{dq0j}Q^{*}_{dq0j}-R_{dq0j}Z_{dq0j}\right)=0 \tag{3.29}$$

Equation (3.29) is used to reach the usable modulation functions of MMCs in outer loop controller as (3.30).

$$P_{dq0j}=\left[-Q_{dq0j}-Y_{dq0j}-\left(T_{dq0j}\frac{dQ^{*}_{dq0j}}{dt}+X_{dq0j}Q^{*}_{dq0j}-R_{dq0j}Z_{dq0j}\right)\right] \tag{3.30}$$

The Direct Lyapunov control theory is employed to prove that the proposed MMC's closed-loop error differential equation of OLC is stable. Thus, the Lyapunov function can be defined as,

$$\begin{aligned} E_{dq0j}\left(Z_{dq0j}\right)&=\frac{1}{2}\left(L+\frac{L_p}{2}\right)\left(z_{dj}\right)^2+\frac{1}{2}\left(L+\frac{L_p}{2}\right)\left(z_{qj}\right)^2+\frac{1}{2}L_p\left(z_{cirdj}\right)^2 \\ &+\frac{1}{2}L_p\left(z_{cirqj}\right)^2+\frac{1}{2}L_p\left(z_{cir0j}\right)^2+\frac{1}{2}C_{eq}\left(z_{dc}\right)^2 \end{aligned} \tag{3.31}$$

The error variables of z are the same defined in (3.24). To prove the globally asymptotic stability of (3.31) against the undesirable disturbances, the derivative of (3.31) in the state variables trajectories should definitively be negative. Therefore,

$$\begin{aligned}&\frac{dE_{dq0j}}{dt}\left(Z_{dq0j}\right)=\left(L+\frac{L_p}{2}\right)\frac{dz_{dj}}{dt}z_{dj}+\left(L+\frac{L_p}{2}\right)\frac{dz_{qj}}{dt}z_{qj}+L_p\frac{dz_{cirdj}}{dt}z_{cirdj}\\&+L_p\frac{dz_{cirqj}}{dt}z_{cirqj}+L_p\frac{dz_{cir0j}}{dt}z_{cir0j}+C_{eq}\frac{dz_{dc}}{dt}z_{dc}=T_{dq0j}\frac{dZ_{dq0j}}{dt}Z_{dq0j}\\&=-\left(X_{dq0j}Z_{dq0j}+R_{dq0j}Z_{dq0j}\right)Z_{dq0j}\end{aligned}\tag{3.32}$$

The error variables based equation of (3.28) can be used to demonstrate that the terms generated by injection resistances in (3.32) are more dominant than other terms. Consequently, (3.32) can be summarized as,

$$\begin{aligned}&\frac{dE_{dq0j}}{dt}\left(Z_{dq0j}\right)=-R_{dq0j}Z_{dq0j}Z_{dq0j}\\&=-R_{dj}\left(z_{dj}\right)^2-R_{qj}\left(z_{qj}\right)^2-R_{cirdj}\left(z_{cirdj}\right)^2-R_{cirqj}\left(z_{cirqj}\right)^2\\&-R_{cir0j}\left(z_{cir0j}\right)^2-\left(R_{dcj}\right)^{-1}\left(z_{dcj}\right)^2<0\end{aligned}\tag{3.33}$$

The global asymptotical stability of the proposed outer loop controller can be guaranteed by (3.33). The proposed outer loop controllers of both MMCs used in HVDC system can be illustrated in Figure 3.3. To regulate the MMCs currents for accurate active and reactive power sharing, Figure 3.3 (a) is employed in OLC. On the other hand, to minimize the MMC circulating currents, Figure 3.3 (b) can be used in the global structure of the proposed outer loop controller.

3.3.2 Design of the Central Loop Controller (CLC)

In order to design a central loop controller with robust features, sliding mode controller is used in this sub-section to make a stable controller against MMC parameters changes. A time-varying sliding surface with strong relative degree g_n is considered as (3.34),

$$S_{dq0j}\left(t,Z_{dq0j}\right)=\left(\frac{d}{dt}+k_{dq0j}\right)^{g_n-1}Z_{dq0j}\tag{3.34}$$

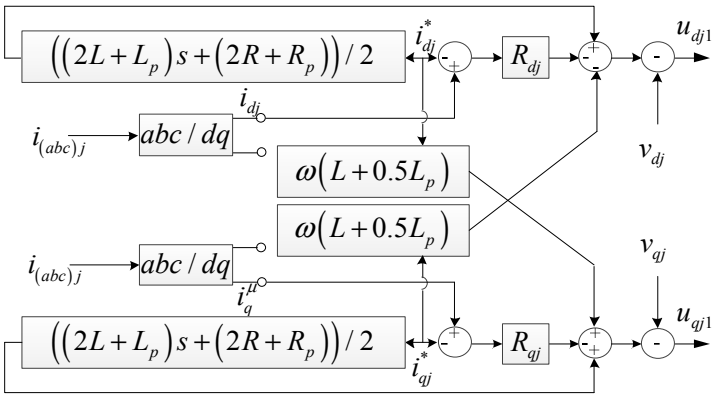

(a)

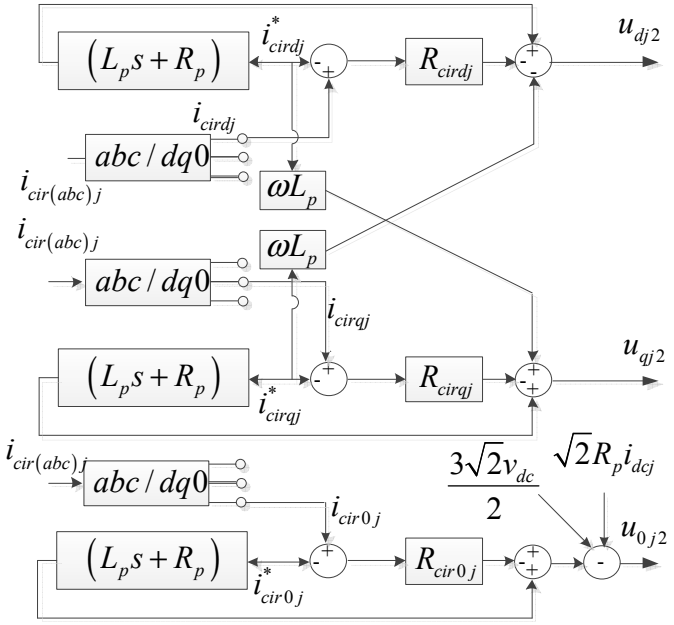

(b)

Figure 3.3 - The proposed outer loop controller for (a) MMCs currents (b) MMCs circulating currents.

The arbitrary constant values of k_{dq0j} help CLC have a faster reaction against any parameter change. By the help of (3.34) and also selecting the relative degree 1 for i_{mj} and i_{cirmj}, MMCs and circulating currents can have the reference sliding surfaces of (3.35) and (3.36), respectively as,

$$S_{dqj1}\left(t,\mathrm{z}_{dqj}\right)=z_{(dq)j}=i_{(dq)j}-i^{*}_{(dq)j} \tag{3.35}$$

$$S_{dq0j2}\left(t,\mathrm{z}_{cirdq0j}\right)=z_{cir(dq0)j}=i_{cir(dq0)j}-i^{*}_{cir(dq0)j} \tag{3.36}$$

The derivative of the reference sliding surfaces should be considered to provide the desired motion for MMCs and circulating currents on the sliding surfaces. Consequently, (3.37) and (3.38) can be achieved as,

$$\frac{dz_{(dq)j}}{dt}=\frac{di_{(dq)j}}{dt}-\frac{di^{*}_{(dq)j}}{dt}=-\psi_{(dq)j}\,\mathrm{sgn}\left(z_{(dq)j}\right) \tag{3.37}$$

$$\frac{dz_{cir(dq0)j}}{dt}=\frac{di_{cir(dq0)j}}{dt}-\frac{di^{*}_{cir(dq0)j}}{dt}=-\psi_{cir(dq0)j}\,\mathrm{sgn}\left(z_{cir(dq0)j}\right) \tag{3.38}$$

Using the sign function and also choosing properly $\psi_{(dq)j}$ and $\psi_{cir(dq0)j}$, can lead to improving the operation of central loop controller against MMCs parameters. The global structure of the proposed central loop controller for both MMCs and circulating currents is shown in Figure 3.4.

The Lyapunov function of (3.39) is introduced to evaluate the stability of the central loop controller performance by considering the sliding law of (3.35)-(3.38) as,

$$J_j(Q)=\frac{1}{2}\left(z_{dj}\right)^2+\frac{1}{2}\left(z_{qj}\right)^2+\frac{1}{2}\left(z_{cirdj}\right)^2+\frac{1}{2}\left(z_{cirqj}\right)^2+\frac{1}{2}\left(z_{cir0j}\right)^2 \tag{3.39}$$

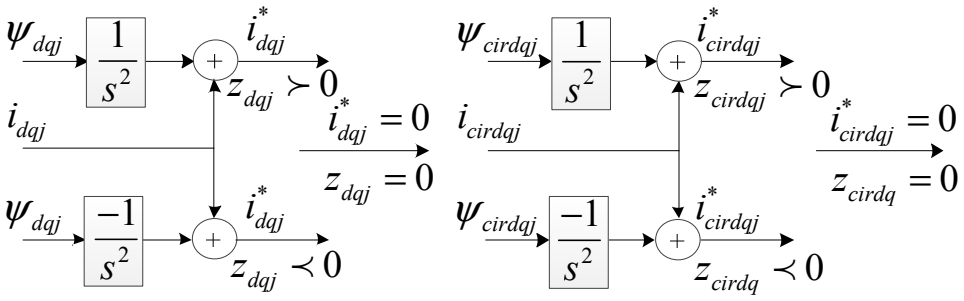

Figure 3.4 - The Proposed Central Loop Controller for (a) MMCs currents (b) MMCs circulating currents.

The equation of (3.40) is achieved by differentiating (3.39) in the trajectories of MMCs and circulating currents as,

$$\begin{aligned}&\frac{dJ_j(Q)}{dt}=z_{dj}\frac{dz_{dj}}{dt}+z_{qj}\frac{dz_{qj}}{dt}+z_{cirdj}\frac{dz_{cirdj}}{dt}+z_{cirqj}\frac{dz_{cirqj}}{dt}+z_{cir0\,j}\frac{dz_{cir0\,j}}{dt}=-z_{dj}\psi_{dj}\,\mathrm{sgn}\left(z_{dj}\right)\\&-z_{qj}\psi_{qj}\,\mathrm{sgn}\left(z_{qj}\right)-z_{cirdj}\psi_{cirdj}\,\mathrm{sgn}\left(z_{cirdj}\right)-z_{cirqj}\psi_{cirqj}\,\mathrm{sgn}\left(z_{cirqj}\right)-z_{cir0\,j}\psi_{cir0\,j}\,\mathrm{sgn}\left(z_{cir0\,j}\right)\le 0\end{aligned}\tag{3.40}$$

Since Z_{xj} sgn (Z_{xj})becomes positive or zero value in each condition, the equation of (3.40) is definitely negative or zero. Thus, according to direct Lyapunov method, the proposed sliding mode based loop controller has stable operation in all its operating conditions.

3.3.3 The Design of Inner Loop Controller (ILC)

As discussed, the MMC2 acts as an inverter and also is responsible to supply nonlinear loads connected to the AC side of the MMC2. The d and q components of nonlinear load currents can be expressed as,

$$i_{l(dq)}=I_{1dq}+\sum_{h=1}^{\infty}i_{l(dq)h}\tag{3.41}$$

The term of I_{1dq} is the fundamental component of load currents in d and q reference frame that is dependent on the MMC's CC. To specify the maximum values of I_{1dq} in which MMC is able to supply, the proposed CC can be used. If the total harmonic components of load currents in d-q reference frame are stated as (3.41),

$$\sum_{h=1}^{\infty}i_{l(dq)h}=i_{l(dq)}\left(1-\frac{\omega_{(dq)2}}{s+\omega_{(dq)2}}\right)\tag{3.42}$$

A LPF-based transfer function is used in (3.42) to obtain the harmonic components of load currents in the MMC2 side [95]. To perform a precise active and reactive power sharing of the MMC2, extracting properly the harmonic components is very important and thus an appropriate process of designing inner loop controller must be done as shown in Figure 3.5 (a). This figure is contained PI controllers as well as LPF in which their gains and cut-off frequency should be properly considered. The process of achieving the MMC1 reference values is illustrated in Figure 3.5 (b). As shown in Figure 3.5 (b), to complete the MMC1 reference values, the total reactive power of MMC1 loads Q_{l2} is used.

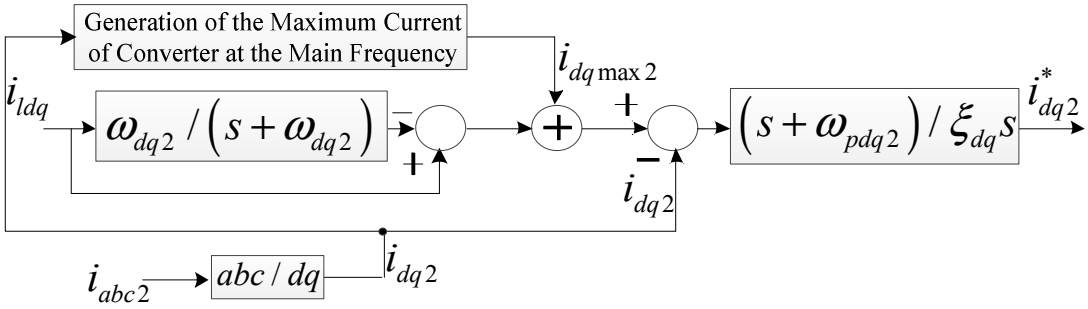

(a)

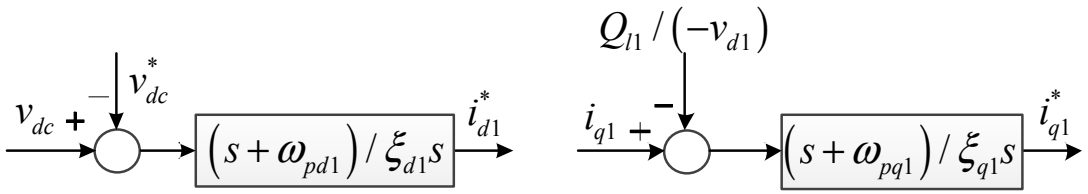

(b)

Figure 3.5 - The Proposed Inner Loop Controller for (a) the MMC2 reference currents (b) the MMC1 reference currents.

3.4 Convergence Evaluation and Stability Analysis

In this section, the ability of MMC2 in load compensation is investigated based on a transfer function established from the Figure 3.5 (a). Then, the DC-link voltage stability of the proposed model is assessed based on the dynamic equations obtained from Figure 3.1 (b).

3.4.1 The Load Compensation Capability Analysis of MMC2

In order to evaluate the capability of MMC2 for tracking the reference current components in d-q frame, the ratio of i_{dq2} and i^*_{dq2} are defined as the objective functions. Following equations describe the relations between the load current and the maximum value of currents of the MMC2 at the fundamental frequency,

$$i_{ldq2} = \alpha i_{ldq2} \ , \ i_{\mathrm{dq\,max\,2}} = \beta \left(\frac{\omega_{\mathrm{dq\,max\,2}}}{s + \omega_{\mathrm{dq\,max\,2}}} \right) i_{dq2} \tag{3.43}$$

By combination of (3.43) and the equation obtained from Figure 5 (a), following transfer function can be achieved,

$$H_{dq2}(s)=\frac{i_{dq2}}{i_{dq2}^{*}}=\frac{\xi_{dq}s^{3}+\xi_{dq}\left(\omega_{dq2}+\omega_{\mathrm{dq\,max\,2}}\right)s^{2}+\xi_{dq}\omega_{dq2}\omega_{\mathrm{dq\,max\,2}}s}{\left(\begin{array}{l}(\alpha-1)s^{3}+\left((\alpha+\beta)\omega_{\mathrm{dq\,max\,2}}-\left(\omega_{dq2}+\omega_{\mathrm{dq\,max\,2}}\right)+\omega_{pdq2}(\alpha-1)\right)s^{2}\\+\left((\beta-1)\omega_{dq2}\omega_{\mathrm{dq\,max\,2}}+(\alpha+\beta)\omega_{pdq2}\omega_{\mathrm{dq\,max\,2}}-\omega_{pdq2}\left(\omega_{dq2}+\omega_{\mathrm{dq\,max\,2}}\right)\right)s\\+(\beta-1)\omega_{pdq2}\omega_{dq2}\omega_{\mathrm{dq\,max\,2}}\end{array}\right)} \quad (3.44)$$

Equation (3.44) can be used to specify appropriate values for the utilized LPF, PI controller gains, α and β. For a normal operation, the values of α and β are almost in the range of 0 and 1, and also the LPF has the cut-off frequency of $\omega_{dq2}=\omega_{dq\,max\,2}=2\pi f_c(f_c=f_s/2)$, which promises the extraction of the DC part and also low harmonic components from the nonlinear load currents. Consequently, by analysing the transfer function of (3.44), the proportional and integral gains of the PI controller (i.e.,$1/\xi_{dq}$ and ω_{pdq}/ξ_{dq}) can be calculated.

3.4.2 Dynamic Model Analysis of the DC-Link Voltage

Dynamic model analysis of the DC-link voltage is investigated to validate the appropriate performance of the proposed HVDC model shown in Figure 3.1 (b). By applying KCL's into the point A, following equation can be obtained [40],

$$C_{eq}\frac{dv_{dc}}{dt}=-\frac{v_{dc}}{R_{dc}}+i_{dc1}-i_{dc2} \quad (3.45)$$

The relationship between the MMCs DC-link and AC side voltages is presumed to be: $i_{dcj}v_{dc}=v_{dtj}i_{dj}+v_{qtj}i_{qj}$. Then, (45) can be rewritten as,

$$C_{eq}\frac{dv_{dc}}{dt}=-\frac{v_{dc}}{R_{dc}}+\frac{\left(v_{dt1}i_{d1}+v_{qt1}i_{q1}\right)-\left(v_{dt2}i_{d2}+v_{qt2}i_{q2}\right)}{v_{dc}} \quad (3.46)$$

By neglecting the instantaneous power on impedances of MMCs, the term $v_{dtj}i_{dj} + v_{qtj}i_{qj}$ is approximately equal to $v_{dj}i_{dj}$; and consequently, (3.46) can be simplified as,

$$C_{eq}\frac{dv_{dc}}{dt} = \frac{-v_{dc}^2 + R_{dc}\left(P_1 - P_2\right)}{R_{dc}v_{dc}} \tag{3.47}$$

The zero dynamic stability of (3.47) is studied to verify the internal stability of the proposed model. The zero dynamic value of DC-link voltage is obtained by $dv_{dc}^*/dt = 0$. Therefore,

$$v_{dc}^* = \sqrt{R_{dc}^*\left(P_1^* - P_2^*\right)} = \sqrt{R_{dc}^*}\sqrt{\left(i_{d1}^* v_{d1}^* - i_{d2}^* v_{d2}^*\right)} \tag{3.48}$$

Equation (3.48) confirms that the desired value of DC-link voltage does entirely rely on the accurate control of active power for the MMCs. In addition to the precise values for the d-component of MMCs currents, the output AC voltages of MMCs required to be finely regulated in order to achieve a desired DC-link voltage. To plot the phase diagram of the DC-link voltage, (3.47) is rearranged as,

$$\begin{aligned} &\frac{dv_{dc}}{dt} = \frac{-v_{dc}^2 + R_{dc}\left(P_1 - P_2\right)}{R_{dc}C_{dc}v_{dc}} = \frac{-v_{dc}^2 + a}{bv_{dc}} \\ &a = R_{dc}\left(P_1 - P_2\right), b = R_{dc}C_{dc} \end{aligned} \tag{3.49}$$

The phase diagrams for dynamic equation of the DC-link voltage are depicted in Figure 3.6. As can be seen, the zero dynamic value of HVDC system DC-link voltage is completely stable in both states, which confirms that the proposed HVDC model reaches a desired DC-link voltage in different operation scenarios.

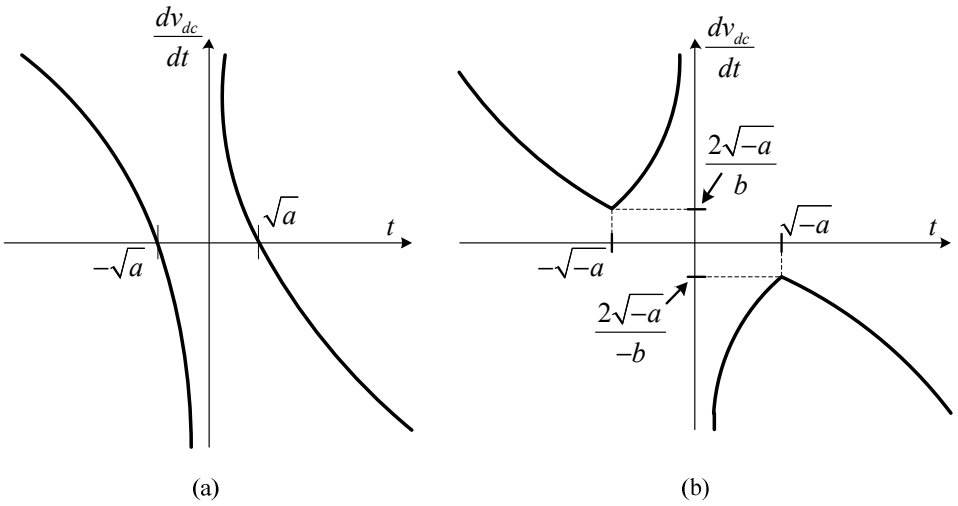

Figure 3.6 - The phase diagrams of the DC-link voltage (a) a>0 and (b) a<0.

3.5 Convergence Evaluation and Stability Analysis

The ability of the proposed multi-loop controller is evaluated in this section. For this, a three-level MMC-HVDC system is considered based on the proposed model in Figure 3.1 (a) and is modelled in the Matlab/Simulink environment in discrete-time mode with sample time of $20\mu s$. Stringent and comprehensive simulation results are provided in this section, alongside a solid mathematical background, to validate operation of the proposed control technique in HVDC power system. Simulation results are presented in order to confirm high performance of the proposed control technique in DC-link voltage control, capacitor voltage balancing, and circulating current minimization. In addition, performance of the proposed MMC-based HVDC model in Figure 3.1 (a) including power and control subsystems are evaluated under various operating conditions. System parameters are provided in Table 3.1 and the schematic diagram and principle of the proposed control technique in MMC-HVDC system is shown in Figure 3.7.

Table 3.1 – Simulation Parameters

f_{ac}	60 Hz	C	25mF
f_s	10 kHz	C_{fi}	615μF
v_{dc}	42kV	R_{dc}	4kΩ
v_c	14kV	P^{μ}, Q^{μ}	150MW ,75MVAR
L_{jk}	25mH	Transformer power rating	23kV/130kV (Δ/Y)
R_{jk}	1Ω	load I of MMC1	65MW,-20MVAR
L_k	6mH	load II of MMC1	70MW,80MVAR
R_k	0.3Ω	load I of MMC2	20MW,7MVAR
n	3	load II of MMC2	30MW,20MVAR
Grid Resistance	0.3 Ω	HVDC line Inductance	10 mH
Grid Inductance	3 mH		

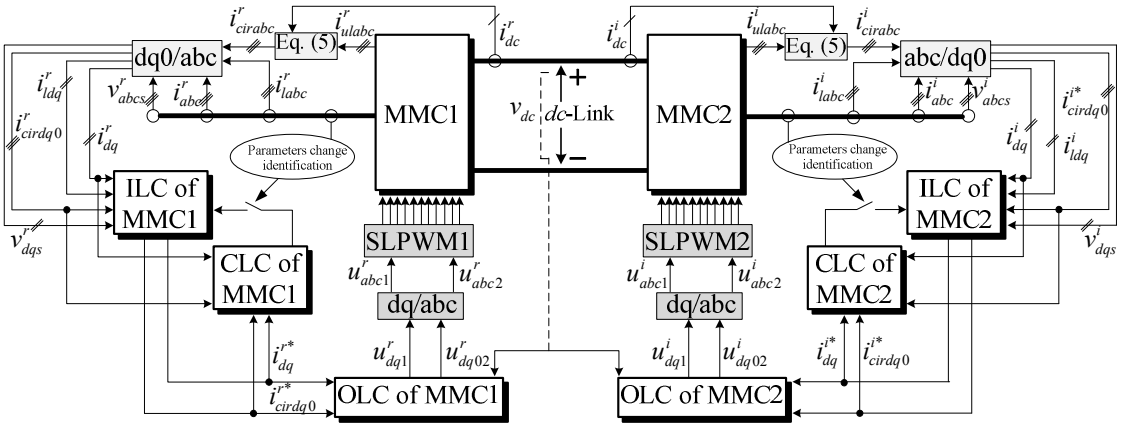

Figure 3.7 - Block diagram of the proposed control technique for the MMC-HVDC system in Figure 3.1.

3.5.1 The Load Variations Based Assessment of the Proposed Control Technique

Dynamics and steady state responses of the proposed model including assigned parameter values in table I are evaluated in this subsection. The scenarios for evaluation of OLC and ILC performance during the load changes are defined as following. At the beginning, in the time interval of 0<t<1/2 sec, a 65MW-j20MVAR load and a 20MW+j7MVAR load are connected to the AC sides of MMC1 and MMC2 respectively and the MMCs are supplying these loads in the steady state operating conditions. This process is continued up to t=1/2 sec where a step load increment is occurring for both MMCs so that in the time interval of 1/2<t<1 sec, a 70MW+j80MVAR load and a 30MW+j20MVAR load are added to the prior loads of MMC1 and MMC2 respectively. The phase "a" of the upper and lower switching functions of MMCs can be seen in Figure 3.8. As it can be observed from this figure, the upper and lower switching functions of MMC2 experiences a little more transient response because of more responsibilities of MMCs in supplying load variations. These switching functions are employed for SLPWM of MMCs in HVDC system. Figure 3.9 shows the DC-link voltage of the system, which is subject to the change of power demand. However as evident, it is regulated with minimum fluctuations (maximum 0.05 kV) around its nominal value at 42 kV. In addition, during the entire processing time, the SM capacitor voltages of both MMCs are kept balanced around their desired values of $v_{dc}/3$ (v_{dc}/N for $N = 3$) with very low ripples considering its response to the power variations.

Figure 3.10 shows three phase balanced AC voltages of MMCs in the proposed HVDC system in the steady state operating condition. As shown in this figure during load variations, the AC voltages of MMCs maintain sinusoidal waveforms without any noticeable distortions. The quality of the proposed control technique to minimize circulating currents of converter arms is demonstrated in Figure 3.11. As given in the figure, the circulating currents of MMCs are reduced to small values during both dynamic and steady state operating conditions. The dynamic response of the proposed control technique to the step variations in active and reactive power commands is shown in Figure 3.12. As it can be seen, MMC1 is almost set at the desired values with 65 MW and -20 MVAR. MMC2 produces the active power required for line resistances and nonlinear load I and also sinks the reactive power generated by the output filter to allow the voltage to settle the desired output voltages as depicted in Figure 3.10. Injected active and reactive power from MMC1 follows the load power variations, which confirms merits of the proposed OLC and ILC closed-loop controllers in control of interfaced MMC in the proposed HVDC model.

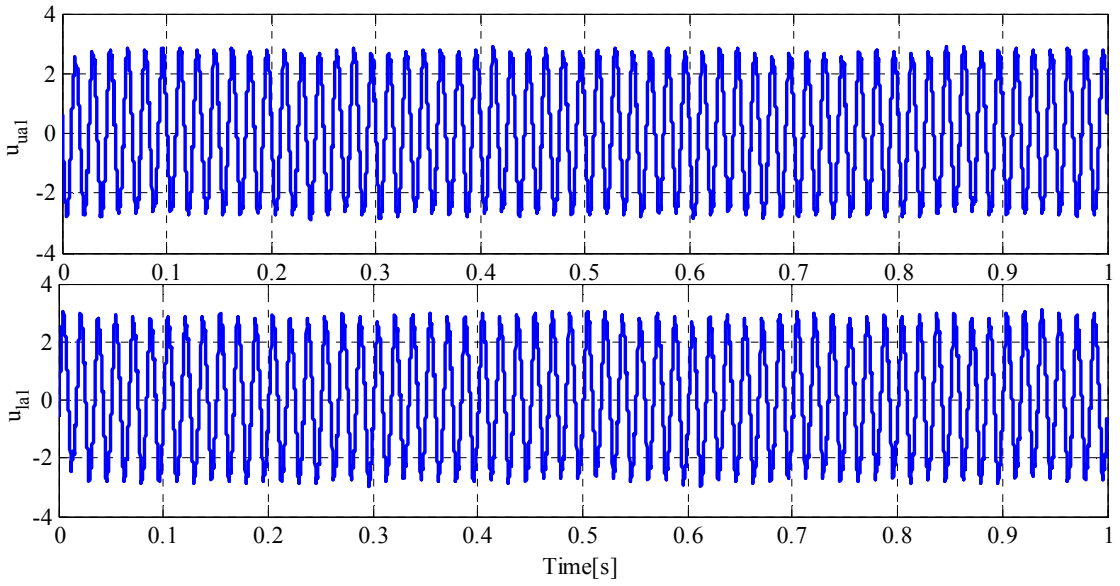

(a)

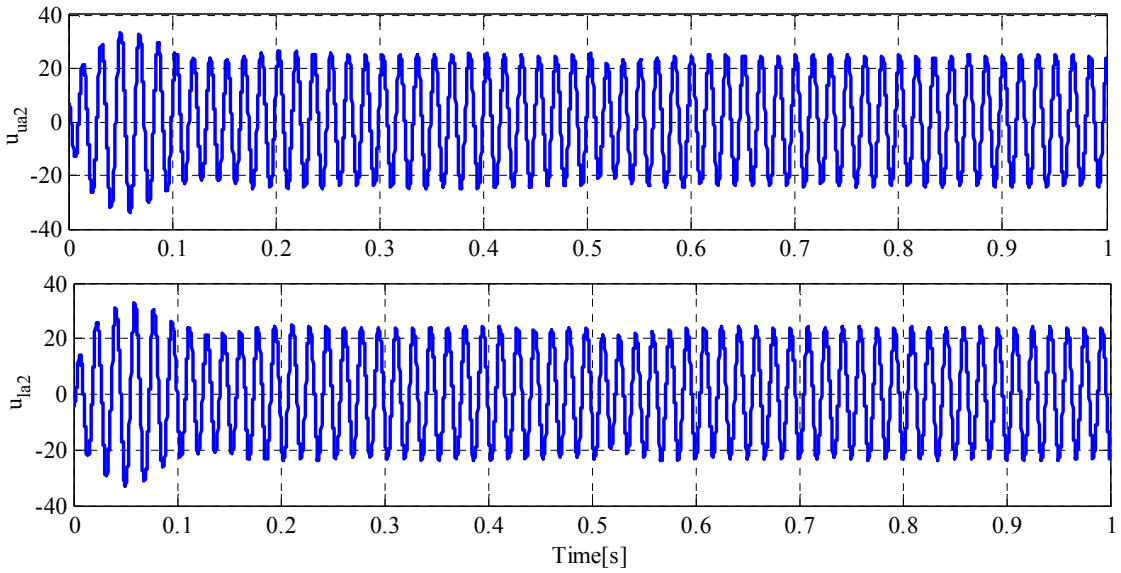

(b)

Figure 3.8 - The upper and lower switching functions of phase "a' of (a) MMC1 (b) MMC2, under load changes.

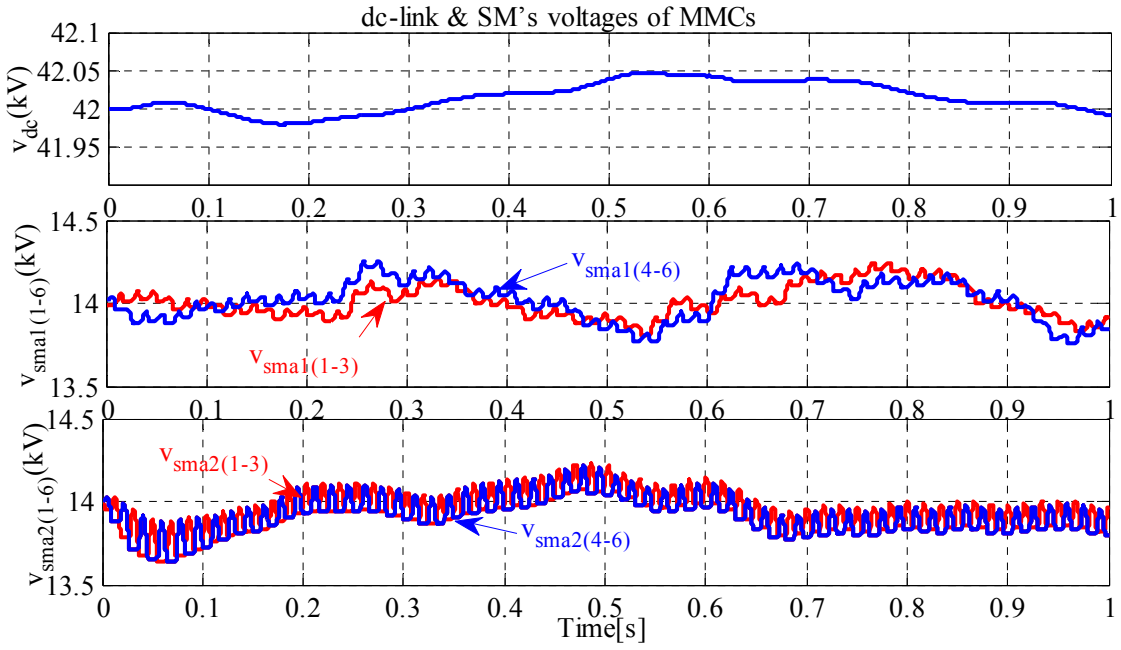

Figure 3.9 - MMCs DC-link and Sub-Module's voltages with load changes.

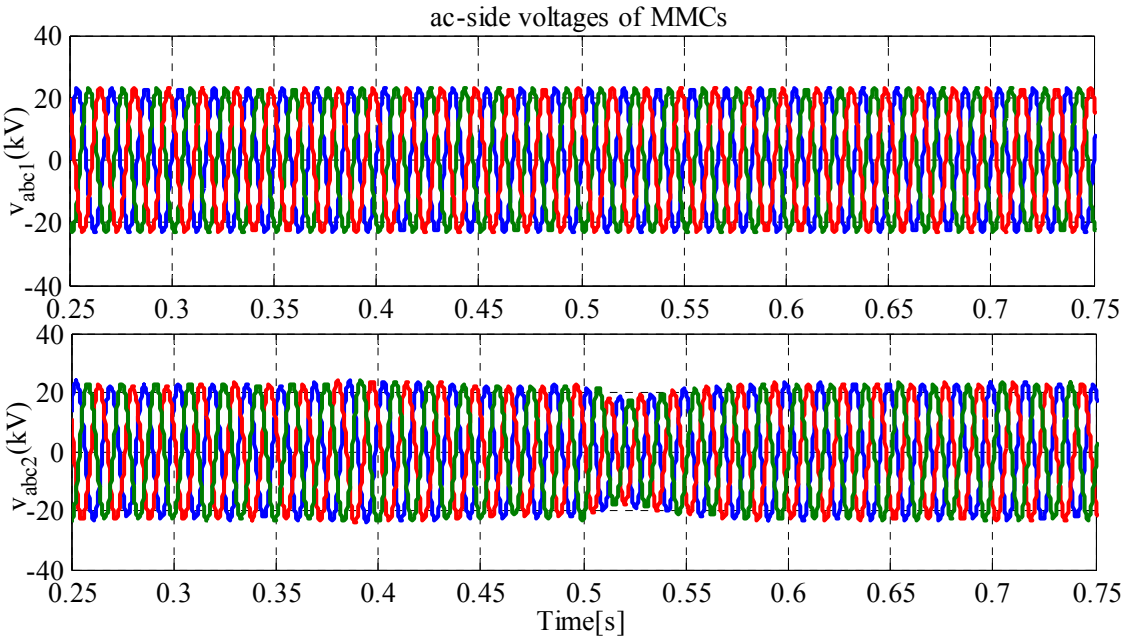

Figure 3.10 - MMCs AC voltages with load changes.

Figure 3.12 indicates the capability of the proposed control technique to pursue a consecutive increment through MMC2 during the dynamic operating condition. As it can be seen, MMC2 is able to generate required active power of additional loads with a short transient time. Reactive power changes of MMC2 is proportional to output filter variations for reaching a balanced three phase voltage.

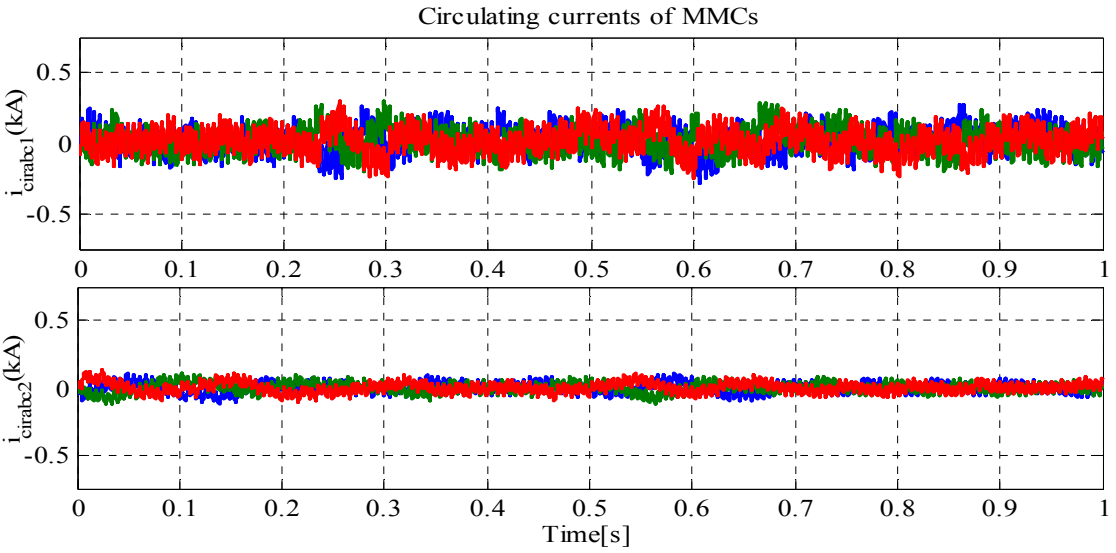

Figure 3.11- MMCs Circulating currents with load changes.

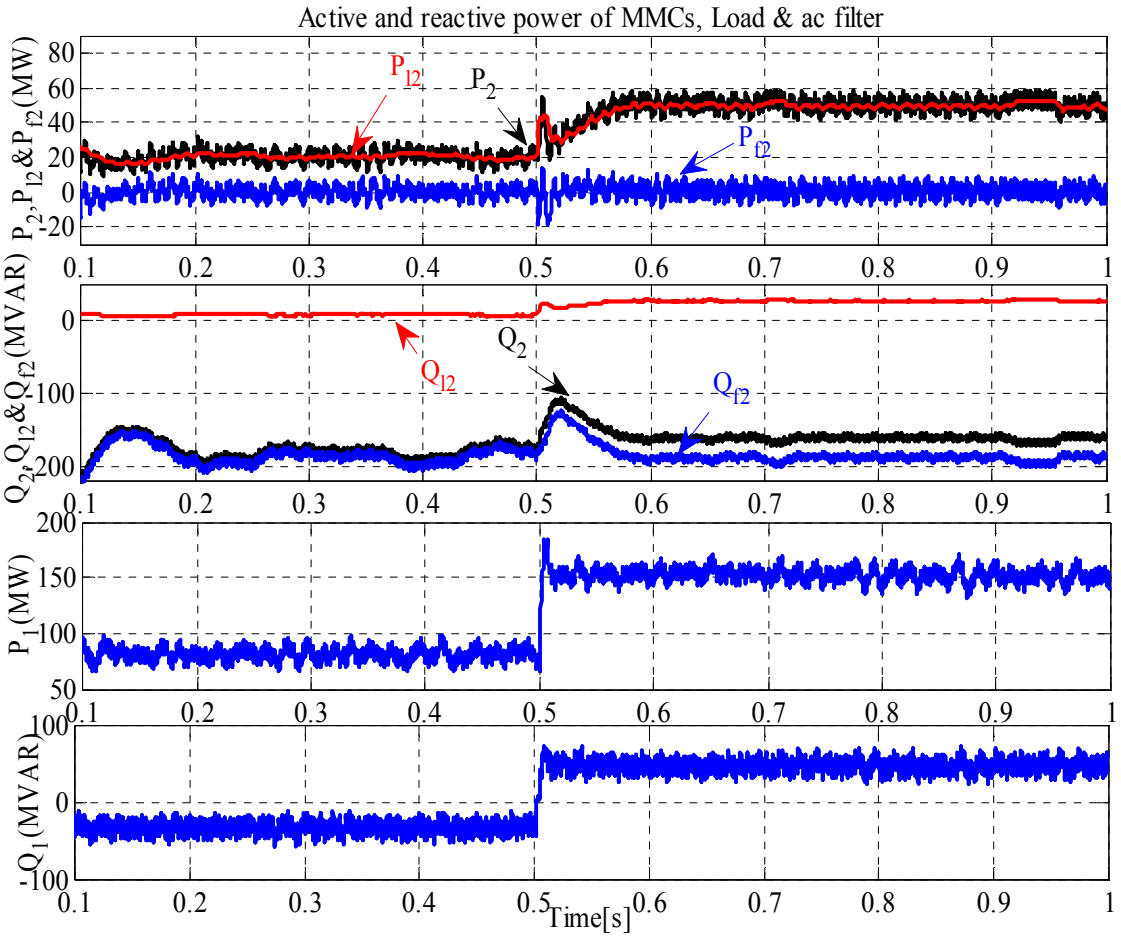

Figure 3.12 - Active and reactive power of MMCs, load, and AC filter with load changes.

3.5.2 The Parameter Variations Based Assessment of the Proposed Control Technique

The designed central loop controller operation of the MMCs once dealing with the parameter change is evaluated in this subsection. Figure 3.13 shows the changes in resistances and inductances of MMCs considered in this sub-section.

Figure 3.14 illustrates the upper and lower switching functions of the phase "a" of MMC1 and MMC2 under parameters changes. For both upper and lower switching functions, more transient state can be seen in the middle of the MMC's parameters changes and more stability is governed in the other time interval of MMC's parameters variations. The DC-link voltage of the proposed HVDC system and SM capacitor voltages of MMCs in presence of MMC parameters variations are depicted in Figure 3.15. Based on this figure, the reference values can be followed by the proposed controller with allowable transient response which verifies the accurate operation of both designed CLC and ILC.

In this condition, three phase balanced AC voltages can be properly generated by MMCs as shown in Figure 3.16. The MMCs circulating currents are shown in Figure 3.17. According to this figure, the proposed controller is able to minimize MMCs circulating currents within acceptable values along with slight transient responses in the time of dynamic change.

In presence of parameters variations, the loads of 140MW+j45MVAR and 35MW+j25MVAR are supplied through MMC1 and MMC2, respectively as depicted in Figure 3.18. As it can be observed from Figure 3.18, the active and reactive power sharing of both MMCs can be accomplished. However, some slight changes happen for both active and reactive power of MMCs because of reactive and resistance variations that are located in acceptable range according to Figure 3.18.

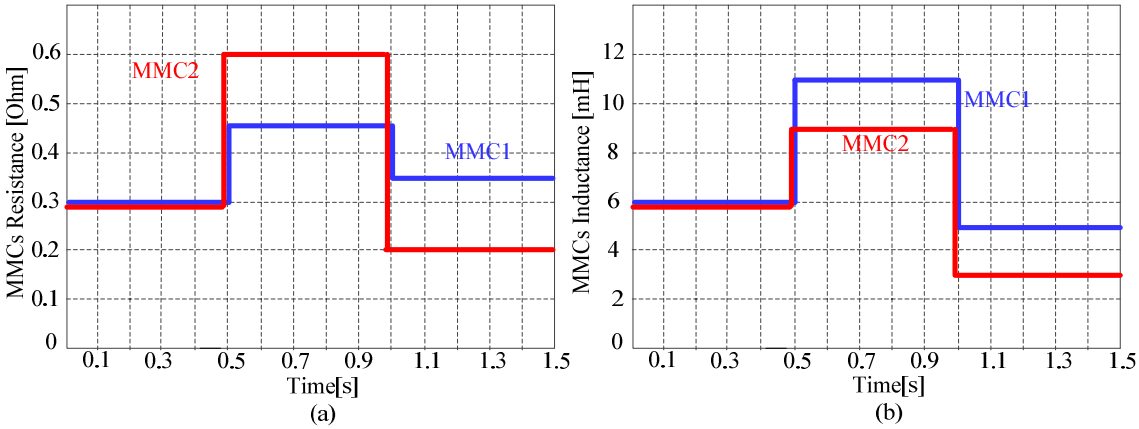

Figure 3.13 - Parameters changes for (a) the resistance of MMCs (b) the inductance of MMCs.

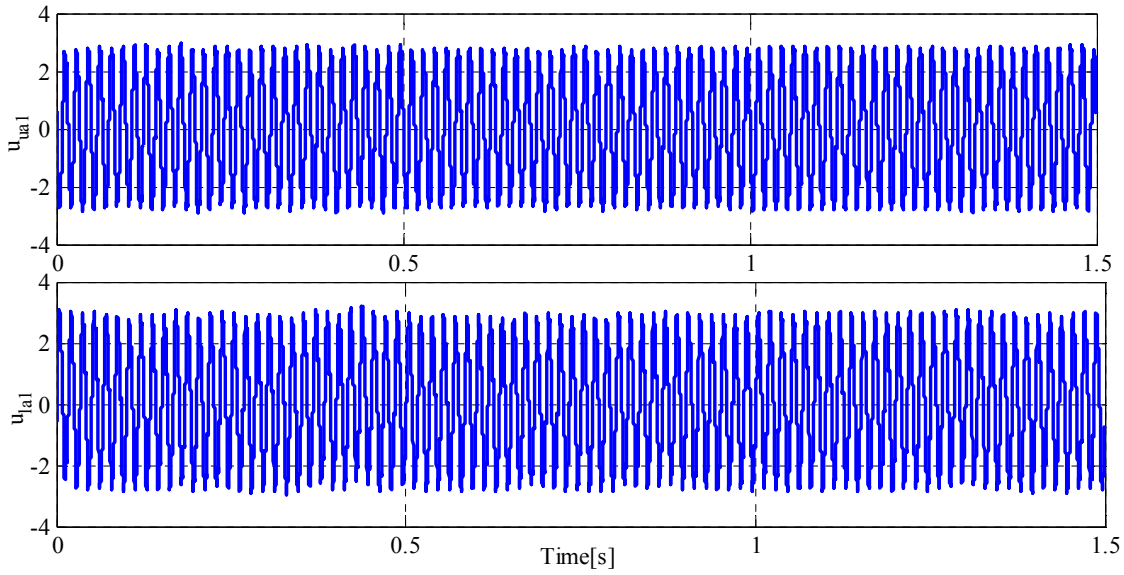

(a)

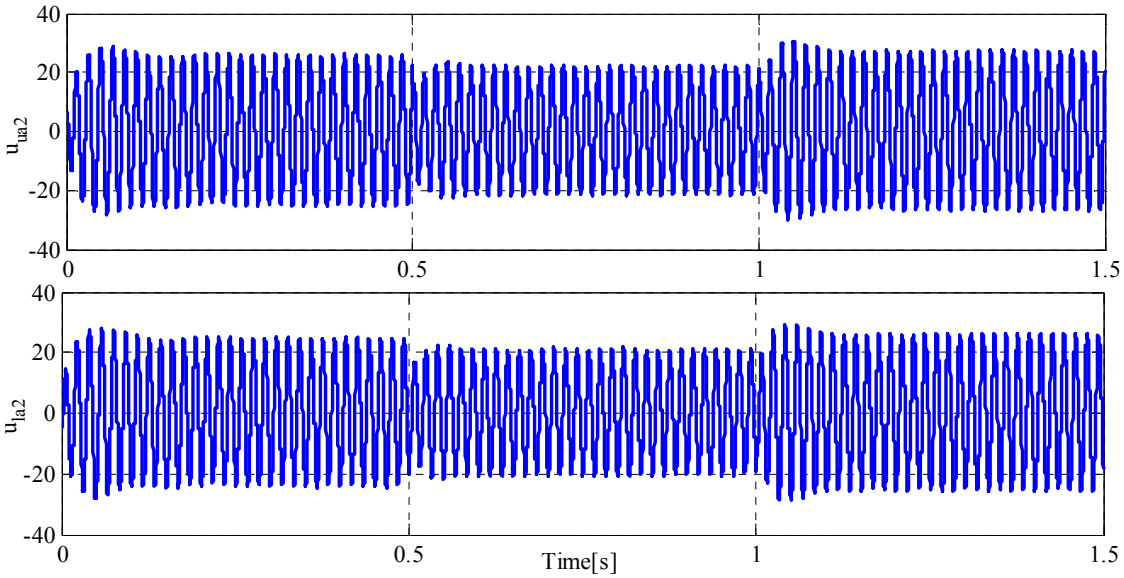

(b)

Figure 3.14 - The upper and lower switching functions of phase "a'' of (a) MMC1 (b) MMC2, under MMC parameters changes.

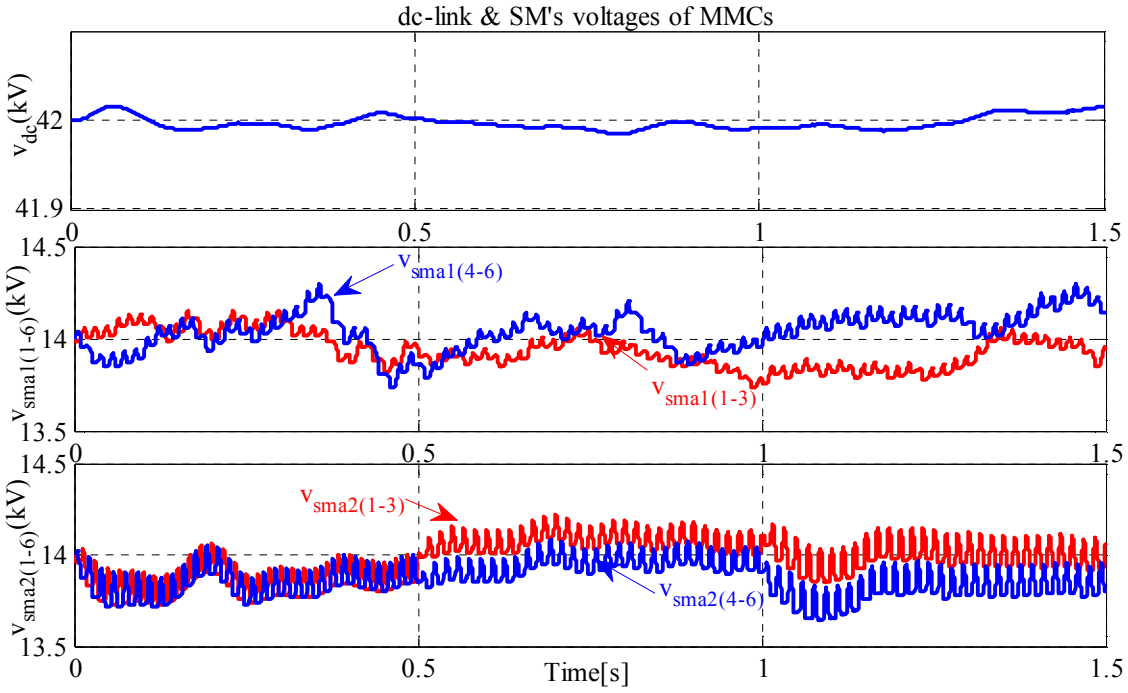

Figure 3.15 - MMCs DC-link and SM's voltages with parameters changes.

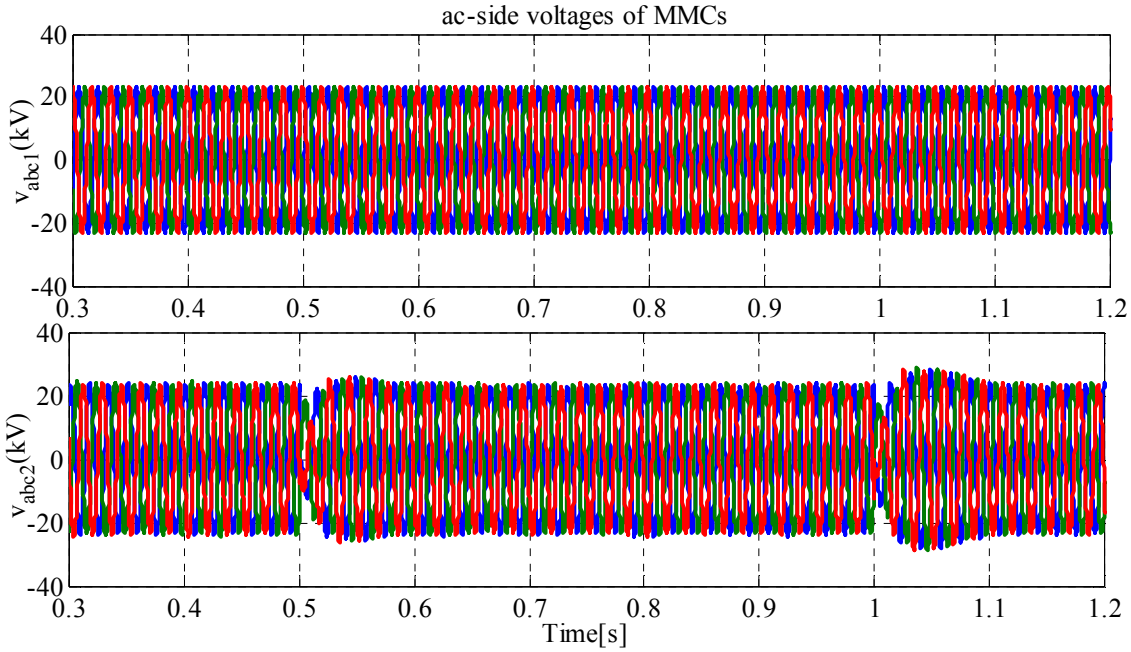

Figure 3.16 - MMCs AC voltages with the parameters changes.

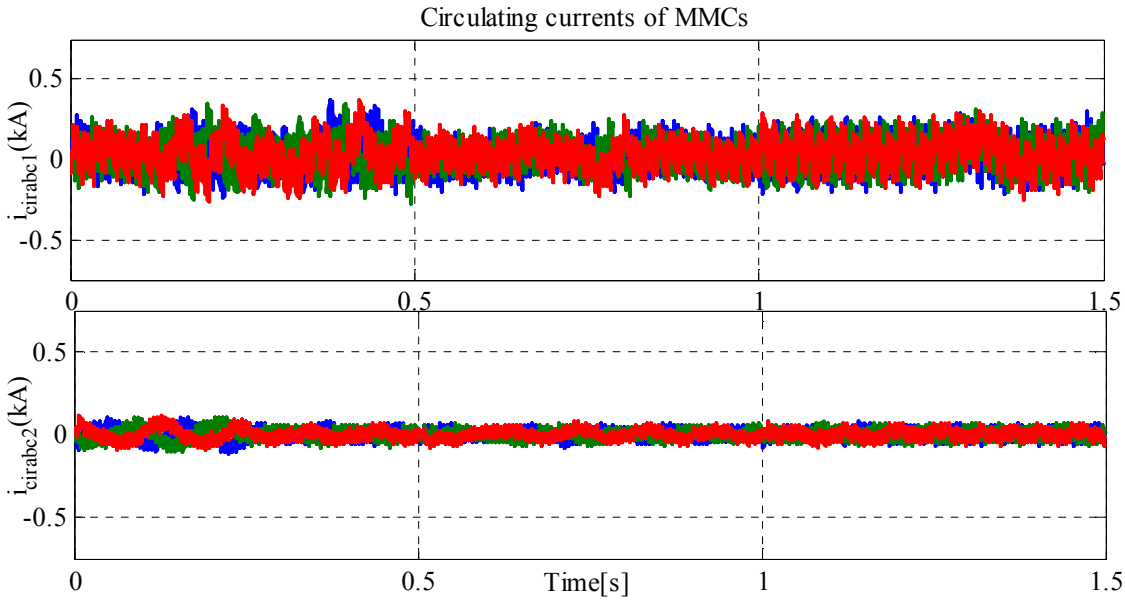

Figure 3.17 - MMCs circulating currents with parameters changes.

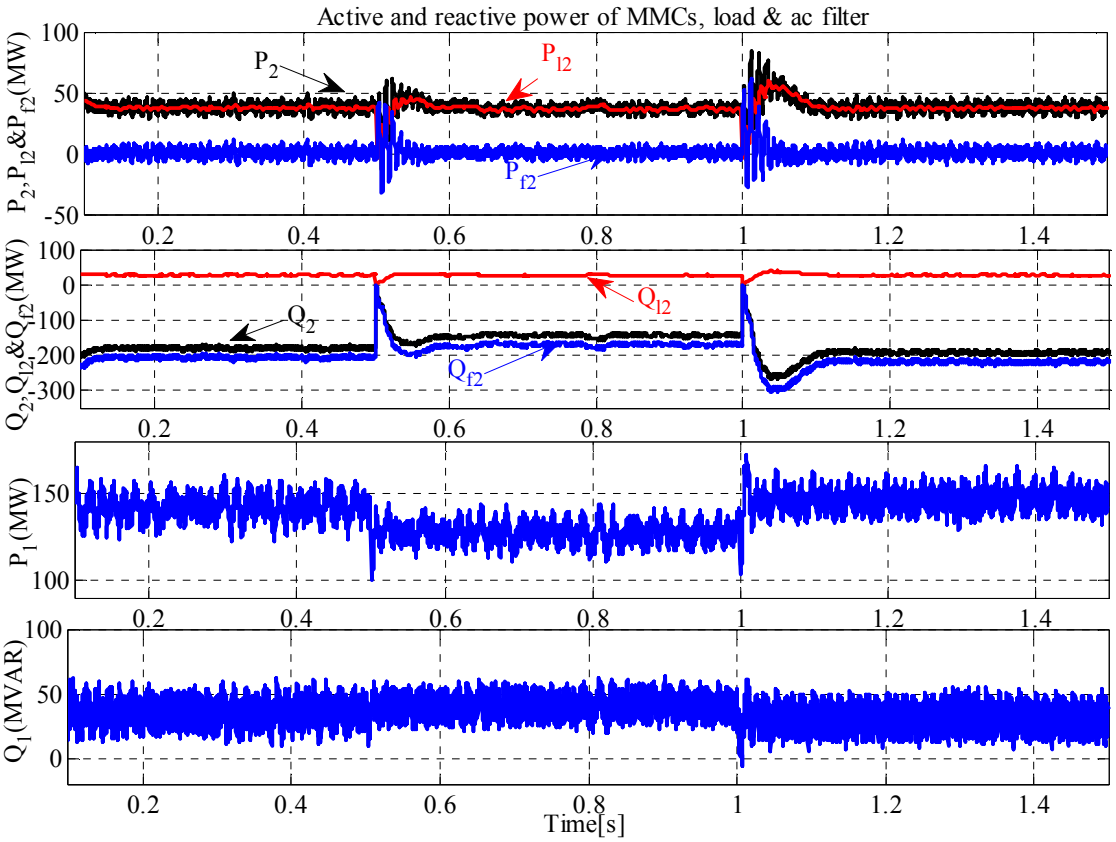

Figure 3.18 - Active and reactive power of MMCs, load, and AC filter with parameters changes.

3.6 Chapter Conclusions

A multi-loop control strategy for the stable operation of MMCs in HVDC system was proposed in this chapter under both load and MMCs parameters variations. Firstly, a six-order dynamic equation was achieved for both MMCs and subsequently a curve based on active and reactive power of MMC was introduced to analyze in depth the MMCs capability of generating both powers. Based on this dynamic model, as the first advantage, a capability curve based on MMC active and reactive power was proposed and the R and L variations effects on the curve were assessed that could provide some control considerations to understand more about the simulation results of the MMC's performance. To design the first loop of the proposed controller, the passivity based control technique was employed to shape OLC for increasing the MMCs convergence ability in dynamic changes. In the next step, to add the robustness feature against MMCs parameters changes, the sliding mode controller was considered to shape the central loop controller. As the second important advantage of the proposed controller, it was able of simultaneously being robustness against MMC´s arm inductance and resistance variations and also having very good dynamic tracking responses against the MMC's load changes. As the third feature of the proposed controller, accurate reference values for MMCs state variables were generated through the inner loop controller using appropriate LPF and regulated PI controllers that could generate instantaneously the requested reference values of both MMCs in all considered operating conditions. To further analyze the MMC based HVDC system, the DC-link voltage stability study was also carried out. Finally, to confirm the validity of the proposed control technique, Matlab/Simulink was used to achieve stringent simulation results of MMCs based HVDC system under both load and MMCs parameters changes.

Chapter 4

Function-Based Modulation Control for Modular Multilevel Converters under Varying Loading and Parameters Conditions

This chapter presents a new function-based modulation control technique for modular multilevel converters (MMC). The main contribution of the study is the formulation of two new modulation functions for the required switching signals of the MMC's upper and lower sub-modules, respectively. The output and circulating current equations of the converter are employed to attain the arm's currents which are utilized for the proposed modulation functions, having two important features: i) it is much less complex compared to the existing control methods of MMC; and ii) the proposed controller can be regulated properly to deal with parameter variations in a bid to ensure stable and accurate performance. In this controller, the MMC output current magnitude and phase angle required for special active and reactive power sharing can be easily applied to the modulation functions. Also, the equivalent capacitors of upper and lower sub-modules are discussed based on the proposed modulation functions. Finally, simulations are performed in Matlab/Simulink environment to evaluate the performance of the proposed control technique in both the dynamic conditions of load as well as varying parameters.

4.1 Introduction

The high attentions to renewable energy resource-based distribution generation systems [96]-[98] lead to considering multilevel converter for high power generation. Various characteristics of modular multilevel converters (MMCs) in high-power and medium-voltage applications lead to the essential need to design appropriate controllers [43], [99]-[101] and proposing effective modulation techniques [50], [102], for these kinds of converters. One of the significant trends for controlling the MMC is to present a dynamic model based on the considered state variables of the controller. For example, in [103], the sum of the capacitor voltage in each arm is used instead of the individual capacitor voltages to shape the MMC model. To complete the MMC evaluation, an effective DC-bus model from the sub-module capacitors is derived in [103]. For a grid-connected MMC, a natural charge level mechanism for branch capacitor voltages as well as the branch power equations based on the consumed active and reactive power in the respective resistance and inductance are investigated in [49]. The study, in addition to enhancement of the voltage ripple estimation concept using accurate model, two independent explicit control loops have also been designed for the line and circulating currents in a decoupled manner.

Another dynamic model-based assessment for the MMC-based multi-terminal HVDC (MTDC) system is performed in [104]. Two different dynamic models are proposed in the study. The first dynamic model of MMC-MTDC system is included the AC side circuit, the inner controllers, the modulation strategies, the outer controllers and the MTDC circuit. The second one as a simplified model contains the outer controllers and partial dynamics of the MTDC circuit based on a quantitative analysis of the detailed model's dynamic processes [104].

In addition to proposing a continuous equivalent model [47], a corresponding single-phase circuit and a load model consisting of current sources [71], and a dynamic model with four independent dynamical components of the arm currents with the effect of AC and DC systems [105]. Others include a discrete-time mathematical model with a predictive model [84], a linearized analytical models with droop control [106] for MMCs under balanced conditions, and other literatures that present more dynamic models and respective controllers for assessment of the MMC operation under other operating conditions [107]–[109].

Similarly, a number of new pulse-width modulation (PWM) techniques and capacitor voltage balancing methods have been proposed to control MMCs in different industrial applications [110], [111]. A phase-disposition (PD) sinusoidal PWM strategy with a voltage balancing method [112], a voltage-balancing control method with phase shifted carrier-based PWM [113], an improved PWM method of which no phase-shifted carrier is needed [114] and a modified nearest level modulation method with the increased level number of AC output voltage [115] have been employed for MMCs. In [116], a discontinuous modulation technique based on adding a zero-sequence to the original modulation signals is proposed which can achieve a significant reduction in the capacitor voltage ripples as well as in the switching power losses for most of the operating points.

To avoid the major drawbacks of the present voltage balancing methods, such as voltage sorting algorithm, extra switching actions, interference with output voltage, the authors of [117] proposed an improved PWM based general control structure for the MMC inverters. The designed control technique is appropriate for both voltage-based and energy-based control methods, and also includes voltage balancing between the upper and lower arms [117]. With the aim of dominating the magnitude modulation for few numbers of cells and also reducing the sorting efforts for cell balancing purposes, tolerance band methods are used for MMC in [118] to obtain switching instants and also cell selection. Moreover, two different modulation patterns for multilevel selective harmonic elimination (MSHE) PWM as well as a method for selecting the number of sub-modules are proposed for control of MMC operation [119]. Among the different control and modulation methods for MMCs [120], multi-carrier PWM techniques have an effect not only on output waveforms and number of levels derived out of a given configuration of the MMC but also on DC-link voltage and arm currents of the converter [121].

In this chapter, two new modulation functions are proposed for control of the MMC operation in inverter mode which can appropriately achieve the main control purposes included regulating the sub-modules voltages and executing accurate active and reactive power sharing. These modulation functions are obtained by making the circulating currents approach zero value and using the arm's currents in the basic differential equations of the MMC in a-b-c reference frame. Moreover, the effects of the MMC parameters and currents changes are considered as the assessment factors of the proposed modulation functions performance in both steady-state and dynamic conditions. In addition, using the proposed functions, the instantaneous powers of the MMC arms and the equivalent capacitors of the upper and lower sub-modules are evaluated. Simulation results are presented to justify the proposed modulation-based method.

4.2 The Proposed Modulation Functions

The basic structure of the proposed three-phase MMC considered in the chapter is shown in Figure 4.1 (a). The DC-link voltage generates the input power needed for the MMC operation. Each arm consists of resistance and inductance, and N series-connected sub-modules, illustrated in Figure 4.1. (b). Each sub-module acts as a voltage source which is actually a half-bridge rectifier with determined output capacitor corresponding to its required DC voltage. Based on Figure 4.1 (b), complementary state exists for the upper and lower switches of the sub-module. It means that if the upper switch is on, the lower switch will be off and vice versa. Moreover, the output of MMC contains inherent resistance and filter inductance. A point of common coupling (PCC) is considered in the proposed MMC in stand- alone mode as depicted in Figure 4.1 (a), to which the output capacitance filter and the consumable three-phase load are connected. The following discusses the process of obtaining the proposed modulation function for the described MMC.

4.2.1 Calculation of The MMC' Arms Currents

According to Figure 4.1 (a), supposing that MMC is controlled to reach sinusoidal output voltages at PCC and supply full three-phase load as a linear load. Thus, based on the needed active and reactive power of the load and the above conditions, the output voltage and current of MMC can be written as,

$$\begin{aligned} v_k &= v_m \cos\left(\omega t + j\frac{2\pi}{3}\right) \\ i_k &= I_m \cos\left(\omega t + j\frac{2\pi}{3} + \alpha\right) \end{aligned} \tag{4.1}$$

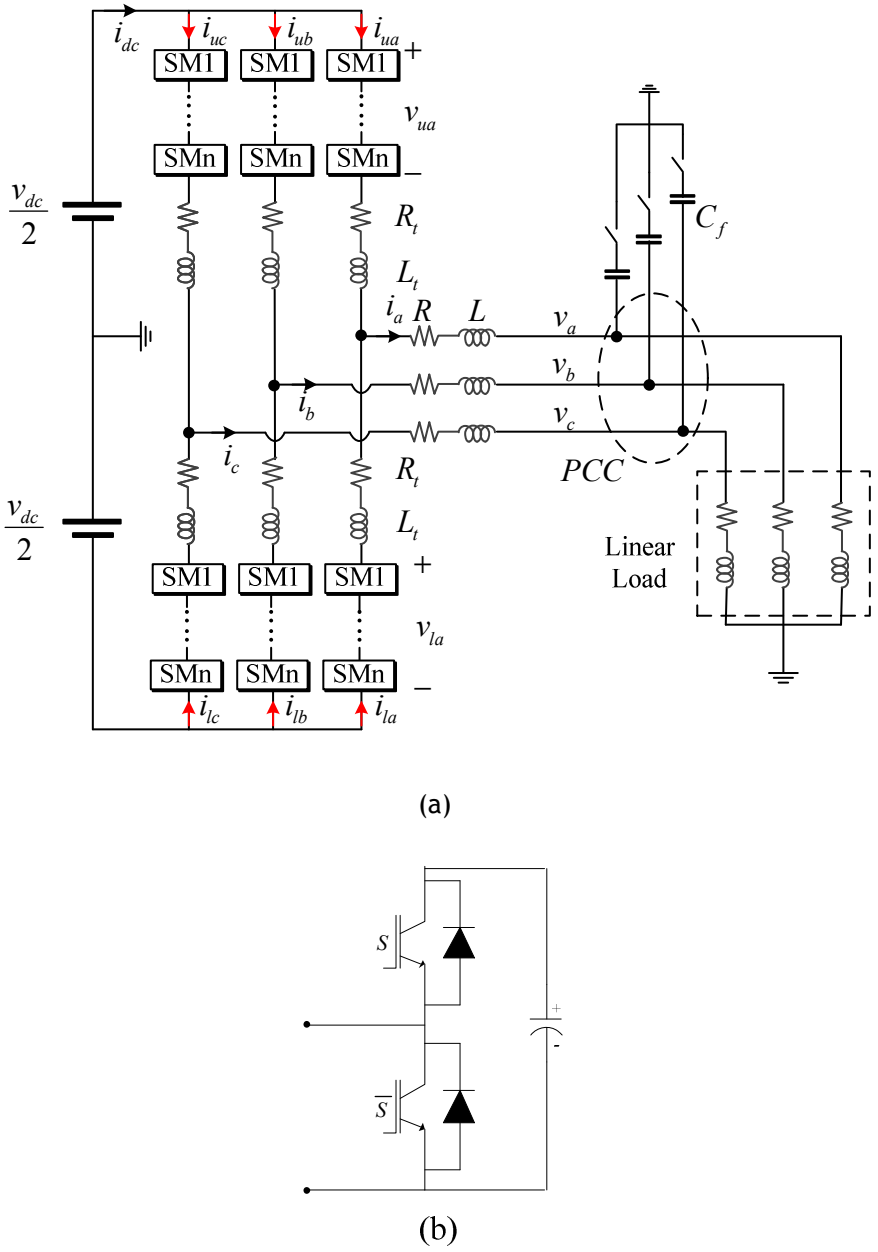

Figure 4.1 - (a) The MMC topology used, (b) sub-module.

The phase angle, α is the determining variable for generating the required active and reactive power of the load in different operating conditions. From Figure 4.1 (a), the relations between output and arm's currents of MMC and also circulating currents can be written as,

$$i_k = i_{uk} + i_{lk} \tag{4.2}$$

$$i_{cirk} = \frac{\left(i_{uk} - i_{lk}\right)}{2} - \frac{i_{dc}}{3} \tag{4.3}$$

For a controlled MMC with accurate operation, the circulating currents should approach zero. Consequently, by applying $i_{cirk} = 0$ to (4.3) and solving two equations achieved from (4.2) and (4.3), the currents of the upper and lower arms of the MMC can be written as,

$$i_{uk} = 0.5I_m \cos\left(\omega t + j\frac{2\pi}{3} + \alpha\right) + i_{dc}/3 \tag{4.4}$$

$$i_{lk} = 0.5I_m \cos\left(\omega t + j\frac{2\pi}{3} + \alpha\right) - i_{dc}/3 \tag{4.5}$$

It is understood from (4.4) and (4.5) that each arm's current is combined with the output AC and input DC currents.

4.2.2 The Proposed Modulation Function

For accurate control of the MMC, a well-designed pulse width modulation should be set. Therefore, two reference waveforms for upper and lower sub-modules of the MMC are proposed in this sub-section to perform a complete switching samples in the used shift-level PWM. Taking into account the neutral point of the DC link in Figure 4.1 (a), and using KVL's law in the determined direction, equations of (4.6) and (4.7) are achieved as,

$$\frac{-v_{dc}}{2} + v_{uk} + L_t\frac{di_{uk}}{dt} + R_t i_{uk} + L\frac{di_k}{dt} + Ri_k + v_k = 0 \tag{4.6}$$

$$\frac{v_{dc}}{2} - v_{lk} + L_t\frac{di_{lk}}{dt} + R_t i_{lk} + L\frac{di_k}{dt} + Ri_k + v_k = 0 \tag{4.7}$$

Substituting (4.1) and (4.4) into (4.6) and assuming $i_{dc} = I_{dc} + i_{dcrip}$, $di_{dcrip}/dt = \tilde{\imath}_{dcrip}$, $L_{eq} = 0.5L_t + L$ and $R_{eq} = 0.5R_t + R$, the upper sub-modules voltages of the MMC can be obtained as,

$$v_{uk} = \frac{v_{dc}}{2} - L_t \tilde{i}_{dcrip} / 3 - i_{dc} R_t / 3 + \left[I_m R_{eq} \sin(\alpha) + L_{eq} I_m \omega \cos(\alpha) \right] \sin\left(\omega t + j \frac{2\pi}{3} \right) + \left[L_{eq} I_m \omega \sin(\alpha) - I_m R_{eq} \cos(\alpha) + v_m \right] \cos\left(\omega t + j \frac{2\pi}{3} \right) \quad (4.8)$$

Using the relation below,

$$\gamma \sin(\omega t) + \lambda \cos(\omega t) = \sqrt{\gamma^2 + \lambda^2} \cos\left(\omega t + tag^{-1}(\lambda / \gamma) - \pi / 2 \right) \quad (4.9)$$

The proposed modulation function related to the switching signals of the upper sub-modules is established as (4.10),

$$u_{uk} = \frac{\frac{v_{dc}}{2} - L_t \tilde{i}_{dcrip} / 3 - i_{dc} R_t / 3 + V_{mu} \cos\left(\omega t + j \frac{2\pi}{3} + \theta_u - \pi / 2 \right)}{v_{dc}} \quad (4.10)$$

Please note that V_{mu} and θ_l are given in appendix A. Applying the same scenario for equation (4.7), the proposed modulation function for lower sub-modules is derived as (4.11),

$$u_{lk} = \frac{\frac{v_{dc}}{2} - L_t \tilde{i}_{dcrip} / 3 - R_t i_{dc} / 3 + V_{ml} \cos\left(\omega t + j \frac{2\pi}{3} + \theta_l - \pi / 2 \right)}{v_{dc}} \quad (4.11)$$

The variables V_{ml} and $\theta_l$are specified in Appendix B. These functions can be used for the MMC control in all operating conditions including both dynamic and steady states. The proposed modulation functions in steady state can be achieved by substituting the reference values of the MMC parameters and specifications in V_{mi} and θ_i as well as using the desired values of DC link voltage and current in (4.10) and (4.11).

4.3 Evaluation of the Instantaneous Power of the MMC Arms

To analyze the effects of the arm's currents obtained in (4.4) and (4.5) on the MMC operation, the instantaneous power of the arms is investigated in this section.

Each arm power of the proposed MMC can be included; instantaneous powers caused by sum capacitors used in the sub-modules as well as the resistance and inductance of the arms. Discussed next is the two types of power.

4.3.1 Calculation of The MMC' Arms Currents

As it can be seen in Figure 4.1 (a), the currents of the upper arms of the MMC enter the positive point of the upper sub-modules voltage. Thus, to comply with the power's law, the instantaneous power of the MMC's upper sub-modules can be written as,

$$p_{uk} = i_{uk} v_{uk} \tag{4.12}$$

Substituting the obtained current and voltage corresponding to the upper sub-modules into (4.12), we achieve equation (4.13) as,

$$\begin{aligned} p_{uk} &= \left(0.5I_m \cos\left(\omega t + j\frac{2\pi}{3} + \alpha\right) + i_{dc}/3\right) \times \left(\frac{v_{dc}}{2} - L_t \tilde{i}_{dcrip}/3 - i_{dc}R_t/3 + V_{mu}\cos\left(\omega t + \theta_u - \pi/2\right)\right) \\ &= 0.25 v_{dc} I_m \cos\left(\omega t + j\frac{2\pi}{3} + \alpha\right) - \frac{I_m L_t \tilde{i}_{dcrip}}{6}\cos\left(\omega t + j\frac{2\pi}{3} + \alpha\right) - \frac{i_{dc}R_t I_m}{6}\cos\left(\omega t + j\frac{2\pi}{3} + \alpha\right) \\ &+ 0.5 I_m V_{mu}\cos\left(\omega t + \theta_u - \pi/2\right)\cos\left(\omega t + j\frac{2\pi}{3} + \alpha\right) + v_{dc} i_{dc}/6 - L_t \tilde{i}_{dcrip} i_{dc}/9 \\ &- R_t i_{dc}^2/9 + \frac{i_{dc}V_{mu}}{3}\cos\left(\omega t + \theta_u - \pi/2\right) \end{aligned} \tag{4.13}$$

After some simplifications, the final equation of the instantaneous power of the MMC upper sub-modules can be obtained as,

$$
\begin{aligned}
&p_{uk} = \beta_{u0} + \beta_{u11}\cos\left(\omega t + j\frac{2\pi}{3} + \alpha\right) + \beta_{u12}\cos\left(\omega t + \theta_u - \pi/2\right) + \beta_{u2}\cos\left(2\omega t + \theta_u + \alpha - \pi/2 + j\frac{2\pi}{3}\right)\\
&\beta_{u0} = v_{dc}i_{dc}/6 - L_t\tilde{i}_{dcrip}i_{dc}/9 - R_t i_{dc}^2/9 + 0.25I_m V_{mu}\cos\left(j\frac{2\pi}{3} - \theta_u + \alpha + \pi/2\right)\\
&\beta_{u11} = 0.25I_m v_{dc} - \frac{I_m L_t \tilde{i}_{dcrip}}{6} - \frac{i_{dc}R_t I_m}{6}\\
&\beta_{u12} = \frac{V_{mu}i_{dc}}{3}\\
&\beta_{u2} = 0.25I_m V_{mu}
\end{aligned}
\tag{4.14}
$$

The same calculations are performed for the power of the lower sub-modules, and consequently,

$$
\begin{aligned}
&p_{lk} = -i_{lk}v_{lk} =\\
&\beta_{l0} + \beta_{l11}\cos\left(\omega t + j\frac{2\pi}{3} + \alpha\right) + \beta_{l12}\cos\left(\omega t + \theta_l - \pi/2\right) + \beta_{l2}\cos\left(2\omega t + \theta_l + \alpha - \pi/2 + j\frac{2\pi}{3}\right)\\
&\beta_{l0} = v_{dc}i_{dc}/6 - R_t i_{dc}^2/9 - i_{dc}L_t\tilde{i}_{dcrip}/9 - 0.25I_m V_{ml}\cos\left(j\frac{2\pi}{3} - \theta_l + \alpha + \pi/2\right)\\
&\beta_{l11} = -0.25I_m v_{dc} + \frac{i_{dc}R_t I_m}{6} - \frac{L_t\tilde{i}_{dcrip}I_m}{6},\ \ \beta_{l12} = \frac{V_{ml}i_{dc}}{3},\ \ \beta_2 = -0.25I_m V_{ml}
\end{aligned}
\tag{4.15}
$$

where, β_i in equations (4.14) and (4.15) are the coefficients of the instantaneous DC power and harmonic components which can be changed by the MMC's specifications such as parameters like currents and voltages. According to (4.14) and (4.15), the instantaneous powers of the upper and lower sub-modules comprise two parts: DC component and harmonic components at the main and second-order frequency of the MMC operating condition.

4.3.2 Instantaneous Power of the Arm's Resistance and Inductance

Another part of the MMC arm is associated with the arm resistance and inductance. From Figure 4.1 (a), the voltage of the upper arm resistance and inductance can be achieved as,

$$
v_{ux} = L_t\frac{di_{uk}}{dt} + R_t i_{uk} \tag{4.16}
$$

Substituting (4.4) in (4.16), the sum of the voltages of the upper arm resistance and inductance can be written as,

$$v_{ux} = -0.5 I_m L_t \omega \sin\left(\omega t + j\frac{2\pi}{3} + \alpha\right) + L_t \tilde{i}_{dcrip} / 3 + 0.5 I_m R_t \cos\left(\omega t + j\frac{2\pi}{3} + \alpha\right) + i_{dc} R_t / 3 \quad (4.17)$$

Thus, the power corresponding to this voltage can be obtained as,

$$p_{ux} = i_{uk} v_{ux} \quad (4.18)$$

Using (4.4) and (4.17), (4.18) can be rewritten as,

$$\begin{aligned} p_{ux} &= \beta_{xu0} + \beta_{xu11}\cos\left(\omega t + j\frac{2\pi}{3} + \alpha\right) + \beta_{xu12}\cos\left(\omega t + j\frac{2\pi}{3} + \alpha - \frac{\pi}{2}\right) \\ &+ \beta_{xu21}\cos\left(2\omega t + j\frac{4\pi}{3} + 2\alpha\right) + \beta_{xu22}\cos\left(2\omega t + j\frac{4\pi}{3} + 2\alpha - \frac{\pi}{2}\right) \end{aligned} \quad (4.19)$$

$$\beta_{xu0} = 0.125 I_m^2 R_t + \frac{L_t \tilde{i}_{dcrip} i_{dc}}{9} + \frac{i_{dc}^2 R_t}{9}$$

$$\beta_{xu11} = \frac{I_m L_t \tilde{i}_{dcrip}}{6} + \frac{i_{dc} R_t I_m}{3}, \quad \beta_{xu12} = -\frac{I_m L_t i_{dc} \omega}{6}$$

$$\beta_{xu21} = 0.125 I_m^2 R_t, \quad \beta_{xu22} = -0.125 \omega L_t I_m^2$$

Again, from Figure 4.1 (a), the below relation can be written for the voltage of the lower arm resistance and inductance as,

$$v_{lx} = L_t \frac{di_{lk}}{dt} + R_t i_{lk} \quad (4.20)$$

Consequently, performing the same scenario for the lower arm resistance and inductance voltage and observing the power law, the instantaneous power of the lower arm resistance and inductance can be achieved as,

$$p_{lx} = -i_{lk}v_{lx} = \beta_{xl0} + \beta_{xl11}\cos\left(\omega t + j\frac{2\pi}{3} + \alpha\right) + \beta_{xl12}\cos\left(\omega t + j\frac{2\pi}{3} + \alpha - \frac{\pi}{2}\right)$$
$$+\beta_{xl21}\cos\left(2\omega t + j\frac{4\pi}{3} + 2\alpha\right) + \beta_{xl22}\cos\left(2\omega t + j\frac{4\pi}{3} + 2\alpha - \frac{\pi}{2}\right)$$

$$\beta_{xl0} = -0.125I_m^2R_t - \frac{L_t\tilde{i}_{dcrip}i_{dc}}{9} - \frac{i_{dc}^2R_t}{9} \quad (4.21)$$
$$\beta_{xl11} = \frac{I_mL_t\tilde{i}_{dcrip}}{6} + \frac{I_mi_{dc}R_t}{6} + \frac{I_mR_ti_{dc}}{6}$$
$$\beta_{xl12} = -\frac{I_mL_t\omega i_{dc}}{6}, \beta_{xl21} = -0.125I_m^2R_t, \beta_{xl22} = 0.125I_m^2L_t\omega$$

where β_{xu} and β_{xl} are the DC and AC component coefficients of the upper and lower arm resistance and inductance instantaneous power. These coefficients are completely dependent on the MMC parameters and its operating conditions at the output and input sides. Thus, accurate calculation of these powers is considerably dependent on the proper operation of the MMC in different conditions of the steady and dynamic states, which can be achieved by executing the appropriate control technique.

4.4 Determination of $I_m$and α

It can be understood from the proposed modulation functions of (4.10) and (4.11) that the main parts of these functions are completely relevant to the specifications of the MMC output currents. On the other hands, considering the obtained equation related to arm's instantaneous powers, it can be seen that the magnitude and angle phase of the MMC output currents have significant effects on all power components. Thus, for presenting an accurate control strategy, the calculation of the output of the MMC current specifications is done in this section based on its rated output active and reactive power. The instantaneous active and reactive power of the proposed MMC are written as,

$$p_{3\varphi} = 1.5V_mI_m\cos(\alpha) \quad (4.22)$$

$$q_{3\varphi} = 1.5V_mI_m\sin(\alpha) \quad (4.23)$$

Dividing (4.23) by (4.22) and using the achieved phase angle in (4.22), the main parts of the MMC output current can be obtained as (4.24),

$$I_m = \frac{p_{3\varphi}}{1.5V_m \cos\left(\tan^{-1}\left(\frac{q_{3\varphi}}{p_{3\varphi}}\right)\right)}, \qquad \alpha = \tan^{-1}\left(\frac{q_{3\varphi}}{p_{3\varphi}}\right) \tag{4.24}$$

For the proposed modulation-based control technique related to the MMC with specified output active and reactive power, (4.24) is employed to perform accurately the controlling operation of the MMC in different working states.

4.5 Accurate Sizing of the Equivalent Sub-Module Capacitors

Considering the output operation of the MMC sub-modules, each sub-module has various output voltage during different operating conditions. Thus, the equivalent capacitor of sum of the upper or lower sub-modules is varied during the MMC performance along with the proposed controller. Taking into account, the upper and lower arm currents of the MMC, the size of the equivalent capacitor can be written as,

$$i_{uk} = C_{equ}\frac{dv_{uk}}{dt} \Rightarrow C_{equ} = \frac{i_{uk}}{\left(dv_{uk}/dt\right)} \tag{4.25}$$

$$i_{lk} = -C_{eql}\frac{dv_{lk}}{dt} \Rightarrow C_{eql} = \frac{-i_{lk}}{\left(dv_{lk}/dt\right)} \tag{4.26}$$

By substituting the obtained equations related to the upper and lower voltages and currents in (4.25) and (4.26), the equivalent capacitors of the upper and lower sub-modules respectively are derived as,

$$C_{equ} = \frac{0.5I_m \cos\left(\omega t + j\frac{2\pi}{3} + \alpha\right) + i_{dc}/3}{0.5\tilde{v}_{dc} - R_l\tilde{i}_{dcrip}/3 - V_{mu}\omega\sin\left(\omega t + \theta_u - \pi/2\right)} \tag{4.27}$$

$$C_{eql}=\frac{-0.5I_m\cos\left(\omega t+j\frac{2\pi}{3}+\alpha\right)+i_{dc}/3}{0.5\tilde{v}_{dc}-R_l\tilde{i}_{dcrip}/3-V_{ml}\omega\sin\left(\omega t-\theta_l-\pi/2\right)} \tag{4.28}$$

Equations (4.27) and (4.28) are drawn in Figure 4.2. As it can be seen from these figures, both equivalent capacitors of upper and lower sub-modules are changed in operation state of MMC which can show the variable feature of arms capacitors. Suitable operation of MMC can lead to accurate calculation of these capacitors.

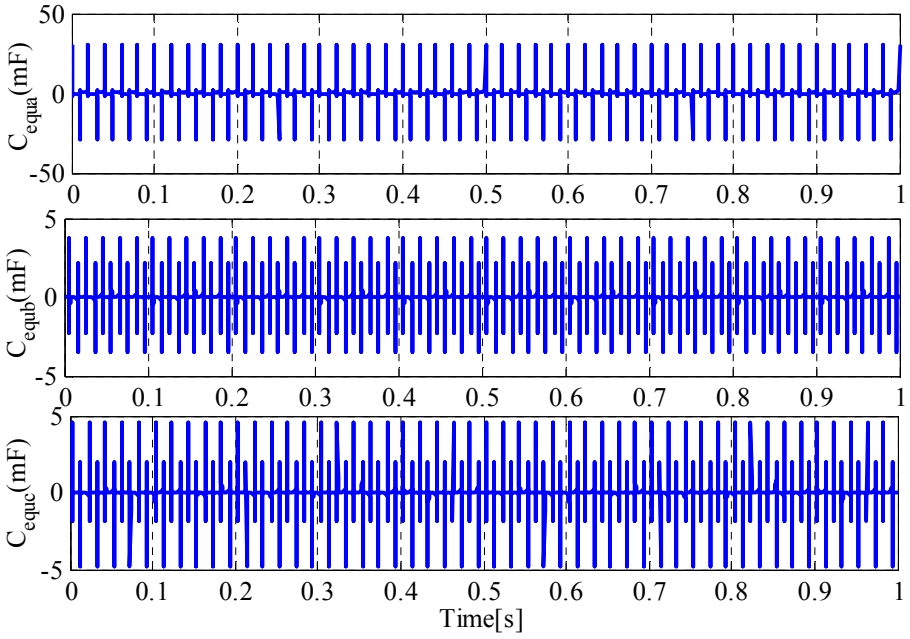

(a)

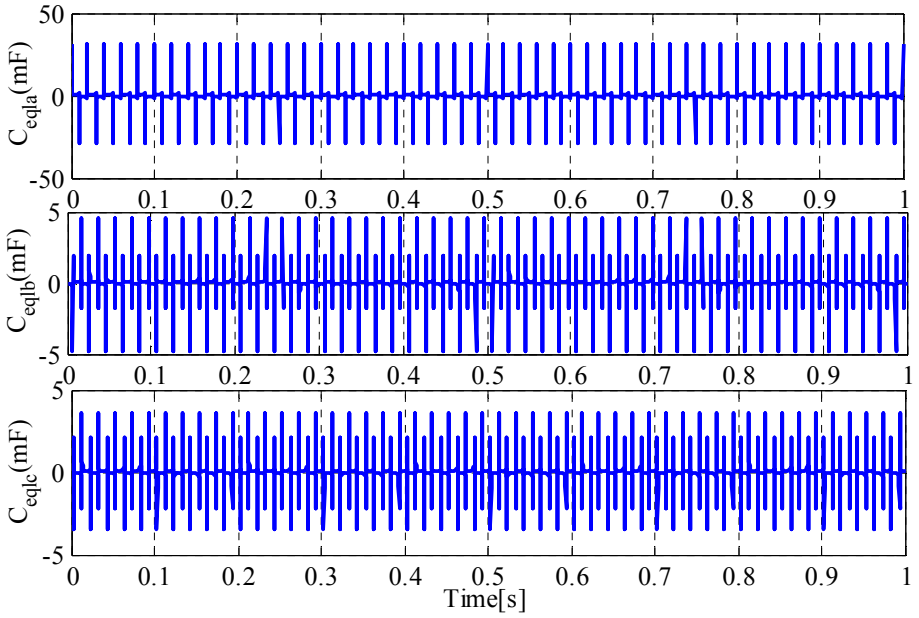

(b)

Figure 4.2 - The equivalent capacitor of (a) upper sub-modules (b) lower sub-modules.

4.6 Simulation Results

Matlab/Simulink environment in discrete mode is employed to evaluate the validity of the proposed modulation function-based control technique under various operating conditions. The overall structure of the proposed controller is drawn in Figure 4.3. As it can be seen from this figure, two processes of the MMC load and parameters changes are applied to the proposed MMC in inverter mode, which shall be further discussed in this section. The values of these processes are given in Table 4.2. Moreover, to fulfil acceptable simulation results, the sample time of the simulation is considered in 1 micro seconds (μs). In both processes, AC capacitor filter is utilized at the PCC, the value of which is presented in Tables 4.1 and 4.2.

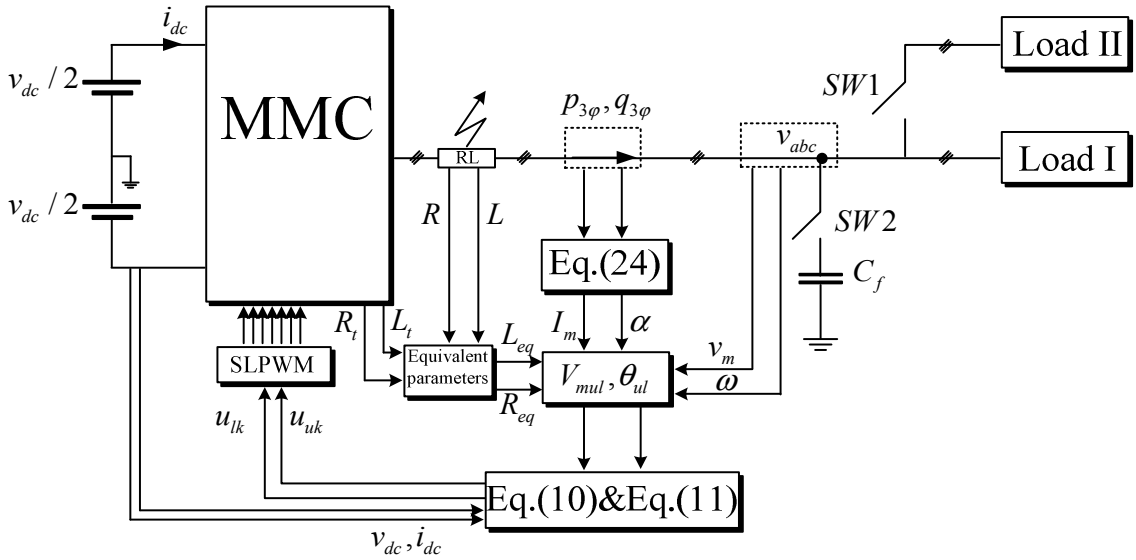

Figure 4.3 - The overall structure of the proposed controller.

Table 4.1 - The parameters of the proposed MMC in load changes conditions

Parameters	Value	Parameters	Value
$L_t(mH)$	15	N	4
$L(mH)$	6	$f(Hz)$	50
$R_t(\Omega)$	0.6	Load Active Power I	50 kW
$R(\Omega)$	0.1	Load Reactive Power I	20 kVAr
$v_{dc}(V)$	11200	Load Active Power II	35 kW
$v_m(V)$	5800	Load Reactive Power II	25 kVAr

Table 4.2 - The parameters of the proposed MMC in parameters changes conditions

Parameters	Value	Parameters	Value
$L_t(mH)$	15	$R_2(\Omega)$	0.15
$L(mH)$	6	$v_{dc}(V)$	11200
$R_{t1}(\Omega)$	0.6	$v_m(V)$	5800
$R_1(\Omega)$	0.1	N	4
L_{t2}(mH)	25	*f(Hz)*	50
L_2(mH)	9	Load Active Power	50 kW
$R_{t2}(\Omega)$	0.9	Load Reactive Power	20 kVAr

4.6.1 Load Changes Evaluation

Firstly, the proposed MMC is set to supply the load of 50 kW and 20 kVAr in the time duration of [0 s, 0.2 s] that is considered as steady-state period. Then, at t=0.2 s, a load of 35 kW and 25 kVAr will be connected to the PCC and the MMC is responsible for the generation of the needed power to cope with additional load. For the specified active and reactive power of the MMC, the variables I_m and α will be calculated from (4.24) to be used in the proposed modulation function. The MMC parameters in this section are given in Table 4.2. The proposed upper and lower modulation functions of the MMC-based control technique with its carrier waves during load dynamic change are illustrated in Figure 4.4 (a). The changes created in these functions at t=0.2s are used to make a proper control performance for generating the needed switching signals of the MMC sub-modules. Figures 4.4 (b) and (c) show the generated switching signals for sub-modules of phase "a". It can be realized from these figures that there is an inverse pattern for upper and lower sub-modules so that the needed switching signals are generated through SLPWM shown in Figure 4.4 (a) for reaching the control aims under load change.

The performance of the proposed controller at the desired control of the sub-modules voltages is shown in Figure 4.5 (a). According to this figure, the sub-module voltages in steady state are kept within the desired value region of 2.8 kV. After load dynamic change, the desired value of the sub-module voltages can be properly achieved with negligible transient response which proves the proper dynamic operation of the proposed controller. The output AC voltages of the MMC before and after using AC filter capacitor $(C_f = 50\mu F)$ are shown in Figure 4.5 (b), which validates the accurate performance of the designed modulation-based controller in both operating conditions.

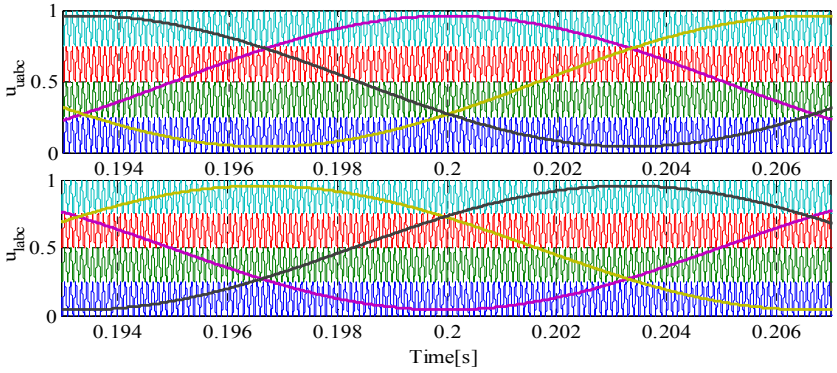

(a)

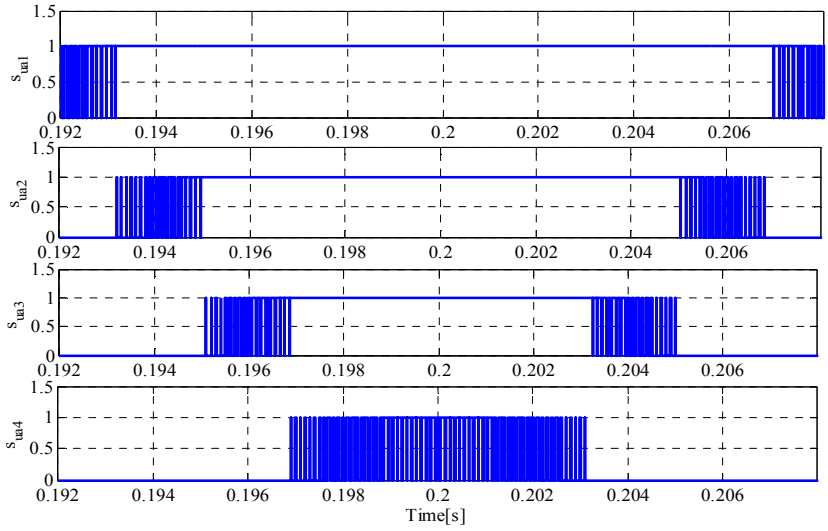

(b)

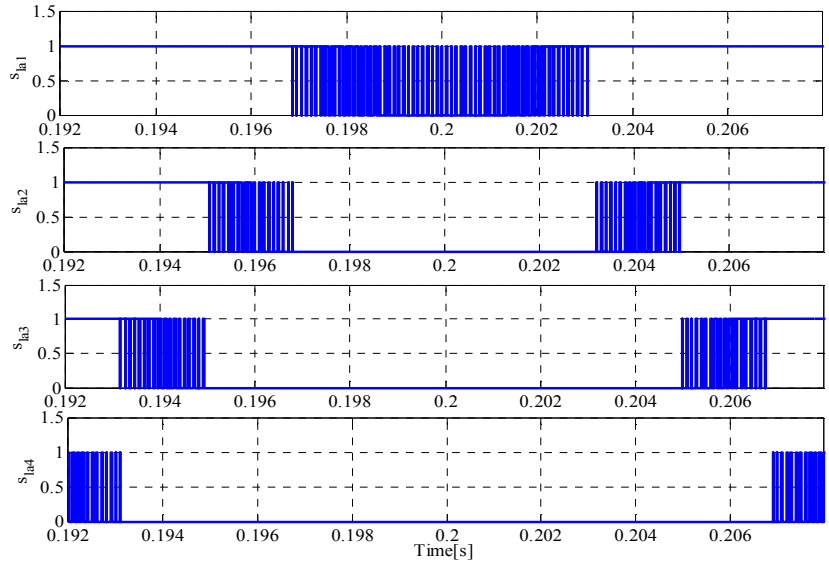

(d)

Figure 4.4 - In load changes process, a) The proposed three-phase upper and lower modulation functions with its carrier waves, b) the generated switching signals for upper sub-modules in phase “a” c) the generated switching signals for lower sub-modules in phase “a”.

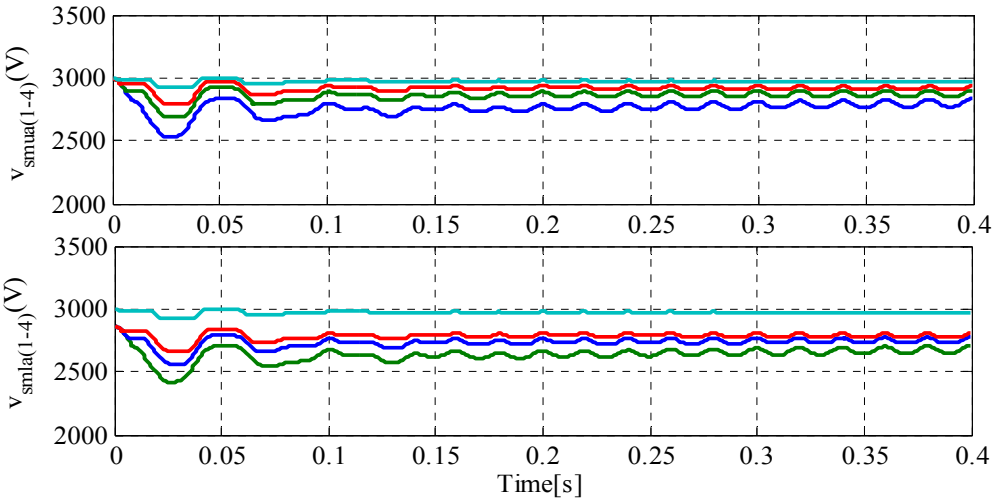

(a)

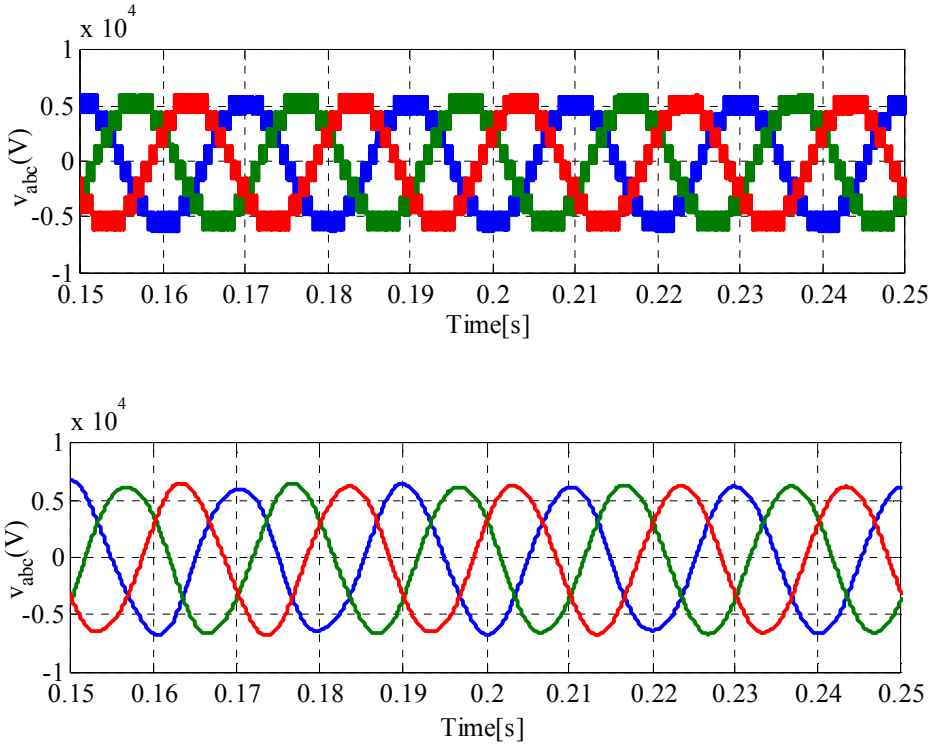

(b)

Figure 4.5 - (a) The sub-module voltages of phase "a" (b) The output voltages of MMC before and after connecting AC filter capacitor under load change condition.

The output and circulating currents assessment of the MMC is accomplished in Figure 4.6 (a). This figure verifies the capability of the MMC at generating suitable output currents in both steady state and dynamic operating conditions. Moreover, as can be seen, the MMC's circulating currents almost tend to be zero with the slight fluctuations.

The capability of MMC for active and reactive power sharing is indicated in Figure 4.6 (b). According to this figure, the MMC's active power properly follows the total load active power in both operating conditions. Figure 4.6 (b) demonstrates the ability of the proposed controller at tracking the reactive power of load in both conditions. Figure 4.7 shows the angle difference between output MMC voltages and Currents under load changes condition. As it can be seen in Figure 4.7, this angle is appropriately changed according to the MMC active and reactive power needed for load.

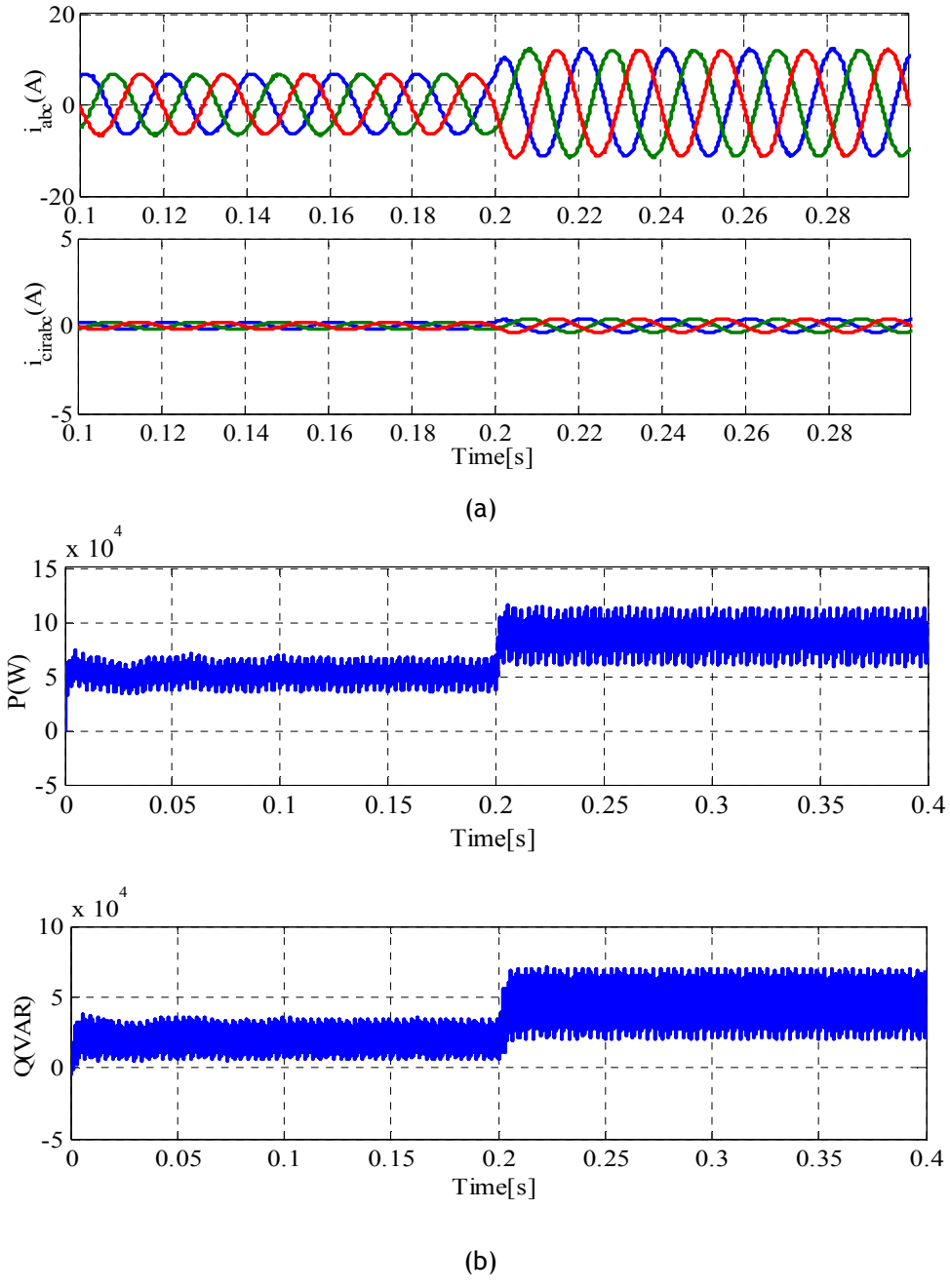

Figure 4.6 - (a) The output and circulating currents of the MMC. (b) Active and reactive power of the MMC under load changes condition.

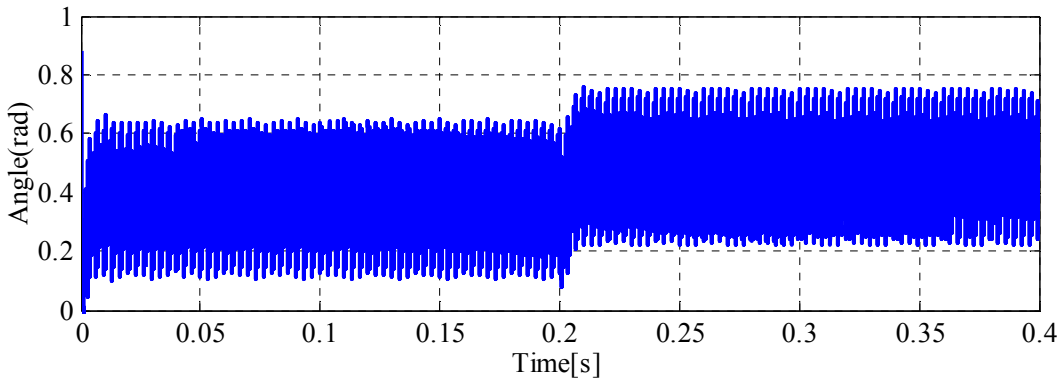

Figure 4.7 - Angle Difference between output MMC voltages and Currents under load changes condition.

4.6.2 Parameters Changes Evaluation

In this section, the effects of varying the MMC parameters on the proposed modulation-based control technique are investigated. Two collections of the parameters corresponding to the MMC's resistances and inductances are given in Table 4.2, which presents the MMC parameters in two different operation conditions. The MMC parameters are varied to the second condition in t=0.2 s. In this process, the MMC supplies a constant load of 50 kW and 20 kVAr. In the presence of the parameters alterations, the proposed modulation functions varied as depicted in Figure 4.8 (a). The related carrier waves are also given in Figure 4.8 (a). The changes made in the functions leads to a different trend for the applied PWM, upon which the appropriate control operation will be finally executed for the proposed MMC. By using SLPWM presented in Figure 4.8 (a), the switching signals for upper and lower sub-modules of phase "a" are achieved illustrated in Figure 4.8 (b) and (c), respectively. The same pattern is governed in this section. However, the control aim is following the reference values under MMC parameters changes in which switching signals are adapted according this aim.

The first aim of the proposed controller is to regulate the sub-module voltages. As it can be seen in Figure 4.9 (a), after varying the parameters at t=0.2s, the proposed controller is able to maintain the sub-module voltages around the desired value regardless of the small fluctuations in short transient time. The output voltages of MMC during AC filter capacitor $(C_f = 50\mu F)$ connection and disconnection are shown in Figure 4.9 (b). The proposed controller is able to keep these voltages at its desired values in parameters changes condition as shown in Figure 4.9 (b).

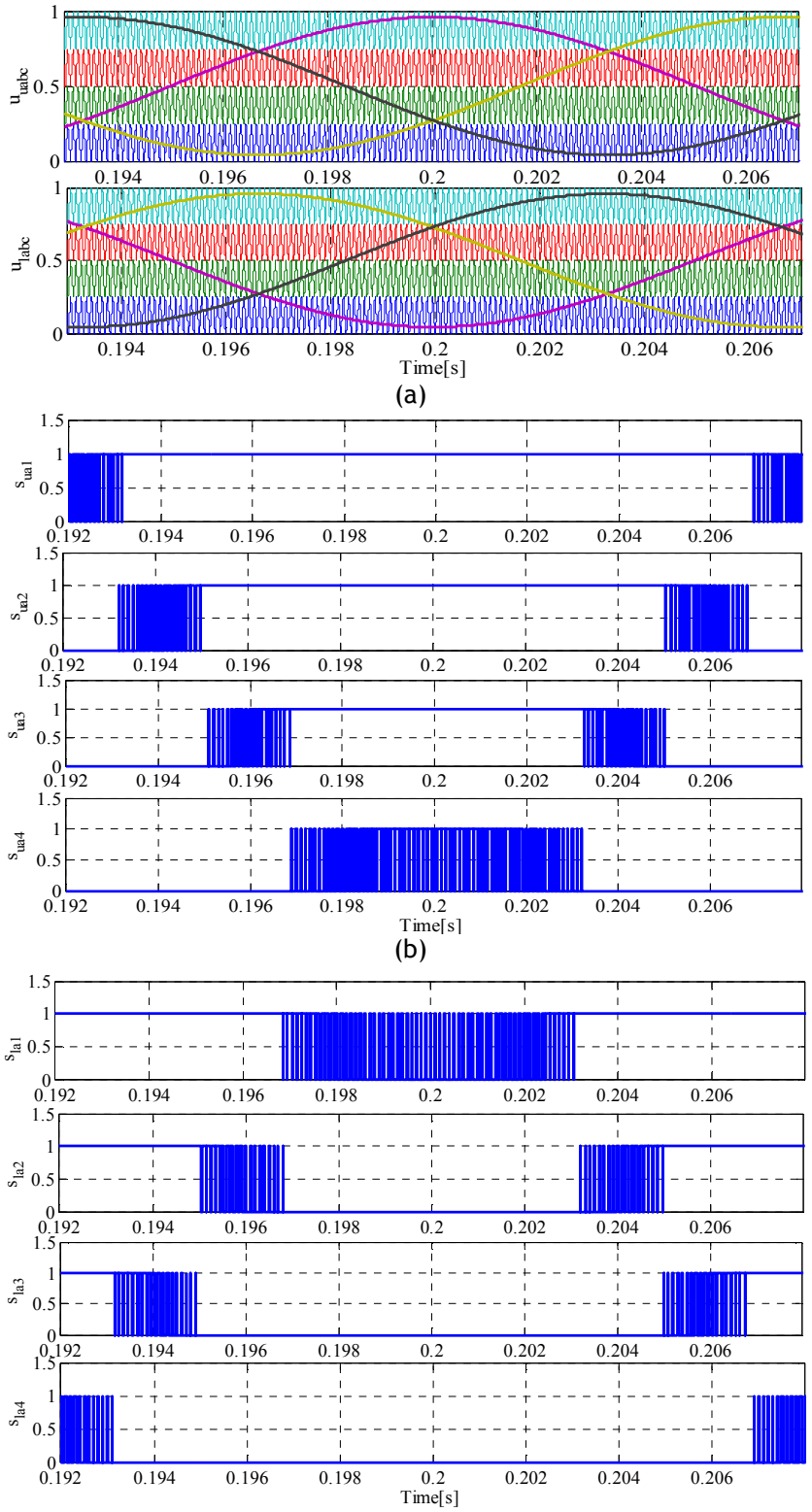

Figure 4.8 - In parameters changes condition, a) The proposed three-phase upper and lower modulation functions with its carrier waves, b)the generated switching signals for upper sub-modules in phase “a” c) the generated switching signals for lower sub-modules in phase “a”.

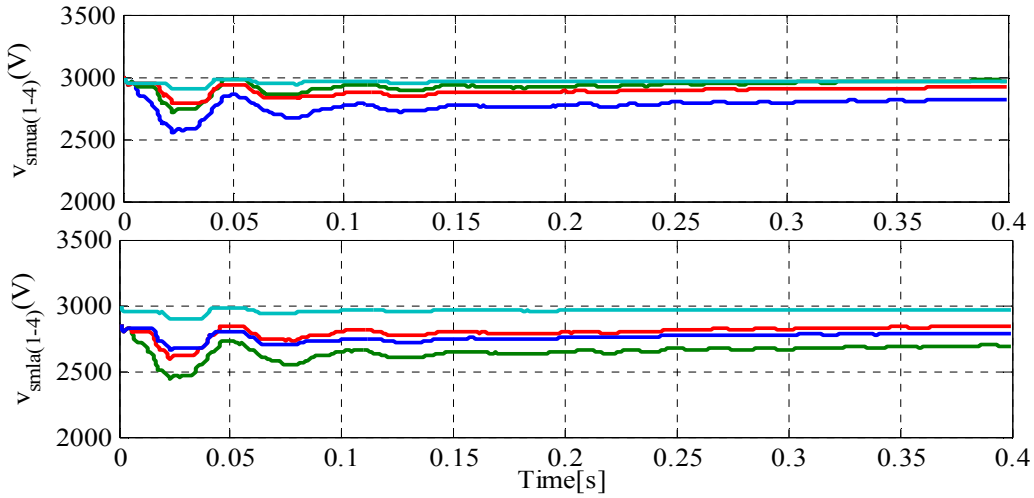

(a)

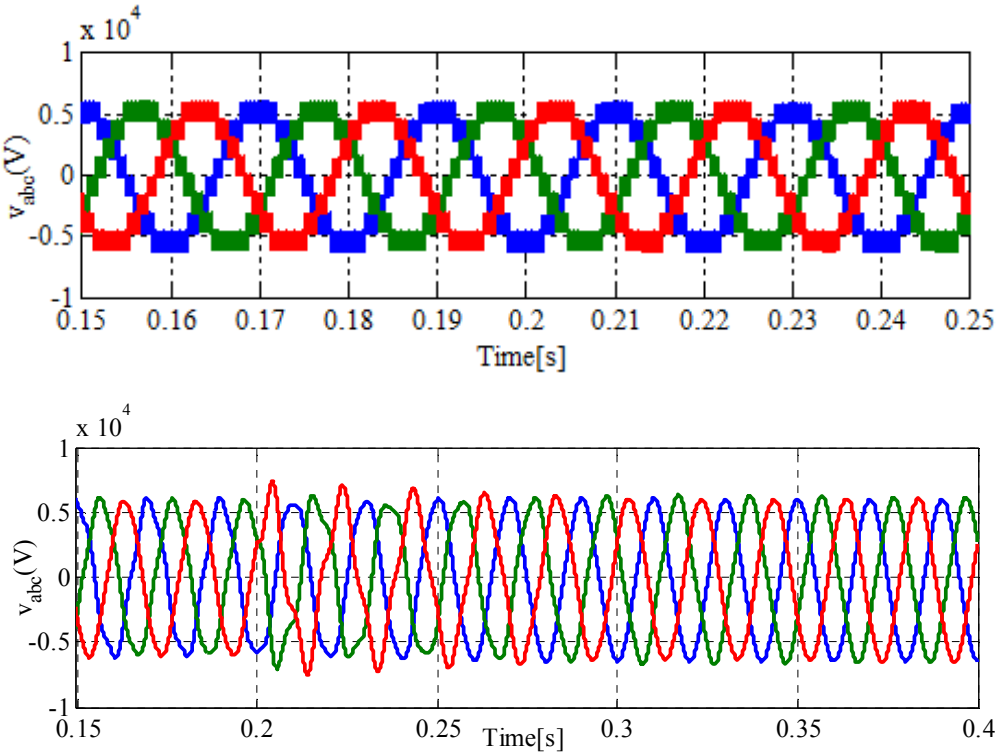

(b)

Figure 4.9 - (a) The sub-modules voltages of phase "a" (b) Output voltages of MMC before and after connecting AC filter under parameters change condition.

The output and circulating currents of MMC are shown in Figure 4.10 (a). According to this figure, the sinusoidal output current is proportional to the consumed load. Also, it is realized form Figure 4.10 (a) that the proposed controller is able to reach the desired value of the output currents with the existence of MMC parameters variations.

Moreover, it can be observed from Figure 4.10 (a) that the operation of the proposed controller in both steady and dynamic state for minimizing the circulating current is good. The active and reactive powers of the MMC are displayed in Figure 4.10 (b). According to this figure, the MMC parameters variation have no significant effects on the active and reactive power sharing of the MMC, as the MMC properly generates the required active power of the load. Figure 4.11 shows the angle difference between output MMC voltages and Currents under MMC parameters changes condition. It can be understood from Figure 4.11 that the angle values are kept in limited area with suitable instantaneous alterations leading to constant active and reactive power in presence of MMC parameters changes.

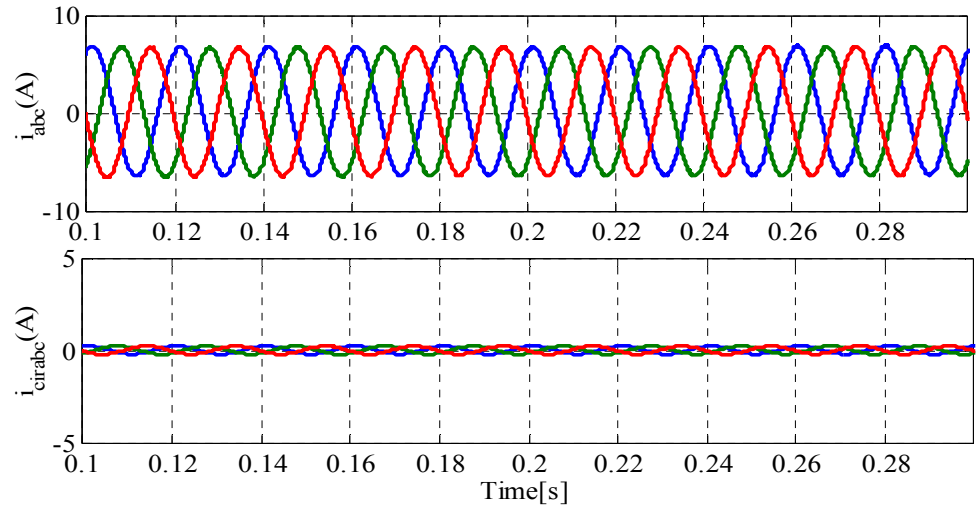

(a)

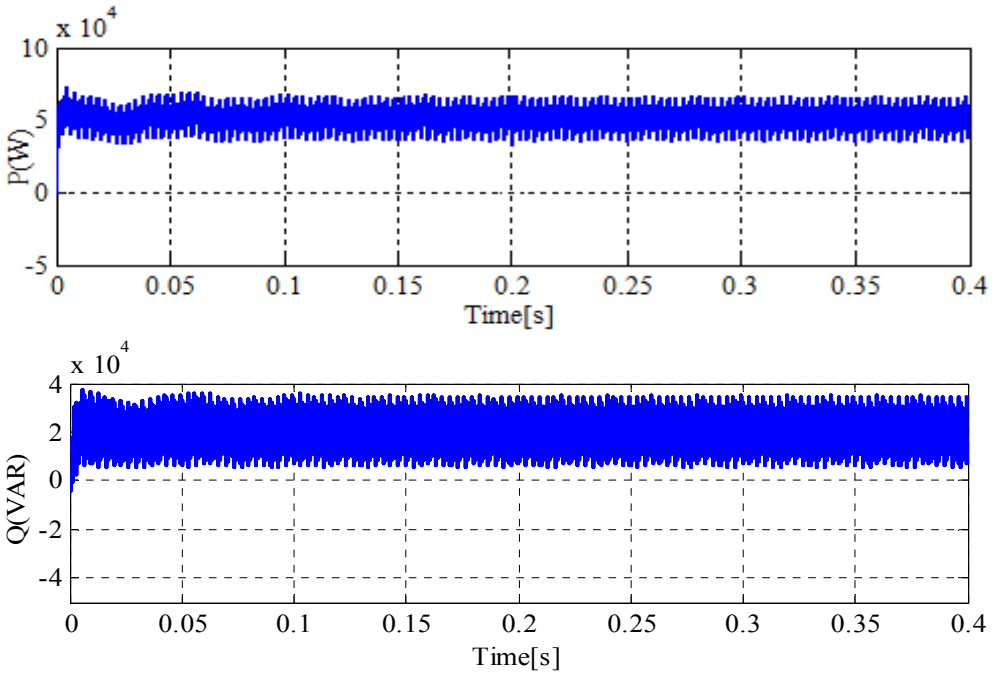

(b)

Figure 4.10 - (a) Output and circulating currents of the MMC (b) Active and reactive power of the MMC under parameters changes condition

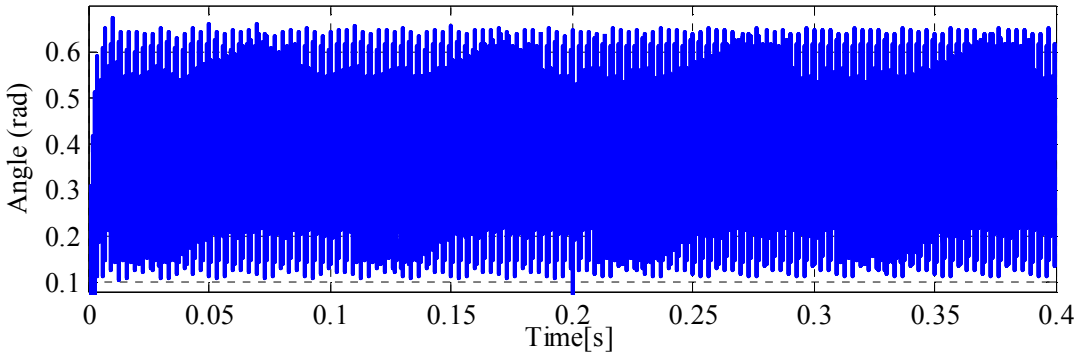

Figure 4.11 - Angle Difference between output MMC voltages and Currents under parameters changes condition.

4.7 Chapter Conclusions

The main contributions of this chapter are two separate modulation functions proposed for the generation of the switching signals of the MMC upper and lower sub-modules. The MMC arms currents, driven from circulating and output currents are applied to the mathematical model of the converter in a-b-c reference frame. This proposed modulation functions are simple in construction when compared with other control methods. It also stabilized the operation of the system in periods of parameters varying conditions. Changing the load connected to the PCC and MMC parameters was considered for the assessment of the designed controller, which was responsible for the control of the sub-modules voltages and accurate active and reactive power sharing performance. To complete the evaluation of the proposed controller, the instantaneous power of the MMC arms and the equivalent capacitors of the sub-modules were investigated. The simulation results in Matlab/Simulink environment demonstrated the capability of the proposed controller for reaching the main control purposes.

Chapter 5

A Novel Modulation Function-Based Control of Modular Multilevel Converters for High Voltage Direct Current Transmission Systems

In this chapter, a novel modulation function-based method including analyses of the modulation index and phase is proposed for the operation of modular multilevel converters (MMCs) in high voltage direct current (HVDC) transmission systems. The proposed modulation function-based control technique is developed based on thorough and precise analyses of all MMC voltages and currents in the a-b-c reference frame in which the alternating current (AC)-side voltage is the first target to be obtained. Using the AC-side voltage, the combination of the MMC upper and lower arm voltages is achieved as the main structure of the proposed modulation function. The main contribution of this chapter is to obtain two very simple new modulation functions to control MMC performance in different operating conditions. The features of the modulation function-based control technique are as follows: (1) this control technique is very simple and can be easily achieved in a-b-c reference frame without the need of using Park transformation; and (2) in addition, the inherent properties of the MMC model are considered in the proposed control technique. Considering these properties leads to constructing a control technique that is robust against MMC parameters changes and also is a very good tracking method for the components of MMC input currents. These features lead to improving the operation of MMC significantly, which can act as a rectifier in the HVDC structure. Simulation studies are conducted through MATLAB/SIMULINK software, and the results obtained verify the effectiveness of the proposed modulation function-based control technique.

5.1 Introduction

Because of existing large-scale renewable energy sources [122]–[124], the needs for specifying a multilevel converter as one of the best option for high power and medium voltage applications seem to be necessary in these years [37], [125], [126]. Owing to remarkable advantages of multilevel modular converters (MMC) in high-voltage and high-power applications including modular structure, dynamic increment of sub-module (SM) numbers, common direct current (DC)-bus and distributed DC capacitors [43], [127]–[129], many pulse width modulation (PWM) techniques have been recently proposed to improve control features of these converters [50], [102].

However, although there are many existing control methods, designing new control techniques with more simplicity, more efficiency, faster steady state operation and better transient response with respect to the type of application are always required. In [114], an improved PWM method for half-bridge based MMCs is proposed that is able to generate an output voltage with maximally 2N + 1 levels. The method discussed in this article is as great as a carrier-phase-shifted PWM (CPSPWM) method.

A popular PWM technique, which is the most commonly used method in the Cascaded H-bridge converters (CHB) [130], [131], is the phase-shifted carrier (PSC). Because of the following features [110], the PSC modulation is also attractive to MMCs [132]–[135]: (1) high modularity and scalability of MMC; (2) easily reaching capacitor voltage balancing control; (3) MMC is able to generate an output voltage with a high switching frequency and a low total harmonic distortion (THD); and (4) MMC structure is able to distribute the semiconductor stress and the power of SMs. For instance, in [110], a mathematical analysis of PSC modulation is presented in order to identify the PWM harmonic characteristics of the MMC output voltage and the circulating current. In addition, the influence of carrier displacement angle between the upper and lower arms on those harmonics is evaluated in this work. The nearest level modulation (NLM) method, which is also known as the round method, is exhaustively discussed in [86], [136], [137]. This method is suitable for MMCs particularly with a large number of SMs. In comparison with the conventional NLM, a modified NLM method in which the number of output alternating current (AC) voltage levels is as great as the CPSPWM and the improved SM unified PWM (SUPWM) is proposed for MMCs in [115]. Through this method, the number of AC voltage levels increased to 2N + 1, which is almost double; and the height of the step in the step wave is halved, leading to a better quality for the MMC AC output voltage waveform. By adding a zero-sequence to the original modulation signals, a new discontinuous modulation technique is achieved in [116] along with a circulating current control technique the MMC arms are clamped to the upper or lower terminals of the DC-link bus. In order to minimize the switching losses of the MMC, the clamping intervals can be regulated by the use of the output current absolute value. In [116], a significant reduction in the capacitor voltage ripples with low modulation indices is also obtained. A multilevel selective harmonic elimination pulse-width modulation (MSHE-PWM) technique is schemed in [138] to perform a tight control of the low-order harmonics and the lowest switching frequency for the MMC [119]. Moreover, two different modulation patterns for MSHE-PWM as well as a method for selecting the number of SMs in the phase-legs of the converter are proposed in [119]. According to [111], [139], the amplitude modulation is widely employed to control MMC-based high voltage direct current (HVDC) transmission systems. The main idea of the method is to first calculate how many SMs should be put into action, and then the capacitors sorting voltage and the final working sequence should be determined by the direction of the arm current. However, in the case of large numbers of SMs, problems related to frequent sorting of capacitor voltage are issued [140].

A novel modulation function accompanied by its index is figured out in this chapter by accurately analyzing all MMC voltages and currents in the a-b-c reference frame in order to improve MMC performance in HVDC applications. Working the AC-side voltage out, a combination of the MMC upper and lower's arm voltages is achieved. The proposed modulation function that completely depends on MMC parameters and also the specifications of MMC input voltages and currents can be derived by using the AC-side voltage. In order to reach an accurate evaluation of MMC operation under different operational conditions, the impact of parameters and input current variations on the proposed modulation function and its index is investigated that ends up improving MMC control. MATLAB/SIMULINK (version, Manufacturer, City, State Abbr. if USA or Canada, Country) based simulation results show the effectiveness of the proposed modulation function-based control.

5.2 Modular Multilevel Converter's Alternating Current-Side Voltages

The structure of a three-phase MMC is illustrated in Figure 5.1(a). The "2N" numbers of SMs are utilized in each arm, whereas their detailed configuration is depicted in Figure 5.1(b). According to the figure, two complementary insulated-gate bipolar transistor (IGBT)-Diode switches are controlled so that each SM may be placed at either connected or bypassed states based on an appropriate switching method and also required controlling aims. In order to suppress the circulating current and also to restrict the fault current during a DC side fault, an inductor is used in either sides of each arm. The series resistor of each arm represents the combination of the arm losses and the inner inductor resistance.

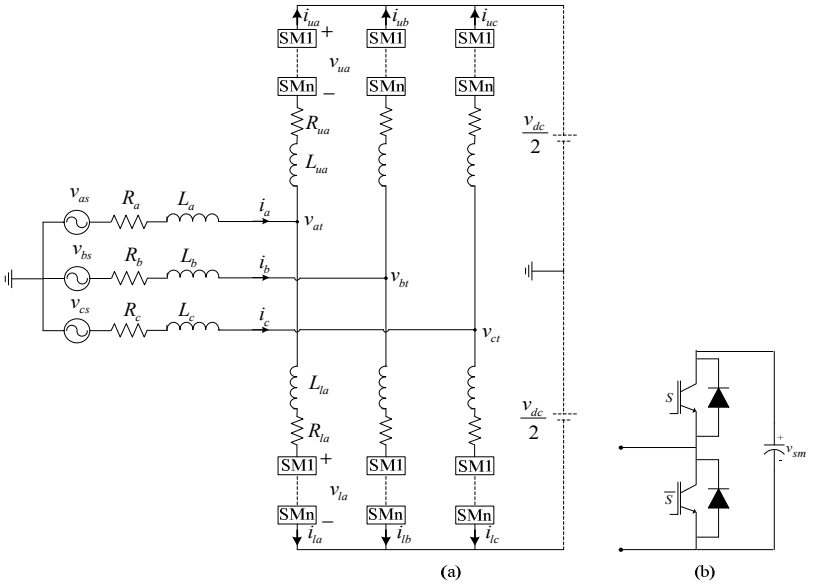

Figure 5.1 - (a) Generic circuit for an MMC and (b) sub-module (SM).

Detailed Calculation of the Alternating Current-Side Voltage

The operation of the used SMs in MMC is highly dependent on the AC-side voltages. As can be inferred from Figure 5.1 (a), the AC-side voltages are directly related to the input variables and parameters. Suppose that MMC input voltage and current of phase "a" are:

$$v_{as} = v_m \cos(\omega t), i_a = I_{ma} \cos(\omega t + \alpha_a) \tag{5.1}$$

Based on the proposed MMC structure shown in Figure 5.1 (a), the relationship between the input and the AC-side voltages of phase "a" can be written as:

$$v_{as} - v_{at} = L_a \frac{\mathrm{d}i_a}{\mathrm{d}t} + R_a i_a \tag{5.2}$$

By substituting Equation (5.1) into Equation (5.2), the AC-side voltage of phase "a" can be achieved as Equation (5.3):

$$\begin{aligned} v_{at} = & \sqrt{\begin{array}{l} L_a^2 I_{ma}^2 \omega^2 + R_a^2 I_{ma}^2 + v_m^2 + \\ 2 v_m L_a I_{ma} \omega \sin(\alpha_a) - 2 v_m R_a I_{ma} \cos(\alpha_a) \end{array}} \times \\ & \cos\left(\omega t + tag^{-1} \left(\frac{\left[v_m + L_a I_{ma} \omega \sin(\alpha_a) - R_a I_{ma} \cos(\alpha_a) \right]}{\left[L_a I_{ma} \omega \cos(\alpha_a) + R_a I_{ma} \sin(\alpha_a) \right]} \right) - \pi / 2 \right) \end{aligned} \tag{5.3}$$

To present more explanations, Equation (5.3) can be rewritten as Equation (5.4):

$$\begin{aligned} v_{kt} = & \sqrt{\begin{array}{l} L_k^2 I_{mk}^2 \omega^2 + R_k^2 I_{mk}^2 + v_m^2 + \\ 2 v_m L_k I_{mk} \omega \sin(\alpha_k) - 2 v_m R_k I_{mk} \cos(\alpha_k) \end{array}} \times \\ & \cos(\omega t + tag^{-1} \left(\frac{\left[v_m + L_k I_{mk} \omega \sin(\alpha_k) - R_k I_{mk} \cos(\alpha_k) \right]}{\left[L_k I_{mk} \omega \cos(\alpha_k) + R_k I_{mk} \sin(\alpha_k) \right]} \right) + \frac{2\pi j}{3} - \frac{\pi}{2}) \end{aligned} \tag{5.4}$$

where *j* is equal to 0, −1 and 1 for the phases of "a", "b" and "c", respectively. The indices of k are the phases sign of "a", "b" and "c". Equation (4.4) shows the general three phase AC-side voltages. As can be realized from Equation (4.4), the AC-side voltages of MMC can be completely affected by input parameters and variables.

5.3 Analysis of Proposed Modulation Function

The proposed modulation function is obtained in this section involving AC-side voltages. The voltages placed in entire upper and lower SMs can be aimed to generate signals required for SM switches. Thus, applying Kirchhoff's voltage law's (KVL's) on phase "a" arms of the MMC, the following equations are derived as:

$$v_{at} - v_{dc}/2 = L_{au}\frac{\mathrm{d}i_{au}}{\mathrm{d}t} + R_{au}i_{au} - v_{au} \tag{5.5}$$

$$v_{at} + v_{dc}/2 = L_{al}\frac{\mathrm{d}i_{al}}{\mathrm{d}t} + R_{al}i_{al} + v_{al} \tag{5.6}$$

By summing up two sides of the equations in Equations (5.5) and (5.6) and also assuming $L_{au} = L_{al} = L_{at}$, the following equation is attained:

$$v_{al} - v_{au} = 2v_{at} - L_{at}\frac{\mathrm{d}i_a}{\mathrm{d}t} - R_{al}i_a \tag{5.7}$$

By substitution of Equations (1) and (3) into Equation (7), Equation (8) can be achieved as:

$$\begin{aligned} v_{al} - v_{au} = &\sqrt{\begin{array}{l}(2L_a + L_{at})^2 I_{ma}^2\omega^2 + (2R_a + R_{at})^2 I_{ma}^2 + 4v_m^2 + \\ 4v_m(2L_a + L_{at})I_{ma}\omega\sin(\alpha_a) - 4v_m(2R_a + R_{at})I_{ma}\cos(\alpha_a)\end{array}} \\ &\cos\left(\omega t + tag^{-1}\left(\frac{\left[2v_m + (2L_a + L_{at})I_{ma}\omega\sin(\alpha_a) - (2R_a + R_{at})I_{ma}\cos(\alpha_a)\right]}{\left[(2L_a + L_{at})I_{ma}\omega\cos(\alpha_a) + (2R_a + R_{at})I_{ma}\sin(\alpha_a)\right]}\right) - \frac{\pi}{2}\right) \end{aligned} \tag{5.8}$$

As been discussed in former section, Equation (8) can be rewritten in a general form as Equation (4.9):

$$\begin{aligned} v_{kl} - v_{ku} = &\sqrt{\begin{array}{l}(2L_k + L_{kt})^2 I_{mk}^2\omega^2 + (2R_k + R_{kt})^2 I_{mk}^2 + 4v_m^2 + \\ 4v_m(2L_k + L_{kt})I_{mk}\omega\sin(\alpha_k) - 4v_m(2R_k + R_{kt})I_{mk}\cos(\alpha_k)\end{array}} \times \\ &\cos(\omega t + \frac{2\pi j}{3} - \frac{\pi}{2} + \\ &tag^{-1}\left(\frac{\left[2v_m + (2L_k + L_{kt})I_{mk}\omega\sin(\alpha_k) - (2R_k + R_{kt})I_{mk}\cos(\alpha_k)\right]}{\left[(2L_k + L_{kt})I_{mk}\omega\cos(\alpha_k) + (2R_k + R_{kt})I_{mk}\sin(\alpha_k)\right]}\right)) \end{aligned} \tag{5.9}$$

The term "$v_{kl} - v_{ku}$" is used to acquire reference waveforms for shift level pulse width modulation (SLPWM). As evident in Equation (5.10), the reference signals of the proposed PWM can be changed by input and arm parameters of MMC as well as input voltages and currents characteristics. Considering the reference values of I_{mk}^{*}, v_{m}^{*} and α_{k}^{*} as input currents and voltages, the proposed modulation index can be written as:

$$\begin{aligned} m_k &= \frac{V_{kt}(L_k, R_k, L_{kt}, R_{kt}, I_{mk}^{*}, v_m^{*}, \alpha_k^{*})}{v_{dc}} \\ &= \frac{1}{v_{dc}} \sqrt{\begin{array}{l} \left(2L_k + L_{kt}\right)^2 I_{mk}^{*2}\omega^2 + \left(2R_k + R_{kt}\right)^2 I_{mk}^{*2} + 4v_m^{*2} + \\ 4v_m^{*}\left(2L_k + L_{kt}\right) I_{mk}^{*}\omega \sin\left(\alpha_k^{*}\right) - 4v_m^{*}\left(2R_k + R_{kt}\right) I_{mk}^{*} \cos\left(\alpha_k^{*}\right) \end{array}} \end{aligned} \tag{5.10}$$

Based on Equations (5.9) and (5.10), and also assuming the reference values of input variables, the proposed modulation functions can be achieved as:

$$u_{ku} = m_k \left(\begin{array}{l} 1 - \cos(\omega t + \frac{2\pi j}{3} - \frac{\pi}{2} + \\ tag^{-1}\left(\frac{\left[2v_m + \left(2L_k + L_{kt}\right) I_{mk}\omega \sin\left(\alpha_k\right) - \left(2R_k + R_{kt}\right) I_{mk} \cos\left(\alpha_k\right)\right]}{\left[\left(2L_k + L_{kt}\right) I_{mk}\omega \cos\left(\alpha_k\right) + \left(2R_k + R_{kt}\right) I_{mk} \sin\left(\alpha_k\right)\right]} \right) \end{array} \right) \tag{5.11}$$

$$u_{kl} = m_k \left(\begin{array}{l} 1 + \cos(\omega t + \frac{2\pi j}{3} - \frac{\pi}{2} + \\ tag^{-1}\left(\frac{\left[2v_m + \left(2L_k + L_{kt}\right) I_{mk}\omega \sin\left(\alpha_k\right) - \left(2R_k + R_{kt}\right) I_{mk} \cos\left(\alpha_k\right)\right]}{\left[\left(2L_k + L_{kt}\right) I_{mk}\omega \cos\left(\alpha_k\right) + \left(2R_k + R_{kt}\right) I_{mk} \sin\left(\alpha_k\right)\right]} \right) \end{array} \right) \tag{5.12}$$

The proposed modulation functions configurations for phase “a” are drawn in Figure 5.2. With respect to Equations (5.11) and (5.12), the proposed index and function are plotted in Figure 5.3 for $I_{mk}^{*} = 50A$ and $\alpha_k^{*} = 0$. As evident in Figure 5.3, the index modulation is quite close to unity. The effects of MMC parameters and input currents on the proposed modulation functions are comprehensively investigated in the next section. The parameters of V_{at} and θ_{at} are given in Appendix C.

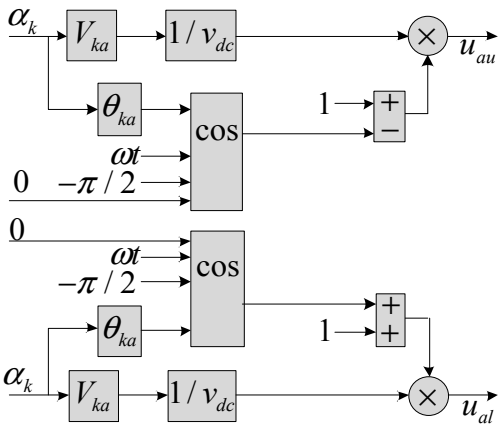

Figure 5.2 - The proposed modulation functions for phase "a".

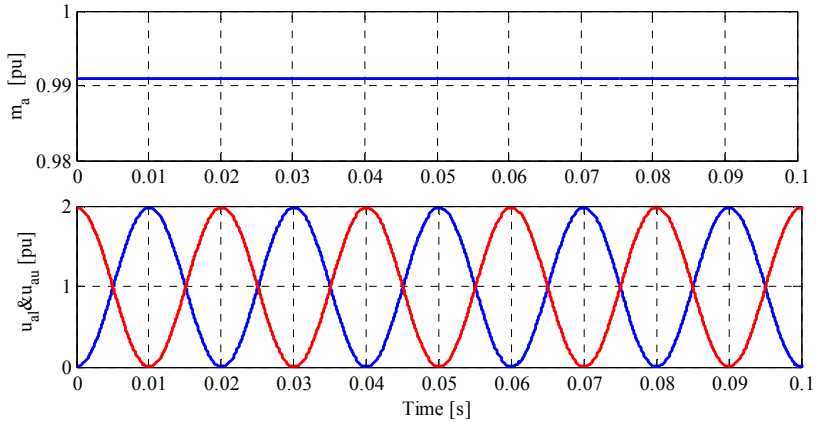

Figure 5.3 - The proposed modulation index and function as to parameters given in Table 5.1.

5.3.1 Parameters Variation Effects on the Proposed Modulation Function

In this section, system parameters are changed to the ones given in Table 5.2 in order to evaluate the effects of the parameters variations on the proposed modulation function. The base parameters are as given in Table 5.1. By increasing the system parameters, the proposed modulation indexes are decreased as depicted in Figure 5.4. The variation trend of the proposed modulation function is also illustrated in Figure 5.4. According to this figure, in addition to the index changes, the phase angles of both upper and lower modulation functions in three conditions slightly tend to be shifted. For the two obtained modulation functions, a typical shifted-level PWM in intervals of $5ms \leq t \leq 10ms$ is shown in Figure 5.5. Figure 5.5 demonstrates that the switching numbers of the second and third levels are decreased, and, instead, the numbers of the lowest level switching is increased. The scenario is inversed for the proposed lower modulation function but not with a similar change in the numbers.

As depicted in Figure 5.6, the presented SLPWM results in a raise in the switching numbers of the second and the third levels and a drop in the switching numbers of the first levels. The sum of the switching generations in both proposed upper and lower modulation functions should lead to a constant value in each level.

Table 5.1 - Simulated system parameters. AC: alternating current; DC: direct current.

Parameter	Value	Unit
Input resistance	0.6	Ohm
Input inductance	15	mH
Arm resistance	0.5	□
Arm inductance	5	mH
AC voltage	6	kV
DC voltage	12	kV
N	4	-
Input frequency	50	Hz
Carrier frequency	10	kHz
SM capacitance	5	mF
SM voltage	3	kV

Table 5.2 - Changes in MMC parameters in Condition 2.

Parameter	Value	Unit
Input resistance	1.2	□
Input inductance	25	mH
Arm resistance	1.5	Ohm
Arm inductance	10	mH
AC voltage	6	kV
I_{mk}	50	A
α_k	0	-

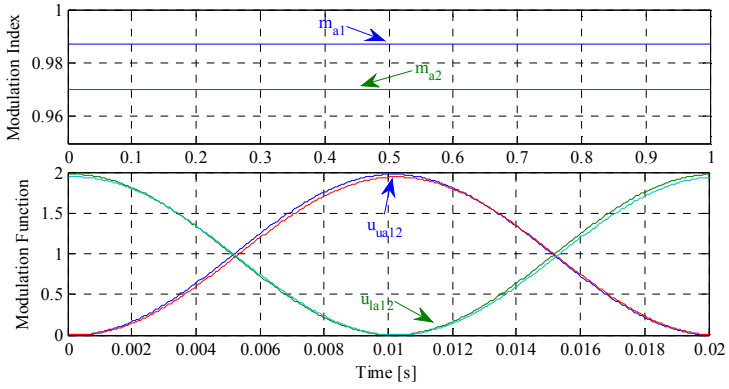

Figure 5.4 - The proposed modulation index and function based on parameters variations given in Table 2.

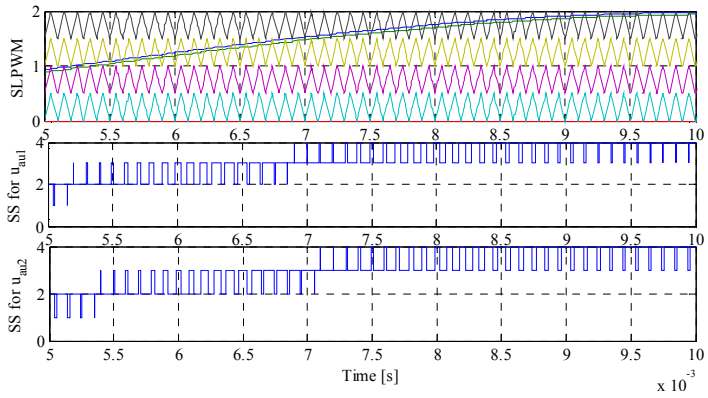

Figure 5.5 - A typical shifted-level pulse width modulation (PWM) for proposed upper modulation function with parameter changes.

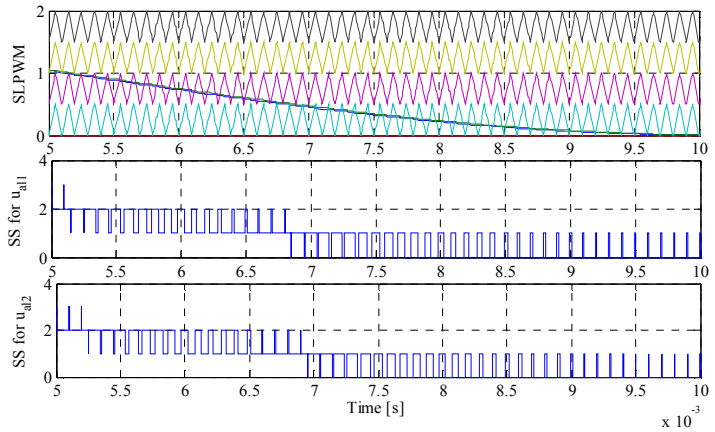

Figure 5.6 - A typical shifted-level PWM for proposed lower modulation function with parameter changes.

5.3.2 Input Current Variation Effects on the Proposed Modulation Function

The magnitude and phase angle of the input currents impact on the proposed modulation function that is reviewed in this section. The specifications of the input current are changed to $I_{mk} = 100A$ and $\alpha_k = -\pi/6$ at $t = 0.2s$. In comparison with parameter variations, the MMC input current variations can make more reduction in the modulation index and phase angle of the proposed modulation functions as illustrated in Figure 5.7. The effects of the input current changes on the applied SLPWM are shown in Figures 5.8 and 5.9. The proposed upper modulation function with its shifted-level triangle waveforms as well as the respective generated signals for two different input currents are drawn in Figure 5.8. It can be seen that the number of switching signals (SS) in the second level is significantly increased for the MMC operating in the second condition compared with the first one.

On the other hand, the first and the second levels of SS are slightly increased for SLPWM applied to the proposed lower modulation function as shown in Figure 5.9. Considering the interval of $5ms \leq t \leq 10ms$ as a sampling period, the input current changes impact more on the operation of the proposed upper modulation function.

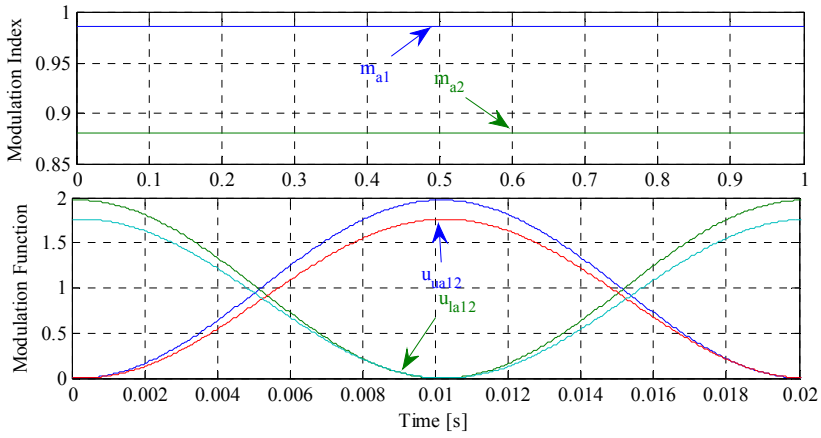

Figure 5.7 - The proposed modulation index and function based on input variable variations.

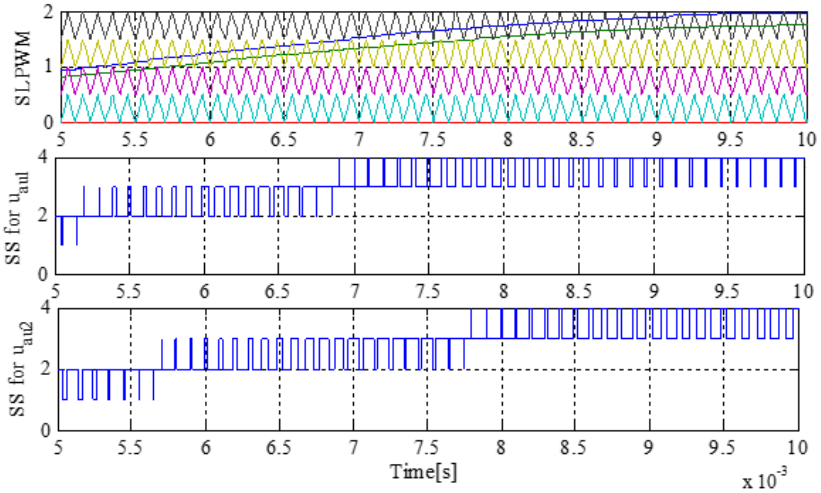

Figure 5.8 - A typical shifted-level PWM for proposed upper modulation function with input current changes.

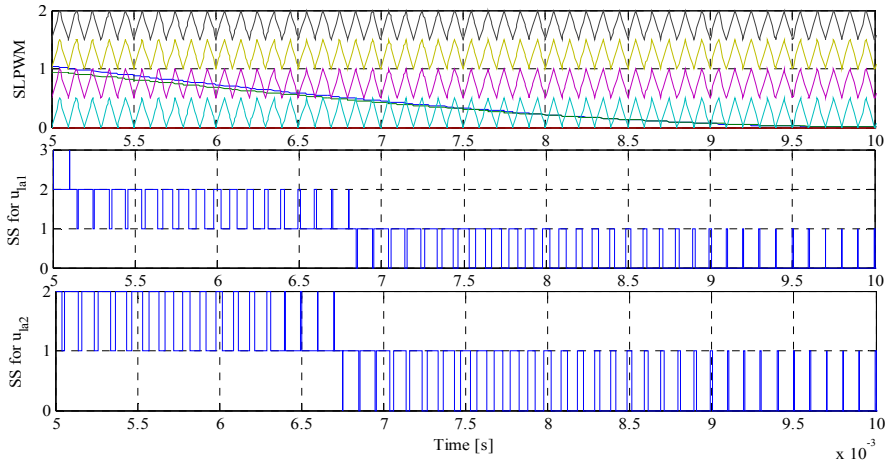

Figure 5.9 - A typical shifted-level PWM for proposed lower modulation function with input current changes.

5.4 Simulation Results

In this section, the control of MMC is executed by the use of proposed modulation function as given in Figure 5.10. MATLAB/SIMULINK environment in discrete mode is used to perform the overall control structure modelling based on the information given in Tables 5.1 and 5.2. Throughout the evaluation process of MMC operation as a rectifier in HVDC application, the simulation sampling time is selected at the value of one micro second. In addition, initial value of 3 kV is considered for all SM capacitors.

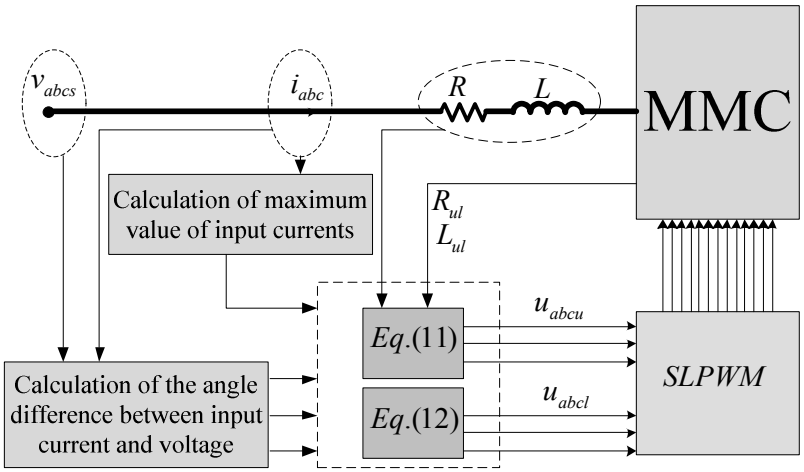

Figure 5.10 - The overall structure of the proposed modulation functions for MMC.

5.4.1 Parameter Variation Evaluation

The obtained functions in Equations (5.11) and (5.12) are considered as carrier waveforms in SLPWM in these simulations. As can be observed, both amplitude and phase angle of the proposed modulation functions can be controlled by varying MMC arm and input parameter changes. In the first section of simulation that is (0, 0.2) seconds, MMC operates in a steady state with parameters given in Table 5.1. Then, at $t = 0.2\,s$, the MMC parameters are changed to the values given in Table 5.2. As can be seen in Figure 5.11, voltages of SMs in phase "a" are kept at their desired values of 3 kV with initial parameters. After parameter variations, the proposed modulation function-based controller is able to acceptably regulate SM voltages, except for a slight deviation from the desired value at $t = 0.2s$. Figure 5.12 shows the DC-link voltage of the MMC. Initially, MMC can reach targeted DC-link voltage after a short transient response. With a very small undershoot, the modulation algorithm continues to attain MMC's desired DC-link voltage after parameter alterations. Phase "a" current of MMC is illustrated in Figure 5.13. According to this figure, MMC can generate the assumed current with the amplitude of 50 for both sets of parameters; however, there are negligible transient responses. The active and reactive power sharing of MMC with parameter changes are illustrated in Figure 5.14. As it can be seen in this figure, the MMC active and reactive powers follow the desired values, even after MMC parameter changes, along with their proportional alterations. The appropriate operation of a designed controller for MMC must lead to minimization of circulating currents. The proposed controller is capable of achieving minimized circulating currents of MMC as depicted in Figure 5.15. As shown in this figure, the circulating current of phase "a" remains at an acceptable level in both operation states.

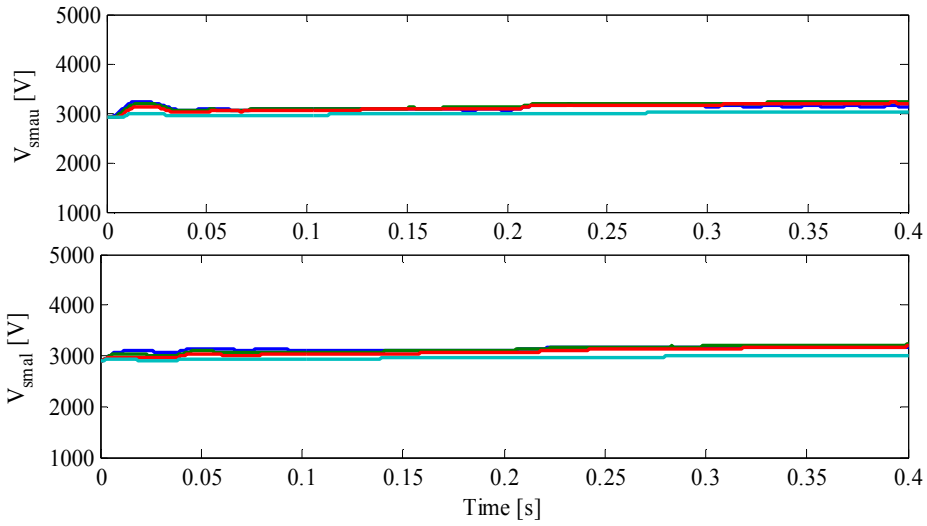

Figure 5.11 - SM voltages of MMC with parameter variations.

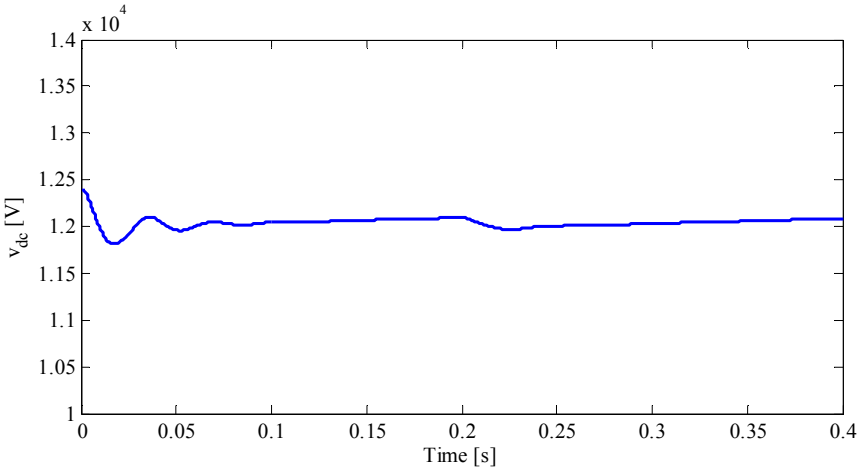

Figure 5.12 - DC-link voltage of MMC with parameter variations.

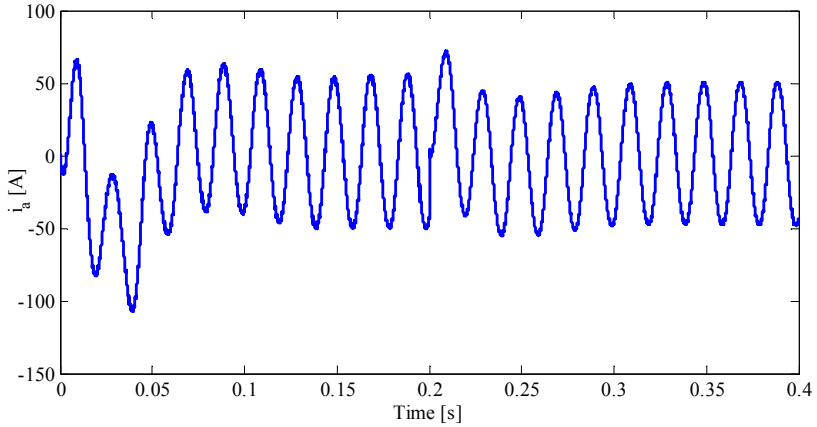

Figure 5.13 - MMC current of phase "a" with parameter variations.

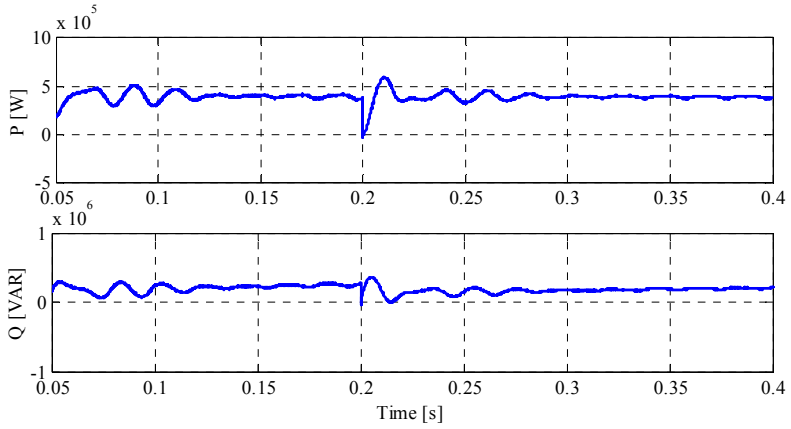

Figure 5.14 - The active and reactive power of MMC with parameter variations.

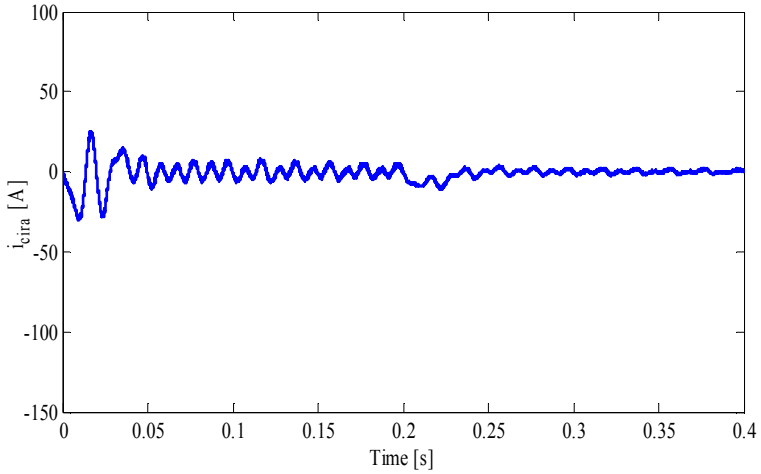

Figure 5.15 - Circulating current of MMC in phase "a" with parameter variations.

5.4.2 Evaluation of Modular Multilevel Converter Input Current Variation

Changing the input current components of α_k and I_{mk} creates different modulation functions for the proposed modulation function-based controller. Thus, the changes caused by input MMC currents should lead to properly commanding the proposed controller to keep MMC in stable operation. In the primary interval, MMC operates with $\alpha_k = 0$, $I_{mk} = 50\,A$ and the parameters given in Table 5.1. Then, the input MMC currents reach a magnitude of $I_{mk} = 100A$ with the phase angle of $\alpha_k = -\pi/6$ at $t = 0.2\,s$, though keeping the same parameters. The MMC SM voltages of both operation states are demonstrated in Figure 5.16. As can be understood from Figure 5.16, the voltages follow the reference value with a slight transient response and also acceptable steady-state error. Moreover, the DC-link voltage of MMC experiences an undershoot after the current variation at t = 0.2 s as depicted in Figure 5.17. After the transition, the proposed controller shows its dynamic capability in keeping the MMC DC-link voltage with an acceptable deviation from the desired value. Figure 5.18 contains the MMC input current of phase "a". Based on this figure, the MMC input current is changed matching the current magnitude to the command, even though with a short period of transient response. Figure 5.19 shows the active and reactive power of MMC with MMC input current changes. According to this figure, both active and reactive powers of MMC are accurately changed based on the governed MMC input current. The circulating current of MMC is also shown in Figure 20. The curve in this figure implies that minimizing circulating current can be effectively accomplished after variation of the input current.

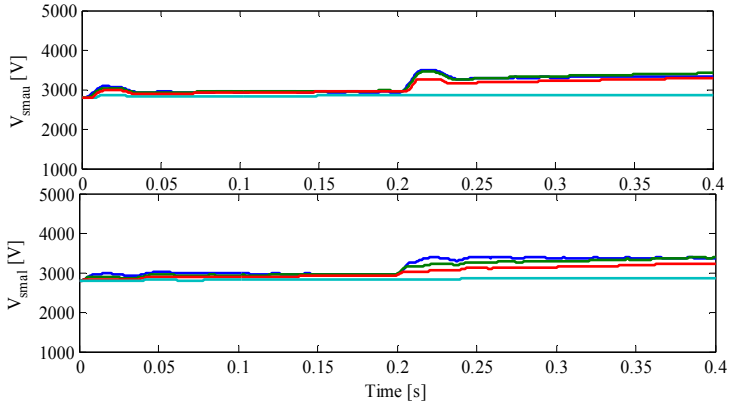

Figure 5.16 - SM voltages of MMC with input MMC current variation.

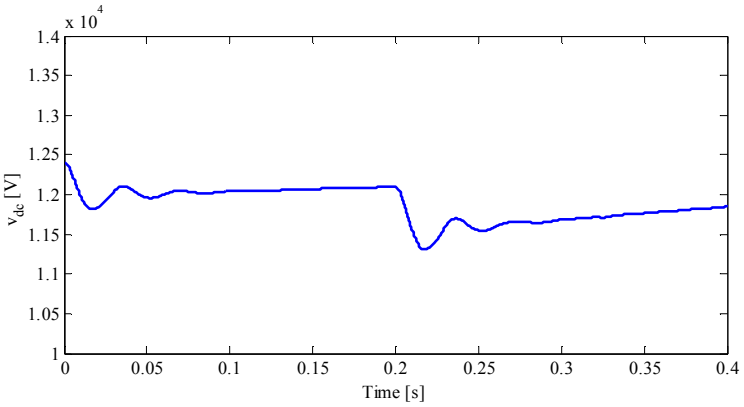

Figure 5.17 - DC-link voltage of MMC with input MMC current variations.

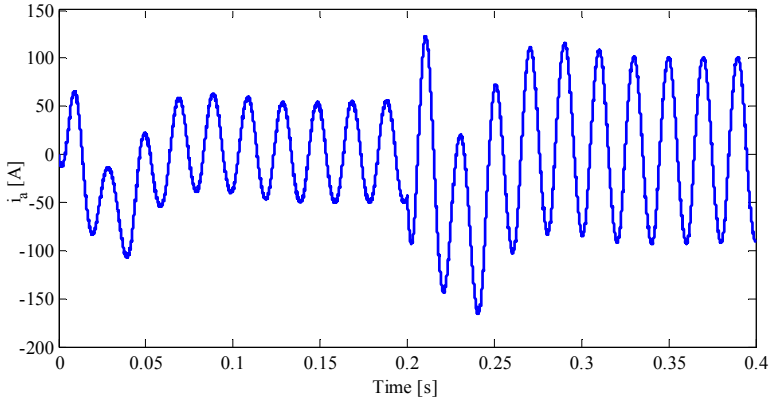

Figure 5.18 - MMC current of phase "a" with MMC input current variations.

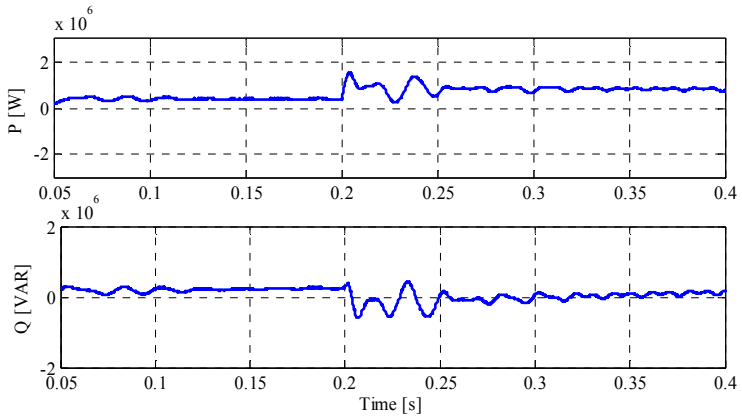

Figure 5.19 - The active and reactive power of MMC with MMC input current variations.

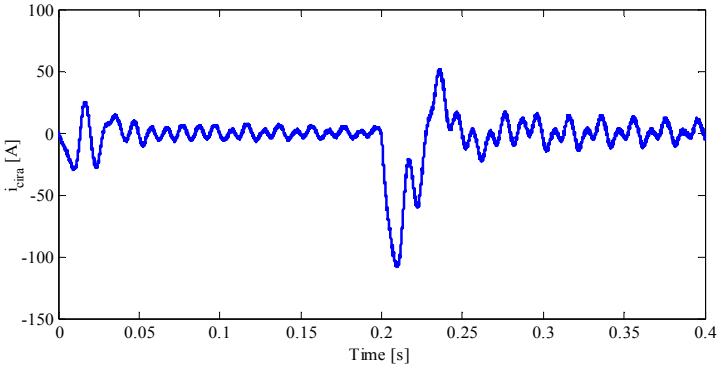

Figure 5.20 - Circulating current of MMC in phase "a" with input MMC current variations.

5.5 Chapter Conclusions

In order to effectively control the operation of MMC in HVDC transmission systems, a novel modulation function with a specified index was proposed in this chapter. For this purpose, analysing all MMC voltages and currents in a-b-c reference frames was performed to primarily obtain the AC side voltage. Then, the combination of the MMC upper and lower arm voltages was achieved by the use of already obtained AC-side voltage. Using this combination led to deriving the proposed modulation function and its modulation index, both depending on MMC parameters, and also the specifications of MMC input voltages and currents. In order to improve the performance of the proposed controller, the impacts of parameters and input current variations on the proposed modulation function and its index were thoroughly investigated in a range of operating points. The main feature of the proposed control technique is its very simple design in a-b-c reference frame, being additionally able to provide a robust performance against MMC parameter changes. MATLAB/SIMULINK allowed verifying the effectiveness of the proposed modulation function-based control technique.

Chapter 6

Dynamic Model, Control and Stability Analysis of MMC in HVDC Transmission Systems

A control technique is proposed in this chapter for control of modular multilevel converters (MMC) in high-voltage direct current (HVDC) transmission systems. Six independent dynamical state variables are considered in the proposed control technique, including two AC currents, three circulating currents, and the DC-link voltage, for effectively attaining the switching state functions of MMCs, as well as for an accurate control of the circulating currents. Several analytical expressions are derived based on the reference values of the state variables for obtaining the MMC switching functions under steady state operating conditions. In addition, dynamic parts of the switching functions are accomplished by direct Lyapunov method (DLM) to guarantee a stable operation of the proposed technique for control of MMCs in HVDC systems. Moreover, the capability curve (CC) of MMC is developed to validate maximum power injection from MMCs into the power grid and/or loads. The impacts of the variations of MMC output and DC-link currents on the stability of DC-link voltage are also evaluated in detail by small-signal analysis.

6.1 Introduction

Nowadays, using different structures of power-electronic converters, the electricity generated through renewable energy resources has been utilized in various forms of industrial applications such as active power filter [141]-[143], grid-connected inverters in micro and smart grids [144]-[149], virtual synchronous generators [150], [151] and distributed generations-based networks [152]-[154]. Among the used power converters, distinguished features of MMCs, including decentralized energy storages, modular structure, easy redundant SMs, simple fault identification and clearance promoted the utilization of MMCs in high and medium voltage/power applications [71], [129]. Attentions have been attracted to designing proper controllers [43], [155], [156], deriving comprehensive general and inner dynamic models [19], [103], [112], [157] and presenting effective modulation methods for the new approach [110], [115], [158] . The most significant technology concerned to connecting remotely located off-shore wind farms interest the major industrial centers and up-to-dated researchers in using the different kinds of MMC in VSC-HVDC transmission systems [104], [106], [159], [160].

Analyzing detailed mathematical models of MMC utilized in HVDC applications offers simultaneous control of active and reactive power and desired DC link voltage in various operating conditions. In [161] an open-loop strategy is designed for controlling the total amount of energy stored inside the MMC. The control technique employs the steady-state solutions of the dynamic equations to make the system globally asymptotically stable [161]. Generic voltage-based and energy-based control structures for MMC inverters are presented in [117] that include voltage balancing between the upper and lower arms. Then, an improved pulse width modulation based control technique is also proposed in the same reference in order to balance the voltage among arm capacitors. The new technique overcomes some major disadvantages corresponding to the applied voltage balancing methods, such as voltage sorting algorithm, extra switching actions, and interference with output voltage. In [162], a digital plug-in repetitive controller is designed to control a carrier-phase-shift pulse-width-modulation (CPS-PWM)-based MMC. The improved circulating current control method with its stability analysis has the merits of simplicity, versatility, and better performance of circulating harmonic current elimination in comparison with the traditional proportional integral controller [162]. Three cost functions based on an MPC are presented in [88] that result in a reduced number of states considered for the AC-side current, circulating current, and capacitor voltage-balancing controls of an MMC. The duty of the first cost function is controlling the AC-side current without considering redundancy. The second one is for the control of the DC-link current ripple, the transient characteristics of the unbalanced voltage condition, and the circulating current. Finally, the last one is designed for reaching the capacitor voltage balancing and reducing the switching frequency of the SM [88]. In addition to the modeling and control schemes analyzed in [163], a switching-cycle state-space model based on the unused switching states of an MMC and the corresponding control method is proposed in [60].

By calculating the average voltage of all SMs in one arm during each control cycle and comparing it with the capacitor voltage of each SM, the switching state of each SM in MMCs is obtained in [61]. In this method, a little sorting of the capacitor voltages is employed and consequently the calculation burden on the controller is significantly decreased.

In order to investigate the impact of the voltage-balancing control on the switching frequency in an MMC, the dynamic relations between the SM's capacitor unbalanced voltage and converter switching frequency are achieved in [164]. Furthermore, by considering negative effects of the unbalanced voltage on the SM capacitor voltage ripple and voltage/current harmonics, the design interaction between switching frequency and SM capacitance, as well as the selection of unbalanced voltage, are also accomplished in [164]. A control technique targeting independent management of capacitor's average voltage in each MMC arm is performed in [165]. In this method, a decomposition of arms energy in different components is considered based on the symmetries of MMC arms. By considering the effects of AC and DC systems, a dynamic MMC model with four independent components of upper and lower arm currents are introduced in [105]. By using this model, dynamical analysis of currents and also design and implementation of current controllers are become simplified.

A dynamic model, control and stability analysis of MMC-HVDC transmission systems is presented in this chapter. This chapter is organized into the following sections. Following the introduction, the dynamic model of MMC-based HVDC is presented in Section 6.2. Steady state analysis of the proposed model is provided in Section 6.3, while dynamic stability analysis is assessed in Section 6.4. In Section 6.5, capability curve analysis of MMC is executed, and DC-link voltage stability analysis is performed in Section 6.6. Simulation results and the highlighted points of this chapter are presented in Sections 6.7 and 6.8.

6.2 The Proposed MMC-Based HVDC Model

The proposed MMC-based HVDC transmission system with two three-phase transformers utilized for the aims of insulation and voltage conversion are illustrated in Figure 6.1. Each MMC is composed of six SMs in its either upper or lower arms along with relevant resistance and inductance to mimic arm losses and limit arm-current harmonics and fault currents, respectively. R_{dc} is the total switching loss of MMCs. Considering each SM to be an IGBT half-bridge converter, rudimentary operational manner of SMs can be explicitly seen throughout dynamic analysis of MMC. Furthermore, the two AC systems are linked to the transformers through resistances and inductances of AC side as shown in Figure 6.1.

The mathematical model

As can be seen in Figure 6.1, grounding points are considered at each neutral point of AC systems and transformers with Y connection. Ascertaining another grounding point in the DC-link voltage of MMCs, (6.1) and (6.2) are obtained by applying KVL law to the loop including DC-link and MMC AC-side voltages as,

$$v_{ki} + L\frac{di_{ki}}{dt} + Ri_{ki} + L_u\frac{di_{uki}}{dt} + R_u i_{uki} - \frac{v_{dc}}{2} + v_{uki} = 0 \tag{6.1}$$

$$-v_{ki} - L\frac{di_{ki}}{dt} - Ri_{ki} + L_l\frac{di_{lki}}{dt} + R_l i_{lki} - \frac{v_{dc}}{2} + v_{lki} = 0 \tag{6.2}$$

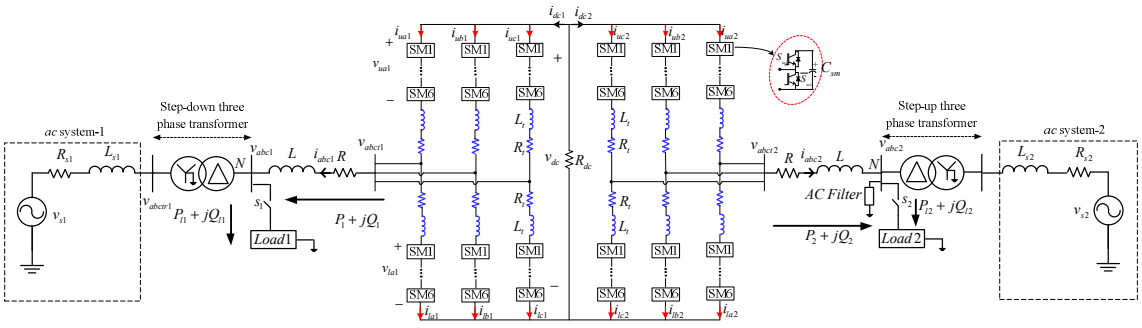

Figure 6.1 - General model of the proposed MMC-based HVDC system.

Following variables are defined as,

$$i_{ki}=i_{uki}-i_{lki},\ i_{cirki}=\frac{i_{uki}+i_{lki}}{2}-\frac{i_{dci}}{3},\ u_{k1i}=\frac{v_{uki}-v_{lki}}{2},\ u_{k2i}=\frac{v_{uki}+v_{lki}}{2} \tag{6.3}$$

Subtracting and summing up (6.1) from and to (6.2), besides using the defined terms in (6.3), the dynamic equations of MMCs can be achieved as,

$$\left(\frac{2L+L_t}{2}\right)\frac{di_{ki}}{dt}+\left(\frac{2R+R_t}{2}\right)i_{ki}+u_{k1i}+v_{ki}=0 \tag{6.4}$$

$$L_t\frac{di_{cirki}}{dt}+R_t i_{cirki}+R_t\frac{i_{dci}}{3}+u_{k2i}-\frac{v_{dc}}{2}=0 \tag{6.5}$$

The equivalent circuits of (6.4) and (6.5) are drawn in Figure 6.2. The output currents of MMCs can be controlled by accurate analysis of the circuit shown in Figure 6.2 (a) and thus the switching function of uk1i is a key factor to regulate MMCs active and reactive power acquired by output currents and voltages.

As shown in Figure 6.2 (b), mitigation of circulating currents is depending on the appropriate adjustment of DC link voltage of MMCs. In addition, the switching function of u_{k1i} plays an important role in effective minimization of undesirable distortions caused by MMC's circulating currents.

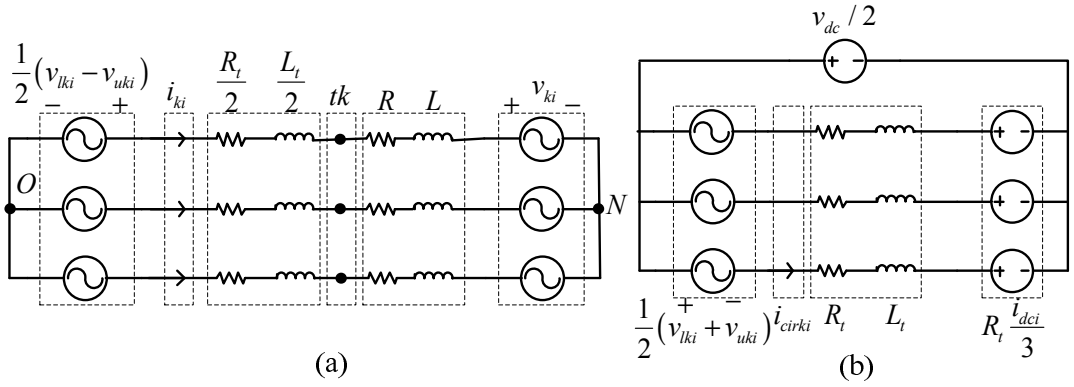

Figure 6.2 - Equivalent circuits of: (a) Dynamic model based on MMC output currents, (b) dynamic model based on circulating currents.

The dynamic relations between DC-link voltage and the upper or lower arms currents can be derived by applying a KCL to the DC-link of Figure 6.1,

$$C_{dc}\frac{dv_{dc}}{dt}+\frac{v_{dc}}{R_{dc}}+\left(i_{uai}+i_{ubi}+i_{uci}\right)+i_{dci'}=0 \tag{6.6}$$

$$C_{dc}\frac{dv_{dc}}{dt}+\frac{v_{dc}}{R_{dc}}+\left(i_{lai}+i_{lbi}+i_{lci}\right)+i_{dci'}=0 \tag{6.7}$$

By adding (6.6) and (6.7) and also using the relationship of circulating current in (6.3), the dynamic relation of DC-link voltage and circulating currents is deduced as,

$$C_{dc}\frac{dv_{dc}}{dt}+\frac{v_{dc}}{R_{dc}}+i_{cirai}+i_{cirbi}+i_{circi}+i_{dc1}+i_{dc2}=0 \tag{6.8}$$

By applying Park's transformation to the (6.4), (6.5), and (6.8), general dynamic equations of the proposed model in $0dq$ reference frame and based on a selected set of state variables including MMC's output currents, circulating currents and also DC-link voltage can be expressed as,

$$
\begin{aligned}
&\left(\frac{2L+L_t}{2}\right)\frac{di_{di}}{dt}+\left(\frac{2R+R_t}{2}\right)i_{di}-\omega\left(\frac{2L+L_t}{2}\right)i_{qi}+u_{d1i}+v_{di}=0\\
&\left(\frac{2L+L_t}{2}\right)\frac{di_{qi}}{dt}+\left(\frac{2R+R_t}{2}\right)i_{qi}+\omega\left(\frac{2L+L_t}{2}\right)i_{di}+u_{q1i}+v_{qi}=0\\
&L_t\frac{di_{cirdi}}{dt}+R_t i_{cirdi}-\omega L_t i_{cirqi}+u_{d2i}=0\\
&L_t\frac{di_{cirqi}}{dt}+R_t i_{cirqi}+\omega L_t i_{cirdi}+u_{q2i}=0\\
&L_t\frac{di_{cir0i}}{dt}+R_t i_{cir0i}+u_{02i}-\frac{3\sqrt{2}v_{dc}}{2}+\sqrt{2}R_t i_{dci}=0\\
&C_{dc}\frac{dv_{dc}}{dt}+\frac{v_{dc}}{R_{dc}}+\sqrt{3}i_{cir0i}+i_{dc1}+i_{dc2}=0
\end{aligned}
\tag{6.9}
$$

The needs for reaching well-designed current control loops and guaranteeing desirably balanced operation of DC-link and SM voltages verify that the different parts of (6.9) should be accurately identified for a fine design of the proposed controller to attain respective aims. The following sections will cover all mentioned points.

6.3 Steady State Analysis

The state variables of the proposed model should be kept in their desired values in steady state operating condition, regardless of experiencing new circumstances such as a step load change. Consequently, the reference values I_{di}^{*} and $I_{qi}^{*}$are calculated as demonstrated in Figure 6.3. As a matter of fact, the q component of AC voltages should be equal to zero for balanced and sinusoidal AC systems. This means that the reference values of MMCs AC voltages are approached to $v_{di}=v_{di}^{*}$ and $v_{di}^{*}=0$. Based on two first terms of (6.9) and with respect to the above points, the first switching state functions of MMC in steady state operating condition are derived as shown in Figure 6.4:

$$
\begin{aligned}
u_{d1i}^{*}&=-\left(\frac{2L+L_t}{2}\right)\frac{di_{di}^{*}}{dt}-\left(\frac{2R+R_t}{2}\right)i_{di}^{*}+\omega\left(\frac{2L+L_t}{2}\right)i_{qi}^{*}-v_{di}^{*}\\
u_{q1i}^{*}&=-\left(\frac{2L+L_t}{2}\right)\frac{di_{qi}^{*}}{dt}-\left(\frac{2R+R_t}{2}\right)i_{qi}^{*}-\omega\left(\frac{2L+L_t}{2}\right)i_{di}^{*}
\end{aligned}
\tag{6.10}
$$

In the same condition, the circulating currents of MMCs should be governed to become zero, $i_{cirdi}^{*}=i_{cirqi}^{*}=i_{cir0i}^{*}=0$. As a result, the second switching functions of MMCs are obtained in accordance to (6.9) and given in Figure 6.5.

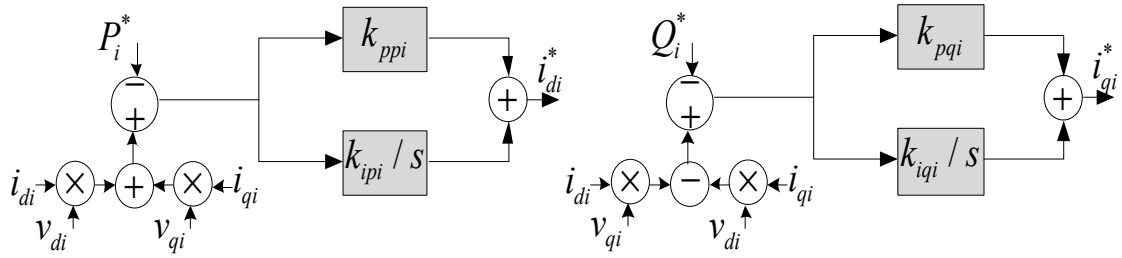

Figure 6.3 - Calculation of MMC output currents.

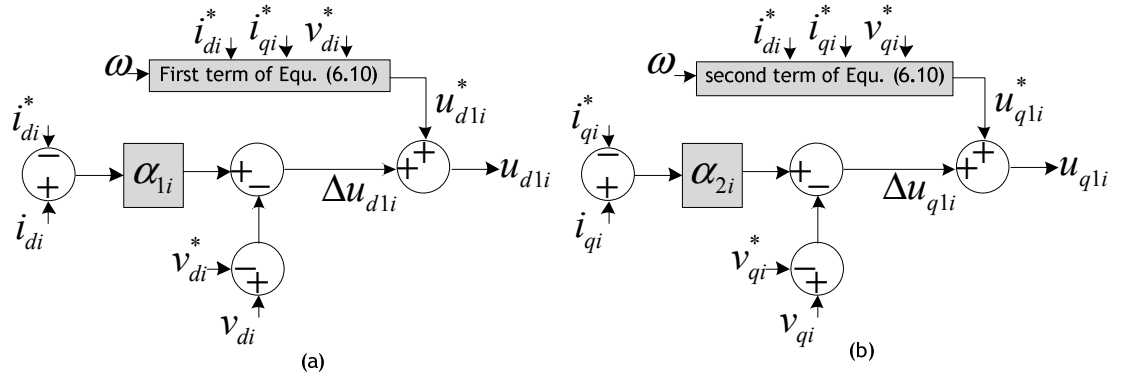

Figure 6.4 - Switching functions based on MMC output currents (a) d-component, (b) q-component.

$$u_{d2i}^* = 0,\ u_{q2i}^* = 0,\ u_{02i}^* = \frac{3\sqrt{2}v_{dc}^*}{2} - \sqrt{2}R_i i_{dci}^* \tag{6.11}$$

Combining (6.10) and (6.11) leads to the main upper and lower switching functions of MMCs in steady state operation. Using the last term of (6.9), the dynamic of DC link voltage in steady state can be expressed as,

$$\frac{dv_{dc}^*}{dt} = -\frac{v_{dc}^*}{C_{dc}R_{dc}} - \frac{i_{dc1}^*}{C_{dc}} - \frac{i_{dc2}^*}{C_{dc}} \tag{6.12}$$

Equation (6.12) shows the dynamic relation between DC link voltage and currents of MMCs. Under the steady state operation, DC link voltage will be equal to,

$$v_{dc}^{*} = -R_{dc}\left(i_{dc1}^{*} + i_{dc2}^{*}\right) \tag{6.13}$$

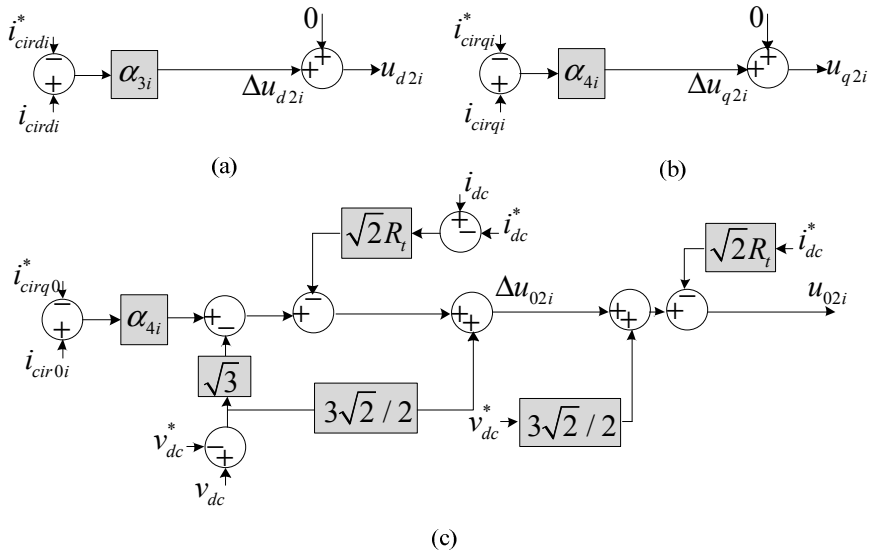

Figure 6.5 - Switching functions based on circulating currents (a) d-component, (b) q-component, (c) 0-component.

Equation (6.13) shows that DC link voltage is dependent on DC currents of MMCs in steady state operating condition. Since DC currents of MMCs are related to the lower and upper MMCs currents, it is understood from (6.13) that a proper control of output and circulating currents of MMCs yields a balanced value for DC link voltage of MMCs.

6.4 Dynamic Stability Analysis

An accurate operation of the system can be provided by taking all possible dynamic changes into account. Dynamic presentation of all state variables involved in the proposed HVDC system can be stated as,

$$\begin{aligned} &x_{1i} = i_{di} - i_{di}^{*},\ x_{2i} = i_{qi} - i_{qi}^{*},\ x_{3i} = i_{cirdi} - i_{cirdi}^{*} \\ &x_{4i} = i_{cirqi} - i_{cirqi}^{*},\ x_{5i} = i_{cir0i} - i_{cir0i}^{*},\ x_{6i} = v_{dc} - v_{dc}^{*} \end{aligned} \tag{6.14}$$

Total dynamic saved energy is a basic requirement for DLM. Following the points discussed above, the dynamic energy function of the proposed model can be calculated as,

$$H(\bar{x}_i)=\frac{2L+L_t}{4}x_{1i}^2+\frac{2L+L_t}{4}x_{2i}^2+\frac{L_t}{2}x_{3i}^2+\frac{L_t}{2}x_{4i}^2+\frac{L_t}{2}x_{5i}^2+\frac{C_{dc}}{2}x_{6i}^2 \tag{6.15}$$

The time-based derivation of (6.15) can be expressed as,

$$\begin{aligned}\dot{H}(\bar{x}_i)=&\frac{2L+L_t}{2}x_{1i}\dot{x}_{1i}+\frac{2L+L_t}{2}x_{2i}\dot{x}_{2i}+L_t x_{3i}\dot{x}_{3i}+\\&L_t x_{4i}\dot{x}_{4i}+L_t x_{5i}\dot{x}_{5i}+C_{dc}x_{6i}\dot{x}_{6i}\end{aligned} \tag{6.16}$$

Each part of (6.16) can be obtained from (6.9) and (6.14) as,

$$\begin{aligned}&\frac{2L+L_t}{2}\dot{x}_{1i}x_{1i}=-\left(\frac{2R+R_t}{2}\right)x_{1i}^2+\omega\left(\frac{2L+L_t}{2}\right)x_{2i}x_{1i}\\&-\left(u_{d1i}-u_{d1i}^*\right)x_{1i}-\left(v_{di}-v_{di}^*\right)x_{1i}\\&\frac{2L+L_t}{2}\dot{x}_{2i}x_{2i}=-\left(\frac{2R+R_t}{2}\right)x_{2i}^2-\omega\left(\frac{2L+L_t}{2}\right)x_{1i}x_{2i}\\&-\left(u_{q1i}-u_{q1i}^*\right)x_{2i}-\left(v_{qi}-v_{qi}^*\right)x_{2i}\\&L_t\dot{x}_{3i}x_{3i}=-R_t x_{3i}^2+\omega L_t x_{4i}x_{3i}-\left(u_{d2i}-u_{d2i}^*\right)x_{3i}\\&L_t\dot{x}_{4i}x_{4i}=-R_t x_{4i}^2-\omega L_t x_{3i}x_{4i}-\left(u_{q2i}-u_{q2i}^*\right)x_{4i}\\&L_t\dot{x}_{5i}x_{5i}=-R_t x_{5i}^2-\left(u_{02i}-u_{02i}^*\right)x_{5i}+\\&\frac{3\sqrt{2}}{2}\left(v_{dc}-v_{dc}^*\right)x_{5i}-\sqrt{2}R_t\left(i_{dci}-i_{dci}^*\right)x_{5i}\\&c_{dc}\dot{x}_{6i}x_{6i}=-\frac{x_{6i}^2}{R_{dc}}-\sqrt{3}x_{5i}x_{6i}-\left(i_{dc1}-i_{dc1}^*\right)x_{6i}\\&-\left(i_{dc2}-i_{dc2}^*\right)x_{6i}\end{aligned} \tag{6.17}$$

In addition, the MMCs switching functions are extended to (6.18) with dynamic components which are used by the proposed controller during dynamic changes,

$$u_{dq(12)i}=\Delta u_{dq(12)i}+u_{dq(12)i}^* \tag{6.18}$$

The first part of (6.18), $\Delta u_{dq(12)i}$, is the dynamic part of the MMC switching functions in d-q reference frame that can be achieved by DLM. This part is responsible to maintain the stability of the proposed model against load variations. Second part of (6.18) is related to the steady state part of MMC switching functions shown as $u^*_{dq(12)i}$. This part is employed so that the state variables of the proposed model follow a special reference values without any dynamic change.

By substitution of (6.17) and (6.18) in (6.16), the summarized derivation of MMCs total saved energy is attained as (6.19),

$$\begin{aligned}
\dot{H}(\bar{x}_i) = &-\left(\frac{2R+R_t}{2}\right)x_{1i}^2-\left(\frac{2R+R_t}{2}\right)x_{2i}^2-R_t x_{3i}^2-R_t x_{4i}^2-R_t x_{5i}^2\\
&-\left(\Delta u_{d1i}+\left(v_{di}-v_{di}^*\right)\right)x_{1i}-\left(\Delta u_{q1i}+\left(v_{qi}-v_{qi}^*\right)\right)x_{2i}-\left(\Delta u_{d2i}\right)x_{3i}\\
&-\left(\Delta u_{q2i}\right)x_{4i}-\left(\Delta u_{02i}-\frac{3\sqrt{2}}{2}x_{6i}+\sqrt{2}R_t\left(i_{dci}-i_{dci}^*\right)+\sqrt{3}x_{6i}\right)x_{5i}\\
&-\left(\left(\left(i_{dc1}-i_{dc1}^*\right)+\left(i_{dc2}-i_{dc2}^*\right)\right)x_{6i}+\frac{x_{6i}^2}{R_{dc}}\right)
\end{aligned} \tag{6.19}$$

According to DLM, a time-varying system with certain state variables will become asymptotically globally stable, if the total saved energy function of system is positive and its derivative is definitely negative.

Therefore, taking into account DLM principle and all terms present in (6.19), the dynamic components of the MMCs switching functions are,

$$\begin{aligned}
&\Delta u_{d1i}=\alpha_{1i}x_{1i}-\left(v_{di}-v_{di}^*\right),\ \Delta u_{q1i}=\alpha_{2i}x_{2i}-\left(v_{qi}-v_{qi}^*\right)\\
&\Delta u_{d2i}=\alpha_{3i}x_{3i},\quad \Delta u_{q2i}=\alpha_{4i}x_{4i}\\
&\Delta u_{02i}=\alpha_{5i}x_{5i}-\left(-\frac{3\sqrt{2}}{2}x_{6i}+\sqrt{2}R_t\left(i_{dci}-i_{dci}^*\right)+\sqrt{3}x_{6i}\right)
\end{aligned} \tag{6.20}$$

The coefficients of α_{3i} are the effective factors for regulating the dynamic parts of the proposed controller that should be chosen appropriately [125]. Terms of (6.20) guarantee the ultimate designed controller operation against any sudden dynamic changes. As can be seen in (6.20), due to presence of steady state values in (6.20), the accurate performance of dynamic parts of switching function are highly reliant on the correct functioning of the proposed model in steady state conditions. Considering (6.20), all terms available in (6.19) can evidently identified to be negative values or zero except for the last term that is,

$$-\left(\left(\left(i_{dc1}-i_{dc1}^{*}\right)+\left(i_{dc2}-i_{dc2}^{*}\right)\right)x_{6i}+\frac{x_{6i}^{2}}{R_{dc}}\right) \tag{6.21}$$

By assuming balanced MMCs circulating currents, equation (6.8) can be rewritten as,

$$C_{dc}\frac{dv_{dc}}{dt}+\frac{v_{dc}}{R_{dc}}+i_{dc1}+i_{dc2}=0 \tag{6.22}$$

Equation (6.21) can also be restated with respect to (6.14) and (6.22) as,

$$C_{dc}x_{6i}\frac{dx_{6i}}{dt} \tag{6.23}$$

In order to investigate the impact of (6.23) on (6.19), the various possible amounts that exist for (6.23) are discussed in this section. Figure 6.6 shows the various states of (6.23). Noticing the reference value demonstrated in red, two possible constant and fluctuated states are considered for DC-link voltage as shown in Figure 6.6. The constant states specified with state 1 and 2 can be more or less than the reference value (for equal value, $x_{6i}=0$). For fluctuated cases, three states are considered. As can be seen in Figure 6.6, for the states of 1 and 2, (6.23) is equal to zero $(dx_{6i}/dt=0)$. Moreover, for fluctuated states, since the sign of dx_{6i}/dt is varying due to the variation of voltage slopes, the ultimate value of (6.23) becomes periodically positive or negative as depicted in Figure 6.6. This is indicating that (6.23) is always close to zero in other states and consequently not able to noticeably impact the negative value of (6.19). Therefore, the whole term of (6.19) is definitely negative or zero.

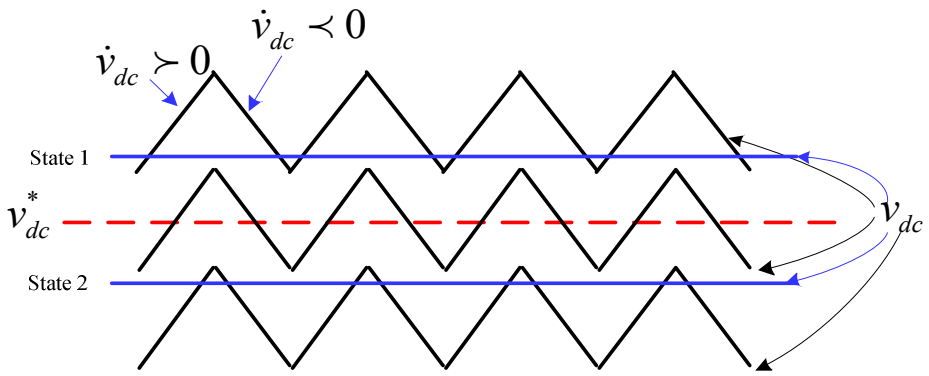

Figure 6.6 - Different states of v_{dc} and dv_{dc}/dt.

6.5 Capability Curve Analysis of the MMCs

Identifying maximum capability of each MMC in active and reactive power injection during operating condition of HVDC system leads to a more accurate design for the controller. The relation between the DC-link voltage and the AC side voltage of each MMC shown in Figure 6.1 can be achieved as,

$$v_{dc} i_{dci} = v_{tdi} i_{di} + v_{tqi} i_{qi} \tag{6.24}$$

In addition, the relation between the AC side and the output voltage of each MMC in d-q frame can be driven by applying KVL's law to Figure 6.1,

$$\begin{aligned} v_{tdi} &= v_{di} + L\frac{di_{di}}{dt} + Ri_{di} - \omega L i_{qi} \\ v_{tqi} &= v_{qi} + L\frac{di_{qi}}{dt} + Ri_{qi} + \omega L i_{di} \end{aligned} \tag{6.25}$$

By assuming $di_{aqi}/dt = I_{avdqi}$ and substituting (6.25) in (6.24), the following circle is obtained as,

$$\begin{aligned}
&\left(i_{di}+\psi\right)^2+\left(i_{qi}+\chi\right)^2=r^2\\
&\psi=\frac{LI_{avdi}+v_{di}}{2R},\chi=\frac{LI_{avqi}+v_{qi}}{2R}\\
&r=\sqrt{\frac{\left(LI_{avdi}+v_{di}\right)^2+\left(LI_{avqi}+v_{qi}\right)^2+4Rv_{dc}i_{dci}}{4R^2}}
\end{aligned} \tag{6.26}$$

Equation (6.26) is a circle with the center of $(-\psi,-\chi)$and radius of r. This circle describes a given area of MMC output current based on a dq frame in which the maximum and minimum values of the current can be accurately calculated. By substituting $i_{di}=P_i/v_{di}$ and $i_{qi}=Q_i/v_{di}$ in (6.26), the following relation is obtained as,

$$\left(P_i+\psi'\right)^2+\left(Q_i+\chi'\right)^2=r'^2\Rightarrow\psi'=v_{di}\psi,\ \chi'=-v_{di}\chi,\ r'=v_{di}r \tag{6.27}$$

The relation described in (6.27) is the capability curve of MMC as a circle with the center of $(-\psi',-\chi')$ and radius of r'. Capability curve of MMCs are plotted in Figure 6.7. The smallest circles shown in Figure 6.7(a) and Figure 6.7(b) are typical MMC CC with $i_{dc}>0$ and $i_{dc}<0$ respectively. By increasing the positive values of i_{dc} and decreasing the negative values of i_{dc}, CC can vary as depicted in Figure 6.7 for different DC-link current values. As shown in these figures, the positive and negative areas of CC are significantly altered for both active and reactive power by changing DC-link currents. This has to be noted while designing any control process.

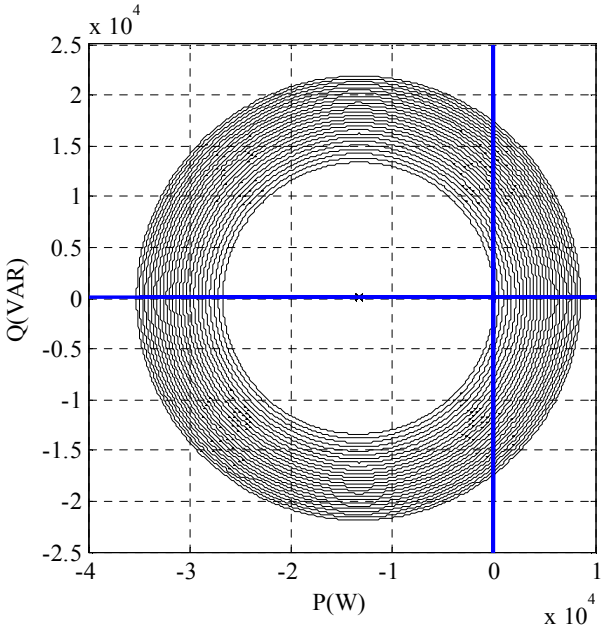

(a)

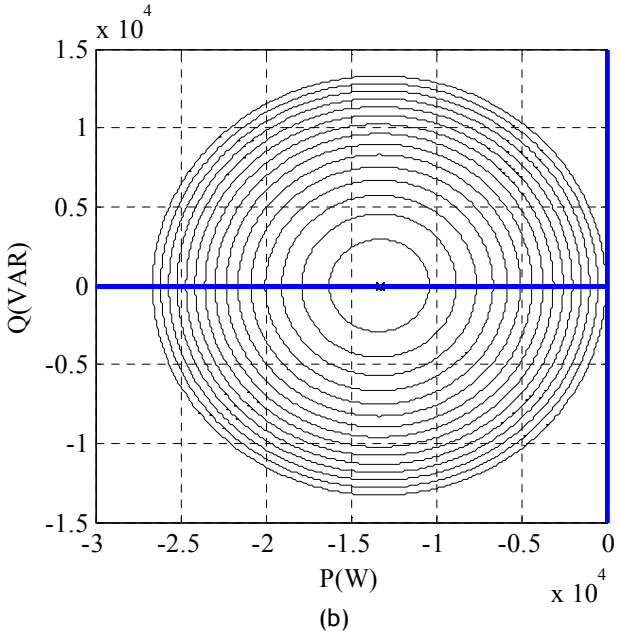

(b)

Figure 6.7 - Capability curve of MMCs (a) increasing $i_{dc} > 0$, (b) decreasing $i_{dc} < 0$.

6.6 DC-Link Voltage Stability Analysis

How the changes of different variables available in the proposed HVDC system affect the DC-link voltage stability is discussed in this section. With respect to (6.22), next equation can be inferred as,

$$C_{dc}\frac{dv_{dc}}{dt} + \frac{v_{dc}}{R_{dc}} = -\frac{P_1 + P_2}{v_{dc}} \tag{6.28}$$

Applying small signal linearization to (6.28), the relation between DC link voltage and MMC active power variation is obtained as,

$$\left(C_{dc}s + \frac{1}{R_{dc}} - \frac{P_1^* + P_2^*}{v_{dc}^{*2}}\right)\Delta v_{dc} = -\frac{\Delta P_1 + \Delta P_2}{v_{dc}^*} \tag{6.29}$$

By substituting (6.25) in (6.24), (6.30) is achieved as,

$$v_{dc}i_{dci} = P_i + \frac{L}{2}\frac{di_{di}^2}{dt} + Ri_{di}^2 + \frac{L}{2}\frac{di_{qi}^2}{dt} + Ri_{qi}^2 \tag{6.30}$$

Another relation between Δv_{dc} and ΔP_i can be derived by the use of small signal linearization for (6.30) as,

$$\Delta P_i = \Delta v_{dc} i_{dci}^* + v_{dc}^* \Delta i_{dci} - (Ls + 2R) i_{di}^* \Delta i_{di} - (Ls + 2R) i_{qi}^* \Delta i_{qi} \tag{6.31}$$

By substituting (6.31) in (6.29), the effects of active power of MMC1 and MMC2 on the DC link voltage can be stated as (6.32) and (6.33) respectively,

$$\left[\Delta v_{dc} \middle| \langle \Delta P_2 = 0 \rangle\right] = [\Delta v_{dc1}] =$$
$$\begin{bmatrix} \frac{(Ls+2R) i_{d1}^*}{\Delta_1} & \frac{(Ls+2R) i_{q1}^*}{\Delta_1} & -\frac{v_{dc}^*}{\Delta_1} \end{bmatrix} \begin{bmatrix} \Delta i_{d1} \\ \Delta i_{q1} \\ \Delta i_{dc1} \end{bmatrix} = \begin{bmatrix} f_{11} & f_{12} & f_{13} \end{bmatrix} \begin{bmatrix} \Delta i_{d1} \\ \Delta i_{q1} \\ \Delta i_{dc1} \end{bmatrix} \tag{6.32}$$

$$\left[\Delta v_{dc} \middle| \langle \Delta P_1 = 0 \rangle\right] = [\Delta v_{dc2}] =$$
$$\begin{bmatrix} \frac{(Ls+2R) i_{d2}^*}{\Delta_2} & \frac{(Ls+2R) i_{q2}^*}{\Delta_2} & -\frac{v_{dc}^*}{\Delta_2} \end{bmatrix} \begin{bmatrix} \Delta i_{d2} \\ \Delta i_{q2} \\ \Delta i_{dc2} \end{bmatrix} = \begin{bmatrix} f_{21} & f_{22} & f_{23} \end{bmatrix} \begin{bmatrix} \Delta i_{d2} \\ \Delta i_{q2} \\ \Delta i_{dc2} \end{bmatrix} \tag{6.33}$$

Considering steady state operational condition of (6.28), Δ_i is equal to,

$$\Delta_i = \left(C_{dc} v_{dc}^* s + \frac{2 v_{dc}^*}{R_{dc}} + i_{dci}^* \right) \tag{6.34}$$

Using (6.32) and (6.33), each part of DC-link voltage variations can be rewritten as follows,

$$\Delta v_{dci} = f_{i1} \Delta i_{di} + f_{i2} \Delta i_{qi} + f_{i3} \Delta i_{dci} \tag{6.35}$$

Thus, the effects of the MMC d-q components and DC-link currents variation on DC-link voltage stability can be evaluated by (6.35). The Nyquist diagrams of each f_{ij} for various positive increasing values of DC-link current are separately depicted in Figure 6.8. As realized from Figure 6.8 (a) and Figure 6.8 (b), f_{i1} and f_{i2} cannot lead to a noticeable instability in DC-link voltage. But, according to Figure 6.8 (c), f_{i3} significantly increases the instability margins in both generation and control processes of DC-link voltage in HVDC system. For this case, regulating DC-link current at desired value is a vital operation in order to reach a stable DC-link voltage. The same discussion is governed for various negative decreasing values of DC-link current as shown in Figure 6.9. However, by decreasing the negative values of DC-link current, f_{i3} diagram is gone to the right-hand part and its magnitude is drastically decreased as illustrated in Figure 6.9 (c) and consequently improves the stabilizing properties of f_{i3}.

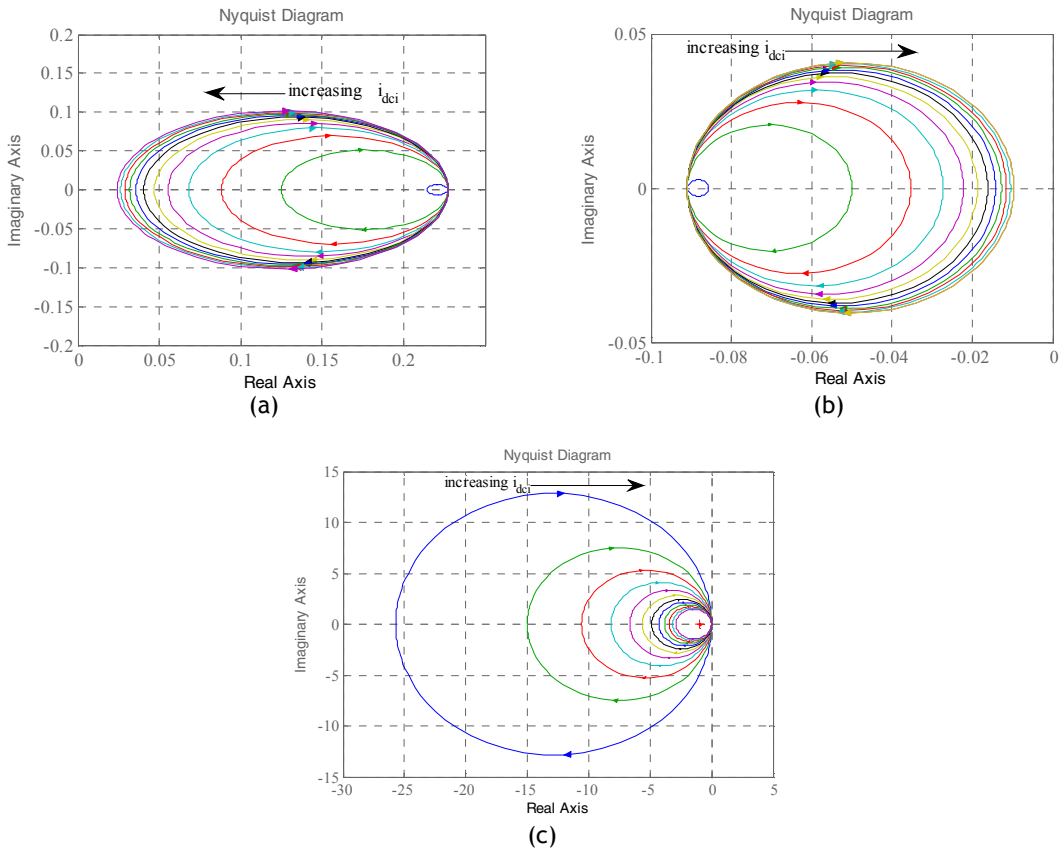

Figure 6.8 - Nyquist diagram of DC-link voltage variations for $i_{dci} > 0$ due to (a) d-component variations of MMC current (f_{i1}) (b) q-component variations of MMC current (f_{i2}) (c) DC-link current variations (f_{i3}).

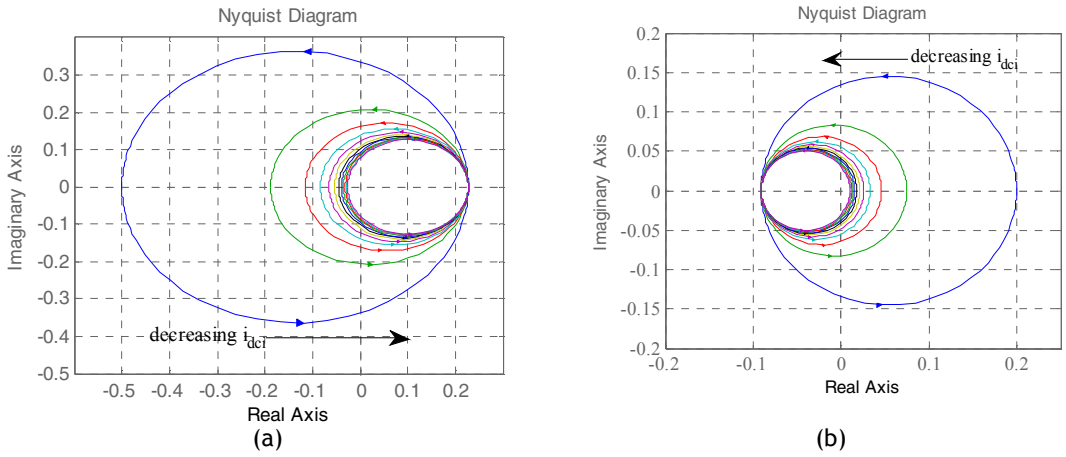

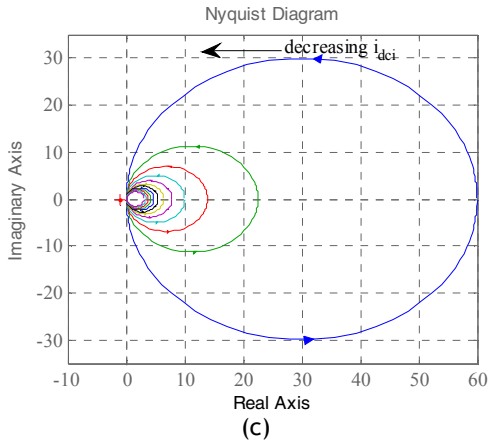

(c)

Figure 6.9 - Nyquist diagram of DC-link voltage variations for $i_{dci} < 0$ due to: (a) d-component variations of MMCs currents (f_{i1}), (b) q-component variations of MMCs currents (f_{i2}), and (c) DC-link current variations (f_{i3}).

6.7 Simulation Results

The purpose of this section is to assess the capability of the proposed control scheme at reaching the desired values of MMC currents, voltages, and active and reactive power under both dynamic and steady state operating conditions. System parameters and the MMC rated values are listed in Table 6.1. SimPower package of Matlab software is utilized to execute this assessment process as structured in Figure 6.10. For the modulation method, SLPWM technique is selected to synthesize gate switching signals for MMCs.

Table 6.1 - Units for Simulated MMC-based System

f_{ac}	60 Hz	C	4 mF
f_s	10 kHz	C_{fi}	65 0μF
v_{dc}^*	18 kV	P_i	20 MW
v_c	3 kV	Q_i	10 MVAR
L	45 mH	Transformer power rating	8 kV/23kV (Δ/Y)
R	0.3 Ω	MMC1 load I	75 MW,-25 MVAR
L_t	12 mH	MMC1 load II	85 MW,80 MVAR
R_t	1 Ω	MMC2 load I	20 MW,7 MVAR
n	6	MMC2 load II	35 MW,25 MVAR

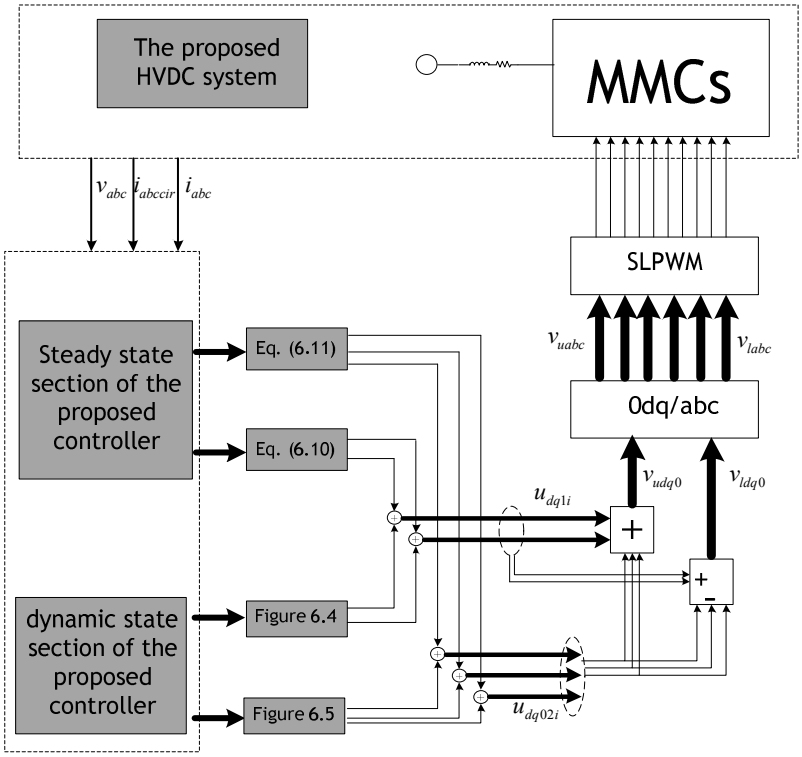

Figure 6.10 - Overall structure of the proposed controller.

To show effectively the impact of DLM on the stability of the proposed controller, two simulation processes will be considered. As a common operation in both processes, firstly the proposed HVDC system works in steady state and each MMC is responsible to supply active and reactive power required by the respective loads. Then, in the second time of each simulation, load changes take place at $t = 0.4\ s$ and $t = 0.6\ s$ for MMC1 and MMC2, respectively, in which, in the first process DLM is not used, while the completed proposed controller with DLM is employed in the second process. The results are presented and discussed in the following section.

6.7.1 DC-Link and AC Voltages Evaluation

Figures 6.11 and 6.12 shows SM voltages and also DC and AC side voltages of MMCs in two simulation processes: without and with DLM. As can be observed, appropriate steady-state operation for DC-link voltage, upper and lower SMs voltages, and AC side voltages of MMCs are achieved with DLM.

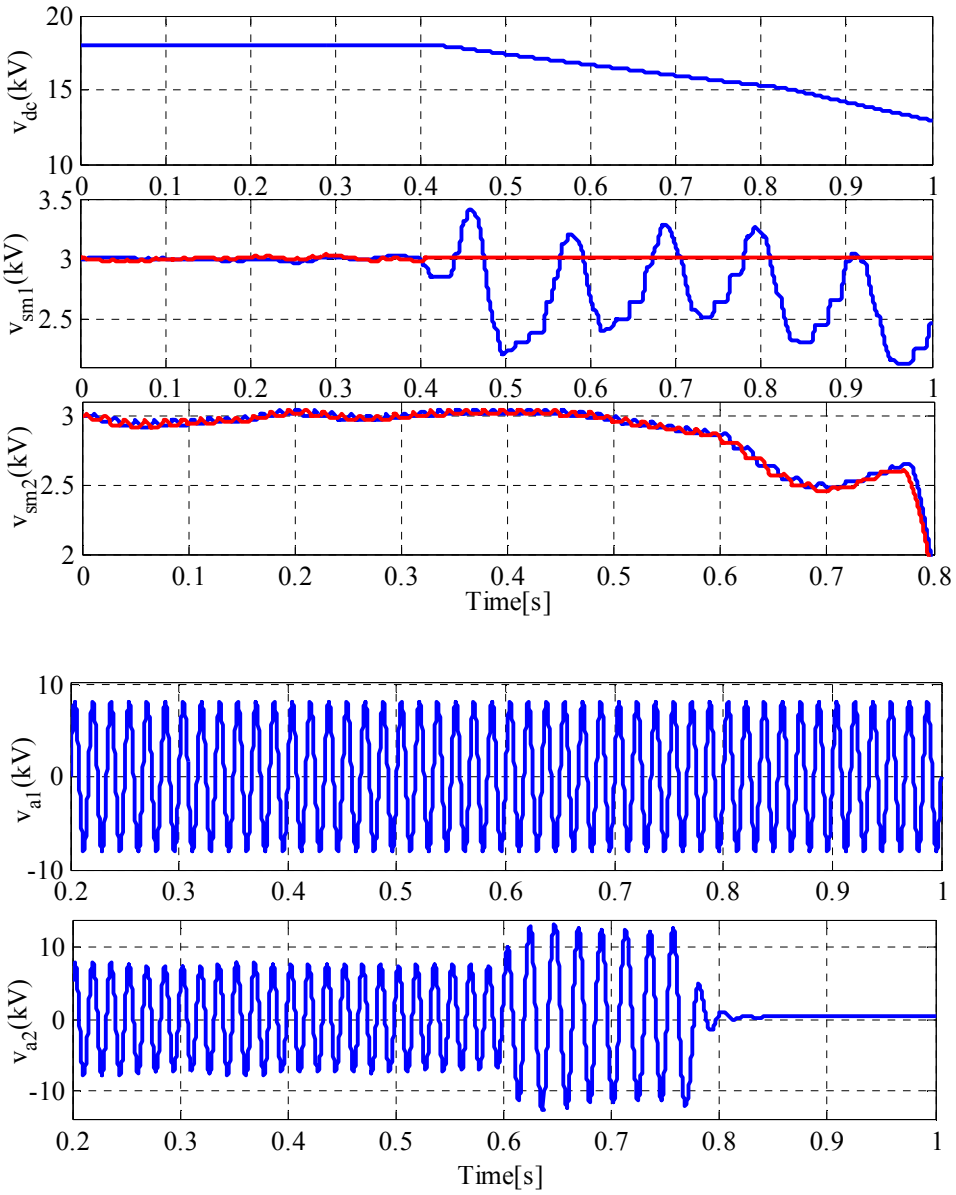

Figure 6.11 - SM voltages and DC and AC side voltages of MMCs without DLM.

Figure 6.11 shows that not using DLM in the proposed controller leads to the divergence of MMCs voltages from its desired values when the load changes happen for MMC1 and MMC2 at $t = 0.4\,s$ and $t = 0.6\,s$, respectively. Figure 6.12 demonstrates the accurate operation of the proposed controller included DLM in both dynamic and steady states. According to this figure, in response to a transient variation, the DC link voltage is kept in desired value with small deviations. In addition, during both dynamic and steady operation of the proposed controller, the upper and lower SMs voltages follow the reference value of $v_{dc}^{*}/6$ with acceptable fluctuations. The appropriate AC side voltages of MMCs are also obtained as shown in Figure 6.12. The MMC2

should act as an inverter and consequently generation of sinusoidal and balanced AC voltages is a main duty of MMC2, which is completely performed as depicted in Figure 6.12.

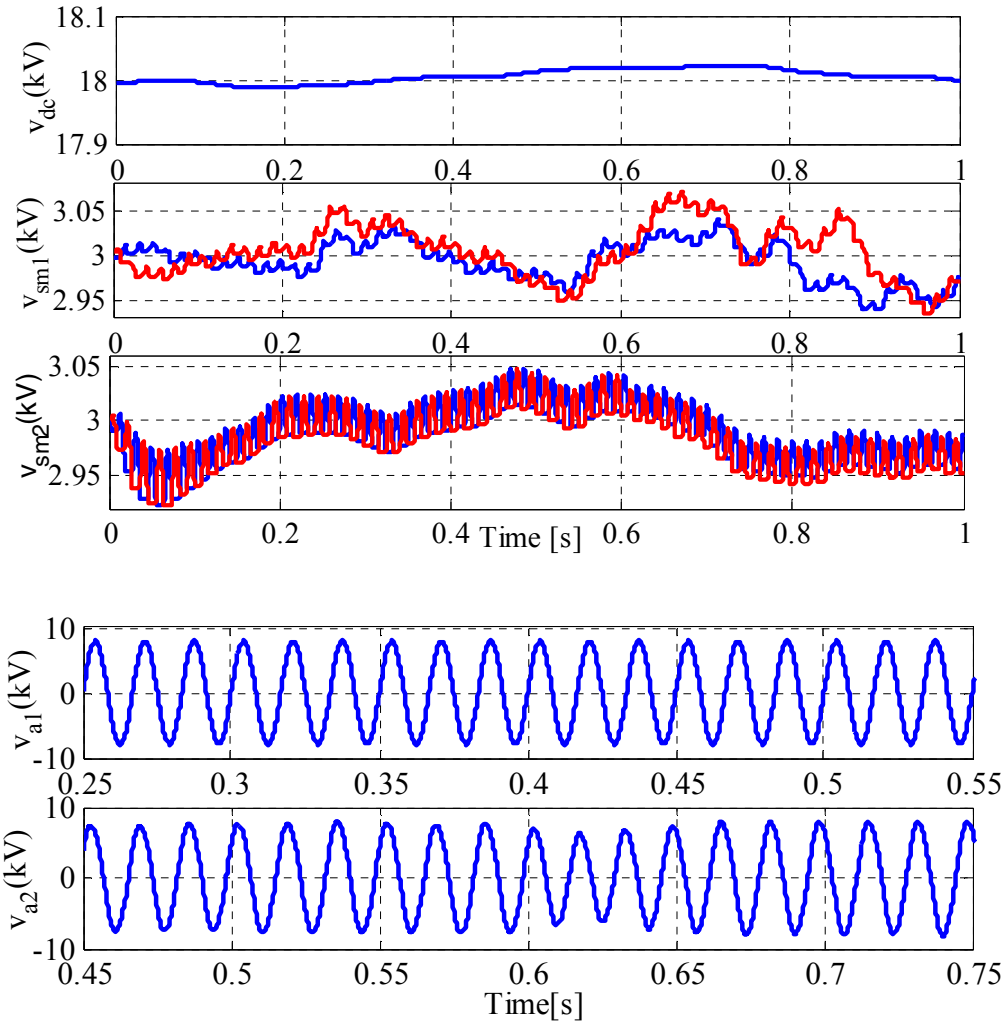

Figure 6.12 - SM voltages and DC and AC side voltages of MMCs with DLM.

6.7.2 Analysis of MMC Currents

To verify suitable performance of the proposed control technique for minimizing MMC circulating currents and regulating DC-link and AC currents of MMCs, Figures 6.13 and 14 can be referred to.

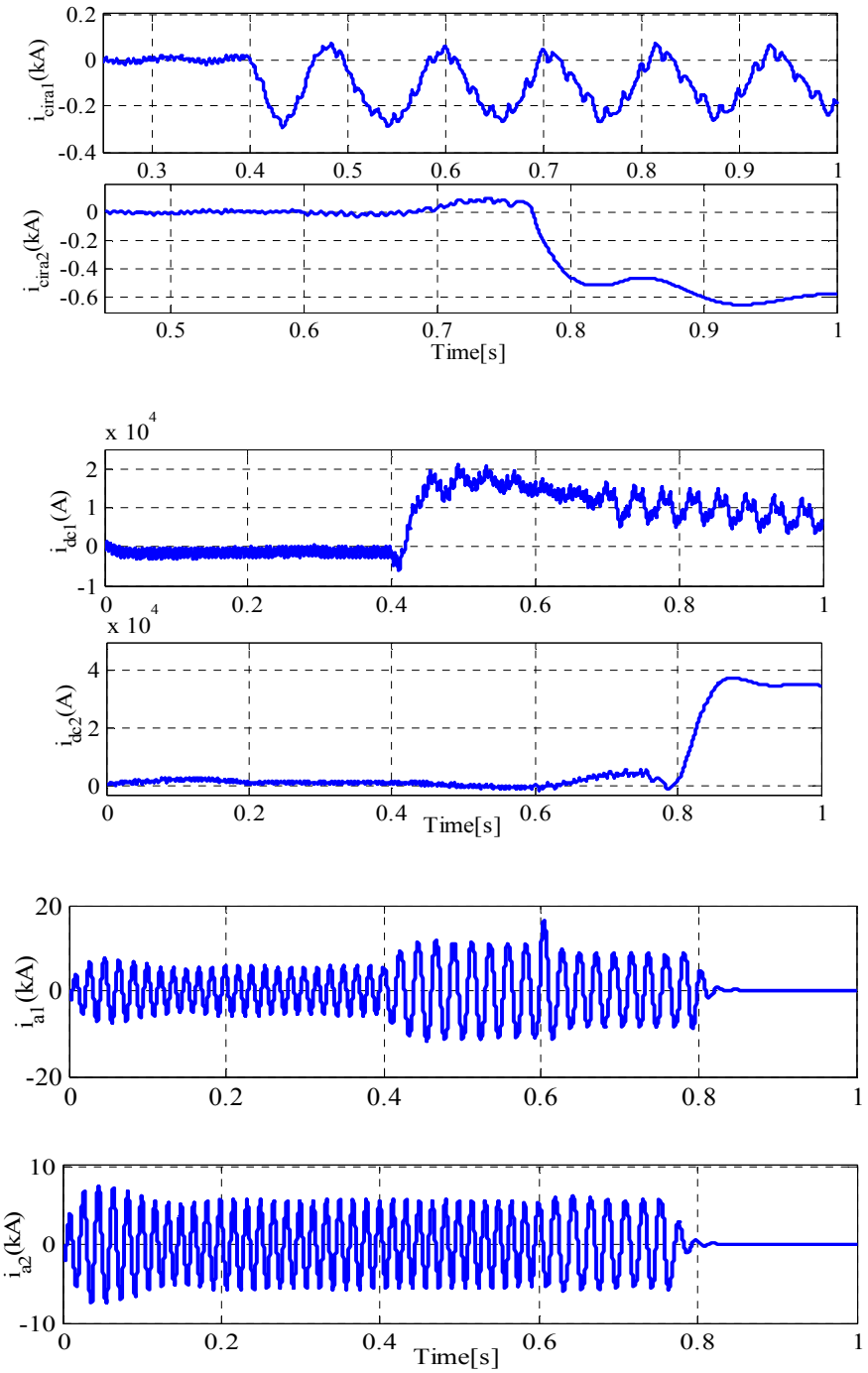

Figure 6.13 - Circulating, DC-link and AC-side currents of the interfaced MMCs without DLM.

Figure 6.13 shows the simulation results of the proposed MMC-based HVDC system under operation of the proposed controller without DLM. As it can be understood from this figure, when load changes take place for MMCs, the controller without DLM is not able to keep the proposed system in stable operation and consequently the currents of MMC1 and MMC2 become unstable at $t = 0.4\ s$ and $t = 0.6\ s$, respectively. From circulating current waveforms of Figure

6.14, it can be derived that minimizing these currents in both MMCs are properly done by the steady state section of the proposed controller and subsequently, in case of sudden loads changes, DLM fully provides dynamic control requirements in order to keep the currents at the minimized values.

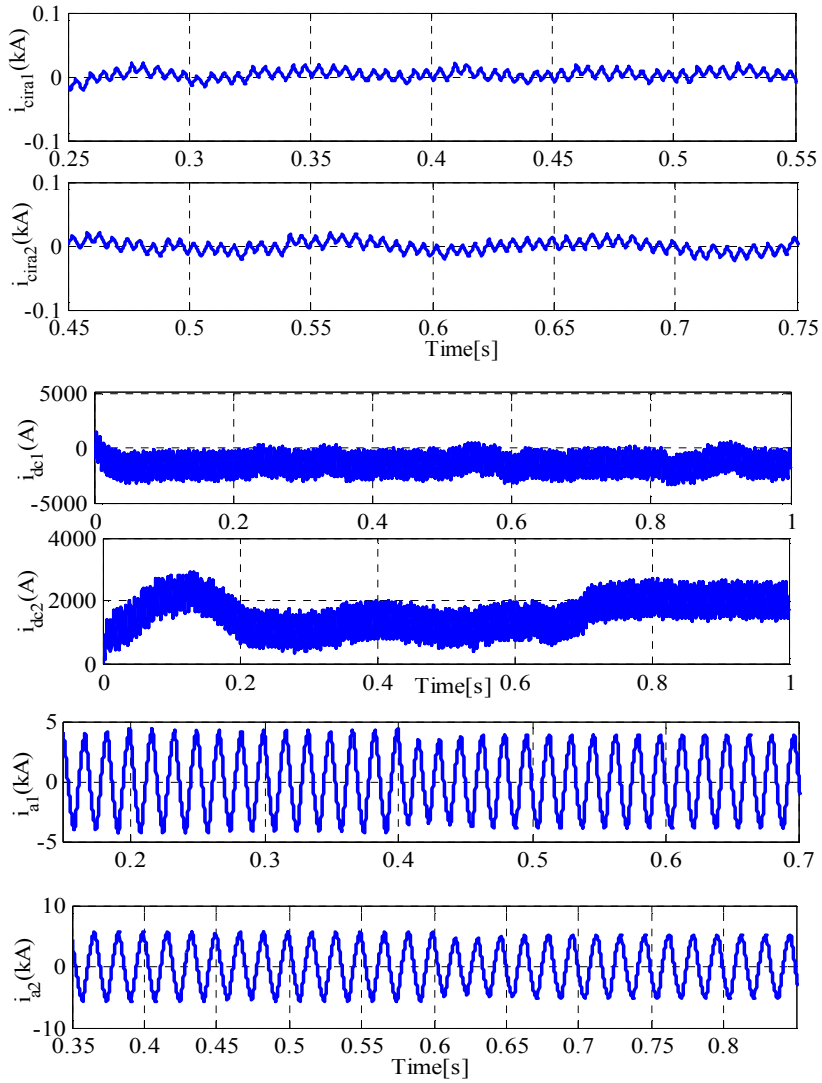

Figure 6.14 - Circulating, DC-link and AC-side currents of the interfaced MMCs with DLM.

Moreover, Figure 6.14 shows the DC link currents of MMC1 and MMC2 respectively in both dynamic and steady states. Considering the dynamic step change time $t = 0.4\,s$ and $t = 0.6\,s$ for MMC1 and MMC2 respectively, the duration of transient time and transient error values are insignificant in the second simulation process with DLM. Also the AC-side currents of MMCs are shown in Figure 6.14. As can be seen, current waveforms and their changes are proportional to the instantaneous needs of the load. They are also influenced by the function of keeping output

voltages of MMC2 sinusoidal and balanced. The d and q components of MMC currents are shown in Figures 6.15 and 6.16. As can be seen, these components become unstable when DLM is not considered in the proposed control technique. When DLM is used in dynamic state operation of the proposed HVDC system, these currents move on their desired values with a small transient response time.

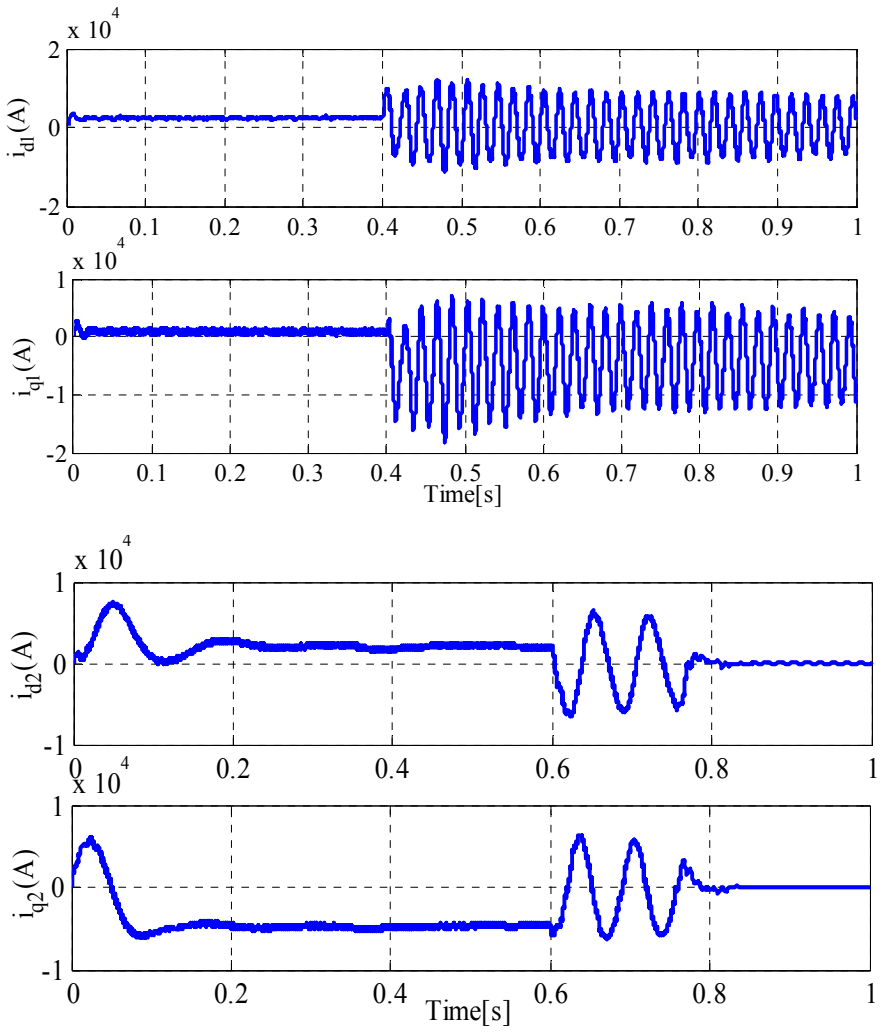

Figure 6.15 - d and q components of MMCs currents without DLM.

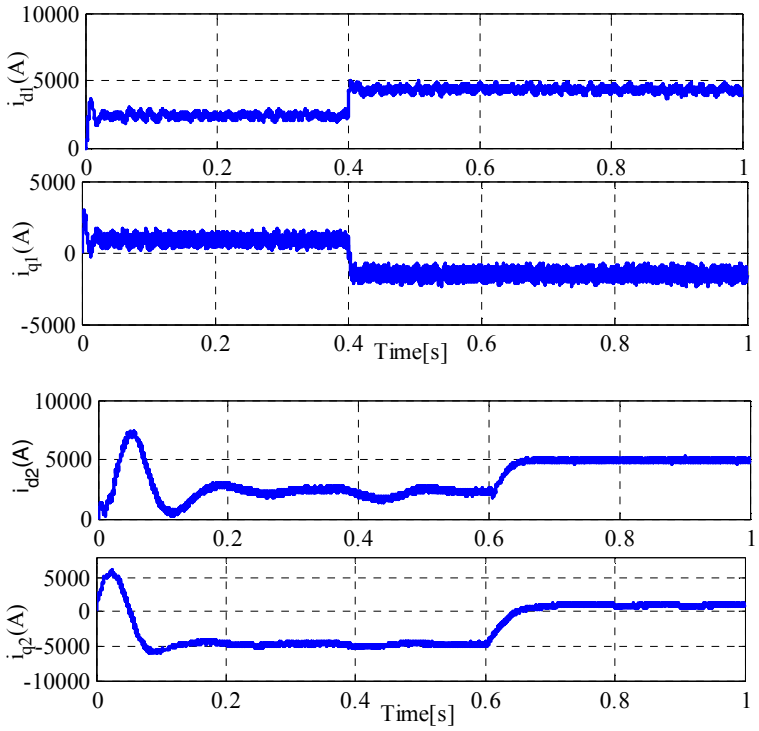

Figure 6.16 - d and q components of MMCs currents with DLM.

6.7.3 Active and Reactive Power Sharing Assessment

The proposed control technique of MMC is also responsible to provide the active and reactive power demanded from the proposed HVDC system. MMCs active and reactive power waveforms are illustrated in Figures 6.17 and 6.18.

Firstly, MMC1 and MMC2 are aimed to supply loads of 10MW+j(-10)MVAR and 3MW+j0.7MVAR respectively. Then, another set of loads as 8MW+j9MVAR and 7MW+j4MVAR are connected to MMC1 and MMC2 respectively at $t = 0.4\,s$ and $t = 0.6\,s$, respectively. Figure 6.17 verifies that the proposed controller without DLM cannot lead to a stable active and reactive power sharing for MMCs in dynamic operating condition.

On the other hand, as can be seen in Figure 6.18, MMCs active power orientation is in the direction of its respective load active power. Also the dynamic change of loads is highly compensated with a fast transient response, due to the proper controlled reaction operated by the designed DLM as depicted in Figure 6.18. Moreover, according to Figure 6.18, the reactive power injection by MMC1 is due to the presence of respective reactive loads in both steady state and dynamic operating conditions of the proposed HVDC system, even though the scenario is different for MMC2. Figure 6.18 also shows that due to presence of filter capacitance at the output of MMC2 for the aim of achieving the desired sinusoidal voltages, MMC2 consumes reactive power.

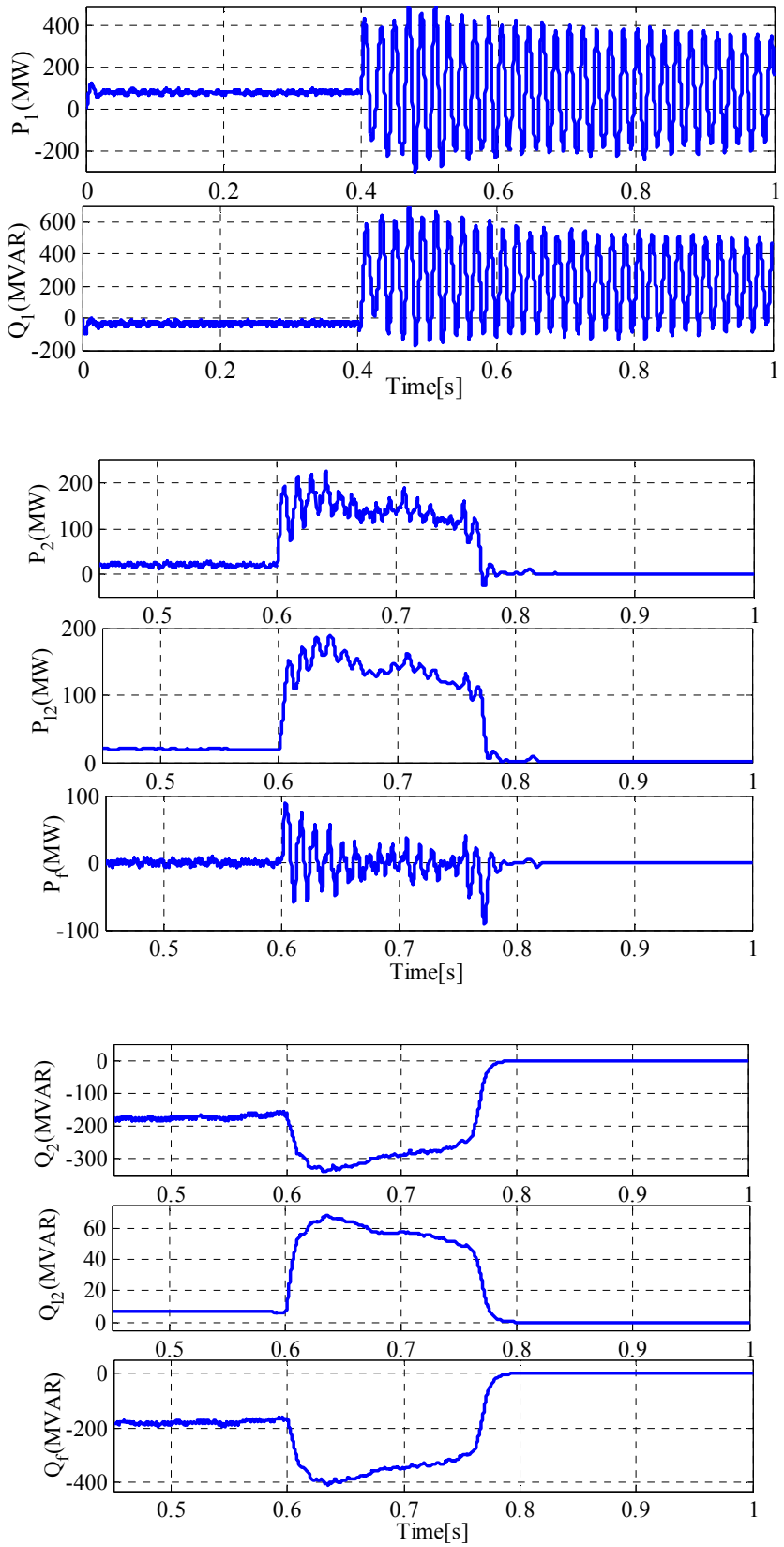

Figure 6.17 - MMC1 and MMC2 active and reactive power waveforms without DLM.

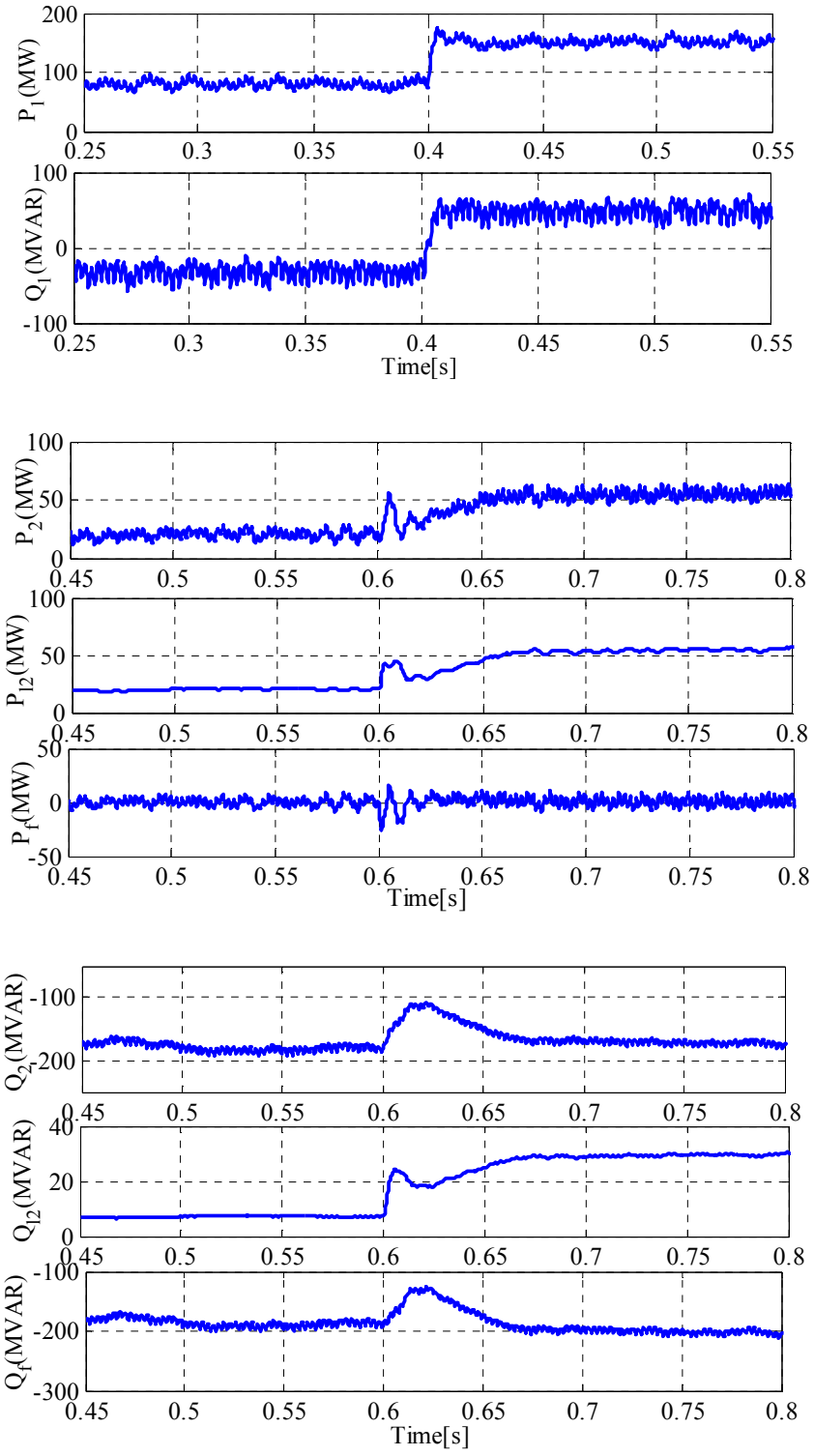

Figure 6.18 - MMC1 and MMC2 active and reactive power waveforms with DLM.

6.8 Chapter Conclusions

This chapter presented a d-q frame based model of MMC-HVDC with six independent dynamical state variables, including AC and circulating currents and also DC-link voltage, to effectively obtain the switching functions of MMC as well as for an accurate circulating current control. Based on the reference values of selected state variables, the MMC switching functions under steady state were obtained to regulate the MMC operation. Moreover, DLM was employed to develop dynamic parts of switching functions to reach globally asymptotically stability. In fact, using DLM leads to a proper operation of the designed controller and a better stabilization of MMC-HVDC against dynamic changes. Then, the capability curve analysis of the interfaced MMCs in the proposed system was carried out by considering the effects of DC-link current changes. Furthermore, the effects of MMC output and DC-link current variations on the DC-link voltage stability were evaluated in detail. Finally, the validity of the proposed controller for the proposed MMC-HVDC system was thoroughly verified and demonstrated by analyzing the simulation results achieved in Matlab/Simulink environment modeling.

Chapter 7

Conclusions, Directions for Future Work and Contributions

In this chapter, the main conclusions of the thesis are highlighted on the basis of answering the research questions that constituted the main motivation of this research. The limitations of the work in this thesis, and some directions of future work are also discussed. Finally, the contributions of this work are highlighted by presenting the set of publications in journals, book chapters or conference proceedings of high standard (IEEE), leading to this thesis work.

7.1 Main Conclusions

The main conclusions drawn from the thesis work, pertaining to the research questions presented in Section 1.3, are summarized as follows. For the sake of clarity, the research questions are reproduced here.

> • ***How can various parts of the dynamic model of the MMC impact on providing an accurate power sharing of renewable energy resources-based HVDC in the presence of model uncertainties and errors?***
>
> A flat outputs-based dynamic model which consists of both active and reactive power as their main state variables contributes to an accurate active and reactive power sharing in both steady state and load changes in the first step. The aforementioned feature considered as one of the main contribution of thesis will be enhanced by adding the integral-proportional terms of the flat output errors to the initial inputs in the proposed DFT. Adding theses terms leads to achieving the robustness ability for the designed ultimate DFT. In fact, this robustness feature is constructed to suppress the negative effects of the input disturbance, model errors, and system uncertainties. Also, it should be said that the robustness feature can be achieved by defining a control Lyapunov function ensuring the stability of the MMC under various operating points.

• What are the results of using the proposed multi-loop control technique on the stable operation of MMCs in HVDC Transmission Systems, and how will each loop with its duties be appropriately led to stable outputs in various operating conditions?

The results of using a multi-loop control technique are dependent on the duties of each control loop. In this thesis, a multi-loop control strategy consisting of three loops, named Outer Loop Controller (OLC), Central Loop Controller (CLC) and Inner Loop Controller (ILC), is designed. Initially, the details of each control loop are explained. OLC is designed based on passivity theory-based control technique to force all considered state variables of MMC-based HVDC system to track their reference values in both steady state and load variations. Sliding mode controller is used to shape CLC. Indeed, CLC is designed to provide stable robustness responses for the considered state variables in the presence of parameters changes. ILC is responsible to generate instantaneously accurate reference values for MMCs used in the HVDC transmission system in both operating modes of inverter and rectifier. As a result, by noticing the mentioned duties of each control loop, the results of using the proposed multi-loop control technique are tracking reference values, robustness ability and generating accurate reference values provided by OLC, CLC and ILC, respectively. As it was mentioned above, OLC, CLC and ILC can lead to stable outputs in various operating conditions by the help of designing a passivity theory-based control technique, defining appropriately the sliding surface and choosing a suitable reference generation algorithm, respectively.

• Which state variables should be more important in a detailed analysis of the MMC structure at reaching flexible modulation functions when the parameter alterations exist in the overall performance of the power system?

Many state variables pertaining to MMC exist that can be used at presenting an accurate analysis for different applications. For instance, the state variables can include the output voltage, output current, DC link voltage, SM capacitor voltage, circulating current, etc. In the frame of inverter mode, MMC output voltages and currents as well as MMC circulating currents are considered in this thesis to perform a detailed analysis of MMC and also to achieve the proposed flexible modulation functions. Since two upper and lower switching functions with detailed parts are aimed to accurately be achieved, using the aforementioned state variables, both upper and lower arms currents are also driven. Various parts of the proposed switching functions can be formed based on reaching appropriate responses with the existence of parameters changes.

• ***How much considering detailed calculations of MMC PWM modulation functions can ease reaching the desired values for the modulation index and phase, and also what is the effect of the system parameters considered by proposing the modulation index and phase?***

Detailed calculations of PWM modulation functions can prevent the undesired approximations which are frequently applied to the ultimate modulation functions. On the other hand, detailed calculations of PWM modulation functions will lead to achieving very accurate values for different parts of modulation functions. Thus, considering detailed calculations of MMC PWM modulation functions can cause very accurate values for the modulation index and phase, which have been accomplished in this thesis. Moreover, various parts of the proposed modulation index and phase can be changed according to the alterations of system parameters to result in a stable operating condition.

• ***Whether by considering the circulating currents components can cause that the ultimate designed controller shows positive results at controlling MMC in the HVDC system or not?***

Circulating currents of MMC can produce a collection of dynamic mathematical equations that have been comprehensively discussed in this thesis. These proposed dynamic equations provide new switching functions that are dependent on the circulating currents variations. Since the dynamic models of the circulating currents in a-b-c reference frame are related to DC link voltage, several effective switching functions are achieved. Accurate calculations of theses effective switching functions in d-q can be led to positive results at controlling MMC in the HVDC system, which has been executed in this thesis.

• ***What results can be achieved by accurately analyzing the proposed detailed curve based on the active and reactive power generated through MMC and which factors can be used to show other aspects of the proposed curve?***

Identifying the maximum capability of each MMC in active and reactive power injection during the operating condition of the HVDC system leads to a more accurate design for the controller. The proposed power curve of the considered MMC-based HVDC system is one of the main contributions of this thesis. It can be understood from this curve that the maximum and minimum amount of the MMC's active and reactive power are completely dependent on MMC's output parameters and also the operation of the proposed MMC through the proposed controller. According to this curve, the center and radius of the power curve are definitely changed by MMC's output parameters, DC link specifications and also output currents and voltages of MMC in d-q reference frame. Moreover, the various parameters effects of the MMC on the power curve can be better assessed.

Increasing the MMC's resistance causes the power curve to become smaller with decreasing the radius and center. On the other hand, the scenario gets inverse when the MMC's inductance increases. In addition, by increasing the positive values of the DC-link current, the capability curve becomes smaller. Also, decreasing the negative values of DC-link current leads to making the radius of capability bigger. The positive and negative areas of capability curve are significantly altered for both active and reactive power by changing DC-link currents. By noticing the aforementioned discussions, changing the MMC parameters, DC link voltage, DC link current and output voltage components can show other aspects of the proposed curve

7.2 Directions for Future Works

The following points may be further studied in order to broaden the understanding of the topics treated in this thesis:

- Considering uncertainties that exist in the SM capacitors in the detailed proposed PWM modulation functions;
- Proposing a suitable SM capacitors voltage balancing method for more effective stable operation when parameters alteration occurs;
- Providing more details for the proposed DFT in various operating conditions by the use of average capacitor voltages;
- Considering unbalanced grid conditions for all proposed control techniques in which the grid is supplying an unbalanced and nonlinear load.

7.3 Relevant Contributions of this Work

7.3.1 Publications in Peer-Reviewed Journals

1. **M. Mehrasa**, E. Pouresmaeil, S. Zabihi, J.C.T. Caballero, J.P.S. Catalão, "A novel modulation function-based control of modular multilevel converters for HVDC transmission systems", **Energies**, Vol. 9, No. 11, pp. 1-14, November 2016. http://dx.doi.org/10.3390/en9110867

2. **M. Mehrasa**, E. Pouresmaeil, S. Zabihi, J.P.S. Catalão, "Dynamic model, control and stability analysis of MMC in HVDC transmission systems", **IEEE Transactions on Power Delivery**, Vol. 32, No. 3, pp. 1471-1482, June 2017. http://dx.doi.org/10.1109/TPWRD.2016.2604295

3. **M. Mehrasa**, E. Pouresmaeil, M.F. Akorede, S. Zabihi, J.P.S. Catalão, "Function-based modulation control for modular multilevel converters under varying loading and parameters conditions", **IET Generation, Transmission and Distribution**, Vol. 11, No. 13, pp. 3222-3230, September 2017.
http://dx.doi.org/10.1049/iet-gtd.2016.1028

4. **M. Mehrasa**, E. Pouresmaeil, S. Zabihi, I. Vechiu, J.P.S. Catalão, "A multi-loop control technique for the stable operation of modular multilevel converters in HVDC transmission systems", **International Journal of Electrical Power & Energy Systems (ELSEVIER)**, Vol. 96, pp. 194-207, March 2018.
http://dx.doi.org/10.1016/j.ijepes.2017.10.006

5. **M. Mehrasa**, E. Pouresmaeil, S. Taheri, I. Vechiu, J.P.S. Catalão, "Novel control strategy for modular multilevel converters based on differential flatness theory", **IEEE Journal of Emerging and Selected Topics in Power Electronics**, Vol. 6, No. 2, pp. 888-897, June 2018.
http://dx.doi.org/10.1109/JESTPE.2017.2766047

7.3.2 Publications in International Conference Proceedings

1. **M. Mehrasa**, S.K. Hosseini, S. Taheri, E. Pouresmaeil, J.P.S. Catalão, "Dynamic performance control of modular multilevel converters in HVDC transmission systems", in: Proceedings of the 2016 **IEEE** Electrical Power and Energy Conference – ***EPEC 2016***, Ottawa, Ontario, Canada, USB flash drive, October 12-14, 2016.
https://doi.org/10.1109/EPEC.2016.7771779

2. **M. Mehrasa**, E. Pouresmaeil, S. Zabihi, J.P.S. Catalão, "Dynamic model, control and stability analysis of MMC in HVDC transmission systems", in: Proceedings of the **IEEE *Power Tech 2017 Conference***, Manchester, UK, USB flash drive, June 18-22, 2017.
https://doi.org/10.1109/PTC.2017.7981256

3. **M. Mehrasa**, M. Sharifzadeh, A. Sheikholeslami, E. Pouresmaeil, J.P.S. Catalão, K. Al-Haddad, "A control strategy based on the upper and lower's arms modulation functions of MMC in HVDC applications", in: Proceedings of the 2018 **IEEE** International Conference on Industrial Technology – ***ICIT 2018***, Lyon, France, USB flash drive, February 20-22, 2018.
https://doi.org/10.1109/ICIT.2018.8352471

Bibliography

[1] L. Zhang *et al.*, "Modeling, control, and protection of modular multilevel converter-based multi-terminal HVDC systems: A review," *CSEE J. Power Energy Syst.*, vol. 3, no. 4, pp. 340–352, Dec. 2017.

[2] P. Briff, "Optimality in the sense of Arm Current Distribution of MMC VSC-HVDC," *IEEE Trans. Power Electron.*, pp. 1–1, 2018.

[3] J. Lyu, X. Cai, and M. Molinas, "Optimal Design of Controller Parameters for Improving the Stability of MMC-HVDC for Wind Farm Integration," *IEEE J. Emerg. Sel. Top. Power Electron.*, vol. 6, no. 1, pp. 40–53, Mar. 2018.

[4] D. Ruimin, C. Kangsheng, W. Jun, L. Rong, Y. Han, and Z. Xiaobin, "Harmonic suppressing control strategy for MMC–HVDC," *J. Eng.*, vol. 2017, no. 13, pp. 1035–1039, Jan. 2017.

[5] H. Saad, Y. Fillion, S. Deschanvres, Y. Vernay, and S. Dennetiere, "On Resonances and Harmonics in HVDC-MMC Station Connected to AC Grid," *IEEE Trans. Power Deliv.*, vol. 32, no. 3, pp. 1565–1573, Jun. 2017.

[6] J. Wang, J. Liang, C. Wang, and X. Dong, "Circulating current suppression for MMC-HVDC under unbalanced grid conditions," *IEEE Trans. Ind. Appl.*, vol. 53, no. 4, pp. 3250–3259, 2017.

[7] Q. Hao, Z. Li, F. Gao, and J. Zhang, "Reduced-Order Small-Signal Models of Modular Multilevel Converter and MMC-Based HVdc Grid," *IEEE Trans. Ind. Electron.*, vol. 66, no. 3, pp. 2257–2268, Mar. 2019.

[8] E. Sanchez-Sanchez, E. Prieto-Araujo, A. Junyent-Ferre, and O. Gomis-Bellmunt, "Analysis of MMC Energy-Based Control Structures for VSC-HVDC Links," *IEEE J. Emerg. Sel. Top. Power Electron.*, vol. 6, no. 3, pp. 1065–1076, Sep. 2018.

[9] M. Mehrasa, E. Pouresmaeil, A. Sepehr, B. Pournazarian, M. Marzband, and J. P. S. Catalão, "Control technique for the operation of grid-tied converters with high penetration of renewable energy resources," *Electr. Power Syst. Res.*, vol. 166, pp. 18–28, Jan. 2019.

[10] M. Mehrasa, R. Godina, E. Pouresmaeil, I. Vechiu, R. L. Rodríguez, and J. P. Catalão, "Synchronous active proportional resonant-based control technique for high penetration of distributed generation units into power grids," in *Innovative Smart Grid Technologies Conference Europe (ISGT-Europe), 2017 IEEE PES*, 2017, pp. 1–6.

[11] M. Mehrasa, M. Rezanejhad, E. Pouresmaeil, J. P. S. Catalão, and S. Zabihi, “Analysis and Control of Single-Phase Converters for Integration of Small-Scaled Renewable Energy Sources into the Power Grid,” in *2016 7th Power Electronics and Drive Systems Technologies Conference (PEDSTC)*, Tehran, Iran, 2016, pp. 384–389.

[12] E. Pouresmaeil, H. R. Shaker, M. Mehrasa, M. A. Shokridehaki, E. M. G. Rodrigues, and J. P. S. Catalão, “Integration of renewable energy for the harmonic current and reactive power compensation,” in *Power Engineering, Energy and Electrical Drives (POWERENG), 2015 IEEE 5th International Conference on*, 2015, pp. 31–36.

[13] E. Pouresmaeil, B. Nørregaard, M. Mehrasa, O. Erdinc, and J. P. Catalão, “A control algorithm for the stable operation of interfaced converters in microgrid systems,” in *Innovative Smart Grid Technologies Conference Europe (ISGT-Europe), 2014 IEEE PES*, 2014, pp. 1–6.

[14] T. Tanaka, K. Ma, H. Wang, and F. Blaabjerg, “Asymmetrical Reactive Power Capability of Modular Multilevel Cascade Converter (MMCC) based STATCOMs for Offshore Wind Farm,” *IEEE Trans. Power Electron.*, pp. 1–1, 2018.

[15] A. António-Ferreira, C. Collados-Rodríguez, and O. Gomis-Bellmunt, “Modulation techniques applied to medium voltage modular multilevel converters for renewable energy integration: A review,” *Electr. Power Syst. Res.*, vol. 155, pp. 21–39, Feb. 2018.

[16] F. Shahnazian, J. Adabi, E. Pouresmaeil, and J. P. S. Catalão, “Interfacing modular multilevel converters for grid integration of renewable energy sources,” *Electr. Power Syst. Res.*, vol. 160, pp. 439–449, Jul. 2018.

[17] M. González, V. Cárdenas, H. Miranda, and R. Álvarez-Salas, “Conception of a modular multilevel converter for high-scale photovoltaic generation based on efficiency criteria,” *Sol. Energy*, vol. 125, pp. 381–397, Feb. 2016.

[18] A. Lesnicar and R. Marquardt, “An innovative modular multilevel converter topology suitable for a wide power range,” in *Power Tech Conference Proceedings, 2003 IEEE Bologna*, 2003, vol. 3, p. 6–pp.

[19] H. Saad *et al.*, “Dynamic Averaged and Simplified Models for MMC-Based HVDC Transmission Systems,” *IEEE Trans. Power Deliv.*, vol. 28, no. 3, pp. 1723–1730, Jul. 2013.

[20] D. Jovcic and A. Jamshidi Far, “Phasor Model of Modular Multilevel Converter With Circulating Current Suppression Control,” *IEEE Trans. Power Deliv.*, vol. 30, no. 4, pp. 1889–1897, Aug. 2015.

[21] N. Ahmed, L. Angquist, S. Norrga, A. Antonopoulos, L. Harnefors, and H.-P. Nee, “A Computationally Efficient Continuous Model for the Modular Multilevel Converter,” *IEEE J. Emerg. Sel. Top. Power Electron.*, vol. 2, no. 4, pp. 1139–1148, Dec. 2014.

[22] A. Jamshidi Far and D. Jovcic, “Small-Signal Dynamic DQ Model of Modular Multilevel Converter for System Studies,” *IEEE Trans. Power Deliv.*, vol. 31, no. 1, pp. 191–199, Feb. 2016.

[23] H. Yang, Y. Dong, W. Li, and X. He, “Average-Value Model of Modular Multilevel Converters Considering Capacitor Voltage Ripple,” *IEEE Trans. Power Deliv.*, vol. 32, no. 2, pp. 723–732, Apr. 2017.

[24] M. Mehrasa and M. Ahmadigorji, “Input/Output Feedback Linearization Control for Three Level/phase NPC Voltage-Source Rectifier Using its Dual Lagrangian Model,” in *11th International Conference on Environment and Electrical Engineering*, Venice, Italy, 2012.

[25] M. Mehrasa, M. Ahmadigorji, and N. Amjady, “A New Dual Lagrangian Model and Input/Output Feedback Linearization Control of 3-Phase/Level NPC Voltage-Source Rectifier,” *Automatika*, vol. 55, no. 1, pp. 99–111, Jan. 2014.

[26] M. Mehrasa, A. Abedi, M. Ahmadigorji, and M. A. Reykandeh, “Dual Lagrangian modeling and Lyapunov-based control of four-wire three-level three-phase NPC voltage-source rectifier,” in *Environment and Electrical Engineering (EEEIC), 2012 11th International Conference on*, 2012, pp. 744–751.

[27] M. Mehrasa, E. Pouresmaeil, and J. P. S. Catalao, “Direct Lyapunov Control Technique for the Stable Operation of Multilevel Converter-Based Distributed Generation in Power Grid,” *IEEE J. Emerg. Sel. Top. Power Electron.*, vol. 2, no. 4, pp. 931–941, Dec. 2014.

[28] M. Mehrasa, M. Ahmadigorji, and A. Abedi, “Dual Lagrangian modeling and Lyapunov-based control of three-level three-phase NPC voltage-source rectifier,” in *Environment and Electrical Engineering (EEEIC), 2012 11th International Conference on*, 2012, pp. 737–743.

[29] R. A. Kordkheili and M. Mehrasa, “Sliding mode control for three-phase ac/dc voltage-source boost converter,” in *Power Electronics Electrical Drives Automation and Motion (SPEEDAM), 2010 International Symposium on*, 2010, pp. 1213–1217.

[30] M. Mehrasa, S. Lesan, S. N. Hoseini Emeni, and A. Sheikholeslami, “Passivity-based control with dual lagrangian model of four-wire three-level three-phase NPC voltage-source rectifier,” *Compatibility and Power Electronics*, pp. 411–418, 2009.

[31] M. Mehrasa, M. E. Adabi, E. Pouresmaeil, and J. Adabi, “Passivity-based control technique for integration of DG resources into the power grid,” *Int. J. Electr. Power Energy Syst.*, vol. 58, pp. 281–290, Jun. 2014.

[32] A. M. Shotorbani, X. Meng, L. Wang, and B. Mohammadi-Ivatloo, “A Decentralized Multiloop Scheme for Robust Control of a Power Flow Controller With Two Shunt Modular Multilevel Converters,” *IEEE Trans. Ind. Inform.*, vol. 14, no. 10, pp. 4309–4321, Oct. 2018.

[33] S. Yang, P. Wang, and Y. Tang, “Feedback linearization-based current control strategy for modular multilevel converters,” *IEEE Trans. Power Electron.*, vol. 33, no. 1, pp. 161–174, 2018.

[34] S. Shao, P. W. Wheeler, J. C. Clare, and A. J. Watson, “Fault Detection for Modular Multilevel Converters Based on Sliding Mode Observer,” *IEEE Trans. Power Electron.*, vol. 28, no. 11, pp. 4867–4872, Nov. 2013.

[35] Q. Yang, M. Saeedifard, and M. A. Perez, “Sliding Mode Control of the Modular Multilevel Converter,” *IEEE Trans. Ind. Electron.*, vol. 66, no. 2, pp. 887–897, Feb. 2019.

[36] M. Mehrasa, E. Pouresmaeil, S. Taheri, I. Vechiu, and J. P. S. Catalao, “Novel Control Strategy for Modular Multilevel Converters Based on Differential Flatness Theory,” *IEEE J. Emerg. Sel. Top. Power Electron.*, vol. 6, no. 2, pp. 888–897, Jun. 2018.

[37] M. Mehrasa, E. Pouresmaeil, S. Zabihi, I. Vechiu, and J. P. S. Catalão, “A multi-loop control technique for the stable operation of modular multilevel converters in HVDC transmission systems,” *Int. J. Electr. Power Energy Syst.*, vol. 96, pp. 194–207, Mar. 2018.

[38] M. Mehrasa, E. Pouresmaeil, M. F. Akorede, S. Zabihi, and J. P. S. Catalão, “Function-based modulation control for modular multilevel converters under varying loading and parameters conditions,” *IET Gener. Transm. Distrib.*, vol. 11, no. 13, pp. 3222–3230, Sep. 2017.

[39] M. Mehrasa, E. Pouresmaeil, S. Zabihi, J. Trujillo Caballero, and J. Catalão, “A Novel Modulation Function-Based Control of Modular Multilevel Converters for High Voltage Direct Current Transmission Systems,” *Energies*, vol. 9, no. 11, p. 867, Oct. 2016.

[40] M. Mehrasa, E. Pouresmaeil, S. Zabihi, and J. P. S. Catalao, “Dynamic Model, Control and Stability Analysis of MMC in HVDC Transmission Systems,” *IEEE Trans. Power Deliv.*, vol. 32, no. 3, pp. 1471–1482, Jun. 2017.

[41] M. Mehrasa, E. Pouresmaeil, B. Pournazarian, A. Sepehr, M. Marzband, and J. Catalão, “Synchronous Resonant Control Technique to Address Power Grid Instability Problems Due to High Renewables Penetration,” *Energies*, vol. 11, no. 9, p. 2469, Sep. 2018.

[42] S. K. Hosseini, M. Mehrasa, S. Taheri, M. Rezanejad, E. Pouresmaeil, and J. P. S. Catalão, "A Control Technique for Operation of Single-Phase Converters in Stand-alone Operating Mode," in *IEEE Electrical Power and Energy Conference (EPEC)*, Ottawa, ON, Canada, 2016.

[43] E. Pouresmaeil, M. Mehrasa, M. A. Shokridehaki, E. M. Rodrigues, and J. P. Catalão, "Control of modular multilevel converters for integration of distributed generation sources into the power grid," in *Smart Energy Grid Engineering (SEGE), 2015 IEEE International Conference on*, 2015, pp. 1–6.

[44] F. Ma *et al.*, "A Railway Traction Power Conditioner Using Modular Multilevel Converter and Its Control Strategy for High-Speed Railway System," *IEEE Trans. Transp. Electrification*, vol. 2, no. 1, pp. 96–109, Mar. 2016.

[45] D. Montesinos-Miracle, M. Massot-Campos, J. Bergas-Jane, S. Galceran-Arellano, and A. Rufer, "Design and Control of a Modular Multilevel DC/DC Converter for Regenerative Applications," *IEEE Trans. Power Electron.*, vol. 28, no. 8, pp. 3970–3979, Aug. 2013.

[46] A. A. Gebreel and L. Xu, "DC-AC Power Conversion Based on Using Modular Multilevel Converter With Arm Energy Approximation Control," *IEEE Power Energy Technol. Syst. J.*, pp. 1–11, 2016.

[47] B. Chen, Y. Chen, C. Tian, J. Yuan, and X. Yao, "Analysis and Suppression of Circulating Harmonic Currents in a Modular Multilevel Converter Considering the Impact of Dead Time," *IEEE Trans. Power Electron.*, vol. 30, no. 7, pp. 3542–3552, Jul. 2015.

[48] A. Hassanpoor, A. Roostaei, S. Norrga, and M. Lindgren, "Optimization-Based Cell Selection Method for Grid-Connected Modular Multilevel Converters," *IEEE Trans. Power Electron.*, vol. 31, no. 4, pp. 2780–2790, Apr. 2016.

[49] M. Vasiladiotis, N. Cherix, and A. Rufer, "Accurate Capacitor Voltage Ripple Estimation and Current Control Considerations for Grid-Connected Modular Multilevel Converters," *IEEE Trans. Power Electron.*, vol. 29, no. 9, pp. 4568–4579, Sep. 2014.

[50] J. Mei, B. Xiao, K. Shen, L. M. Tolbert, and J. Y. Zheng, "Modular Multilevel Inverter with New Modulation Method and Its Application to Photovoltaic Grid-Connected Generator," *IEEE Trans. Power Electron.*, vol. 28, no. 11, pp. 5063–5073, Nov. 2013.

[51] R. Vidal-Albalate, H. Beltran, A. Rolan, E. Belenguer, R. Pena, and R. Blasco-Gimenez, "Analysis of the Performance of MMC Under Fault Conditions in HVDC-Based Offshore Wind Farms," *IEEE Trans. Power Deliv.*, vol. 31, no. 2, pp. 839–847, Apr. 2016.

[52] Y. Wang, W. Zhao, G. Chen, Y. Hu, and M. Wang, “Application of modular multilevel converter in medium voltage high power permanent magnet synchronous generator wind energy conversion systems,” *IET Renew. Power Gener.*, vol. 10, no. 6, pp. 824–833, Jul. 2016.

[53] A. Edpuganti and A. K. Rathore, “Optimal Pulsewidth Modulation for Common-Mode Voltage Elimination Scheme of Medium-Voltage Modular Multilevel Converter-Fed Open-End Stator Winding Induction Motor Drives,” *IEEE Trans. Ind. Electron.*, vol. 64, no. 1, pp. 848–856, Jan. 2017.

[54] B. Zhao, Q. Song, J. Li, Y. Wang, and W. Liu, “High-Frequency-Link Modulation Methodology of DC–DC Transformer Based on Modular Multilevel Converter for HVDC Application: Comprehensive Analysis and Experimental Verification,” *IEEE Trans. Power Electron.*, vol. 32, no. 5, pp. 3413–3424, May 2017.

[55] T. Soong and P. W. Lehn, “Internal Power Flow of a Modular Multilevel Converter With Distributed Energy Resources,” *IEEE J. Emerg. Sel. Top. Power Electron.*, vol. 2, no. 4, pp. 1127–1138, Dec. 2014.

[56] G. Liu, Z. Xu, Y. Xue, and G. Tang, “Optimized Control Strategy Based on Dynamic Redundancy for the Modular Multilevel Converter,” *IEEE Trans. Power Electron.*, vol. 30, no. 1, pp. 339–348, Jan. 2015.

[57] B. S. Riar, T. Geyer, and U. K. Madawala, “Model Predictive Direct Current Control of Modular Multilevel Converters: Modeling, Analysis, and Experimental Evaluation,” *IEEE Trans. Power Electron.*, vol. 30, no. 1, pp. 431–439, Jan. 2015.

[58] J. Xu, C. Zhao, W. Liu, and C. Guo, “Accelerated Model of Modular Multilevel Converters in PSCAD/EMTDC,” *IEEE Trans. Power Deliv.*, vol. 28, no. 1, pp. 129–136, Jan. 2013.

[59] J. Xu, A. M. Gole, and C. Zhao, “The Use of Averaged-Value Model of Modular Multilevel Converter in DC Grid,” *IEEE Trans. Power Deliv.*, vol. 30, no. 2, pp. 519–528, Apr. 2015.

[60] Jun Wang, R. Burgos, and D. Boroyevich, “Switching-Cycle State-Space Modeling and Control of the Modular Multilevel Converter,” *IEEE J. Emerg. Sel. Top. Power Electron.*, vol. 2, no. 4, pp. 1159–1170, Dec. 2014.

[61] F. Yu, W. Lin, X. Wang, and D. Xie, “Fast Voltage-Balancing Control and Fast Numerical Simulation Model for the Modular Multilevel Converter,” *IEEE Trans. Power Deliv.*, vol. 30, no. 1, pp. 220–228, Feb. 2015.

[62] A. J. Korn, M. Winkelnkemper, and P. Steimer, “Low output frequency operation of the modular multi-level converter,” in *Energy Conversion Congress and Exposition (ECCE), 2010 IEEE*, 2010, pp. 3993–3997.

[63] A. Antonopoulos, L. Angquist, S. Norrga, K. Ilves, L. Harnefors, and H.-P. Nee, “Modular Multilevel Converter AC Motor Drives With Constant Torque From Zero to Nominal Speed,” *IEEE Trans. Ind. Appl.*, vol. 50, no. 3, pp. 1982–1993, May 2014.

[64] S. Debnath, J. Qin, and M. Saeedifard, “Control and Stability Analysis of Modular Multilevel Converter Under Low-Frequency Operation,” *IEEE Trans. Ind. Electron.*, vol. 62, no. 9, pp. 5329–5339, Sep. 2015.

[65] J. Kolb, F. Kammerer, M. Gommeringer, and M. Braun, “Cascaded Control System of the Modular Multilevel Converter for Feeding Variable-Speed Drives,” *IEEE Trans. Power Electron.*, vol. 30, no. 1, pp. 349–357, Jan. 2015.

[66] M. Spichartz, V. Staudt, and A. Steimel, “Analysis of the module-voltage fluctuations of the modular multilevel converter at variable speed drive applications,” in *Optimization of Electrical and Electronic Equipment (OPTIM), 2012 13th International Conference on*, Tehran, Iran, 2012, pp. 384–389.

[67] M. Pahlevaninezhad, P. Das, J. Drobnik, P. K. Jain, and A. Bakhshai, “A New Control Approach Based on the Differential Flatness Theory for an AC/DC Converter Used in Electric Vehicles,” *IEEE Trans. Power Electron.*, vol. 27, no. 4, pp. 2085–2103, Apr. 2012.

[68] P. Thounthong and S. Pierfederici, “A New Control Law Based on the Differential Flatness Principle for Multiphase Interleaved DC–DC Converter,” *IEEE Trans. Circuits Syst. II Express Briefs*, vol. 57, no. 11, pp. 903–907, Nov. 2010.

[69] E. Song, A. F. Lynch, and V. Dinavahi, “Experimental validation of a flatness-based control for a voltage source converter,” in *American Control Conference, 2007. ACC’07*, 2007, pp. 6049–6054.

[70] M. Fliess, J. LéVine, P. Martin, and P. Rouchon, “Flatness and defect of non-linear systems: introductory theory and examples,” *Int. J. Control*, vol. 61, no. 6, pp. 1327–1361, Jun. 1995.

[71] H. Fehr, A. Gensior, and M. Müller, “Analysis and trajectory tracking control of a modular multilevel converter,” *IEEE Trans. Power Electron.*, vol. 30, no. 1, pp. 398–407, 2015.

[72] M. Mehrasa, S. K. Hosseini, S. Taheri, E. Pouresmaeil, and J. P. S. Catalao, “Dynamic performance control of modular multilevel converters in HVDC transmission systems,” in *Electrical Power and Energy Conference (EPEC), 2016 IEEE*, 2016, pp. 1–6.

[73] K. Ilves, A. Antonopoulos, S. Norrga, and H.-P. Nee, “Steady-State Analysis of Interaction Between Harmonic Components of Arm and Line Quantities of Modular Multilevel Converters,” *IEEE Trans. Power Electron.*, vol. 27, no. 1, pp. 57–68, Jan. 2012.

[74] M. Thathan and A. Alexander, “Modelling and analysis of modular multilevel converter for solar photovoltaic applications to improve power quality,” *IET Renew. Power Gener.*, vol. 9, no. 1, pp. 78–88, Jan. 2015.

[75] S. Debnath and M. Saeedifard, “A New Hybrid Modular Multilevel Converter for Grid Connection of Large Wind Turbines,” *IEEE Trans. Sustain. Energy*, vol. 4, no. 4, pp. 1051–1064, Oct. 2013.

[76] Y. Zhang, J. Ravishankar, J. Fletcher, R. Li, and M. Han, “Review of modular multilevel converter based multi-terminal HVDC systems for offshore wind power transmission,” *Renew. Sustain. Energy Rev.*, vol. 61, pp. 572–586, Aug. 2016.

[77] A. Antonopoulos, L. Angquist, L. Harnefors, and H.-P. Nee, “Optimal Selection of the Average Capacitor Voltage for Variable-Speed Drives With Modular Multilevel Converters,” *IEEE Trans. Power Electron.*, vol. 30, no. 1, pp. 227–234, Jan. 2015.

[78] A. Nami, J. Liang, F. Dijkhuizen, and G. D. Demetriades, “Modular Multilevel Converters for HVDC Applications: Review on Converter Cells and Functionalities,” *IEEE Trans. Power Electron.*, vol. 30, no. 1, pp. 18–36, Jan. 2015.

[79] I. A. Gowaid, G. P. Adam, S. Ahmed, D. Holliday, and B. W. Williams, “Analysis and Design of a Modular Multilevel Converter With Trapezoidal Modulation for Medium and High Voltage DC-DC Transformers,” *IEEE Trans. Power Electron.*, vol. 30, no. 10, pp. 5439–5457, Oct. 2015.

[80] S. Du and J. Liu, “A Study on DC Voltage Control for Chopper-Cell-Based Modular Multilevel Converters in D-STATCOM Application,” *IEEE Trans. Power Deliv.*, vol. 28, no. 4, pp. 2030–2038, Oct. 2013.

[81] S. Debnath, J. Qin, B. Bahrani, M. Saeedifard, and P. Barbosa, “Operation, Control, and Applications of the Modular Multilevel Converter: A Review,” *IEEE Trans. Power Electron.*, vol. 30, no. 1, pp. 37–53, Jan. 2015.

[82] V. R. Disfani, L. Fan, Z. Miao, and Y. Ma, “Fast model predictive control algorithms for fast-switching modular multilevel converters,” *Electr. Power Syst. Res.*, vol. 129, pp. 105–113, Dec. 2015.

[83] A. A. Gebreel and L. Xu, “Power quality and total harmonic distortion response for MMC with increasing arm inductance based on closed loop-needless PID controller,” *Electr. Power Syst. Res.*, vol. 133, pp. 281–291, Apr. 2016.

[84] Jiangchao Qin and M. Saeedifard, “Predictive Control of a Modular Multilevel Converter for a Back-to-Back HVDC System,” *IEEE Trans. Power Deliv.*, vol. 27, no. 3, pp. 1538–1547, Jul. 2012.

[85] G. Bergna *et al.*, “A Generalized Power Control Approach in ABC Frame for Modular Multilevel Converter HVDC Links Based on Mathematical Optimization,” *IEEE Trans. Power Deliv.*, vol. 29, no. 1, pp. 386–394, Feb. 2014.

[86] K. Ilves, A. Antonopoulos, S. Norrga, and H.-P. Nee, “A New Modulation Method for the Modular Multilevel Converter Allowing Fundamental Switching Frequency,” *IEEE Trans. Power Electron.*, vol. 27, no. 8, pp. 3482–3494, Aug. 2012.

[87] X. Li, Q. Song, W. Liu, Q. Li, H. Rao, and S. Xu, “Zero-sequence voltage injection control scheme of modular multilevel converter supplying passive networks under unbalanced load conditions,” *Electr. Power Syst. Res.*, vol. 121, pp. 270–278, Apr. 2015.

[88] J.-W. Moon, J.-S. Gwon, J.-W. Park, D.-W. Kang, and J.-M. Kim, “Model Predictive Control With a Reduced Number of Considered States in a Modular Multilevel Converter for HVDC System,” *IEEE Trans. Power Deliv.*, vol. 30, no. 2, pp. 608–617, Apr. 2015.

[89] M. Vasiladiotis and A. Rufer, “Analysis and Control of Modular Multilevel Converters With Integrated Battery Energy Storage,” *IEEE Trans. Power Electron.*, vol. 30, no. 1, pp. 163–175, Jan. 2015.

[90] H. Barnklau, A. Gensior, and J. Rudolph, “A Model-Based Control Scheme for Modular Multilevel Converters,” *IEEE Trans. Ind. Electron.*, vol. 60, no. 12, pp. 5359–5375, Dec. 2013.

[91] R. Li and J. E. Fletcher, “A novel MMC control scheme to increase the DC voltage in HVDC transmission systems,” *Electr. Power Syst. Res.*, vol. 143, pp. 544–553, Feb. 2017.

[92] R. Li, J. E. Fletcher, L. Xu, and B. W. Williams, “Enhanced Flat-Topped Modulation for MMC Control in HVDC Transmission Systems,” *IEEE Trans. Power Deliv.*, vol. 32, no. 1, pp. 152–161, Feb. 2017.

[93] R. Li, L. Xu, L. Yao, and B. W. Williams, “Active Control of DC Fault Currents in DC Solid-State Transformers During Ride-Through Operation of Multi-Terminal HVDC Systems,” *IEEE Trans. Energy Convers.*, vol. 31, no. 4, pp. 1336–1346, Dec. 2016.

[94] R. Li, L. Xu, D. Holliday, F. Page, S. J. Finney, and B. W. Williams, “Continuous Operation of Radial Multiterminal HVDC Systems Under DC Fault,” *IEEE Trans. Power Deliv.*, vol. 31, no. 1, pp. 351–361, Feb. 2016.

[95] E. Pouresmaeil, M. Mehrasa, and J. P. S. Catalao, “A Multifunction Control Strategy for the Stable Operation of DG Units in Smart Grids,” *IEEE Trans. Smart Grid*, vol. 6, no. 2, pp. 598–607, Mar. 2015.

[96] M. Mehrasa, A. Sepehr, E. Pouresmaeil, M. Marzband, J. P. Catalão, and J. Kyyrä, "Stability Analysis ofa Synchronous Generator-Based Control Technique used in Large-Scale Grid Integration of Renewable Energy," in *2018 International Conference on Smart Energy Systems and Technologies (SEST)*, 2018, pp. 1–5.

[97] E. Pouresmaeil, M. Mehrasa, M. A. Shokridehaki, and E. M. G. Rodrigues, "Control and Stability Analysis of Interfaced Converter in Distributed Generation Technology," in *International Conference on Computer as a Tool (EUROCON), IEEE EUROCON 2015*, Salamanca, Spain, 2015.

[98] S. N. H. Eimeni, A. Radan, and M. Mehrasa, "The Single-Phase Single-Switch PWM Three-Level High Power Factor Rectifier for DC Network Application," in *4th IEEE Conference on Industrial Electronics and Applications*, Xi'an, China, 2009.

[99] B.-T. Ooi and C. Wang, "Incorporating deadbeat and low-frequency harmonic elimination in modular multilevel converters," *IET Gener. Transm. Distrib.*, vol. 9, no. 4, pp. 369–378, Mar. 2015.

[100] M. Mehrasa, M. Sharifzadeh, A. Sheikholeslami, E. Pouresmaeil, J. P. Catalão, and K. Al-Haddad, "A control strategy based on the upper and lower's arms modulation functions of MMC in HVDC applications," in *2018 IEEE International Conference on Industrial Technology (ICIT)*, 2018, pp. 1873–1878.

[101] F. Shahnazian, J. Adabi, E. Pouresmaeil, M. Mehrasa, and J. P. S. Catalão, "Circulating Current Elimination of Grid-Connected Modular Multilevel Converters," in *2018 IEEE International Conference on Environment and Electrical Engineering and 2018 IEEE Industrial and Commercial Power Systems Europe (EEEIC / I&CPS Europe)*, Palermo, Italy, 2018.

[102] Qingrui Tu, Zheng Xu, and Lie Xu, "Reduced Switching-Frequency Modulation and Circulating Current Suppression for Modular Multilevel Converters," *IEEE Trans. Power Deliv.*, vol. 26, no. 3, pp. 2009–2017, Jul. 2011.

[103] L. Harnefors, A. Antonopoulos, S. Norrga, L. Angquist, and H.-P. Nee, "Dynamic Analysis of Modular Multilevel Converters," *IEEE Trans. Ind. Electron.*, vol. 60, no. 7, pp. 2526–2537, Jul. 2013.

[104] S. Liu, Z. Xu, W. Hua, G. Tang, and Y. Xue, "Electromechanical Transient Modeling of Modular Multilevel Converter Based Multi-Terminal HVDC Systems," *IEEE Trans. Power Syst.*, vol. 29, no. 1, pp. 72–83, Jan. 2014.

[105] R. Lizana, M. A. Perez, D. Arancibia, J. R. Espinoza, and J. Rodriguez, "Decoupled Current Model and Control of Modular Multilevel Converters," *IEEE Trans. Ind. Electron.*, vol. 62, no. 9, pp. 5382–5392, Sep. 2015.

[106] W. Wang, A. Beddard, M. Barnes, and O. Marjanovic, “Analysis of Active Power Control for VS-HVDC,” *IEEE Trans. Power Deliv.*, vol. 29, no. 4, pp. 1978–1988, Aug. 2014.

[107] C. Wang, B.-T. Ooi, and Q. Hao, “Reduction of low-frequency harmonics in modular multilevel converters (MMCs) by harmonic function analysis,” *IET Gener. Transm. Distrib.*, vol. 8, no. 2, pp. 328–338, Feb. 2014.

[108] R. Guruambeth and R. Ramabadran, “Fuzzy logic controller for partial shaded photovoltaic array fed modular multilevel converter,” *IET Power Electron.*, vol. 9, no. 8, pp. 1694–1702, Jun. 2016.

[109] P. Hu, D. Jiang, Y. Zhou, Y. Liang, J. Guo, and Z. Lin, “Energy-balancing Control Strategy for Modular Multilevel Converters Under Submodule Fault Conditions,” *IEEE Trans. Power Electron.*, vol. 29, no. 9, pp. 5021–5030, Sep. 2014.

[110] B. Li, R. Yang, D. Xu, G. Wang, W. Wang, and D. Xu, “Analysis of the Phase-Shifted Carrier Modulation for Modular Multilevel Converters,” *IEEE Trans. Power Electron.*, vol. 30, no. 1, pp. 297–310, Jan. 2015.

[111] T. C. Lim, B. W. Williams, G. P. Adam, Y. Zhang, and S. J. Finney, “Analysis of modular multilevel converter capacitor voltage balancing based on phase voltage redundant states,” *IET Power Electron.*, vol. 5, no. 6, pp. 726–738, Jul. 2012.

[112] M. Saeedifard and R. Iravani, “Dynamic Performance of a Modular Multilevel Back-to-Back HVDC System,” *IEEE Trans. Power Deliv.*, vol. 25, no. 4, pp. 2903–2912, Oct. 2010.

[113] F. Deng and Z. Chen, “Voltage-Balancing Method for Modular Multilevel Converters Under Phase-Shifted Carrier-Based Pulsewidth Modulation,” *IEEE Trans. Ind. Electron.*, vol. 62, no. 7, pp. 4158–4169, Jul. 2015.

[114] Z. Li, P. Wang, H. Zhu, Z. Chu, and Y. Li, “An Improved Pulse Width Modulation Method for Chopper-Cell-Based Modular Multilevel Converters,” *IEEE Trans. Power Electron.*, vol. 27, no. 8, pp. 3472–3481, Aug. 2012.

[115] P. Hu and D. Jiang, “A Level-Increased Nearest Level Modulation Method for Modular Multilevel Converters,” *IEEE Trans. Power Electron.*, vol. 30, no. 4, pp. 1836–1842, Apr. 2015.

[116] R. Picas, S. Ceballos, J. Pou, J. Zaragoza, G. Konstantinou, and V. G. Agelidis, “Closed-Loop Discontinuous Modulation Technique for Capacitor Voltage Ripples and Switching Losses Reduction in Modular Multilevel Converters,” *IEEE Trans. Power Electron.*, vol. 30, no. 9, pp. 4714–4725, Sep. 2015.

[117] S. Fan, K. Zhang, J. Xiong, and Y. Xue, “An Improved Control System for Modular Multilevel Converters with New Modulation Strategy and Voltage Balancing Control,” *IEEE Trans. Power Electron.*, vol. 30, no. 1, pp. 358–371, Jan. 2015.

[118] A. Hassanpoor, L. Angquist, S. Norrga, K. Ilves, and H.-P. Nee, “Tolerance Band Modulation Methods for Modular Multilevel Converters,” *IEEE Trans. Power Electron.*, vol. 30, no. 1, pp. 311–326, Jan. 2015.

[119] V. Agelidis, M. Ciobotaru, and G. Konstantinou, “Selective harmonic elimination pulse-width modulation of modular multilevel converters,” *IET Power Electron.*, vol. 6, no. 1, pp. 96–107, Jan. 2013.

[120] D. Siemaszko, A. Antonopoulos, K. Ilves, M. Vasiladiotis, L. Ängquist, and H.-P. Nee, “Evaluation of Control and Modulation Methods for Modular Multilevel Converters,” presented at the International Power Electronics Conference , 2010. ECCE ASIA, 2010, pp. 746–753.

[121] G. S. Konstantinou, M. Ciobotaru, and V. G. Agelidis, “Analysis of multi-carrier PWM methods for back-to-back HVDC systems based on modular multilevel converters,” in *IECON 2011-37th Annual Conference on IEEE Industrial Electronics Society*, 2011, pp. 4391–4396.

[122] M. Mehrasa, A. Sepehr, E. Pouresmaeil, M. Marzband, and J. P. S. Catalão, “Angular Frequency Dynamic-Based Control Technique of a Grid-Interfaced Converter Emulated by a Synchronous Generator,” in *2018 International Conference on Smart Energy Systems and Technologies (SEST)*, Sevilla, Spain, 2018.

[123] E. Pouresmaeil, M. Mehrasa, R. Godina, I. Vechiu, R. L. Rodríguez, and J. P. Catalão, “Double synchronous controller for integration of large-scale renewable energy sources into a low-inertia power grid,” in *Innovative Smart Grid Technologies Conference Europe (ISGT-Europe), 2017 IEEE PES*, 2017, pp. 1–6.

[124] M. Mehrasa, E. Pouresmaeil, M. Marzband, and J. P. Catalão, “A Single Synchronous Controller for High Penetration of Renewable Energy Resources into the Power Grid,” in *2018 IEEE International Conference on Environment and Electrical Engineering and 2018 IEEE Industrial and Commercial Power Systems Europe (EEEIC/I&CPS Europe)*, 2018, pp. 1–5.

[125] M. Mehrasa, E. Pouresmaeil, M. F. Akorede, B. N. Jørgensen, and J. P. S. Catalão, “Multilevel converter control approach of active power filter for harmonics elimination in electric grids,” *Energy*, vol. 84, pp. 722–731, May 2015.

[126] E. Pouresmaeil, M. Mehrasa, E. Rodrigues, R. Godina, and J. P. Catalão, “Control of Modular Multilevel Converters Under Loading Variations in Distributed Generation Applications,” in *2018 IEEE International Conference on Environment and Electrical Engineering and 2018 IEEE Industrial and Commercial Power Systems Europe (EEEIC/I&CPS Europe)*, 2018, pp. 1–6.

[127] R. Marquardt, “Modular Multilevel Converter: An universal concept for HVDC-Networks and extended DC-Bus-applications,” in *Power Electronics Conference (IPEC), 2010 International*, 2010, pp. 502–507.

[128] M. Glinka and R. Marquardt, “A New AC/AC Multilevel Converter Family,” *IEEE Trans. Ind. Electron.*, vol. 52, no. 3, pp. 662–669, Jun. 2005.

[129] U. N. Gnanarathna, A. M. Gole, and R. P. Jayasinghe, “Efficient Modeling of Modular Multilevel HVDC Converters (MMC) on Electromagnetic Transient Simulation Programs,” *IEEE Trans. Power Deliv.*, vol. 26, no. 1, pp. 316–324, Jan. 2011.

[130] S. Kouro *et al.*, “Recent Advances and Industrial Applications of Multilevel Converters,” *IEEE Trans. Ind. Electron.*, vol. 57, no. 8, pp. 2553–2580, Aug. 2010.

[131] R. Naderi and A. Rahmati, “Phase-Shifted Carrier PWM Technique for General Cascaded Inverters,” *IEEE Trans. Power Electron.*, vol. 23, no. 3, pp. 1257–1269, May 2008.

[132] M. Hagiwara and H. Akagi, “Control and Experiment of Pulse width Modulated Modular Multilevel Converters,” *IEEE Trans. Power Electron.*, vol. 24, no. 7, pp. 1737–1746, Jul. 2009.

[133] E. Solas, G. Abad, J. A. Barrena, S. Aurtenetxea, A. Carcar, and L. Zajac, “Modular Multilevel Converter With Different Submodule Concepts—Part II: Experimental Validation and Comparison for HVDC Application,” *IEEE Trans. Ind. Electron.*, vol. 60, no. 10, pp. 4536–4545, Oct. 2013.

[134] H. Peng, M. Hagiwara, and H. Akagi, “Modeling and Analysis of Switching-Ripple Voltage on the DC Link Between a Diode Rectifier and a Modular Multilevel Cascade Inverter (MMCI),” *IEEE Trans. Power Electron.*, vol. 28, no. 1, pp. 75–84, Jan. 2013.

[135] N. Thitichaiworakorn, M. Hagiwara, and H. Akagi, “Experimental Verification of a Modular Multilevel Cascade Inverter Based on Double-Star Bridge-Cells (MMCI-DSBC),” presented at the Energy Conversion Congress and Exposition, 2012. ECCE, Raleigh, NC, USA, 2012, pp. 4196–4202.

[136] L. Angquist, A. Antonopoulos, D. Siemaszko, K. Ilves, M. Vasiladiotis, and H.-P. Nee, “Open-Loop Control of Modular Multilevel Converters Using Estimation of Stored Energy,” *IEEE Trans. Ind. Appl.*, vol. 47, no. 6, pp. 2516–2524, Nov. 2011.

[137] Q. Tu and Z. Xu, “Impact of Sampling Frequency on Harmonic Distortion for Modular Multilevel Converter,” *IEEE Trans. Power Deliv.*, vol. 26, no. 1, pp. 298–306, Jan. 2011.

[138] A. K. Harchegani and H. Iman-Eini, “Selective harmonic elimination pulse width modulation in single-phase modular multilevel converter,” in *Power Electronics, Drives Systems & Technologies Conference (PEDSTC), 2015 6th*, 2015, pp. 346–351.

[139] N. Ahmed, A. Haider, L. Angquist, and H.-P. Nee, "M2C-based MTDC system for handling of power fluctuations from offshore wind farms," 2011.

[140] S. P. Teeuwsen, "Modeling the trans bay cable project as voltage-sourced converter with modular multilevel converter design," in *Power and Energy Society General Meeting, 2011 IEEE*, 2011, pp. 1–8.

[141] M. Mehrasa, E. Pouresmaeil, S. Zabihi, E. M. G. Rodrigues, and J. P. S. Catalão, "A control strategy for the stable operation of shunt active power filters in power grids," *Energy*, vol. 96, pp. 325–334, Feb. 2016.

[142] E. Pouresmaeil, M. Mehrasa, M. A. Shokridehaki, M. Shafie-khah, E. M. G. Rodrigues, and J. P. S. Catalão, "Stable operation of grid-interfacing converter during the operation of active power filters in power grids," in *Compatibility and Power Electronics (CPE), 2015 9th International Conference on*, 2015, pp. 132–137.

[143] S. N. Hoseini Eimeni, A. Radan, and M. Mehrasa, "A new single-phase single-switch PWM three-level high power factor rectifier with separate regulation of output capacitors voltage," 4th IEEE Conference on Industrial Electronics and Applications, pp. 1062-1067, 2009.

[144] M. Mehrasa, E. Pouresmaeil, B. N. Jørgensen, and J. P. S. Catalão, "A control plan for the stable operation of microgrids during grid-connected and islanded modes," *Electr. Power Syst. Res.*, vol. 129, pp. 10–22, Dec. 2015.

[145] E. Pouresmaeil, M. Mehrasa, M. A. Shokridehaki, E. M. G. Rodrigues, and J. P. S. Catalão, "Stable operation of distributed generation units in microgrid networks," in *Power Engineering Conference (AUPEC), 2015 Australasian Universities*, 2015, pp. 1–6.

[146] M. Mehrasa, E. Pouresmaeil, H. Mehrjerdi, B. N. Jørgensen, and J. P. S. Catalão, "Control technique for enhancing the stable operation of distributed generation units within a microgrid," *Energy Convers. Manag.*, vol. 97, pp. 362–373, Jun. 2015.

[147] E. Pouresmaeil, H. R. Shaker, M. Mehrasa, M. A. Shokridehaki, E. M. G. Rodrigues, and J. P. Catalão, "Stability analysis for operation of DG units in smart grids," in *Power Engineering, Energy and Electrical Drives (POWERENG), 2015 IEEE 5th International Conference on*, 2015, pp. 447–452.

[148] M. Babaie, M. Sharifzadeh, M. Mehrasa, L-F. Baillargeon, and K. Al-Haddad, "A robust fuzzy-based control technique for grid-connected operation of sensor-less PUC5 inverter," 44th Annual Conference of the IEEE Industrial Electronics Society, pp. 5272-5276, 2018.

[149] M. Mehrasa, M. Sharifzadeh, and K. Al-Haddad, "A droop based-control strategy of stand-alone single-phase converters for microgrid applications," 44th Annual Conference of the IEEE Industrial Electronics Society, pp. 5261-5266, 2018.

[150] M. Mehrasa, E. Pouresmaeil, A. Sepehr, B. Pournazarian, and J. P. S Catalão, “Control of power electronics-based synchronous generator for the integration of renewable energies into the power grid,” International Journal of Electrical Power & Energy Systems, vol. 111, pp. 300-314, 2019.

[151] M. Mehrasa, E. Pouresmaeil, H. Soltani, F. Blaabjerg, M. R. A Calado, and J. P. S Catalão, “Virtual Inertia and Mechanical Power-Based Control Strategy to Provide Stable Grid Operation under High Renewables Penetration,” Journal Applied Sciences, vol. 9, no. 6, pp. 1043, 2019.

[152] M. Mehrasa, M. Ebrahim Adabi, E. Pouresmaeil, J. Adabi, and B. N. Jørgensen, “Direct Lyapunov control (DLC) technique for distributed generation (DG) technology,” *Electr. Eng.*, vol. 96, no. 4, pp. 309–321, Dec. 2014.

[153] E. Pouresmaeil, M. Mehrasa, and J. P. Catalão, “Control strategy for the stable operation of multilevel converter topologies in DG technology,” in *Power Systems Computation Conference (PSCC), 2014*, 2014, pp. 1–7.

[154] M. Ahmadigorji, M. T. Kenari, and M. Mehrasa, “Optimal DG sizing in primary distribution feeders using dynamic programming approach,” in *Environment and Electrical Engineering (EEEIC), 2012 11th International Conference on*, 2012, pp. 371–375.

[155] S. Du, J. Liu, and T. Liu, “Modulation and Closed-Loop-Based DC Capacitor Voltage Control for MMC With Fundamental Switching Frequency,” *IEEE Trans. Power Electron.*, vol. 30, no. 1, pp. 327–338, Jan. 2015.

[156] M. Vatani, M. Hovd, and M. Saeedifard, “Control of the Modular Multilevel Converter Based on a Discrete-Time Bilinear Model Using the Sum of Squares Decomposition Method,” *IEEE Trans. Power Deliv.*, vol. 30, no. 5, pp. 2179–2188, Oct. 2015.

[157] A. Beddard, M. Barnes, and R. Preece, “Comparison of Detailed Modeling Techniques for MMC Employed on VSC-HVDC Schemes,” *IEEE Trans. Power Deliv.*, vol. 30, no. 2, pp. 579-589, Apr. 2015.

[158] A. Dekka, B. Wu, and N. R. Zargari, “A Novel Modulation Scheme and Voltage Balancing Algorithm for Modular Multilevel Converter,” presented at the Applied Power Electronics Conference and Exposition ,2015. APEC, 2015, pp. 1227–1233.

[159] G. Bergna *et al.*, “An Energy-Based Controller for HVDC Modular Multilevel Converter in Decoupled Double Synchronous Reference Frame for Voltage Oscillation Reduction,” *IEEE Trans. Ind. Electron.*, vol. 60, no. 6, pp. 2360–2371, Jun. 2013.

[160] P. Wang, X.-P. Zhang, P. F. Coventry, and R. Zhang, “Start-Up Control of an Offshore Integrated MMC Multi-Terminal HVDC System With Reduced DC Voltage,” *IEEE Trans. Power Syst.*, vol. 31, no. 4, pp. 2740–2751, Jul. 2016.

[161] A. Antonopoulos, L. Angquist, L. Harnefors, K. Ilves, and H.-P. Nee, "Global Asymptotic Stability of Modular Multilevel Converters," *IEEE Trans. Ind. Electron.*, vol. 61, no. 2, pp. 603–612, Feb. 2014.

[162] M. Zhang, L. Huang, W. Yao, and Z. Lu, "Circulating Harmonic Current Elimination of a CPS-PWM-Based Modular Multilevel Converter With a Plug-In Repetitive Controller," *IEEE Trans. Power Electron.*, vol. 29, no. 4, pp. 2083–2097, Apr. 2014.

[163] M. A. Perez, S. Bernet, J. Rodriguez, S. Kouro, and R. Lizana, "Circuit Topologies, Modeling, Control Schemes, and Applications of Modular Multilevel Converters," *IEEE Trans. Power Electron.*, vol. 30, no. 1, pp. 4–17, Jan. 2015.

[164] Y. Li, E. A. Jones, and F. F. Wang, "The Impact of Voltage-Balancing Control on Switching Frequency of the Modular Multilevel Converter," *IEEE Trans. Power Electron.*, vol. 31, no. 4, pp. 2829–2839, Apr. 2016.

[165] R. Lizana, M. A. Perez, S. Bernet, J. R. Espinoza, and J. Rodriguez, "Control of Arm Capacitor Voltages in Modular Multilevel Converters," *IEEE Trans. Power Electron.*, vol. 31, no. 2, pp. 1774–1784, Feb. 2016.

Appendices

Appendix A

All the matrixes used in (3.23) are the following:

$$Q_{dq0j}=\begin{bmatrix} i_{dj} \\ i_{qj} \\ i_{cirdj} \\ i_{cirqj} \\ i_{cir0j} \\ v_{dc} \end{bmatrix}, T_{dq0j}=\begin{bmatrix} R+0.5R_p & 0 & 0 & 0 & 0 & 0 \\ 0 & R+0.5R_p & 0 & 0 & 0 & 0 \\ 0 & 0 & L_p & 0 & 0 & 0 \\ 0 & 0 & 0 & L_p & 0 & 0 \\ 0 & 0 & 0 & 0 & L_p & 0 \\ 0 & 0 & 0 & 0 & 0 & C_{eq} \end{bmatrix} \tag{A.1}$$

$$X_{dq0j}=\begin{bmatrix} \left(R+0.5R_p\right) & -\omega\left(L+0.5L_p\right) & 0 & 0 & 0 & 0 \\ \omega\left(L+0.5L_p\right) & \left(R+0.5R_p\right) & 0 & 0 & 0 & 0 \\ 0 & 0 & R_p & -\omega L_p & 0 & 0 \\ 0 & 0 & \omega L_p & R_p & 0 & 0 \\ 0 & 0 & 0 & 0 & R_p & -\dfrac{3\sqrt{2}}{2} \\ 0 & 0 & 1 & 1 & 1 & \dfrac{1}{R_{dc}} \end{bmatrix} \tag{A.2}$$

$$P_{dq0j}=\begin{bmatrix} u_{dj1} \\ u_{qj1} \\ u_{dj2} \\ u_{qj2} \\ u_{0j2} \\ 0 \end{bmatrix}, O_{dq0j}=\begin{bmatrix} 0 \\ 0 \\ 0 \\ 0 \\ \sqrt{2}R_p i_{dcj} \\ i_{dc1}+i_{dc2} \end{bmatrix}, Y_{dq0j}=\begin{bmatrix} v_{dj} \\ v_{qj} \\ 0 \\ 0 \\ 0 \\ 0 \end{bmatrix} \tag{A.3}$$

Appendix B

Expressions of the variables V_{mu}, θ_u, V_{ml} and θ_l, respectively:

$$V_{mu} = \sqrt{\left[I_m R_{eq}\sin(\alpha) + L_{eq} I_m \omega\cos(\alpha)\right]^2 + \left[L_{eq} I_m \omega\sin(\alpha) - I_m R_{eq}\cos(\alpha) + v_m\right]^2}, \theta_u = tag^{-1}\left(\frac{\left[L_{eq} I_m \omega\sin(\alpha) - I_m R_{eq}\cos(\alpha) + v_m\right]}{\left[I_m R_{eq}\sin(\alpha) + L_{eq} I_m \omega\cos(\alpha)\right]}\right) \quad \text{(B.1)}$$

$$V_{ml} = \sqrt{\left[I_m R_{eq}\sin(\alpha) + L_{eq} I_m \omega\cos(\alpha)\right]^2 + \left[-v_m - R_{eq} I_m\cos(\alpha) + L_{eq} I_m \omega\sin(\alpha)\right]^2}, \theta_l = tag^{-1}\left(\frac{\left[-v_m - R_{eq} I_m\cos(\alpha) + L_{eq} I_m \omega\sin(\alpha)\right]}{\left[L_{eq} I_m \omega\cos(\alpha) + R_{eq} I_m\sin(\alpha)\right]}\right) \quad \text{(B.2)}$$

Appendix C

Expressions of the variables V_{at} and θ_{at}, respectively:

$$V_{at} = \sqrt{\begin{array}{l}\left(2L_a + L_{at}\right)^2 I_{ma}^2 \omega^2 + \left(2R_a + R_{at}\right)^2 I_{ma}^2 + 4v_m^2 + \\ 4v_m \left(2L_a + L_{at}\right) I_{ma} \omega \sin\left(\alpha_a\right) - 4v_m \left(2R_a + R_{at}\right) I_{ma} \cos\left(\alpha_a\right)\end{array}}$$

$$\theta_{at} = tag^{-1}\left(\frac{\left[2v_m + \left(2L_a + L_{at}\right) I_{ma} \omega \sin\left(\alpha_a\right) - \left(2R_a + R_{at}\right) I_{ma} \cos\left(\alpha_a\right)\right]}{\left[\left(2L_a + L_{at}\right) I_{ma} \omega \cos\left(\alpha_a\right) + \left(2R_a + R_{at}\right) I_{ma} \sin\left(\alpha_a\right)\right]}\right) \quad \text{(C.1)}$$